UNIVERSITÀ
DEGLI STUDI
DEL MOLISE

Numerical Modelling for Performance Assessment of Bridges Including VBI

Department of Biosciences and Territory
Ph.D Program in Biosciences and Territory: Applied Science Curriculum

Thesis submitted in partial fulfillment of the requirements for the degree of
Doctor of Philosophy

2024

SSD ICAR/09 - Tecnica delle costruzioni

Supervisor:
Prof. Giovanni Fabbrocino

Candidate:
Stefano Ercolessi

Co-supervisor:
Prof. Carlo Rainieri

Coordinator:
Prof. Filippo Santucci de Magistris

Abstract

Numerical simulations focusing on Vehicle-Bridge Interaction (VBI) are pivotal for enhancing our comprehension of bridge safety and longevity. Such simulations are intricate, encapsulating a broad spectrum of influences including traffic loads, environmental factors, and roadway conditions. Traffic loads, a fundamental aspect, impose varying degrees of operational stress on bridges, characterized by diverse magnitudes and frequencies. Environmental factors, such as fluctuations in temperature, wind forces, and seismic activities, pose additional long-term challenges to structural integrity. Road roughness also plays a critical role, impacting both vehicle performance and the bridge's structural health. Through the meticulous incorporation of these variables into numerical simulations, engineers and researchers can adeptly predict and scrutinize the multifaceted interactions between vehicles and bridges under authentic operational scenarios. This analytical approach fosters more robust design methodologies, improved maintenance protocols, and heightened safety standards, underscoring the indispensable value of comprehensive VBI simulations within contemporary structural engineering paradigms. This research delves into an exhaustive numerical examination of VBI, spotlighting the adoption of a beam finite element model poised for integration into a broader VBI analytical framework. The investigative journey spans from simple one-dimensional analyses to more sophisticated three-dimensional beam models that account for shear deformation and torsional dynamics. A notable aspect of this research addresses the calibration of vehicle dynamics, bridging a gap in existing literature concerning finite element model implementations and vehicle dynamics definition. Vehicle dynamic definition based on the processing data made available by Weigh in Motion Databases facilitates a systematic approach to traffic pattern analysis. The study further extends to evaluate environmental influences, including temperature variations. Furthermore, the development of the *Ghost project*, a C++ based finite element analysis software, marks a significant stride towards simulating VBI scenarios, accommodating diverse traffic configurations and analytical approaches. This work showcases several numerical simulations, each exploring varied traffic conditions and methodological perspectives, to evaluate the framework's efficacy and precision. These simulations entail a comparative analysis of direct and indirect VBI methodologies, focusing on the interplay between driving frequencies, environmental factors, and their cumulative effects on both bridge structures and vehicular dynamics. The overarching goal of this dissertation is to assess the effectiveness of a numerical framework rooted in beam model finite element formulations for VBI simulations. Through this research, the aim is to provide a comprehensive tool that bridges the gap between computational efficiency and modeling fidelity, thereby offering practical insights into bridge design, vehicle dynamics, and structural analysis, in order to obtain an estimate of bridges responses under several scenarios. This endeavor underscores the significance of a holistic approach to VBI simulations, promising substantial advancements in the field of structural engineering.

Contents

List of Figures

List of Tables

Chapter 1

Introduction

Bridges are more than just strategic infrastructures; they are vital lifelines, playing an indispensable role in every community's fabric. Their importance transcends merely serving as a means to traverse natural obstacles such as rivers or valleys. Instead, bridges should be regarded as essential tools that facilitate the connection of places and people, fostering economic growth, cultural exchange, and social cohesion. Integral to the seamless functioning of transportation networks, they significantly impact everything from daily commutes to international trade and on the local and global environment [1–4]. Thus, preserving bridges goes beyond safeguarding against extreme scenarios like structural collapse [5–7]. It is equally important to maintain their operational conditions to ensure safety, efficiency, and longevity. This maintenance involves regular inspections, timely repairs, and proactive upgrades to meet evolving demands and environmental challenges. In bridge maintenance, recognizing the roots of many catastrophic failures in neglected supervision and inadequate upkeep is crucial. These dramatic incidents often attract significant attention, overshadowing the silent yet pervasive issue of gradual deterioration. The consequences of such neglect are not only costly in terms of repairs and replacements but also pose significant risks to public safety. They can disrupt the economic and social activities dependent on these critical structures. Hence, a comprehensive approach to bridge maintenance is essential, including both routine checks and long-term strategic planning. This proactive approach addresses potential issues before they escalate into serious problems, ensuring bridges continue to serve as indispensable connectors in our communities and support the continuous flow of people, goods, and services [8–10]. In structural engineering, the application of numerical simulations is paramount for assessing the impact of moving loads on bridges. These simulations offer a detailed and accurate representation of bridge behavior under stress from varying loads, such as moving vehicles. Advanced computational models enable engineers to predict the dynamic response of bridge structures, including factors like vibration, deflection, and potential stress points. This is crucial for ensuring bridge safety and durability, as it allows for identifying and mitigating risks not apparent in standard static load analysis. Furthermore, these simulations are invaluable during the design phase, enabling engineers to optimize bridge designs for both strength and efficiency. They consider the complex interactions between the bridge structure and the moving loads. Insights gained from these simulations are essential for prolonging bridge lifespans, ensuring reliability under varied traffic conditions, and safeguarding public safety. In a broader context, they significantly contribute to developing sustainable, resilient infrastructure, adapting to challenges posed by increasing traffic volumes and heavier vehicles in modern transportation networks. In this context numerical simulations play a pivotal role, particularly in the design, analysis, and maintenance of bridges. These simulations serve as a crucial tool for engineers, allowing them to model

and analyze complex bridge structures under various loading conditions, including traffic loads, environmental stresses, and natural disasters like earthquakes.

Figure 1.1: Bridge and its interaction with traffic and the environmental conditions[1].

By employing advanced computational methods such as the Finite Element Method (FEM), engineers can predict how bridges will respond to these diverse stresses, identifying potential weak points, stress concentrations, and deformation patterns. This predictive power is invaluable not only in the design phase, where it aids in optimizing structural integrity and material efficiency, but also in the maintenance and retrofitting of existing bridges. Numerical simulations enable the assessment of a bridge's durability and the longevity of its components, guiding decisions on necessary repairs or upgrades. Furthermore, in an era where sustainability and resilience are paramount, these simulations assist in ensuring that bridge designs are not only safe and reliable but also environmentally sustainable and economically viable. This integration of numerical simulations in bridge engineering enhances public safety, optimizes resource use, and contributes to the development of infrastructure capable of withstanding the challenges of the 21st century. Moreover, accurate numerical simulations of traffic phenomena are essential in structural engineering, offering comprehensive descriptions of the various components, both natural and artificial, that bridges encounter. These simulations enable the modeling of traffic loads and their effects on bridge structures through diverse methodologies, each suited to particular scenarios and specific issues. The scientific literature often presents multiple approaches for addressing the same phenomenon, making it crucial to analyze the benefits and trade-offs of each method. This analysis aids in selecting the most appropriate technique for a given situation. The primary computational differences lie in the methods used to model the bridge structure and traffic. While closed-form solutions are available for simpler problems, numerical analyses, especially within the finite element framework, are more widely employed. The finite element method (FEM) offers versatility in modeling and simulating mechanical phenomena, with outcomes varying based on the specific analysis goal. Detailed finite element models that use 2D and 3D elements are possible, as demonstrated in studies (e.g. [11, 12]), but these are typically confined to scenarios requiring static responses or examining the kinematics of a single vehicle's effect on the bridge. Despite advances in software that facilitate the modeling of complex geometries, the necessary domain discretization for accurate responses often involves a large number

[1]Image generated by ChatGPT 4.0

of elements, which significantly impacts computational times. Additionally, the modeling of vehicles, which can still rely on 3D elements, and their interaction with the bridge structure is often approached through a multi-body framework [13]. These complexities present major challenges, particularly in scenarios where multiple vehicles are analyzed to simulate a bridge under operational conditions with full traffic flow. Hence, these factors must be carefully considered when choosing the most effective simulation approach for accurate and efficient analysis. To address the limitations of 3D and 2D modeling in bridge engineering, transitioning to 1D finite element models presents a viable alternative. These models describe the same physical systems but with fewer degrees of freedom, offering several advantages in various scenarios. One key benefit is reduced computational time, as these models are derived from distributed mass systems. In simpler cases, this approach even allows for analytical solutions, useful for verifying the accuracy of associated numerical problems [14–19]. Additionally, coupling the sub-systems, namely the bridge and vehicles, becomes more straightforward in 1D models. This coupling avoids complex mathematical constructs like Lagrange multipliers, relying instead on basic assumptions like perfect contact between the sub-systems. Although this assumption may seem restrictive given the mechanical behavior of vehicle suspension systems, its validity has been demonstrated in various studies. Moreover, the vehicle's impact on the bridge, the primary sub-system, can be idealized through three main approaches: moving forces, moving masses, or dynamic systems like sprung-mass or half-car models. These methodologies have been extensively explored, highlighting the conditions where one technique is preferable over others [20]. The moving force approach, the simplest to implement and calibrate, was initially developed to study the effects of moving loads on bridges. This approach models a sequence of forces, derived from the vehicle masses, moving across the bridge structure, thereby inducing a dynamic response. Numerically, this method is efficient as the number of degrees of freedom is largely determined by the beam's geometric discretization, and the time-varying elements are confined to the force intensities and contact point locations [21–23]. However, this method has drawbacks, such as the inability to account for road roughness and, more critically, the omission of inertial interactions between the bridge and vehicles. The previously mentioned limitation regarding the neglect of inertial interaction can be effectively addressed by adopting the moving masses approach [24, 25]. In this approach, forces are substituted with moving masses, significantly impacting the simulation by incorporating the inertial effects between the bridge and vehicle sub-systems. This approach, as a numerical tool for traffic simulation, offers reliability and specific numerical advantages over more complex mechanical systems, which will be discussed subsequently. From the perspective of finite element analysis, replacing forces with masses does not alter the total number of degrees of freedom required in a simulation. This is because the inertial contributions are accounted for within the bridge's mass matrix, which is recalculated at each time step. This method's efficacy has been supported by various studies [26, 27], which have presented both analytical and numerical simulations of the same problem, demonstrating the approach's reliability and accuracy, particularly in certain scenarios. The moving mass approach is particularly advantageous over the moving force method when the vehicle masses are comparable to the bridge's mass, and when the dynamic behavior of the overall system is significantly influenced by their interaction [28]. Despite advancements in the moving masses approach compared to the moving forces approach, it may still fall short in comprehensively addressing the interaction between bridge structures and vehicles. Notably, the inertial interaction isn't the sole mechanical phenomenon affecting bridges under live traffic. Vehicles, equipped with suspension systems designed for passenger comfort, significantly mitigate vibration impacts. These systems, typically spring-damper setups, can have a non-negligible in-

teraction with bridges. Bridges and vehicles constantly exchange mutual forces through contact points, influenced by the vehicles' mechanical characteristics. This interaction can notably affect the bridge's structural damping, either positively or negatively. This phenomenon is recognized in international codes, such as Eurocode 1's 'Additional Damping Method', and is documented in scientific works [29]. Moreover, the presence of road roughness [30] on bridge structures significantly impacts the interaction between vehicles and bridges, particularly in severe cases. Overcoming the limitations of previous approaches, such as the moving masses method, is possible by idealizing vehicles as mechanical systems [31–33]. These systems, designed to travel across bridges under the assumption of perfect contact, aim to accurately depict the dynamic behavior of the vehicle sub-system with minimal degrees of freedom. Various proposed models, characterized by elements like masses, springs, and dampers, achieve this (fig. 4.1).

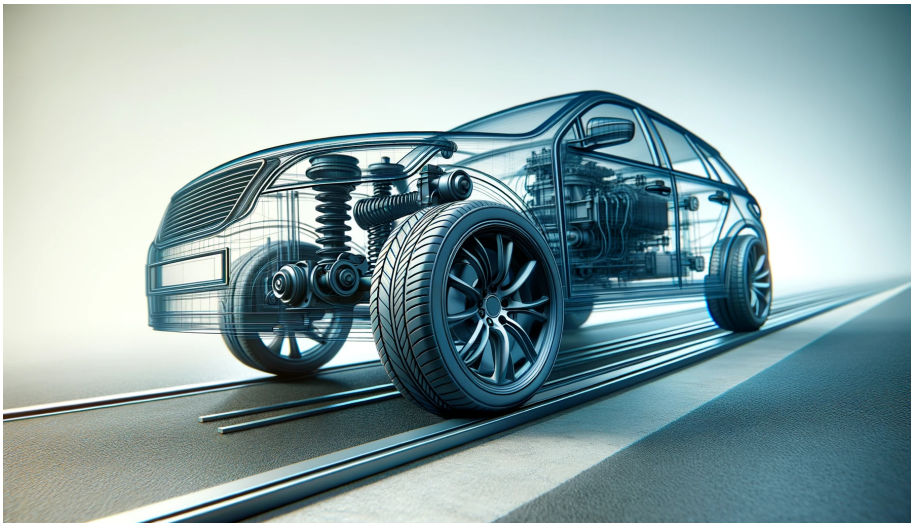

Figure 1.2: Idealization of a vehicle with simple mechanical devices[2].

The simplest of these is the sprung mass system [34, 35], which evolves into the damped sprung mass system by adding a damper [36]. The quarter-car model [37–39] introduces an additional mass element and spring. Its evolution, the half-car model [40–43], adds two spring-damper systems to simulate vehicle pitching. These models, however, are idealizations and can be adapted to specific scenarios [44–46]. The sophistication of vehicle models depends on the phenomenon analyzed and the responses required from simulations. In scenarios with many vehicles, simpler dynamic vehicle models are more suitable, whereas highly detailed responses from a few vehicles, like in railway bridges, necessitate more complex models with an adequate number of degrees of freedom. Numerical frameworks in traffic simulations, utilized for various purposes like direct and indirect methods, assist in the dynamic identification of bridges. Direct methods, part of experimental modal analysis [47–49], use data like acceleration and velocity measured directly on bridges. Operational modal analysis [50–52], an alternative, doesn't require known excitation sources and has become popular for its simplicity and cost-effectiveness. Indirect methods [53, 54], in contrast, record responses on vehicles to estimate bridge modal parameters. However, using moving vehicles on short bridges can lead to poor frequency resolution. Lower vehicle speeds help mitigate this, enhancing the accuracy of dynamic estimations related to the *driving frequency* [55–57], closely linked to the *critical velocity*. In general, the concepts of *driving frequency* and *critical speed* are paramount for ensuring structural in-

[2]Image generated by ChatGPT 4.0

tegrity and safety. Driving frequency refers to the rate at which a vehicle's load moves across a bridge. This factor is critical in the dynamic analysis of bridges, as it can lead to resonance if the driving frequency aligns with the bridge's natural frequency. Resonance can cause amplified structural vibrations, which, if not properly managed, might lead to potential structural damage or failure. On the other hand, critical speed in bridge engineering is defined as the speed at which a moving load, such as a vehicle, induces the maximum dynamic response in the bridge. This speed is crucial in the design and health monitoring of bridges, as exceeding the critical speed can result in significant dynamic effects, including uncomfortable vibrations or even structural damage. Understanding and calculating these factors is essential for bridge design, helping to avoid resonance conditions and ensuring that bridges can safely accommodate typical traffic loads and speeds. These scenarios can be seamlessly integrated into the previously mentioned numerical framework, both to assess the quality and reliability of known techniques and to serve as a platform for developing new approaches. For instance, the application of operational modal analysis techniques to indirect methods is notable. It has been demonstrated that classical tools, such as *Frequency Domain Decomposition* (FDD) and *Covariance-Driven Stochastic Subspace Identification* (CoV-SSI) from the operational modal analysis realm, can be effectively applied within an indirect framework, yielding reliable results [58, 59].

Figure 1.3: Weigh in motion system idealization[3].

Furthermore, over the past two decades, modal estimation of structures has become an essential tool, incorporated into various national codes. However, there are certain restrictions, as seen in the Italian scenario, particularly when responses are obtained from bridges with active traffic flow. These restrictions often mandate the use of *Weigh In Motion* (WIM) systems to support bridge response data [60] (fig. 1.3). Additionally, the impact of various disturbance phenomena, like road roughness and environmental factors on modal estimation, can be evaluated and studied. Many scholars have explored how different natural and anthropogenic conditions affect the dynamic estimation of bridge structures. These factors include temperature-induced frequency variations, weak and strong environmental excitations, wind intensity, and traffic loads [61–63]. The behavior of bridges is influenced by various factors, but not all to the same extent. It has been demonstrated, primarily through principal component analysis, that environmental temperature variations and traffic loads are the most significant factors affecting bridge responses [64, 65].

[3]Image generated by ChatGPT 4.0

Consequently, incorporating all these external factors into numerical simulations presents a substantial but challenging task. Often, simulations aimed at describing Vehicle-Bridge Interactions neglect these physical interactions, a notable shortcoming, especially when the simulations are part of a broader framework such as big data generation for artificial intelligence applications or in the context of digital twins. The integration of digital twin technology and big data analytics into the study of vehicle-bridge interaction phenomena marks a significant leap forward in civil engineering and infrastructure management.

Figure 1.4: Bridge digital twin idealization[4].

A digital twin (fig. 1.4), essentially a virtual replica of a physical bridge, enables engineers and researchers to monitor, analyze, and predict the behavior of bridge structures under vehicle loads in real-time. This dynamic tool leverages big data, collected from numerous sensors on the bridge, to gather detailed information about structural responses to traffic, environmental conditions, and material fatigue. Continuously updated with real-time data, the digital twin offers an evolving and accurate model for predictive maintenance, structural health monitoring, and decision-making processes. The vast volumes of data generated from vehicle-bridge interactions are meticulously analyzed using advanced algorithms, including Artificial Intelligence (AI) techniques, which provide critical insights into stress patterns, potential weaknesses, and the long-term effects of traffic loads. The incorporation of Artificial Intelligence allows for more efficient processing and interpretation of data, leading to enhanced safety and reliability of bridge structures and laying the groundwork for innovative design and construction practices. The use of digital twins, coupled with big data and Artificial Intelligence, signals a shift towards a more proactive, data-driven approach in infrastructure management. This new approach aims to optimize bridge lifespans and ensure their safe operation amidst increasing traffic demands and evolving environmental challenges. However, there remains a noticeable gap in the literature regarding an algorithm or methodology for automatically setting up and calibrating the mechanical parameters of vehicle dynamic models for monitoring systems on bridges. Additionally, the significance of horizontal and torsional responses in bridges, which many beam-model-based studies tend to overlook, needs more emphasis. The integration of Artificial Intelligence could potentially address these gaps by enabling more comprehensive and multi-dimensional analysis of bridge data, accounting for all critical aspects of bridge dynamics.

[4]Image generated by ChatGPT 4.0

This work primarily concentrates on examining Vehicle-Bridge Interaction (VBI) phenomena through a numerical lens. A novel finite element framework has been developed, extending the capabilities of these simulations to encompass the complete three-dimensional behavior of bridge structures under traffic, while utilizing only beam finite elements. The analysis explores several facets, including the selection of adequate finite elements necessary for these simulations and the development of specialized numerical software capable of performing the required simulations. Numerical benchmark are provided with some commercial software and the developed one for both the finite element formulations and for the interactions of the vehicle with the principal system. Furthermore, various error estimation parameters for signals have been introduced into the analysis to evaluate the strengths and weaknesses of these metrics. The primary objective in this case is to interpret the performance of non-standard indicators to assess their estimations for processes that have a mean close to zero. Moreover, common aspects related to VBI are extensively examined to understand how various phenomena influence the overall numerical simulations and identify the key factors to consider in specific scenarios. Both *direct* and *indirect* methods are scrutinized, along with a range of environmental and intrinsic factors that could affect the analysis, necessitating their incorporation into the simulation process. Several test layout are explored and the incidence of several external factors are included, such as thermal variations, environmental excitation or the impact of road roughness in the analysis. The main objective of the work is to define a new framework for obtaining estimates of the responses of bridges subjected to vehicular traffic, rationally defining a procedure to take into account various disturbance factors, such as temperature and environmental noise. Not of secondary importance is the definition of traffic loads which, although introduced with simplified dynamic models, are determined through a procedure based on real data derived from WIM. Moreover, this framework is particularly suitable for generating data that can then be processed with the various tools arising from the era of big data. The dissertation outline is briefly reported below:

- **Chapter 2** is dedicated to elucidating the beam finite element problem. It provides a detailed formulation of a Timoshenko finite element capable of describing non-uniform torsion. This is complemented by several numerical benchmarks aimed at testing its accuracy in dynamic applications;

- **Chapter 3** delves into the dynamic coupling between two sub-systems: vehicles, represented as simple dynamic systems, and the bridge. Following the presentation of the mathematical relationships, the quality and accuracy of the implementation are rigorously tested through numerical comparisons with *Abaqus 2023*;

- **Chapter 4** centers on calibrating factors in the simulations that are traffic-related. It particularly addresses the calibration of quarter-car models, which serve as the primary unit for representing traffic, as well as the calibration of the so-called road roughness;

- **Chapter 5** is devoted to the calibration of environmental effects that are integrated into the numerical framework. It specifically addresses the modulation of thermal variations and the calibration of environmental excitation, which is achieved by employing a set of equivalent forces to accurately represent these environmental influences.

- **Chapter 6** introduces and describes the *ghost project*, a versatile finite element software specifically designed for the numerical simulation of Vehicle-Bridge Interaction

problems. The chapter outlines the software's class structure and overall architecture. Additionally, it includes examples to demonstrate the software's capabilities and applications in simulating these interactions.

- **Chapter 7** is focused on conducting numerical simulations through the aforementioned software. It comprehensively explores and analyzes various traffic scenarios and methodologies. The primary objective is to discern the potential advantages and limitations that may emerge from simulating both *direct* and *indirect methods*. This analysis aims to provide a deeper understanding of the effectiveness and challenges inherent in these simulation approaches.

- **Conclusion and future developments** it naturally aims to briefly and concisely report the results obtained in the discussion in all its aspects, as well as to define the future research developments stemming from the work presented.

Chapter 2

Finite Element Formulation of the Beam problem

Finite element formulation for the Vehicle-Brige Interaction problem needs to be strongly improved, especially for cases where beam elements are employed to describe the mechanical behavior of bridge structures. As stated in the introduction, beam elements are suitable for modeling the three-dimensionality of the problem, similar to 2D and 3D elements, with considerable computational benefits. However, the majority of scientific literature focuses on the description of the mechanical problem restricted only to its flexural behavior, often neglecting the torsional behavior and its coupling with other acts of motion in real structures. Moreover, most recent works focus on slender beams, usually modeled according to the Euler-Bernoulli hypothesis without considering the shear deformability. However, from a beam theory perspective a lot of theory have been developed over the last centuries. Indeed, The first historical traces associated with significant contributions in the field of beam mechanics date back to the 17th century, when a great scientist, Galileo, in the "i discorsi" investigated for the first time from a scientific perspective the beam elements. Indeed, in his studies aimed at determining the ultimate strength of a member subjected to bending, he analyzed the case of a cantilever beam subjected to its own weight and a concentrated load at its end, deriving functional expressions that, although not very accurate, were able to estimate the strength of such structural elements. Obviously, these studies stemmed from practical needs rather than purely analytical ones, but they were fundamentally important because they initiated a series of considerations that allowed the advancement of such studies. This led to one of the most significant contributions from the point of view of beam mechanics, attributed to Bernoulli. In 1861, he made the first analytical contribution focused on the problem of elastic bending of beam elements. This study laid the groundwork for the beam element known today as the Euler-Bernoulli beam, which is still used and implemented in different finite element codes and proves to be a good tool for analyzing those structures that can be schematized and idealized as slender beams. However, this theory leads to a series of simplifications that do not allow for a general description of the beam phenomenon in its entirety. Indeed, the analysis of which type of element to implement must necessarily be commensurate with the final objective, which can only be an accurate description of the physical phenomenon. This reality is the engine that has allowed scholars who came later to undertake that critical process that has led to the evolution of models to this day. In fact, significant contributions are not only attributed to modern and contemporary scholars but have roots in the past. Indeed, not too long after Bernoulli's elegant theory, an important figure of the time named Lord Rayleigh (1877) brought an evolution to the beam theory by including the beam element's rotational inertia within the problem, a condition previously completely

neglected by Bernoulli's studies. About fifty years later, S.P. Timoshenko [66] applied a corrective factor to the beam already presented by Rayleigh, capable of describing the shear deformability in beam elements more accurately than previous models. This theory has proven to be the one that returns the most accurate mechanical quantities for thick beam elements. Until that time, structural elements, and in particular the sections characterized by them, were essentially of a massive type, or it was very rare for the profiles analyzed to have a thin thickness compared to the characteristic dimensions of the sections. It is in this context that a theory was developed by V.Z. Vlasov in 1959 [67], where the previous ones were further developed, including in the mechanical description those effects due to such particular geometries, whether they are characterized by open or closed sections. Here, the mechanical phenomenon of non-uniform torsion is accentuated by the particular type of section analyzed. Adding another building block to the theory of beam elements. These four theories, which may at first seem distinct but are in fact one the evolution of the other, are the cornerstones of the development of this type of element and the starting point for the studies and advancements that researchers have brought to our day. Indeed, during the last century, there were several works aimed at extending or deepening the aforementioned theories as well as their formulations from a numerical standpoint in different finite element solutions, which can be found in most of today's calculation codes. Research, of course, has moved on different fronts, analyzing the various formulations differently. There are different works that can be found in the literature on the Euler-Bernoulli formulation. One of the first studies focused on this theory is attributed to M.M. Black [68, 69] who in two works studied the behavior of thin-walled beam elements in the field of large displacements. This work not only developed the theoretical results of this theory but also some experimental tests are conducted from which emerged how such profiles are subject to nonlinear instability phenomena when subjected to combined bending and torsion stresses. However, the experimental results of the time were limited, as stated by the author himself due to the layout that was executed for such types of tests at the time, which did not allow for a complete and exhaustive understanding of the strongly nonlinear behavior exhibited by the elements. Furthermore, in 1965 the work was further extended to structures formed by the union of multiple thin walled Euler-Bernoulli beams in order to constitute a single continuous structure. Also in this case, the author, leveraging experimental and numerical tests naturally deriving from his previous works, was able to demonstrate how even in the case of these structures subjected to combined bending and torsion stresses, instability phenomena are present and how the approximate formulations of the time behaved positively for stress-strain levels normally present in structures under normal operating conditions. Subsequently, R.E.D. Bishop [70, 71], who made significant contributions to beam theory, driven by the study of thin-walled profiles used especially in the naval industry, delved into the study of asymmetric thin-walled sections. In particular, he with two different works based on the Euler-Bernoulli and Vlasov theory analyzed the dynamic behavior of such elements, first deriving the equations of motion through the principle of virtual works and then solving the differential equations that regulate the dynamics of the elements both for the case of free and forced oscillations. In particular, he focused on the consequences that warping has on this type of profiles highlighting how crucial this phenomenon is especially in calculating the natural frequencies of thin-walled beam elements. In the same years, P.O. Friberg [72, 73] presented a series of works also aimed at describing the dynamic behavior of thin-walled beams, approaching the problem by exploiting the method of the dynamic stiffness matrix, which allows to simplify considerably the equations that regulate the phenomenon even in the presence of warping, and these studies resulted in a numerical implementation of the problem. Along with the theoretical formulations, the first implementations of such

models within calculation codes also began, and naturally, a series of works made for the implementation of such models to finite elements began to appear. In [74] a finite element formulation was proposed, neglecting the flexural-torsional coupling of the problem, which was then subsequently revisited in [75], where the beam element was schematized as a bar with two nodes with seven degrees of freedom per node. Simulations were then proposed for profiles with open and closed sections exploiting the approach of the mixed variational principal for the reduction of the shear locking phenomenon. In this context, it was thus concluded that following the modified Hellinger-Reissner variational principle it is possible to develop both linear and quadratic beam elements that provided adequate performance and accuracy especially in function of the negative phenomenon of shear locking that was present on the models presented previously. The study of such models, naturally continued presenting increasingly accurate and complex models as in the work of S.M. Hashemi et al. [76] where using the principle of virtual works together with approximations directly coming from the shape functions of the element it was possible to obtain a matrix solution that takes into account the contributions of mass and stiffness as a function of a single vibration frequency showing excellent results in terms of accuracy. Subsequently, at the beginning of the new century, A. Arpaci et al. with two works [77, 78] derived numerically the roots of the fundamental equation of the beam analyzing the effects that rotational inertia has on the dynamic problem, also focusing on the flexural-torsional coupling of the general problem. Moreover, attempts to develop the theory did not stop, and the desire to try and apply new techniques to the problem made its way as in the works of L. Jun [79, 80] where the main focus was the application of the dynamic matrix transfer method to derive the vibrational properties of the system investigated under the effect of an axial load. Shortly after, the same problem in the absence of axial stress was taken up by J.R. Banerjee et al. [81] who through the dynamic stiffness matrix applied to the system the Wittrick-Williams algorithm obtaining interesting results from the point of view of the vibration frequencies of the analyzed beam. Notable were then the results, from the numerical point of view, brought by Y.L. Kuo et al. [82] who presented a finite element formulation based on stress, which allowed thanks to the compatibility relations to have continuity not only on displacements and rotations but also stress continuity on the nodes of the element, a drawback that previous finite element formulations based on displacements suffered from. Subsequently, many scholars have continued to investigate thin-walled Euler-Bernoulli beams with or without various kinds of mechanical couplings [83, 84] or have continued to propose finite element formulations that can be found in various calculation codes [85]. However, in this context, the aforementioned Euler-Bernoulli formulation was not the only one that has been developed over the years, in fact, the same fate befell the Timoshenko formulation. Although similar, but profoundly different this formulation has had a notable development especially starting from the 70s of the last century. For example, in 1973 T.M. Wang [86], began to analyze the impact that such elements have in their application to frame structures, providing an analytical solution to the problem and highlighting the contribution of rotational inertia in such operating conditions of the profiles. At the same time, the influence of shear deformability on the modes of vibration of the beam was analyzed in [87] which highlighted how especially in stocky structures the presence of the phenomenon can significantly influence the simulated dynamic behavior of the elements. In the same years, J.R. Bishop et al. [88] again, driven by the desire to investigate the contribution that such theory could have on naval engineering and in particular in its application as the structure of boat keels, studied the effect that warping has on the free oscillations of thin-walled Timoshenko type profiles, focusing on the presence of the so-called principal modes of antisymmetric motion, which at the time was thought to be particularly complicated to take into account, but J.R. Bishop demon-

strated how it was not necessary to resort to unusual methods to keep them in account in dynamic analyses. Already at the beginning of the early 80s, the first formulations of Timoshenko type beam elements began to appear especially regarding the context of finite elements. Two examples to mention are [89, 90] where two finite element formulations with a modified definition of sectorial area were presented. Always in this period still J.R. Banerjee et al. [91–93] exploited the concept of dynamic stiffness matrix and applied it also to the Timoshenko formulation in the presence of flexural-torsional coupling in the static field also providing a numerical implementation of the problem, which allowed the authors to bring to the forefront a series of numerical comparisons with classic approximate methods for such structural elements that were commonly used at the time. However, the authors also analyzed the dynamic behavior of the structure and in particular how the presence of warping and the theory of thin-walled profiles went to severely influence the dynamic behavior in free oscillation of the structural elements that are characterized by these sections and once again the convergence of the analyses was improved referring to the so-called Wittrick-Williams algorithm. But the studies did not stop here, in fact later R.D. Ambrosini et al. [94, 95] analyzed the problem in the frequency domain focusing on the effects of rotational inertia and shear deformability of the problem arising from the coupling of the Timoshenko and Vlasov theory. At the end of the 90s, there were several attempts to expand the knowledge and concepts of the Timoshenko beam problem, among these attempts it is fair to mention the work of A.N. Bercin et al. [96] who studied the interaction of torsion and bending in such types of beams providing an analytical solution of the problem and introducing in the analysis the rotational inertia of the element. Or the two finite element formulations due to Back et al. [97] and Hutchinson [98] and especially that of Reddy et al. [99] which presented a super convergent finite element based on reduced integration that gave significant performance from the computational and accuracy point of view. However, such elements were not implemented or developed only for finite element solutions, in fact, Sapontzakis et al [100] proposed a BEM formulation and the comparisons they brought with finite element calculation software returned interesting results in terms of accuracy. Or still worth mentioning are the formulations of Kahrobaiyan et al [101] who proposed a finite element also based on stress rather than displacements that gave impressive accuracy results.

In this regard, this section is dedicated to the implementation of a beam finite element formulation based on Timoshenko theory, able to account for the coupling between the several kinematic components that this structural element normally exhibits, along with uniform and non-uniform torsion, considering some hypotheses strictly derived from Vlasov's theory [67]. Furthermore, some numerical benchmarks are performed and illustrated to test the quality of the implementation against a commercial software, such as *Abaqus 2023*. Numerical simulations intended as benchmarks for the theoretical formulations are performed using an ad hoc finite element implementation based on software coded in C++, named *ghost project*, which will be fully disclosed in chapter 6. On the other hand, the section properties of the various sections analyzed in the following sections are computed using a Python package called *sectionproperties* [102], which is open-source. Its source code has been modified to obtain all the geometrical quantities needed for the further analysis, indeed in its native formulation some mechanical quantities aimed to the description of warping feature of the section are not immediately provided.

2.1 Flexural-torsional Timoshenko beam element with non uniform torsion

The finite element formulation for mechanical elements can be defined using various methodologies, both for the strong form and the weak form. In finite element analysis of beam elements, three fundamental principles are commonly employed to derive the governing equations: D'Alembert's Principle, Lagrange's Principle, and Hamilton's Principle. D'Alembert's Principle plays a pivotal role in dynamic analysis, transforming dynamic beam problems into equivalent static ones by introducing inertial forces as fictitious external loads, simplifying the analysis of beams under dynamic loading like vibrations, where inertia is significant. Lagrange's Principle, emphasizing the minimization of total potential energy, which includes both strain energy due to deformation and potential energy from external forces, proves invaluable in handling complex boundary conditions and constraints in elastic structural problems, and is particularly effective for systems where forces do not have a potential energy function. Hamilton's Principle extends this concept by considering both kinetic and potential energies, making it essential for the dynamic analysis of beam elements. It leads to the derivation of comprehensive differential equations that describe the motion of beams, accounting for elasticity and mass distribution, and is crucial for analyzing vibrational behaviors like natural frequencies and modes. Collectively, these principles provide a robust and nuanced framework for the finite element modeling of beam elements, enabling precise and reliable modeling for a wide array of structural analysis applications, from basic static scenarios to complex dynamic environments. The subsequent sections detail the methodologies applied to characterize the two formulations for the mechanical problem under investigation. This means to establish the stationarity of the Hamilton's functional, involving the synchronous variated motions, to derive the equations of motion in their strong form, followed by the application of the renowned Galerkin method to derive the displacement-based finite element model. Let's assume the displacement field associated with the beam's cross section, where the coordinate system is depicted in fig. 2.1.

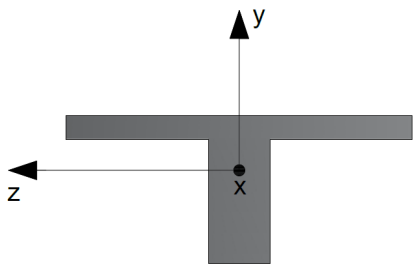

Figure 2.1: Beam cross-section coordinates system.

$$\begin{aligned} u_x(x,y,z) &= w_x - y\theta_z + z\theta_y + \omega(y,z)\cdot\theta_{x,x} \\ u_y(x,y,z) &= w_y - (z-z_s)\cdot\theta_x \\ u_z(x,y,z) &= w_z + (y-y_s)\cdot\theta_x \end{aligned} \tag{2.1}$$

In the aforementioned coordinate system, the displacement components of the cross section are denoted as $u_i(x,y,z)$ with $i = x,y,z$. The quantity θ_x represents the torsional rotation of the element, while $\omega(y,z)$ is the so-called warping function. The notation, $_{,x}$ indicates

the first derivative with respect to x. The point of coordinates (y_s,z_s) correspond to the chosen pole or the center of twist characteristic of the section. In contrast to Euler's theory, the Timoshenko formulation accounts for the shear deformability of the beam element. In this context, quantities associated with deflections along the y and z axes can be divided into contributions from two different mechanical behaviors

$$\begin{aligned} w_y &= w_{y,s} + w_{y,b} \\ w_z &= w_{z,s} + w_{z,b} \end{aligned} \tag{2.2}$$

the shear contributions $w_{y,s}$ and $w_{z,s}$ and the classical deflections $w_{y,b}$ and $w_{z,b}$ due to the bending also present in the Bernoulli formulation. By taking the first derivatives of the relations (2.2) the same additive composition holds for the associated quantities

$$\begin{aligned} \frac{\partial w_y}{\partial x} &= \frac{\partial w_{y,s}}{\partial x} + \frac{\partial w_{y,b}}{\partial x} = \gamma_{xy} + \theta_z \\ \frac{\partial w_z}{\partial x} &= \frac{\partial w_{z,s}}{\partial x} + \frac{\partial w_{z,b}}{\partial x} = \gamma_{xz} - \theta_y \end{aligned} \tag{2.3}$$

where γ_{xy} and γ_{xz} are the angular distortions associated with to y and z components and θ_z and θ_y are the section rotations due to bending in the two direction of the coordinate system. Once, that the displacement field is known is trivial to retrieve the associated strain field by considering classical continuum mechanic equations

$$\begin{aligned} \epsilon_x &= \frac{\partial u_x}{\partial x} = w_{x,x} - y \cdot \theta_{z,x} + z \cdot \theta_{y,x} + \omega \cdot \theta_{x,xx} \\ 2\gamma_{xy} &= \frac{\partial u_x}{\partial y} + \frac{\partial u_y}{\partial x} = w_{y,x} - \theta_z - \left[(z - z_s) - \frac{\partial \omega}{\partial y} \right] \cdot \theta_{x,x} \\ 2\gamma_{xz} &= \frac{\partial u_x}{\partial z} + \frac{\partial u_z}{\partial x} = w_{z,x} + \theta_y + \left[(y - y_s) + \frac{\partial \omega}{\partial z} \right] \cdot \theta_{x,x} \end{aligned} \tag{2.4}$$

where ϵ_x is the normal strain along the beam axis. The associate stress field it is compute by assuming an elastic behaviour of the medium and introducing the so-called stress-strain relationships as

$$\begin{aligned} \sigma_x &= E \cdot \epsilon_x \\ \tau_{xy} &= G \cdot \gamma_{xy} \\ \tau_{xz} &= G \cdot \gamma_{xz} \end{aligned} \tag{2.5}$$

Once, that all the previous quantities are defined the system of partial differential equation of motion in its strong form is retrieved by means of the Lagrange principle, which can be formally stated as

$$\delta \int_{t_1}^{t_2} \left[T - (U - V) \right] dt = 0 \tag{2.6}$$

this is a classic variational approach where the variation of the Lagrangian functional is taken with respect to time, here the quantities T, U and V are respectively the kinetic energy the strain potential energy and the work done by the external forces. Moreover, the variations of the above functional are meant to lie within the class of synchronous variated motions [103].

2.1.1 Strain Potential Energy Formulation

The strain energy over the considered finite volume V of the beam element, can be addressed by

$$2U = \int_V (\sigma_x \epsilon_x + \tau_{xy}\gamma_{xy} + \tau_{xz}\gamma_{xz})\, dV \tag{2.7}$$

substituting relations (2.5)-(2.4) into (2.12) the latter takes the following form

$$\begin{aligned} 2U = E \int_V (w_{x,x} - y \cdot \theta_{z,x} + z \cdot \theta_{y,x} + \omega \cdot \theta_{x,xx})^2\, dV \\ +G \int_V \left\{ w_{y,x} - \theta_z - \left[(z - z_s) - \frac{\partial \omega}{\partial y} \right] \cdot \theta_{x,x} \right\}^2 dV \\ +G \int_V \left\{ w_{z,x} + \theta_y + \left[(y - y_s) + \frac{\partial \omega}{\partial z} \right] \cdot \theta_{x,x} \right\}^2 dV \end{aligned} \tag{2.8}$$

by introducing the geometric sectional properties in the (2.8)

$$\begin{aligned} A = \int_A dA \qquad S_y = \int_A z\, dA \qquad S_z = \int_A y\, dA \qquad S_\omega = \int_A \omega\, dA \\ I_z = \int_A z^2 dA \qquad I_y = \int_A y^2 dA \qquad I_{yz} = \int_A yz\, dA \\ I_{\omega z} = \int_A \omega\, y dA \qquad I_{\omega y} = \int_A \omega z\, dA \qquad I_\omega = \int_A \omega^2 dA \\ J = \int_A \left\{ \left[(y - y_s) - \frac{\partial \omega}{\partial y} \right]^2 + \left[(z - z_s) + \frac{\partial \omega}{\partial z} \right]^2 \right\} dA \\ S_{ys} = \int_A (z - z_s)\, dA \qquad S_{zs} = \int_A (y - y_s)\, dA \\ S_{\omega y} \int_A \frac{\partial \omega}{\partial z} dA \qquad S_{\omega z} = \int_A \frac{\partial \omega}{\partial y} dA \end{aligned} \tag{2.9}$$

The development of the strain energy formulation can be further simplified by introducing an hypothesis deriving directly from the Vlaslov theory [67]. Indeed, the Vlaslov assumption states that the tangential stress at the mid-surface of the beam are null or negligible. In this regard, it holds

$$\begin{aligned} 2 \cdot \gamma_{xy,T} = \left[-(z - z_s) + \frac{\partial \omega}{\partial y} \right] \theta_{x,x} = 0 \Longrightarrow \frac{\partial \omega}{\partial y} = (z - z_s) \\ 2 \cdot \gamma_{xz,T} = \left[(y - y_s) - \frac{\partial \omega}{\partial y} \right] \theta_{x,x} = 0 \Longrightarrow \frac{\partial \omega}{\partial z} = -(y - y_s) \end{aligned} \tag{2.10}$$

where $\gamma_{xy,T}$ and $\gamma_{xz,T}$ are the tangential strains due to the presence of torsion in the investigated section. Moreover, those relations can be further elaborated by integrating

over the area of the element, as

$$\begin{aligned} \int_A \frac{\partial \omega}{\partial y} dA = \int_A (z - z_s) dA \Longrightarrow S_{\omega z} = S_{ys} \\ \int_A \frac{\partial \omega}{\partial z} dA = -\int_A (y - y_s) dA \Longrightarrow S_{\omega y} = -S_{zs} \end{aligned} \tag{2.11}$$

working around the equations (2.8), substituting the mechanical quantities (2.9) the following formulation is obtainable

$$\begin{aligned} 2U = EA \int_L w_{x,x}^2 dx + EI_z \int_L \theta_{z,x}^2 dx + EI_y \int_L \theta_{y,x}^2 dx + EI_\omega \int_L \theta_{x,xx}^2 dx \\ -2ES_z \int_L w_{x,x} \cdot \theta_{z,x} dx + 2ES_y \int_L w_{x,x} \cdot \theta_{y,x} dx + 2ES_\omega \int_L w_{x,x} \cdot \theta_{x,xx} dx \\ -2EI_{yz} \int_L \theta_{z,x} \cdot \theta_{y,x} dx - 2EI_{\omega z} \int_L \theta_{x,xx} \cdot \theta_{z,x} dx + 2EI_{\omega y} \int_L \theta_{y,x} \cdot \theta_{x,xx} dx \\ +GA_y \int_L (w_{y,x} - \theta_z)^2 dx + GA_z \int_L (w_{z,x} + \theta_y)^2 dx + GJ \int_L \theta_{x,x}^2 dx \end{aligned} \tag{2.12}$$

here, in the strain potential energy formulation A_y and A_z are respectively the shear areas computed along the y and z axis of the section coordinate system and the integral over L is, naturally, over the total length of the beam.

2.1.2 Kinetic Energy Formulation

Kinetic energy of the mechanical system is retrieved by considering the integral over the volume V of the material density ρ multiplied by the three squared velocity components, which under the assumption of homogeneous medium specialized in

$$2K = \rho \int_V (\dot{u_x}^2 + \dot{u_y}^2 + \dot{u_z}^2) dV \tag{2.13}$$

by substituting the fundamental relations associate with the displacement field of the section (2.1) in (2.13)

$$\begin{aligned} 2K = \rho \int_V (w_x - y \cdot \theta_z + z \cdot \theta_y + \omega \cdot \theta_{x,x})^2 dV \\ +\rho \int_V [w_y - (z - z_s)\theta_x)]^2 dV + \rho \int_V [w_z - (y - y_s)\theta_x)]^2 dV \end{aligned} \tag{2.14}$$

and developing the basic math behind and defining the polar moment of inertia of the section computed considering the shear center as a pole

$$I_{ps} = \int_A (y - y_s)^2 + (z - z_s)^2 dA \tag{2.15}$$

the relation (2.14) assumes the form of

$$\begin{aligned} 2K = \rho A \int_L \left(\dot{w}_x^2 + \dot{w}_y^2 + \dot{w}_z^2\right) dx + \rho I_z \int_L \dot{\theta}_z^2 dx + \rho I_y \int_L \dot{\theta}_y^2 dx + \rho I_\omega \int_L \dot{\theta}_{x,x}^2 dx \\ -2\rho I_{yz} \int_L \dot{\theta}_z \cdot \dot{\theta}_y \, dx - 2\rho I_{\omega z} \int_L \dot{\theta}_z \cdot \dot{\theta}_{x,x} \, dx + 2\rho I_{\omega y} \int_L \dot{\theta}_y \cdot \dot{\theta}_{x,x} \, dx \\ -2\rho S_z \int_L \dot{w}_x \cdot \dot{\theta}_z dx + 2\rho S_y \int_L \dot{w}_x \cdot \dot{\theta}_y dx + 2\rho S_\omega \int_L \dot{w}_x \cdot \dot{\theta}_{x,x} dx \\ +\rho I_{PS} \int_L \dot{\theta}_x^2 dx - 2\rho S_{ys} \int_L \dot{w}_y \cdot \dot{\theta}_x dx + 2\rho S_{zs} \int_L \dot{w}_z \cdot \dot{\theta}_x dx \end{aligned} \tag{2.16}$$

2.1.3 Virtual Work of External Loads

The virtual work of external loads on the displacement field is here depicted. Neglecting the effects of the body forces on the mechanical system, two system of forces are identified. Those are the distributed loads togehther with the nodal generalized forces, which embody the natural conditions of the problem. The virtual work of the external loads is

$$\begin{aligned} V = \int_V \left(q_x \cdot \delta w_x + q_y \cdot \delta w_y + m_z \cdot \delta\theta_z + q_z \cdot \delta m_y + m_x \cdot \delta\theta_x + b_x \cdot \delta\theta_{x,x}\right) dV \\ + \left[N \cdot \delta w_x + T_y \cdot \delta w_y + M_z \cdot \delta\theta_z + T_z \cdot \delta w_z + M_y \cdot \delta\theta_y + M_x \cdot \delta\theta_x + B_x \cdot \delta\theta_{x,x}\right]_0^L \end{aligned} \tag{2.17}$$

where, q_x, q_y and q_z are the distributed loads along the associated direction of the coordinate system; m_x, m_y and m_z are the distributed moments counterparts, finally the quantity b_x is the distributed bi-moment. The formulation for the concentrated loads at the two beam ends can be expanded by considering (2.5), for each contribution as

$$\begin{aligned} N &= \int_A \sigma_x \cdot dA = EA \cdot w_{x,x} - ES_z\theta_{z,x} + ES_y \cdot \theta_{y,x} + ES_\omega \cdot \theta_{x,xx} \\ T_y &= \int_A \tau_{xy} dA = GA_y \cdot (w_{y,x} - \theta_z) - GS_{ys} \cdot \theta_{x,x} + GS_{\omega z} \cdot \theta_{x,x} \\ M_z &= -\int_A \sigma_x \cdot y da = -ES_z \cdot w_{x,x} + EI_z \cdot \theta_{z,x} - EI_{yz} \cdot \theta_{y,x} - EI_{\omega z} \cdot \theta_{x,xx} \\ T_z &= \int_A \tau_{xz} dA = GA_z \cdot (w_{z,x} + \theta_y) - GS_{zs} \cdot \theta_{x,x} + GS_{\omega y} \cdot \theta_{x,x} \\ M_y &= \int_A \sigma_x \cdot z da = ES_y \cdot w_{x,x} + EI_y \cdot \theta_{y,x} - EI_{yz} \cdot \theta_{z,x} - EI_{\omega y} \cdot \theta_{x,xx} \end{aligned} \tag{2.18}$$

$$\begin{aligned} M_x = \int_A -\tau_{xy} \cdot \left[(z - z_s) - \omega_{,y}\right] + \tau_{xz} \cdot \left[(z + z_s) + \omega_{,z}\right] dA \\ = G\left(S_{ys} - S_{\omega z}\right)\left(w_{y,x} - \theta_z\right) + G\left(S_{zs} - S_{\omega y}\right)\left(w_{z,x} + \theta_y\right) + GJ \cdot \theta_{x,x} \end{aligned}$$

$$B_x = \int_A \sigma_x \cdot \omega dA = ES_\omega \cdot w_{x,x} - EI_{\omega z} \cdot \theta_{z,x} + EI_{\omega y} \cdot \theta_{y,x} + EI_\omega \cdot \theta_{x,xx}$$

The latter describes the boundary condition terms of the beam and have an crucial role especially in the further integration by part of the two energy terms in order to reach both the strong form of the equation of motion for the investigated mechanical problem.

2.1.4 Equation of Motion: Strong Form

Once that, the energy components associated with the potential strain energy U, the kinetic energy T and the external virtual work V, are defined, is immediate to achieve the equation of motion in its strong form by applying the calculus of the variations. In the case under consideration, transitioning from the strong form to the definition of the weak form is an essential step. It can be demonstrated that these formulations are equivalent through the Lax-Milgram theorem [104, 105]. This theorem plays a crucial role in establishing a solid foundation for the mathematical analysis of physical systems, especially when employing numerical methods for solving partial differential equations. By ensuring the existence and uniqueness of solutions to the weak form, the Lax-Milgram theorem validates the approach of using the weak form as a viable and effective method for addressing complex engineering and physical problems. In practical terms, the theorem allows for the conversion of differential equations from their strong form (which involves derivatives and can be difficult to solve directly, especially for complex geometries or boundary conditions) to a weak form (which involves integral formulations and can be more readily approximated using numerical techniques). Here, by applying the integration by part of the energy components and simplifying the boundary conditions terms together with the initial condition of the mechanical system the strong formulation is achieved. Hereafter, the three aforementioned energy quantities are treated as separate entities for the sake of clearness, condition which is possible due to the commutative properties of the variation operator *delta*. Starting from equation (2.8) taking the infinitesimal variation, integrating by part and discarding the boundary conditions terms

$$
\begin{aligned}
-U = \int_{t_1}^{t_2} \Big\{ & EA \int_0^L w_{x,xx} \cdot \delta w_x dx - ES_z \int_0^L w_{x,xx} \cdot \delta\theta_z dx - ES_z \int_0^L \theta_{z,xx} \cdot \delta w_x dx \\
& + ES_y \int_0^L w_{x,xx} \cdot \delta\theta_y dx + ES_y \int_0^L \theta_{y,xx} \cdot \delta w_x dx - ES_\omega \int_0^L w_{x,xxx} \cdot \delta\theta_x dx \\
& + ES_\omega \int_0^L \theta_{x,xxx} \cdot \delta w_x dx - EI_{yz} \int_0^L \theta_{z,xx} \cdot \delta\theta_y dx - EI_{yz} \int_0^L \theta_{y,xx} \cdot \delta\theta_z dx \\
& + EI_{\omega y} \int_0^L \theta_{x,xxx} \cdot \delta\theta_y dx - EI_{\omega y} \int_0^L \theta_{y,xxx} \cdot \delta\theta_x dx + EI_{\omega z} \int_0^L \theta_{z,xxx} \cdot \delta\theta_x dx \\
& - EI_{\omega z} \int_0^L \theta_{x,xxx} \cdot \theta_z dx + EI_z \int_0^L \theta_{z,xx} \cdot \delta\theta_z dx + EI_y \int \theta_{y,xx} \cdot \delta\theta_y dx \\
& - EI_\omega \int_0^L \theta_{x,xxxx} \cdot \delta\theta_x dx + GA_y \cdot \left[\int_0^L (w_{y,x} - \theta_z)_{,x} \cdot \delta w_y dx + \int_0^L (w_{y,x} - \theta_z) \cdot \delta\theta_z dx \right] \\
& + GA_z \cdot \left[\int_0^L (w_{z,x} + \theta_y)_{,x} \cdot \delta w_z dx - \int_0^L (w_{z,x} + \theta_y) \cdot \delta\theta_y dx \right] + GJ \int_0^L \theta_{x,xx} \cdot \delta\theta_x dx \Big\}
\end{aligned}
\tag{2.19}
$$

the same formulation can be adopted in order to describe the quantities associated with the kinetic energy. However, for the latter case the integration by part should be applied over the time domain. Thus, the application of the infinitesimal variation together with the integration by part let to write for the relation (2.14) the following

$$
\begin{aligned}
K = \int_0^L \Big\{ & -\rho A \int_{t_1}^{t_2} \ddot{w}_x \cdot \delta w_x dt - \rho A \int_{t_1}^{t_2} \ddot{w}_y \cdot \delta w_y dt - \rho A \int_{t_1}^{t_2} \ddot{w}_z \cdot \delta w_z dt \\
& -\rho I_z \int_{t_1}^{t_2} \ddot{\theta}_z \cdot \delta\theta_z dt - \rho I_y \int_{t_1}^{t_2} \ddot{\theta}_y \cdot \delta\theta_y dt + \rho I_\omega \int_{t_1}^{t_2} \ddot{\theta}_{x,xx} \cdot \delta\theta_x dt \\
& + \rho I_{\omega z} \left(- \int_{t_1}^{t_2} \ddot{\theta}_{z,x} \cdot \delta\theta_x dt + \int_{t_1}^{t_2} \ddot{\theta}_{x,x} \delta\theta_z dx \right) + \rho I_{\omega y} \left(\int_{t_1}^{t_2} \ddot{\theta}_{y,x} \cdot \delta\theta_x dt - \int_{t_1}^{t_2} \ddot{\theta}_{x,x} \delta\theta_y dx \right) \\
& -\rho I_{PS} \int_{t_1}^{t_2} \ddot{\theta}_x \cdot \delta\theta_x dt + \rho S_z \left(\int_{t_1}^{t_2} \ddot{w}_x \cdot \delta\theta_z dt + \int_{t_1}^{t_2} \ddot{\theta}_z \cdot \delta w_x dt \right) \\
& + \rho I_{yz} \left(\int_{t_1}^{t_2} \ddot{\theta}_z \cdot \delta\theta_y dt + \int_{t_1}^{t_2} \ddot{\theta}_y \cdot \delta\theta_z dt \right) - \rho S_y \left(\int_{t_1}^{t_2} \ddot{w}_x \cdot \delta\theta_y dt + \int_{t_1}^{t_2} \ddot{\theta}_y \cdot \delta w_x dt \right) \\
& + \rho S_{ys} \left(\int_{t_1}^{t_2} \ddot{w}_y \cdot \delta\theta_x dt + \int_{t_1}^{t_2} \ddot{\theta}_x \cdot \delta w_y dt \right) - \rho S_{zs} \left(\int_{t_1}^{t_2} \ddot{w}_z \cdot \delta\theta_x dt + \int_{t_1}^{t_2} \ddot{\theta}_x \cdot \delta w_z dt \right) \\
& + \rho S_\omega \left(\int_{t_1}^{t_2} \ddot{w}_{x,x} \cdot \delta\theta_x dt - \int_{t_1}^{t_2} \ddot{\theta}_{x,x} \cdot \delta w_x dt \right) \Big\} dx
\end{aligned}
\tag{2.20}
$$

grouping together the same infinitesimal contribution for the terms associated with the kinetic, potential and the external virtual work the strong formulation of the equation of motion for the investigated mechanical system is reached, which consists in the following system of partial differential equations

$$
\begin{cases}
\begin{aligned}
& EA \cdot w_{x,xx} - ES_z \cdot \theta_{z,xx} + ES_y \cdot \theta_{y,xx} + ES_\omega \cdot \theta_{x,xxx} - \rho A \cdot \ddot{w}_x \\
& \qquad + \rho S_z \cdot \ddot{\theta}_z - \rho S_y \cdot \ddot{\theta}_y - \rho S_\omega \cdot \ddot{\theta}_{x,x} + q_x = 0
\end{aligned} \\
\\
GA_y \cdot (w_{y,x} - \theta_z)_{,x} - \rho A \ddot{w}_y + \rho S_{ys} \ddot{\theta}_x + q_y = 0 \\
\\
\begin{aligned}
& EI_z \cdot \theta_{z,xx} + GA_y \cdot (w_{y,x} - \theta_z) - ES_z \cdot w_{x,xx} - EI_{yz} \cdot \theta_{y,xx} - EI_{\omega z} \cdot \theta_{x,xxx} \\
& \qquad - \rho I_z \cdot \ddot{\theta}_z + \rho I_{\omega z} \cdot \ddot{\theta}_{x,x} + \rho S_z \cdot \ddot{w}_x + \rho I_{yz} \cdot \ddot{\theta}_y + m_z = 0
\end{aligned} \\
\\
GA_z \cdot (w_{z,x} + \theta_y)_{,x} - \rho A \ddot{w}_z - \rho S_{zs} \ddot{\theta}_x + q_z = 0 \\
\\
\begin{aligned}
& EI_y \cdot \theta_{y,xx} - GA_z \cdot (w_{z,x} + \theta_y) + ES_y \cdot w_{x,xx} - EI_{yz} \cdot \theta_{z,xx} + EI_{\omega y} \cdot \theta_{x,xxx} \\
& \qquad - \rho I_y \cdot \ddot{\theta}_y - \rho I_{\omega y} \cdot \ddot{\theta}_{x,x} - \rho S_y \cdot \ddot{w}_x + \rho I_{yz} \cdot \ddot{\theta}_z + m_y = 0
\end{aligned} \\
\\
\begin{aligned}
& GJ \cdot \theta_{x,xx} - ES_\omega \cdot w_{x,xxx} - EI_{\omega y} \cdot \theta_{y,xxx} + EI_{\omega z} \cdot \theta_{z,xxx} - EI_\omega \theta_{x,xxxx} \\
& \qquad - \rho I_{PS} \cdot \ddot{\theta}_x + \rho I_\omega \ddot{\theta}_{x,xx} - \rho I_{\omega z} \cdot \ddot{\theta}_{z,x} + \rho I_{\omega y} \cdot \ddot{\theta}_{y,x} \\
& \qquad + \rho S_{ys} \cdot \ddot{w}_y - \rho S_{zs} \cdot \ddot{w}_z + \rho S_\omega \cdot \ddot{w}_{x,x} + m_x = 0
\end{aligned}
\end{cases}
\tag{2.21}
$$

Those relations are able to describe the mechanical behaviour of the investigated system both by a static and a dynamic point of view and are manipulated in following section in order to achieve a solution which is coherent with the finite element method.

2.1.5 Equation of Motion: Weak Form and Finite Element Formulation

Once, that the strong for of the mechanical problem is exposed, the weak formulation needs to be described to achieve the desired finite element formulation. This is equivalent to writing the first variation of the functional (see (2.6)) above within the class of synchronous variated motions admissible for the structure at hand Many methodologies are available to this purpose, among them the standard Galerkin method is hereafter implemented. This method involves approximating the solution to a PDE using a series of basis or test functions that satisfy certain boundary conditions of the problem. The core idea is to project the error of the approximation onto the space spanned by these basis functions and ensure that this projected error is minimized. In practice, this is achieved by multiplying the residual (the difference between the left and right sides of the PDE) by each basis function and integrating over the domain, setting these integrals to zero. This process transforms the PDE into a set of algebraic equations. The Galerkin method's strength lies in its flexibility; the choice of basis functions can be tailored to the specific problem, leading to efficient and accurate solutions. It is particularly effective in dealing with complex geometries and boundary conditions, making it a cornerstone technique in FEA for structural analysis, fluid dynamics, and other areas requiring the solution of complex differential equations. In current case, the relations are multiplied by test functions hereafter denoted as $\mathcal{H}_i(x)$, with $(i = 1, \dots, 7)$ and integrated by part. Below the several contributions are reported for each considered degree of freedom for the sake of the exposition. In the case of the axial degree of freedom w_x

$$\begin{aligned} &EA\left[\mathcal{H}_1 \cdot w_{x,x}\Big|_0^L - \int_0^L \mathcal{H}_{1,x} \cdot w_{x,x} dx\right] + ES_\omega\left[\mathcal{H}_1 \cdot \theta_{x,xx}\Big|_0^L - \int_0^L \mathcal{H}_{1,x} \cdot \theta_{x,xx} dx\right] \\ &-ES_z\left[\mathcal{H}_1 \cdot \theta_{z,x}\Big|_0^L - \int_0^L \mathcal{H}_{1,x} \cdot \theta_{z,x} dx\right] + ES_y\left[\mathcal{H}_1 \cdot \theta_{y,x}\Big|_0^L - \int_0^L \mathcal{H}_{1,x} \cdot \theta_{y,x} dx\right] \\ &-\rho A \int_0^L \mathcal{H}_1 \cdot \ddot{w}_x dx + \rho S_z \int_0^L \mathcal{H}_1 \cdot \ddot{\theta}_z dx - \rho S_y \int_0^L \mathcal{H}_1 \cdot \ddot{\theta}_y dx \\ &-\rho S_\omega \int_0^L \mathcal{H}_1 \cdot \theta_{x,x} dx + \int_0^L \mathcal{H}_1 \cdot q_x dx = 0 \end{aligned} \tag{2.22}$$

subsequently, for the terms associated with to the deflection w_y and rotation θ_z

$$\begin{aligned} &GA_y\left[\mathcal{H}_2 \cdot (w_{y,x} - \theta_z)\Big|_0^L - \int_0^L \mathcal{H}_{2,x} \cdot (w_{y,x} - \theta_z) dx\right] \\ &-\rho A \int_0^L \mathcal{H}_2 \cdot \ddot{w}_y dx + \rho S_{ys} \int_0^L \mathcal{H}_2 \cdot \ddot{\theta}_x dx + \int_0^L \mathcal{H}_2 \cdot q_y dx = 0 \end{aligned} \tag{2.23}$$

$$
\begin{aligned}
&EI_z\left[\mathcal{H}_4\cdot\theta_{z,x}\Big|_0^L-\int_0^L\mathcal{H}_{4,x}\cdot\theta_{z,x}dx\right]+GA_y\int_0^L\mathcal{H}_4\cdot(w_{y,x}-\theta_z)dx\\
&-ES_z\left[\mathcal{H}_4\cdot w_{x,x}\Big|_0^L-\int_0^L\mathcal{H}_{4,x}\cdot w_{x,x}dx\right]\\
&-EI_{yz}\left[\mathcal{H}_4\cdot\theta_{y,x}\Big|_0^L-\int_0^L\mathcal{H}_{4,x}\cdot\theta_{y,x}dx\right]-EI_{\omega z}\left[\mathcal{H}_4\cdot\theta_{x,xx}\Big|_0^L-\int_0^L\mathcal{H}_{4,x}\cdot\theta_{x,xx}dx\right]\\
&-\rho I_z\int_0^L\mathcal{H}_4\cdot\ddot{\theta}_z dx+\rho I_{\omega z}\int_0^L\mathcal{H}_4\cdot\ddot{\theta}_{x,x}dx+\\
&+\rho I_{yz}\int_0^L\mathcal{H}_4\cdot\ddot{\theta}_y dx+\rho S_z\int_0^L\mathcal{H}_4\cdot\ddot{w}_x dx+\int_0^L\mathcal{H}_4\cdot m_z dx=0
\end{aligned}
\tag{2.24}
$$

the opposite counterparts, which are W_z and θ_y can be stated as

$$
\begin{aligned}
&GA_z\left[\mathcal{H}_3\cdot(w_{z,x}+\theta_y)\Big|_0^L-\int_0^L\mathcal{H}_{3,x}\cdot(w_{z,x}+\theta_y)dx\right]\\
&-\rho A\int_0^L\mathcal{H}_3\cdot\ddot{w}_z dx-\rho S_{zs}\int_0^L\mathcal{H}_3\cdot\ddot{\theta}_x dx+\int_0^L\mathcal{H}_3\cdot q_z dx=0
\end{aligned}
\tag{2.25}
$$

$$
\begin{aligned}
&EI_y\left[\mathcal{H}_5\cdot\theta_{y,x}\Big|_0^L-\int_0^L\mathcal{H}_{5,x}\cdot\theta_{y,x}dx\right]-GA_z\int_0^L\mathcal{H}_5\cdot(w_{z,x}-\theta_y)dx\\
&+ES_y\left[\mathcal{H}_5\cdot w_{x,x}\Big|_0^L-\int_0^L\mathcal{H}_{5,x}\cdot w_{x,x}dx\right]\\
&-EI_{yz}\left[\mathcal{H}_5\cdot\theta_{z,x}\Big|_0^L-\int_0^L\mathcal{H}_{5,x}\cdot\theta_{z,x}dx\right]+EI_{\omega y}\left[\mathcal{H}_5\cdot\theta_{x,xx}\Big|_0^L-\int_0^L\mathcal{H}_{5,x}\cdot\theta_{x,xx}dx\right]\\
&-\rho I_y\int_0^L\mathcal{H}_5\cdot\ddot{\theta}_y dx-\rho S_y\int_0^L\mathcal{H}_5\cdot\ddot{w}_x dx-\rho I_{\omega y}\int_0^L\mathcal{H}_5\cdot\ddot{\theta}_{x,x}dx\\
&+\rho I_{yz}\int_0^L\mathcal{H}_5\cdot\ddot{\theta}_x dx+\int_0^L\mathcal{H}_5\cdot m_y dx=0
\end{aligned}
\tag{2.26}
$$

Finally, the same formulations for the torsional degrees of freedom θ_x and its derivative $\theta_{x,x}$ is achieved by

$$\begin{aligned}
&GJ\left[\mathcal{H}_6\cdot\theta_{x,x}\Big|_0^L-\int_0^L\mathcal{H}_{6,x}\cdot\theta_{x,x}dx\right]-ES_\omega\left[\mathcal{H}_{6,x}\cdot w_{x,xx}\Big|_0^L-\mathcal{H}_{6,xx}\cdot w_{x,x}\Big|_0^L\right.\\
&\left.+\int_0^L\mathcal{H}_{6,xxx}\cdot w_{x,x}dx\right]-EI_{\omega y}\left[\mathcal{H}_6\cdot\theta_{y,xx}\Big|_0^L-\mathcal{H}_{6,x}\cdot\theta_{y,x}\Big|_0^L+\int_0^L\mathcal{H}_{6,xx}\cdot\theta_{y,x}dx\right]\\
&+EI_{\omega z}\left[\mathcal{H}_6\cdot\theta_{z,xx}\Big|_0^L-\mathcal{H}_{6,x}\cdot\theta_{z,x}\Big|_0^L+\int_0^L\mathcal{H}_{6,xx}\cdot\theta_{z,x}dx\right]\\
&-EI_\omega\left[\mathcal{H}_6\cdot\theta_{x,xxx}\Big|_0^L-\mathcal{H}_{6,x}\cdot\theta_{x,xx}\Big|_0^L+\int_0^L\mathcal{H}_{6,xx}\cdot\theta_{x,xx}dx\right]-\rho I_{PS}\int_0^L\mathcal{H}_6\cdot\ddot{\theta}_x dx\\
&+\rho I_\omega\left[\mathcal{H}_6\cdot\ddot{\theta}_{x,x}\Big|_0^L-\int_0^L\mathcal{H}_{6,x}\cdot\ddot{\theta}_{x,x}dx\right]-\rho I_{\omega z}\left[\mathcal{H}_6\cdot\ddot{\theta}_z\Big|_0^L-\int_0^L\mathcal{H}_{6,x}\cdot\ddot{\theta}_z dx\right]\\
&+\rho I_{\omega y}\left[\mathcal{H}_6\cdot\ddot{\theta}_y\Big|_0^L-\int_0^L\mathcal{H}_{6,x}\cdot\ddot{\theta}_y dx\right]+\rho S_{ys}\int_0^L\mathcal{H}_6\cdot\ddot{w}_y dx-\rho S_{zs}\int_0^L\mathcal{H}_6\cdot\ddot{w}_z dx\\
&+\rho S_\omega\left[\mathcal{H}_6\cdot\ddot{w}_x\Big|_0^L-\int_0^L\mathcal{H}_{6,x}\cdot\ddot{w}_x dx\right]+\int_0^L\mathcal{H}_6\cdot m_x=0
\end{aligned}\tag{2.27}$$

Substituting the test functions $\mathcal{H}_i$ with the associated shape functions which approximate the displacement field in a typical Galerkin fashion it is immediate to obtain the formulation for the mass $\tilde{M}$ and stiffness $\tilde{K}$ matrices alongside the force vector $\bar{f}$ of the mechanical system, once that the boundary condition terms are excluded from the previous relations. However, the introduction of a vector notation is more suitable for the clearness of the exposition. As a matter of fact, the displacement field can be approximated by the introduction of the shape functions for each degree of freedom in order to approximate the responses of the element between the two end nodes. In particular, the aforementioned displacement components are approximated as

$$w_x(x,t)=\bar{N}_1(x)\bar{d}_1^T(t)=\begin{bmatrix}N_1^1 N_1^2\end{bmatrix}\begin{bmatrix}w_x^1\\ w_x^2\end{bmatrix}$$

$$w_y(x,t)=\bar{N}_2(x)\bar{d}_2^T(t)=\begin{bmatrix}N_2^1 N_2^2 N_2^3 N_2^4\end{bmatrix}\begin{bmatrix}w_y^1\\ \theta_z^1\\ w_y^2\\ \theta_z^2\end{bmatrix}\quad \theta_z(x,t)=\bar{N}_3(x)\bar{d}_2^T(t)=\begin{bmatrix}N_3^1 N_3^2 N_3^3 N_3^4\end{bmatrix}\begin{bmatrix}w_y^1\\ \theta_z^1\\ w_y^2\\ \theta_z^2\end{bmatrix}$$

$$w_z(x,t)=\bar{N}_4(x)\bar{d}_3^T(t)=\begin{bmatrix}N_4^1 N_4^2 N_4^3 N_4^4\end{bmatrix}\begin{bmatrix}w_z^1\\ \theta_y^1\\ w_z^2\\ \theta_y^2\end{bmatrix}\quad \theta_y(x,t)=\bar{N}_5(x)\bar{d}_3^T(t)=\begin{bmatrix}N_5^1 N_5^2 N_5^3 N_5^4\end{bmatrix}\begin{bmatrix}w_y^1\\ \theta_z^1\\ w_y^2\\ \theta_z^2\end{bmatrix}$$

$$\theta_x(x,t)=\bar{N}_6(x)\bar{d}_4^T(t)=\begin{bmatrix}N_6^1 N_6^2 N_6^3 N_6^4\end{bmatrix}\begin{bmatrix}\theta_x^1\\ \theta_{x,x}^1\\ \theta_x^2\\ \theta_{x,x}^2\end{bmatrix}\tag{2.28}$$

here, the vectors d_i are the row vectors carrying the displacement components for the node 1 and 2, which correspond to the two beam ends, and the vector N_i represent the shape matrix vectors for each displacement components. Substituting the vector representation (2.28) in (2.27) and discarding the boundary conditions out of the problem it is possible to derive the associate stiffness matrix $\tilde{K}$ where for each degree of freedom

$\underline{\mathbf{w_x}}$

$$\begin{aligned} EA\int_0^L N_{1,x}^T\, N_{1,x}\, d_1\, dx + ES_\omega \int_0^L N_{1,x}^T\, N_{6,xx}\, d_4\, dx - ES_z \int_0^L N_{1,x}^T\, N_{3,x}\, d_2\, dx \\ +ES_y \int_0^L N_{1,x}^T\, N_{5,x}\, d_3\, dx \end{aligned} \tag{2.29}$$

$\underline{\mathbf{w_y},\ \theta_\mathbf{z}}$

$$\begin{aligned} GA_y \int_0^L (N_{2,x}^T - N_3^T)(N_{2,x} - N_3)\, d_2\, dx + EI_z \int_0^L N_{3,x}^T\, N_{3,x}\, d_2 dx \\ -ES_z \int_0^L N_{3,x}^T\, N_{1,x}\, d_1\, dx \\ -EI_{yz} \int_0^L N_{3,x}^T\, N_{5,x} d_3 dx - EI_{\omega z} \int_0^L N_{3,x}^T\, N_{6,x}\, d_4\, dx \end{aligned} \tag{2.30}$$

$\underline{\mathbf{w_z},\ \theta_\mathbf{y}}$

$$\begin{aligned} GA_z \int_0^L (N_{4,x}^T + N_5^T)(N_{4,x} + N_5)\, d_3\, dx + EI_y \int_0^L N_{5,x}^T\, N_{5,x}\, d_3 dx \\ +ES_y \int_0^L N_{5,x}^T\, N_{1,x}\, d_1\, dx \\ -EI_{yz} \int_0^L N_{5,x}^T\, N_{3,x} d_2 dx + EI_{\omega y} \int_0^L N_{5,x}^T\, N_{6,xx}\, d_4 dx \end{aligned} \tag{2.31}$$

$\underline{\theta_\mathbf{x},\ \theta_\mathbf{x,x}}$

$$\begin{aligned} GJ \int_0^L N_{6,x}^T\, N_{6,x}\, d_4\, dx + ES_\omega \int_0^L N_{6,xxx}\, N_{1,x}\, d_1 dx \\ +EI_{\omega y} \int_0^L N_{6,xx}\, N_{5,x}\, d_3 dx - EI_{\omega z} \int_0^L N_{6,xx}\, N_{3,x}\, d_2 dx \\ +EI_\omega \int_0^L N_{6,xx}\, N_{6,xx}\, d_4\, dx \end{aligned} \tag{2.32}$$

on the other end the mass matrix $\tilde{M}$ can be defined by considering components related to the kinetic energy of the system, as

$\underline{\mathbf{w_x}}$

$$\begin{aligned}\rho A \int_0^L N_1^T\, N_1 \ddot{d}_1 dx - \rho S_z \int_0^L N_1^T\, N_3 \ddot{d}_3 dx + \rho S_y \int_0^L N_1^T\, N_5 \ddot{d}_3\, dx \\ +\rho S_\omega \int_0^L N_1^T\, N_{6,x}\, \ddot{d}_4\, dx\end{aligned} \tag{2.33}$$

$\underline{\mathbf{w_y},\ \theta_\mathbf{z}}$

$$\begin{aligned}\rho A \int_0^L N_2^T\, N_2 \ddot{d}_2 dx + \rho I_z \int_0^L N_3^T\, N_3\, \ddot{d}_2\, dx - \rho S_{zs} \int_0^L N_2^T \cdot N_6\, d_4\, dx \\ -\rho I_{\omega z} \int_0^L N_3^T \cdot N_{6,x}\, \ddot{d}_4\, dx - \rho I_{yz} \int_0^L N_3^T \cdot N_5\, \ddot{d}_3\, dx - \rho S_z \int_0^L N_3^T \cdot N_1\ ,\ddot{d}_1\, dx\end{aligned} \tag{2.34}$$

$\underline{\mathbf{w_z},\ \theta_\mathbf{y}}$

$$\begin{aligned}\rho A \int_0^L N_4^T\, N_4 \ddot{d}_3 dx + \rho I_y \int_0^L N_5^T\, N_5\, \ddot{d}_3\, dx + \rho S_{ys} \int_0^L N_4^T \cdot N_6\, d_4\, dx \\ +\rho I_{\omega y} \int_0^L N_5^T \cdot N_{6,x}\, \ddot{d}_4\, dx - \rho I_{yz} \int_0^L N_5^T \cdot N_6\, \ddot{d}_4\, dx + \rho S_y \int_0^L N_5^T\, N_1\, \ddot{d}_1 dx\end{aligned} \tag{2.35}$$

$\underline{\theta_\mathbf{x},\ \theta_{\mathbf{x},\mathbf{x}}}$

$$\begin{aligned}\rho I_{PS} \int_0^L N_6^T\, N_6\, \ddot{d}_4\, dx + \rho I_\omega \int_0^L N_{6,x}^T\, N_{6,x} \ddot{d}_4\, dx + \rho S_\omega \int_0^L N_{6,x}\, N_1\, \ddot{d}_1\, dx \\ -\rho I_{\omega z} \int_0^L N_{6,x}^T \cdot N_3\, \ddot{d}_2 dx + \rho I_{\omega y} \int_0^L N_{6,x}^T \cdot N_5\, \ddot{d}_3\, dx - \rho S_{zs} \int_0^L N_6^T \cdot N_2\, \ddot{d}_2\, dx \\ +\rho S_{ys} \int_0^L N_6^T \cdot N_4\, \ddot{d}_3\, dx + \rho S_\omega \int_0^L N_{6,x}^T \cdot N_1\, \ddot{d}_1\, dx\end{aligned} \tag{2.36}$$

finally the associate force vector can be computed isolating the terms derived by the external virtual work in the weak form equation resulting in

$\underline{\mathbf{w_x}}$

$$\int_0^L N_1\ q_x\ dx \tag{2.37}$$

$\underline{\mathbf{w_y},\ \theta_\mathbf{z}}$

$$\int_0^L N_2\ q_y\ dx + \int_0^L N_3\ m_z\ dx \tag{2.38}$$

$\underline{\mathbf{w_z},\ \theta_\mathbf{y}}$

$$\int_0^L N_4\ q_z\ dx + \int_0^L N_5\ m_y\ dx \tag{2.39}$$

$\underline{\theta_\mathbf{x},\ \theta_{\mathbf{x},\mathbf{x}}}$

$$\int_0^L N_6\ m_x\ dx + \int_0^L N_{6,x}\ b_x\ dx \tag{2.40}$$

Once that, all the stiffness and the mass matrix are assembled in the finite element fashion for the whole domain the mechanical problem can be solved for the several cases such as dynamic, static and modal cases.

2.2 Numerical Benchmark

The theoretical definition of the presented finite element, as mentioned earlier, needs to be tested to identify any numerical issues and to assess overall accuracy. Furthermore, the efficacy of the theory and its finite element implementation can be compared with other well-known solutions in the field of computational mechanics. In fact, several approaches can be deployed to numerically model the same mechanical problem, which depend on various factors such as the desired degree of accuracy, available computational resources, and the specific problem to be modeled, among others. Therefore, different approaches can be implemented to test the performance of the computational elements. Specifically, in the present work, the dynamical response of the mechanical model is compared with two different Finite Element software tools, *Abaqus 2023* [106] and *OpenSees* [107]. The former is a sophisticated engineering simulation software used primarily for finite element analysis (FEA) and computer-aided engineering. Developed by Dassault Systèmes, it offers advanced capabilities for modeling, analyzing, and visualizing a wide range of mechanical components and systems. It is particularly renowned for its ability to handle complex non-linear problems, which involve contact, large deformations, or complex material behavior. The software consists of two main parts: *Abaqus/Standard* and *Abaqus/Explicit*. *Abaqus/Standard* is well-suited for static and quasi-static analyses, including stress, thermal, and coupled thermal-mechanical problems. On the other hand, *Abaqus/Explicit* is designed for transient dynamic analyses where rapid changes and severe non-linearities occur, such as in impact and crash scenarios. Moreover, it also includes a wide array of material models, making it adaptable to various industry needs, from metal to rubber and beyond. Its user-friendly interface allows for efficient model setup, while its robust solver technology ensures accurate and reliable results. Nonetheless, *OpenSees* is an open-source software framework designed primarily for simulating the seismic response of structural and geotechnical systems. Developed at the University of California, Berkeley, under the Pacific Earthquake Engineering Research Center (PEER), it has become a widely used tool in the field of earthquake engineering. *OpenSees* provides a robust platform for developing and implementing advanced computational models of structural behavior under seismic loads. It offers a diverse range of modeling elements, materials, and solution algorithms, allowing researchers and engineers to simulate both the nonlinear and dynamic response of structures. One of its key strengths is its flexibility. Users can create complex models of structural systems, incorporating various elements like beams, columns, shells, and solid elements. It supports different material models, including those that capture

the nonlinear behavior of concrete, steel, and soil, crucial for accurately simulating earthquake impacts. As an open-source tool, *OpenSees* benefits from a large community of users and developers who contribute to its continuous improvement and extension, making it a dynamic and evolving resource for seismic analysis and research. Due to their trustworthiness and reliability, both software tools are employed here for a numerical comparison between the proposed finite element model and the same problem modeled with 2D elements, specifically the shell elements. Two types of analysis are implemented: modal analysis and an implicit dynamic analysis, which are described subsequently. Both are intended to evaluate the mechanical behavior of the investigated elements in the dynamic range. The adopted structural element is a classical 15 meters long double-tee beam made up of concrete, which idealized as simply supported at both ends and both the uniform and no uniform torsion are restrained. The geometric characteristics of the cross-section (fig. 2.2) are reported in table 2.1.

Figure 2.2: Beam cross-section

Section geometrical properties			
B_1		2.500	m
B_2		0.500	m
B_3		0.200	m
B_4		1.100	m
H_1		0.525	m
H_2		0.050	m
H_3		0.475	m
Section properties			
Area	A	3.15e-01	m^2
Shear Factor y-y	χ_y	2.80e-02	m^2
Shear Factor z-z	χ_z	3.49e-02	m^2
Second moment of area y-y	I_y	1.46e-01	m^4
Second moment of area z-z	I_z	8.79e-03	m^4
Torsional constant	J	2.23e-03	m^4
Second moment of warping	I_ω	1.63e-02	m^6
Mixed moment ω-y	$I_{\omega y}$	4.22e-02	m^5
Material properties			
Density	ρ	2.50e+03	kg/m^3
Young modulus	E	3.50e+10	N/m^2
Poisson's coefficient	ν	3.00e-01	–

Table 2.1: Section and material properties.

Section properties of the cross sections are obtained considering a python package, also based on the finite element method, named *sectionproperties* [102]. This python package is a specialized tool designed for the analysis and design of structural cross-sections. This open-source package allows engineers and designers to calculate various properties of cross-sections, such as area, centroid, moment of inertia, and torsional properties. It is particularly useful in civil, structural, and mechanical engineering for analyzing the behavior of beams, columns, and other structural elements under various load conditions. The package provides functionality to create complex cross-section geometries, perform finite element analysis for detailed property calculation, and visualize cross-section shapes and stress distributions. Its user-friendly interface and integration with Python make it a valuable tool for both educational purposes and professional engineering applications, simplifying and enhancing the process of structural analysis. Although, the comprehensive number of parameters implemented and computed in the *sectionproperties* package minor modifications to the source code were made in order to obtain all the parameters needed for the numerical analysis.
Abaqus 2023 modelling is carried on by mean of a planar extrusion suitable to two-dimensional meshing, in particular structured meshed is employed considering 3361 S4 linear element with characteristic length equal to 0.125 m and associated with elastic isotropic material. The elastic isotropy is here justified by the fact, that even for the traffic analysis only the service limit states are investigated. Thus, the material choice as a minimum impact on the computational times. Boundary conditions at the two beam ends are enforced by means of reference points which are then coupled with the edge of the beam. Similar, process is implemented to the midpoint of the beam in order to apply time varying generalized forced for the dynamic analysis. Meanwhile, the modelling of the structural model in *OpenSees* is pursued by a pre and post-processor suite named STKO [108]. The same model is introduced in the pre-processor with the same characteristic of the one implemented in *Abaqus 2023* with a structured meshed characterized by the same number of finite ShellMITC4 [109] elements to which the two different associated section, which differ only for the associate shell thickness are characterized by the same elastic isotropic material. The *MITC* in ShellMITC4 stands for *Mixed Interpolation of Tensorial Components*. This refers to the element's formulation, which is designed to mitigate the problem of shear locking, a common issue in finite element analysis of thin shell structures. Shear locking can lead to overly stiff behavior in the numerical model, particularly when the shell is very thin compared to its other dimensions. The ShellMITC4 element achieves this by using a mixed interpolation technique in its formulation. This approach provides more accurate representation of the transverse shear strains, improving the element's performance, especially in bending-dominated problems. This element is widely used in the *OpenSees* community for analyzing shell structures like steel and concrete panels, tanks, bridges, and other structures where shell-like behavior is significant. The ShellMITC4 is appreciated for its robustness in various types of analyses, including nonlinear, dynamic, and static problems. Furthermore, rigid links of beam type are implemented to enforce the continuity between the slab and the beam's tee and equal dof constraints are put in place to enforce the constraints at the two beam ends together with the beam mid point able to distribute the dynamic loading at the beam. Furthermore, both the numerical model show the reference point which are restrained positioned at the level of the elastic centre of the beam. The proposed beam model is implemented in a custom made c++ finite element software, that is *Ghost project*, which is presented in chapter 6. The structural component is discretized by 30 beam finite elements. The three model are then subject to the different analysis; the first one is a simple modal analysis, where both the natural frequencies and the mode shapes are compared, results are depicted in table 2.2 for the

sake of comparison.

Modal analysis comparison				
	Abaqus 2023	OpenSees	Proposed	
	Frequency [Hz]	Frequency [Hz]	Frequency [Hz]	Mode
1	4.32	4.36	4.34	Vert
2	11.40	11.79	11.36	Tors + Hor
3	16.96	17.11	17.04	Vert
4	17.84	18.32	18.40	Tors + Hor
5	27.60	35.88	26.37	Hor + Tors

Table 2.2: Modal analysis comparison: natural frequencies and mode shapes.

The second dynamic test consists in the application in correspondence of the beam midpoint of two time histories of generalized forces. Indeed, in order to investigate the mechanical behaviour of the system both a vertical force and a torsional moment are applied to the structure with magnitude equal respectively to 100 kN and 50 kNm. The variation over the time of the two forcing terms is retrieved by the additive composition of three sinusoidal loads of unitary amplitude and frequencies amounting to 0.2 Hz, 0.5 Hz and 1 Hz; the resulting temporal distribution of the forcing terms is depicted in Fig 2.3.

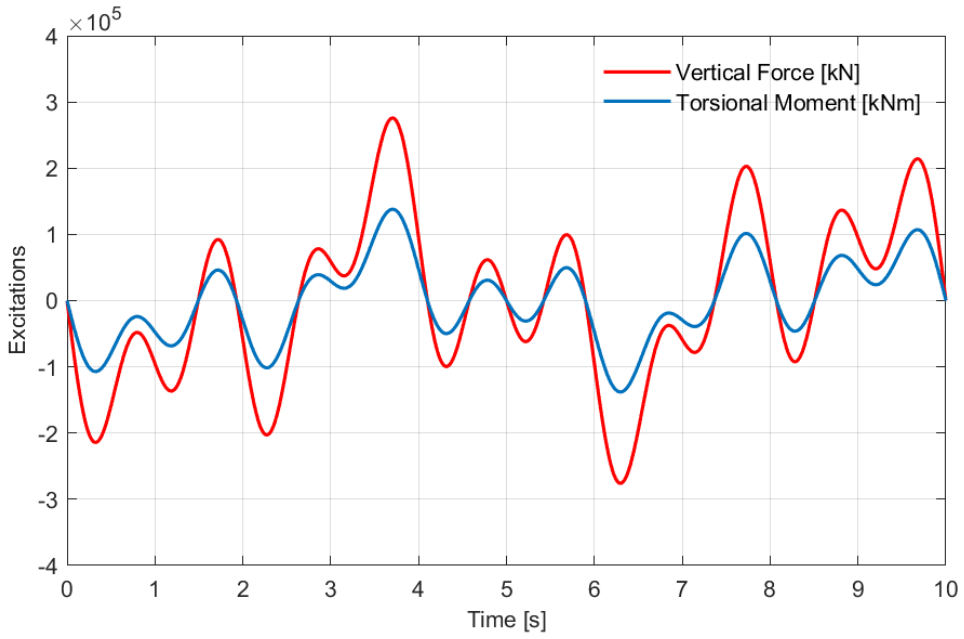

Figure 2.3: Temporal trend of the vertical force and the torsional moment applied to the beam midpoint.

In *Abaqus 2023*, the dynamic analysis is defined as implicit whit a fixed time step equal to 0.01s, which is 100 times smaller of the maximum frequency of which the excitation is composed of. The Hilber Hughes Taylor (HHT) [110] algorithm is employed to solve the equation of motion with a default of $\alpha = -0.05$. The same algorithm with the same property of the numerical damping parameter is employed in *OpenSees* and *Ghost* to solve the equation of motion of the proposed structural element in order to achieve the maximum uniformity between the two mechanical system. The resulting dynamical responses in

terms of vertical displacements, velocities and rotations can be found in figs. 2.4 to 2.6.

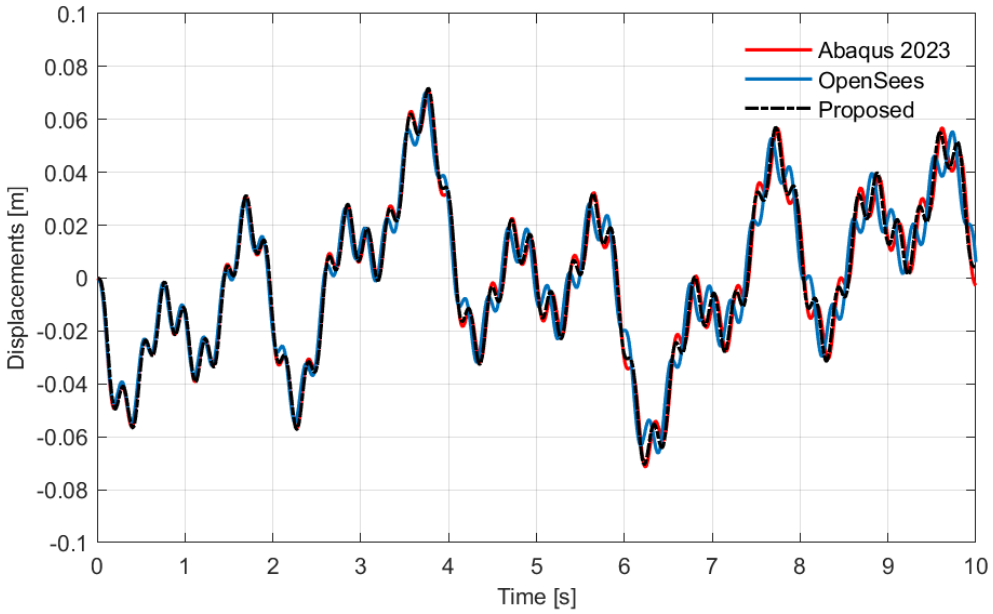

Figure 2.4: Beam midpoint: vertical displacements.

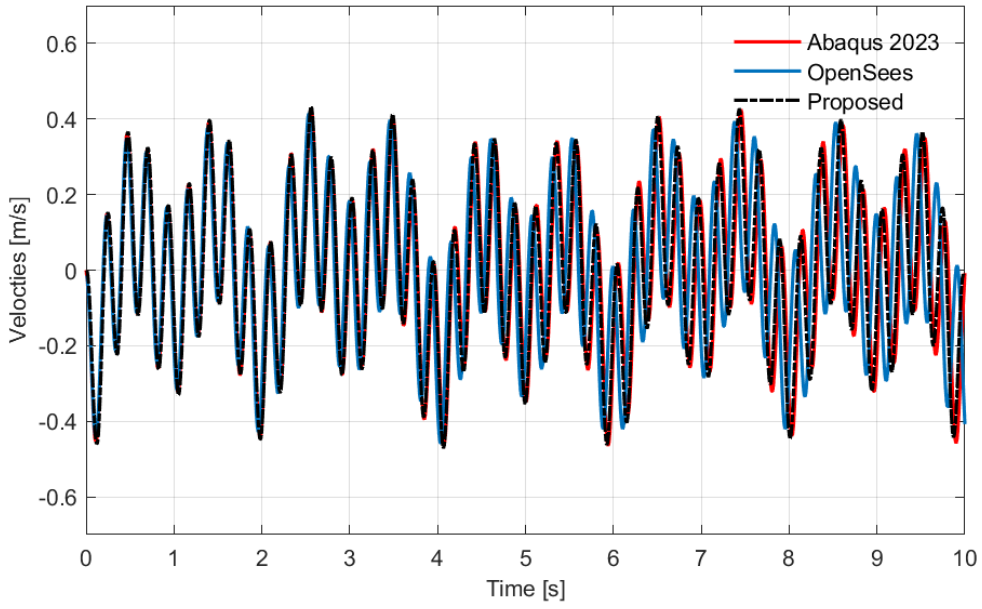

Figure 2.5: Beam midpoint: vertical velocities.

On the other hand, the results pertaining to the torsional rotations, velocities and accelerations are reported in figs. 2.7 to 2.9.

Alongside the qualitative analysis that can be easily drawn from the figures, it is necessary to introduce error indices capable of numerically quantifying the accuracy of the approach deployed. However, what must be considered is the significance of the error

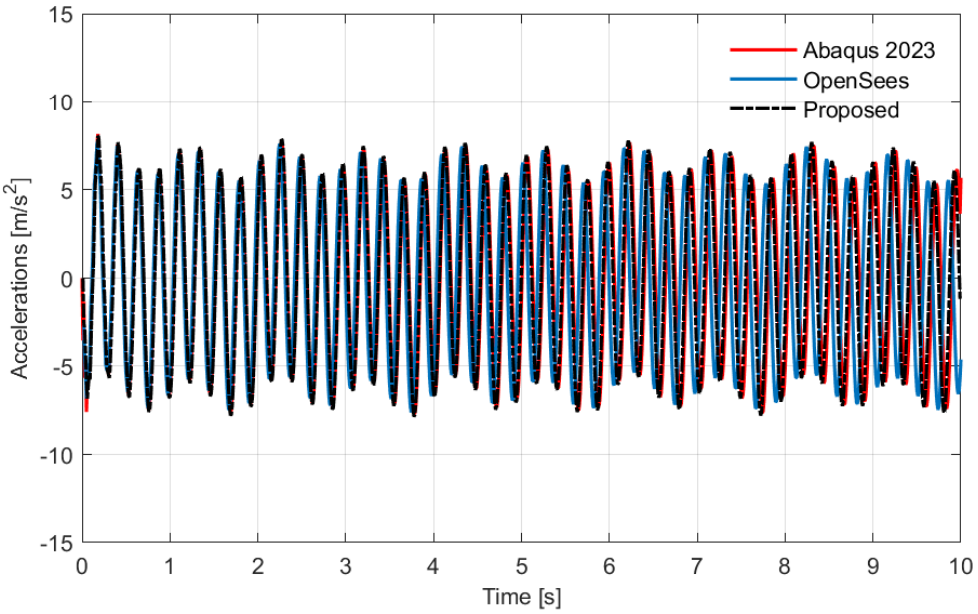

Figure 2.6: Beam midpoint: vertical accelerations.

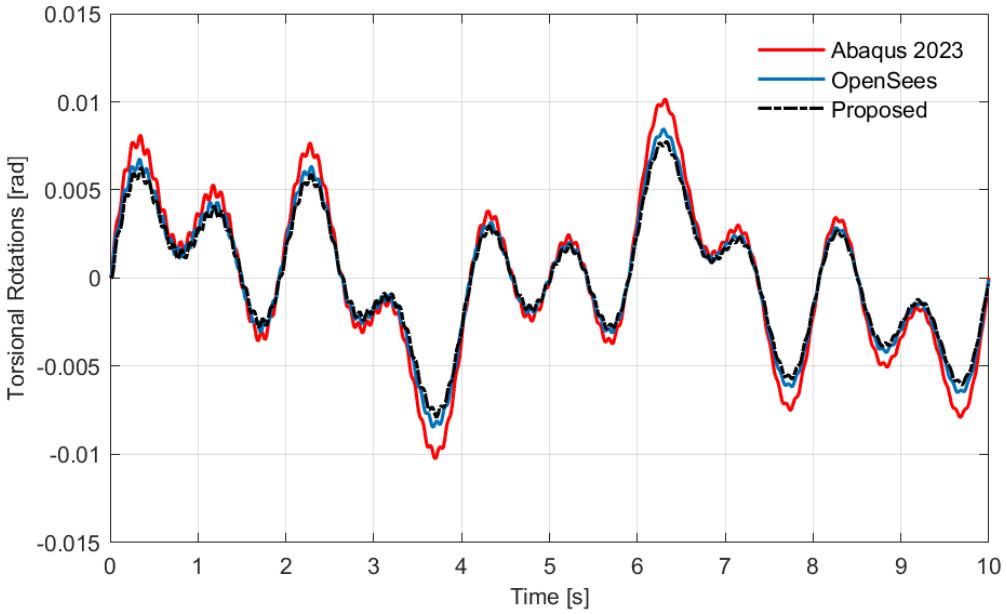

Figure 2.7: Beam midpoint: torsional rotations.

parameter to be used in the analysis. In this regard, it is immediately clear how some of the processes or temporal histories presented may have average values close to zero or anyway very small. Such a condition would lead to the introduction of relatively high measures of relative error given the presence of numbers close to zero in the denominator. Moreover, since this is not a static analysis, from which it would be possible to define a single comparison value, there is a need to resort to error measures capable of quantifying

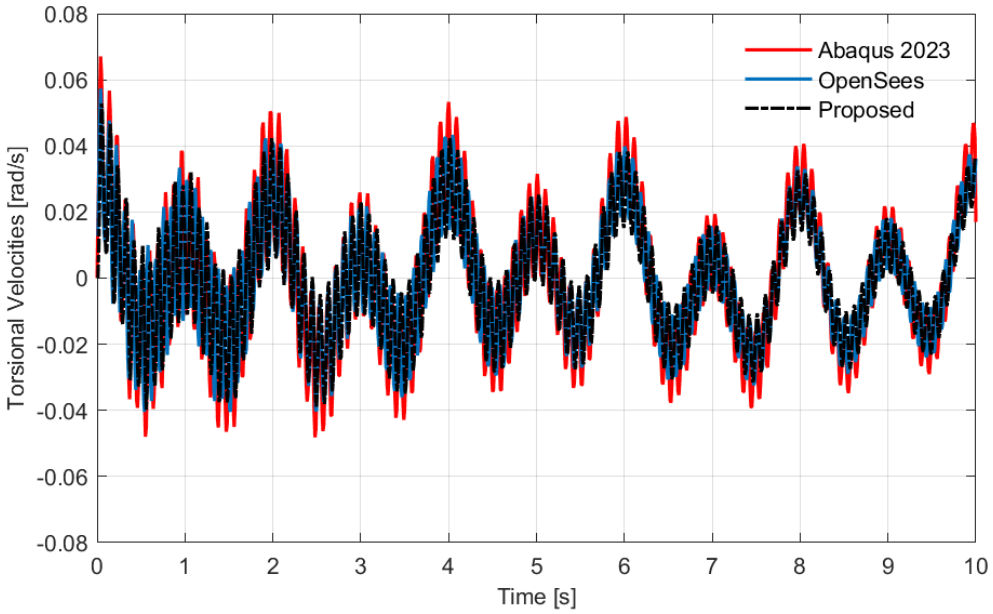

Figure 2.8: Beam midpoint: torsional velocities.

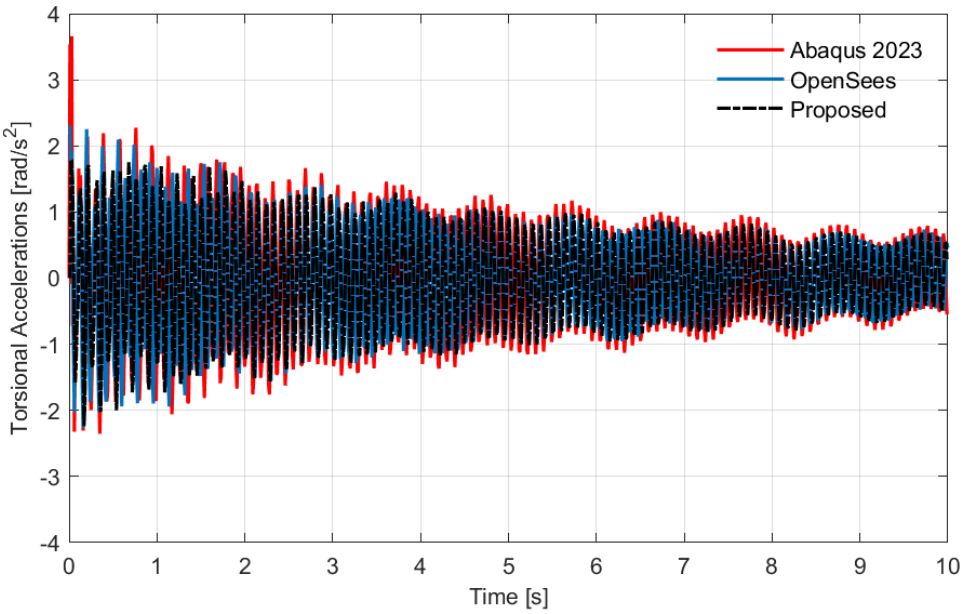

Figure 2.9: Beam midpoint: torsional accelerations.

its magnitude by considering multiple realizations of the phenomenon, i.e., in this case, the temporal histories of the responses analyzed. In this regard, three different error measures are subsequently introduced and further employed: the Mean Absolute Error (MAE), the Root Mean Squared Error (RMSE) and the Normalized Mean Squared Error (NRMSE). Indeed, error metrics critically determine the perceived accuracy of numerical models. While the classical Mean Relative Error (MRE) provides a direct measure of prediction

errors relative to the actual values, its utility diminishes with observed values near zero, necessitating alternative metrics such as RMSE, NRMSE, and MAE for a comprehensive and meaningful accuracy evaluation [111–114].
The MAE is a measure used to quantify the accuracy of predictions or estimates. It calculates the average magnitude of errors between pairs of observations. Mathematically, the MAE is calculated as the average of the absolute differences between benchmark values, *Abaqus 2023* in the investigated case, and the compared values (*Ghost* responses). From a mathematical standpoint it can be defined as

$$MAE = \frac{1}{n}\sum_{i=1}^{n}|y_i - \hat{y}_i| \tag{2.41}$$

where n is the number of samples, y_i is the actual value of the i-th *Abaqus 2023* time history and $\hat{y}_i$ is its **ghost** counterpart. The MAE gives a straightforward indication of the average error magnitude, with a value of 0 indicating no error or perfect matching between two responses. Moreover, the simplicity of MAE makes it highly interpretable; it directly corresponds to the average error magnitude across the investigated responses. RMSE quantifies the square root of the average of the squared differences between predicted values and actual observations. This focus on squaring the errors means that larger discrepancies between predicted and observed values are given disproportionately higher weight, emphasizing the significance of substantial errors. The RMSE is especially valued in contexts where it is crucial to minimize large errors, as it penalizes them more heavily than smaller errors. The formula for RMSE remains:

$$RMSE = \sqrt{\frac{1}{n}\sum_{i=1}^{n}(y_i - \hat{y}_1)^2} \tag{2.42}$$

On the other hand, NRMSE offers a solution to one of the primary limitations of RMSE: the lack of context regarding the scale of the data. By normalizing the RMSE value, NRMSE provides a dimensionless ratio, enabling the comparison of model accuracy across datasets with varying scales and units. The common normalization methods include division by the range (maximum - minimum) of the observed data or by the mean of the observed values $\bar{y}$:

$$NRMSE = \frac{RMSE}{y_{max} - y_{min}} \tag{2.43}$$

$$NRMSE = \frac{RMSE}{\bar{y}} \tag{2.44}$$

NRMSE is particularly advantageous in comparative model evaluation, where it is essential to understand the relative error magnitude independently of the dataset's scale. This normalization allows to objectively assess and compare the performance of different models or methods across diverse datasets. In the following in the computation of the NRMSE it is employed the normalization with respect to the maximum and minimum values associated with the numerical responses. In conclusion, MRE's sensitivity to values

close to zero can significantly distort error interpretation and this is the main reason why this metric it is here not employed. In contrast, MAE, RMSE, and NRMSE offer advantages for a more balanced and meaningful analysis, which can be briefly stated as:

- Robustness: MAE is less sensitive to outliers compared to RMSE, providing a robust measure of central tendency for errors. It ensures that all errors are treated equally, regardless of their magnitude.

- Sensitivity and stability: RMSE's sensitivity to larger errors makes it suitable for applications where such errors are particularly undesirable. Unlike MRE, both RMSE and MAE provide stable measures across values near zero.

- Normalization: NRMSE allows for comparisons across different scales and units, offering a clear, dimensionless metric of model accuracy, which is especially valuable in comparative analyses.

All the aforementioned error metrics are computed and reported in table 2.3, where the benchmark values are referred to the *Abaqus 2023* responses and the compared responses are essentially those derived from the *Ghost* and *OpenSees* numerical simulations.

From both quantitative and qualitative analyses, observations can be made regarding dynamic and modal scenarios, leading to various insights. Specifically, the modal analysis demonstrates a strong concordance between the two models, notably in vertical and torsional modes. Yet, minor discrepancies are noted in the frequency values for the fifth coupled mode, which exhibits a higher frequency in the *OpenSees* formulation. Additionally, the proposed model exhibits coherent alignment with the other two numerical implementations. These dynamic attributes are reflected in the outcomes of the dynamic analysis, representing the second numerical case discussed herein. A notable correlation among the three models is observed, particularly concerning aspects tied to the vertical degree of freedom. This alignment is evident in fig. 2.4, where the plots from the three models showcase similar trends and minimized error values table 2.3, although the *OpenSees* plot reveals slight variances. A commendable match is also achieved for the velocity and acceleration responses of the system, as illustrated in figs. 2.5 and 2.6. In terms of the torsional degree of freedom, the findings align with those from the modal analysis. Despite variances in natural frequencies, only minimal amplitude differences are observed, especially between the proposed model and the *OpenSees* model. Moreover, when juxtaposed with the *Abaqus 2023* responses, both qualitative and quantitative analyses ascertain that the *ghost* responses are more accurate compared to the established finite element benchmark.Furthermore, our investigation extends beyond mere quantitative analysis, integrating error metrics to meticulously evaluate the model's precision across both time and frequency domains. This level of scrutiny, underscored by the detailed responses in eqs. (2.41) to (2.43) and their frequency content in table 2.4, is paramount. A comparative quantitative review across different software platforms in the frequency domain underscores the sustained accuracy of our model, particularly highlighted by the specified error metrics. Notably, the NRMSE remains below 10% across all metrics in the frequency domain, which not only affirms the robustness of the numerical responses but also highlights the effectiveness of our model in simulating dynamic behaviors of bridge structures. Additionally, the modal analysis outcomes presented in table 2.2 resonate within figs. 2.10 and 2.11, particularly noting that the second vertical mode remains elusive due to the beam midpoint acting as a nodal point (zero modal displacements) in the

Abaqus Vs Ghost MAE					
Vertical displacement $[m]$	Vertical velocity $[m/s]$	Vertical acceleration $[m/s^2]$	Torsional rotation $[rad]$	Torsional velocity $[rad/s]$	Torsional acceleration $[rad/s^2]$
2.20e-03	5.97e-02	1.63e+00	8.61e-04	7.20e-03	4.82e-01
Abaqus Vs Ghost RMSE					
Vertical displacement $[m]$	Vertical velocity $[m/s]$	Vertical acceleration $[m/s^2]$	Torsional rotation $[rad]$	Torsional velocity $[rad/s]$	Torsional acceleration $[rad/s^2]$
5.60e-05	2.14e-02	5.91e-02	2.25e-06	3.06e-04	6.23e-03
Abaqus Vs Ghost NRMSE					
Vertical displacement [%]	Vertical velocity [%]	Vertical acceleration [%]	Torsional rotation [%]	Torsional velocity [%]	Torsional acceleration [%]
0.04	2.40	0.37	0.01	0.27	0.37
Abaqus Vs OpenSees MAE					
Vertical displacement $[m]$	Vertical velocity $[m/s]$	Vertical acceleration $[m/s^2]$	Torsional rotation $[rad]$	Torsional velocity $[rad/s]$	Torsional acceleration $[rad/s^2]$
7.10e-03	1.92e-01	5.25e+00	6.37e-04	1.30e-02	9.23e-01
Abaqus Vs OpenSees RMSE					
Vertical displacement $[m]$	Vertical velocity $[m/s]$	Vertical acceleration $[m/s^2]$	Torsional rotation $[rad]$	Torsional velocity $[rad/s]$	Torsional acceleration $[rad/s^2]$
1.47e-03	3.41e-02	1.09e+00	3.65e-06	6.39e-04	1.09e+00
Abaqus Vs OpenSees NRMSE					
Vertical displacement [%]	Vertical velocity [%]	Vertical acceleration [%]	Torsional rotation [%]	Torsional velocity [%]	Torsional acceleration [%]
1.04	3.82	6.84	0.02	0.55	0.32

Table 2.3: MAE, RMSE and NMRSE for the numerical benchmarks presented in chapter 2.

considered modal shapes. It is also worth mentioning that responses from *OpenSees* exhibit minor disturbances for frequencies above 15 Hz. Despite representing Fourier spectra in decibels for both vertical and torsional accelerations, errors in the frequency domain are measured in terms of amplitude, as converting to decibels would unduly amplify discrepancies between numerical responses. In carrying out these numerical simulations to benchmark the theory, it's crucial to acknowledge the underlying assumptions that may influence the results. These include the linear material properties and the assumption of

small deformations, which might not fully capture the complex behaviors under certain real-world conditions. Recognizing these limitations provides a balanced perspective and suggests directions for future research, such as exploring the effects of non-linear material properties or large deformations on the frequency response.

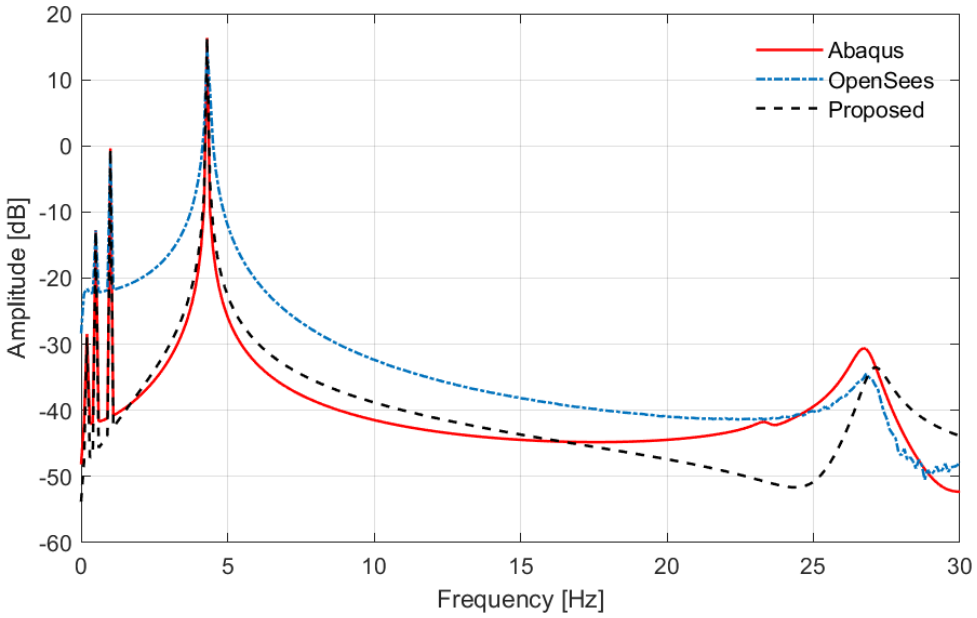

Figure 2.10: Fourier spectra for vertical accelerations responses (figs. 2.6 and 2.9).

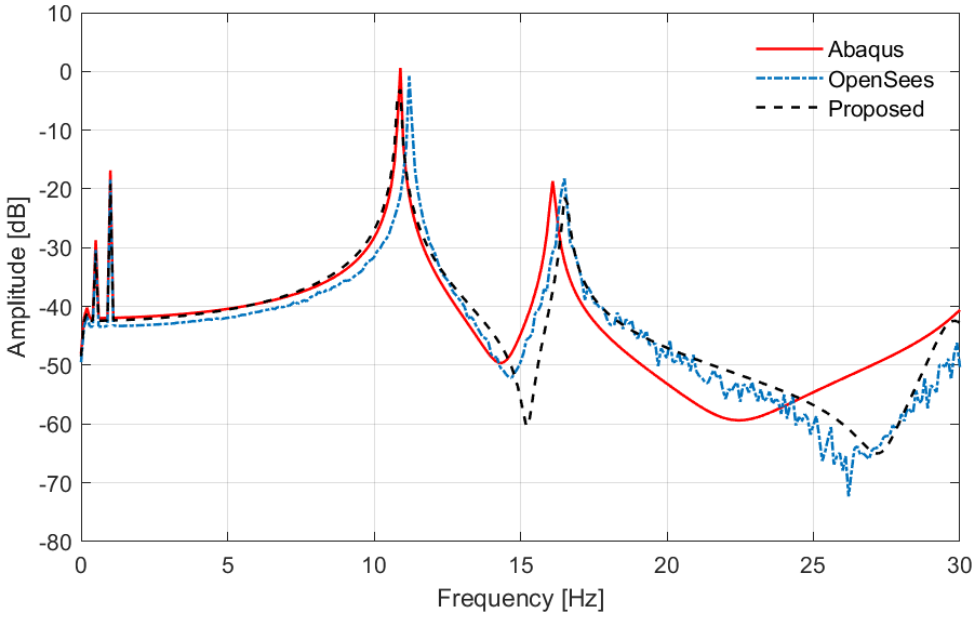

Figure 2.11: Fourier spectra for torsional accelerations responses (fig. 2.9).

In summary, the performance of the beam model is effective, a notable achievement considering it utilizes a mere 30 finite elements—a stark contrast to the more than 3000

Abaqus Vs Ghost					
Vertical accelerations					
MAE	6.16e-03	RMSE	2.99e-04	NRMSE [%]	0.005
Torsional accelerations					
MAE	7.50e-03	RMSE	7.94e-02	NRMSE [%]	7.41
Abaqus Vs OpenSees					
Vertical accelerations					
MAE	3.37e-02	RMSE	5.29e-01	NRMSE [%]	8.07
Torsional accelerations					
MAE	1.16e-02	RMSE	8.68e-02	NRMSE [%]	8.10

Table 2.4: MAE, RMSE and NMRSE for the Fourier spectra of the vertical and torsional accelerations in temrs of amplitude (see figs. 2.6 and 2.9).

shell elements employed in each of the comparative shell models. This remarkable efficiency underscores the model's capability to faithfully represent the complex three-dimensional nature of beam problems with a minimal element count. Moreover, this streamlined approach holds significant promise for advancing Vehicle-Bridge Interaction (VBI) theory. It offers a novel perspective, especially in the realm of beam elements, by potentially incorporating torsional degrees of freedom and warping effects, which are currently overlooked in such models. Furthermore, the examination of the frequency content of the model's responses further validates the accuracy and reliability of this numerical approach. These findings not only corroborate the model's precision in capturing the essential mechanical behaviors of structural elements but also highlight its potential for integration into VBI studies. With its straightforward yet effective formulation, this model paves the way for a more nuanced understanding and simulation of the dynamic interactions between vehicles and bridges. This development is especially critical given the increasing need for efficient and accurate modeling techniques in structural engineering, offering a promising avenue for future research and application in enhancing the fidelity and efficiency of VBI models. Moreover, it's possible to examine the effectiveness and performance that the three considered error metrics have on defining the dynamic problem. Indeed, unlike static or modal analysis cases where comparing individual outputs makes it relatively straightforward to introduce error estimates like absolute or relative error, in dynamic scenarios where temporal motion stories consisting of a large number of data points are analyzed, relying on averaged error estimate values becomes essential. Furthermore, for dynamic responses approaching zero, it is often more reliable from a performance standpoint to refer to error estimation elements such as the RMSE or its standardized version, which, although more robust than the MRE, can still generate misleading error measurements for numbers close to zero. Furthermore, it is possible to conclude how despite some minor aspects which can influence the model accuracy, the overall dynamic response of the beam model seem to behave quite well, in term of estimated of the mechanical response of the system. Especially in comparison with the different levels of computational effort needed between the two different models, the shell model and the beam model.

Chapter 3

Finite Element Coupling for the Vehicle-Bridge Interaction Problem

In the history of structural mechanics, the interaction between vehicle and bridge has always played a crucial role in the scientific community. This interest has led to a constant evolution of models used for such types of analysis, also in function of the different responses to investigate. Indeed, it is easy to imagine how, more than from the interaction of the vehicle, understood as a car or heavy vehicle, the impulse to the discipline was significantly provided with the advent of railways. In fact, from the mid-19th century, researchers began not only to approach the discipline but also to adapt it to the problems of the era in relation to trains and their interaction with the built environment. And it is always thanks to the technological evolution concerning the railway sector in relation to the development of high-speed trains that this discipline has had renewed interest at the beginning of the 90s [31]. In fact, in this case, the use and development of new technologies have led bridge structures to new types of loads and therefore stresses in relation to the new railway vehicles that have had a considerable improvement in both their performance in relation to the type of number of passengers that they are able to move. The first studies aimed at this issue can be traced back to the 50s of the 19th century, when two works stand out among the others. Indeed, Stokes et al. [115] and Willis et al. [116] began the study of the phenomenon of moving loads and the stresses to which the materials in railway bridges are subjected. In particular, the mathematical equations governing the phenomenon were discussed for the first time, and the effects that materials, particularly iron, could undergo under stresses due to moving loads were critically described. Although, from a scientific viewpoint, these works were quite embryonic for our days, they were definitely not only innovative but also an interesting starting point for all subsequent studies in the sector. The first analytical solutions, indeed, allowed scholars to have estimates regarding the mechanical mechanisms that played a role in the analyses. And it is certainly to such works that about fifty years later Timoshenko [117] looked to develop and refine the differential equations governing the problem, exploiting his extensive mathematical knowledge to provide closed-form solutions to the problem, first deriving the equations of motion from energy principles and then obtaining a system response admitting a solution derived by trigonometric functions. However, the problem developed and solved by Timoshenko mainly concerned vehicles, and therefore forces, moving on the beam at a constant speed, a limitation that was immediately overcome almost ten years later by the work of Lowan [118], who extended the theory to include moving loads at non-constant speed, deriving analytical solutions capable of returning an

estimate of the stresses to which such structures are subjected under those load conditions. In all the aforementioned solutions, the description of the forces was essentially aimed at the description of a train passing over a beam. Indeed, it is noteworthy that the characterization of the loads from a railway perspective is less complex and stochastic compared to the description of the traffic phenomenon. This is because the types of trains and their speeds are much less variable compared to vehicular traffic, which is composed of very different vehicles moving at different speeds. To alleviate this issue, Fryba [23] focused his research on the interaction between moving forces associated with traffic investigating the effect that this random nature has on structures. In particular, for the first time, such moving forces were treated as a non-stationary random process, characterized by a constant mean. Along with the random nature of traffic, for the first time, not only the effects of speed on the bridge response but also the effects that such forces have on the damping of the bridge, which in some situations has proven to be not possible to ignore, were brought to the attention of the scientific community. Following the same traces, subsequent studies carried forward by Sniady et al. [15] where the moving forces were represented with random values not only of speed but also of amplitude. In this way, the researcher was able, to give a stochastic nuance to the problem, bringing to light theoretical solutions of the expected values and the variance of the displacement values of the analyzed beam. Although, until then, most of the work was focused on vehicles discretized as simple moving forces, over time and with the evolution of the systems that came into play in the analysis, scholars began to improve the analyses considering also the inertial effects of the various moving vehicles. Indeed, it already seemed clear at the time that considering a system of forces on a beam could mean that some important aspects of the system were neglected. Following this thought, scholars decided to improve the systems by initially including the inertial effects and the consequent actions that the two systems exchange, and it is precisely in this context that the approach to moving masses was born. One of the first cases in which such an approach was presented dates back to the early 80s when T. Dahleberg [19] presented a moving masses approach making a significant contribution to the discipline. He wrote a very interesting work where he presented a parametric study performed on a simply supported beam structure traversed by moving masses. This parametric study then allowed to underline how, especially in some cases, i.e., when the mass ratios between the two subsystems begin to be significant, the approach of moving forces has little accurate prediction of the phenomenon. Therefore, the effects of inertial forces turn out to be a relevant aspect that should be taken into account in relation to the type of application. The very simple and effective method presented by the previous scholar was then further extended from a computational viewpoint by A.O.Cifuentes [24] who extended the previous method by modeling the contact between moving mass and bridge exploiting the technique of Lagrange multipliers capable of imposing compatibility conditions at the interface between the two subsystems. This concept was then deeply investigated in the same year by J.E. Atkin [25] who proposed an analytical and a numerical method for the solution of such problems studying the problem on beams subject to different boundary conditions moving from the basic hypothesis of a simply supported beam. Subsequently, P.K. Chatterjee [119] studied the impact of vehicular traffic, once again considering the model of moving masses, on suspension bridges. Such analysis is focussed on a nonlinear interactive force, exploits the eccentricity of the load, and includes in the analysis the contribution of asphalt roughness generating roughness profiles exploiting Montecarlo simulations derived from the power density function of the profile. The responses in this area are then also tested in reference to other types of vehicles including in the analyses 3D 2D vehicles and sprung mass systems. The evolution of the representation of vehicles was necessary as scholars of the time realized that it is

not only the inertial effects that come into play in this type of problem. Indeed, there are multiple factors that can influence the dynamic response of the bridge structure under traffic conditions. Vehicles normally are equipped with suspension systems that are characterized by a complex spring-damper mechanism; this mechanical apparatus can exert additional forces on the beam that go beyond those inertial. In particular, it is possible to notice how viscous forces come into play that can both excite the structure and bring about a modification of the structural damping, a condition which is necessary to know especially in the dynamic identification phase of the problem. Moreover, the presence of asphalt roughness, which can be conceptually understood as a non-flat profile of the beam, makes the two subsystems mutually exchange elastic and viscous forces essentially due to the suspension of the vehicles mainly dimensioned to ensure comfort to the passengers. And it is precisely in this perspective, that ideal dynamic models capable of simulating the responses of vehicles by assembling basic dynamic units such as masses, springs, and dampers were developed. Indeed, from the composition of such elements, it is possible to obtain mechanical models that, although simplified, are capable of describing the response of the mechanical systems of interest. Numerous are the models developed and that can be found in the literature, such as the sprung-mass system which is characterized by a single vertical degree of freedom, essentially born to describe in a simplified way the behavior of a vehicle axle, or the so-called half-car model in which in addition to the vertical degree of freedom includes the effects of the vehicle pitching on the two axes. These two units were then further developed and complicated to make them able to describe the mechanical behavior of complex vehicles. Here, what is worth highlighting is how the choice of the simplified system should be commensurate and chosen according to the problem to represent; indeed, as the elements that make up the system increase, there will be the simultaneous increase of the degrees of freedom of the problem and therefore the number of equations that come into play in the numerical analyses. Moreover, the computational cost of models characterized by a significant number of degrees of freedom means that these cannot be included in the context of vehicular traffic simulations. For this reason, often in the literature, systems characterized by numerous degrees of freedom are used to describe the response of a single vehicle while in the case where the objective is the estimation of the bridge response subjected to traffic often proceed with the insertion of much simpler models like the quarter-car model. However, the concept of moving mass was not completely abandoned by scholars, indeed, G. Michaltsos [16] studied the response of a simply supported Euler-Bernoulli beam element under conditions of moving masses at constant speed. The main focus of the study was to understand what type of interaction there is between the mass and its speed on the beam and how this interaction conditions the system. In the meantime, in the same period, other scholars continued to develop the models of moving masses, the most known example is probably the one from of H.P Lee [26], who reconsidered the theoretical problem and solved it in matrix form combining the Lagrangian approach with the assumed modes method. One of the most interesting conclusions of this work is the fact that he managed to demonstrate how, in some situations, the results derived from the concentrated forces approach is not always the upper bound for the corresponding formulation of moving masses. The approach of moving masses was then taken up a few years later by M. Ichikawa et al. [17], who focused on continuous Euler-Bernoulli beams subjected to moving masses. Subsequently, M. Dehestani et al. [27] investigated the inertial interaction between vehicles and bridge, but focusing on a fundamental aspect not always considered, namely the impact that the critical speed has on structures of this type. The critical speed is a phenomenon strictly connected to the so-called driving frequency, and it is certainly a mechanical quantity that must be considered both in the design phase and in the maintenance or verification of bridges.

Simultaneously, towards the end of the 90s, we find the beginning of the works of Y.B. Yang [18, 34–36] who, publication after publication, established a theoretical and computational framework for the study of the vehicle-structure interaction phenomenon with different vehicle models. His work had a significant impulse especially for its applications to high-speed trains that were rapidly developing at the time. Assuming some fundamental hypotheses in the mechanical problem investigated, some of which are still accepted, such as the perfect contact of the two systems, he developed primarily closed-form solutions of the problem of the quarter-car model moving over the beam, with particular emphasis on the mechanical phenomena that can reflect on the performance of the structure, such as resonance and cancellation phenomena, or the definition of the so-called speed-parameter strictly connected to the driving-frequency, or still the definition of parametric studies for the study of the so-called impact factor on bridge structures. One of the most significant contributions according to the author, is the definition of a matrix method based on the condensation of the degrees of freedom through contact relations that allow making the problem very efficient from a computational viewpoint. Indeed, he made a problem that on paper needs complicated mechanical constructs to manage like contacts, in a direct and apparently decoupled problem, which is very efficient and easily implementable in a finite element context. Along with the formal determination of the problem, he also investigated the problem associated with the natural frequency shift essentially due to the presence of vehicles on the bridge structure showing that in the case where the mass ratios between the two systems are significant this instantaneous shift could be a critical parameter especially in case of dynamic identification of the system. However, this was not the only theory developed in recent years, in fact, Yang's work turns out to be essentially focused on planar problems where the beam elements behave according to Euler-Bernoulli theory. In the same years, X.Q. Zhu et al. [21] associated the VBI theory to Timoshenko type beam elements, deriving the motion equations exploiting Hamilton's principle and solving it through the modal superposition method accompanied by an optimization methodology for the identification of forces. Hence, he not only applied the above-mentioned principles to different beam elements, but it was also one of the first cases where the so-called inverse problem was addressed, namely the condition in which the objective of the analysis is the identification of the moving forces on the beam starting from a limited number of punctual dynamic information on the structure. At the beginning of the new century, research on vehicle-structure interaction did not stop, in fact, new studies and simulations on the phenomenon were presented, such as in L. Kwasniewski et al. [13] where the authors presented a complete analysis aimed at studying and quantifying the impact factor modeling with three-dimensional elements both the bridge structure and the vehicle in a simulation that modeled the vehicle in a particularly detailed way in all its parts. They obtained very good results compared to experimental data collected on the discretized structure. On the same research field, we can find the work of Q. Xie et al. [12] where the authors performed finite element analyses of an entire structure considering three-dimensional elements for the subsystems. The objective of their research was essentially to study the stress levels that the passage of a heavy vehicle causes in relation to the structural elements of which the bridge is composed. Moreover, in the field of numerical simulations of the mechanical problem related to vehicle-structure interaction deserves to be reported the work of Y. Dong et al. [120] where the authors, aware of the lack of finite elements developed ad hoc for the realization of such numerical task, defined a so called user-defined element in Abaqus able to perform the simulations already presented by Yang a few years earlier. Then, N.Liu et al. [33] investigated the dynamic response of beams subjected to moving loads exploiting an optimization technique called swarm optimization method to obtain a calibration of the physical parameters of the structure for an optimal

response to the stresses caused by moving vehicles at different speeds. Three years later, Q.Li et al. [42] introduced a new iterative technique to determine and solve the problem of non-linear mechanical interaction between bridge and train calculating the value of the forces on the linear theory of klaker. Then, Q.Zou et al. [46] presented a comparative study regarding different calculation models for the vehicle-structure interaction problem. In this work, different computational approaches developed by other authors in previous years were tested on a finite element model of a real bridge structure. They were able to demonstrate how depending on the finite elements selected for the numeric simulations, in the dynamic field, the results that can be obtained turn out to be very different. In particular, this work showed how using shell, solid and beam elements only the last two will provide concordant results unlike the classic beam elements that at least under normal conditions are not able to fully capture the dynamic response of the bridge. This point is crucial for the future treatment and for the numerical simulations presented below. Over time, the concept of vehicle-structure interaction shifted to methodologies of using such tools aimed especially at the monitoring of structures. And it is precisely in this context that the so-called inverse methods, of which we already mentioned that appear as a big innovation, which albeit with limits, is not negligible. A significant contribution to the inverse methods was brought by X.Q.Zhu [21] who presented a work in which he exposed all the previous attempts to solve such a problem that turns out to be ill-conditioned highlighting pros and cons of the techniques presented. At the same time, it is possible to find the first works on indirect methods such as, for example, C. Tan et al. [56] focused on the monitoring of bridge structures from data obtained directly on vehicles moving on the structure aimed at the identification of damage. They implemented an algorithm based on the wavelet transform to overcome the problems notoriously found in the use of FFT which is often characterized by poor frequency resolution that determines inaccurate or not significant results for the purposes of dynamic identification. Moreover, a technique of subtraction of the signals measured by two consecutive axes is presented, a methodology that allows minimizing the impact of some disturbance phenomena on the identification, such as for example asphalt roughness. Subsequently, the work of Q. Zeng et al. [45] modified the theory already exposed by Y.B. Yang proposing an integration scheme for the vehicle-structure interaction problem introducing a fictitious contact point in the dynamic problem, which allows solving the entire problem as two subsets of distinct but iteratively connected problems, the benefits found by the authors are essentially related to the speed of solving the problem from a numerical rather than practical point of view. Finally, it is worth mentioning two works written by the same research group led by C.D Stoura et al. [29, 44] where researchers dissected the complete response observed in the physical phenomenon analyzing step by step how elastic, damping, and inertial forces impact on the total response of the system. Furthermore, in the same works, scientists then proposed a method called "modified bridge system method" which also in this case allows to decouple the contributions in the case where the stiffness ratios of the two systems are rather small that is strongly in favor of the investigated structure. These theories were then put into practice using finite element analysis to solve the indirect problem and try to find the modal information of the system directly from the accelerations measured on the vehicle. In the following, a finite element framework for vehicle-bridge interaction simulations will be proposed aiming to obtain an estimate of the mechanical responses of the bridge and vehicles exploiting the beam element presented in the previous chapter. However, it is worth to noting how all the aformetioned works based on numerical simulation on the Vehicle-Bridge Interaction which take into account the beam problem did not account for the torsional behavioru fo the bridge, since several developed models consider only the vertical deflection of the mechanical system, this results in a simplistic approach, which is

especially unacceptable when a high degree of detail is required. Indeed, some bridge structures exhibit torsional behaviors that need to be adequately addressed, even in simpler models. The focus of this section is to mitigate this mechanical limitation through a coupling mechanism between beam finite elements and vehicles. By integrating the theoretical framework from the previous chapter, the Yang theory [31] is further refined to achieve a more comprehensive framework. This new approach combines the simplicity of the beam element theory with the three-dimensional effects inherent to the bridge structure. The goal is to define a new framework capable of describing the dynamic responses of bridges with minimal computational effort, without neglecting critical physical phenomena such as the inertial interaction between the two subsystems: the primary system (the bridge or beam) and the secondary system (the vehicles). However, inertial interaction is not the only concern within the Vehicle-Bridge Interaction framework. Vehicles are generally equipped with suspension systems that are crucial for occupant comfort, and the mechanical characteristics of these devices introduce additional interactions due to their damping and stiffness properties. These phenomena must be modeled and incorporated into the numerical framework to narrow the gap between fully complex models, usually characterized by a vast number of degrees of freedom, and beam-based models. In this context, the further development of the theory relies on a simple dynamic model designed to describe the vehicle, specifically the quarter-car model, which can characterize a single vehicle axle. This system is in reciprocal interaction with the primary system; this relationship can be modeled by the so-called contact force. This force is used to derive the coupled system of differential equations, which is then solved using the Finite Element Method. Currently, only one disturbing phenomenon is considered in this section, while other issues such as vehicle parameter calibration, traffic modeling, and environmental effects on bridge structures will be addressed in subsequent sections. These advancements in modeling not only contribute to our understanding of Vehicle-Bridge Interactions but also have practical implications. Improved models can lead to better predictive capabilities, informing critical design decisions and maintenance schedules for bridges. Additionally, the computational efficiency achieved through these models enables more extensive simulations, including scenarios involving a larger number of variables or longer time frames. However, it's important to acknowledge that while these models offer significant progress, they may have limitations that require further investigation. Identifying these limitations sets the stage for ongoing research, ensuring that our models continue to evolve and enhance our ability to design and maintain safe and efficient bridge structures.

3.1 Vehicle idealization

Let's consider the i-th quarter-car model fig. 3.1. This is composed of many mechanical apparatus including the *upper mass*, which describe the mass of the vehicle m_{vi}, the *wheel mass* m_{wi}, which is ideally located at correspondence of the contact point between the two sub-systems, and a *spring-damper* system described by its stiffness constant k_{vi} and its damping constant c_{vi}. The latter is introduced in the analysis due its capabilities to reproduce the suspension system of a vehicle. The i-th quarter-car is assumed to be moving at constant speed v_i. Although, this assumption at first impact might seem restrictive, it has two essential justifications. Primarily, in the condition of highway bridges the vehicles do not experience brutal speed variations, especially nowadays where the population is slowly transitioning to autonomous vehicles or to vehicles of last generation which are often equipped with a cruise modality where the speed is kept constant. Furthermore, admitting no velocity variations over the bridge span it is then possible to not take into account the longitudinal forces caused by accelerations or declarations (braking forces).

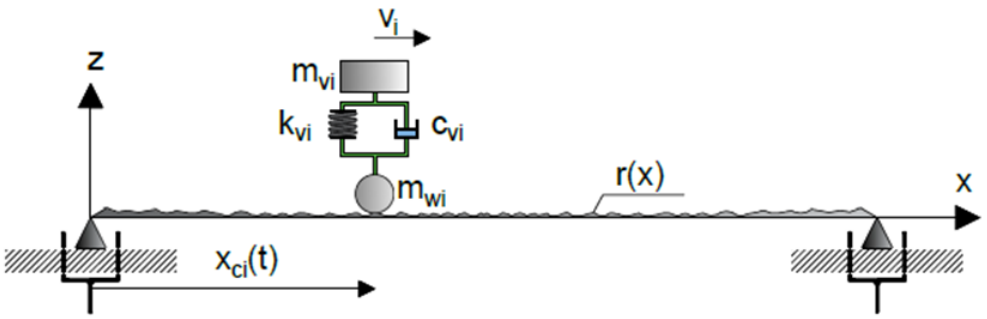

Figure 3.1: i-th vehicle moving along the beam structure.

In addition in the further sections only straight beam are considered hence neglecting the lateral excitation derived from the centripetal components in curved bridges. Moreover, in the analysis the road roughness profile is introduced by $r(x)$ and the coordinate position of the quarter-car as function of the time variable is identified as $x_{ci}(t)$. In this perspective, it trivial to find the equation of motion of the quarter-car model, which act on the beam along the vertical axes y as

$$m_{vi}\ddot{u}_{vi} + c_v(\dot{u}_{vi} - \dot{u}_{wi} - \dot{r}_i) + k_v(u_{vi} - u_{wi} - r_i) = 0 \tag{3.1}$$

here, in eq. (3.1) ($\dot{}$) represents the derivative with respect to time. Consequently, $\ddot{u}_{vi}$, $\ddot{u}_{vi}$, u_{vi} are respectively the acceleration, the velocity and the displacement associated with the vehicle mass m_{vi}, on the other hand $\ddot{u}_{wi}$, $\ddot{u}_{wi}$, u_{wi} are the wheel counterparts. Hereinafter, the introduction of the road roughness arises due to the term r_i and its derivative with respect to time $\dot{r}_i$. Moreover, the i-th quarter-car model excites the beam element by means of the so-called contact force f_{ci}, which is the force experienced in correspondence of the contact point, and might be expressed as function of the spatial coordinate x_{ci}. The spatial coordinate is the road travelled by the vehicle at the considered instant of time t. Hence, the contact force expression can be stated by considering the equilibrium at the contact point, as

$$\begin{gathered} m_{wi}\ddot{u}_w i = f_{ci} + m_{vi}\ddot{u}_{vi} \\ f_{ci} = m_{wi}\ddot{u}_{wi} - c_{vi}(\ddot{u}_{vi} - \ddot{u}_{wi} - \dot{r}_i) - k_{vi}(u_{vi} - u_{wi} - r_i) \end{gathered} \tag{3.2}$$

The reciprocity relation, whose assumption is based on the perfect contact hypothesis leads to the coupling of the two sub-system, which are the j-th finite element and the i-th vehicle idealization. The latter hypothesis implies that there is not any kind of separation among the two-subsystem during the observed time interval. Moreover, the total displacement of a generic point assumed to be solidal with the beam cross-section, can be retrieved by the kinematic composition of the displacement components, which is directly derived from the flexural-torsional behaviour of the structural element, by the introducing of the quantity h_i, which describes the distance along the z axes between the beam elastic axes x and the quarter-car position. Furthermore, by assuming the hypothesis of small displacement the total vertical displacement of the generic point, which is then experienced by the wheel mass of the associated oscillator, might be described as

$$\begin{gathered} u_{wi} = w_z^b(x_{ci}) - h_i \cdot tan[\theta_x^b(x_{ci})] \\ u_{wi} \approx w_z^b(x_{ci}) - h_i \cdot \theta_x^b(x_{ci}) \end{gathered} \tag{3.3}$$

where $w_z^b(x_{ci})$ and $\theta_x^b(x_{ci})$, represent respectively the deflection of the bridge along the vertical axis and the torsional rotation of the element evaluated in correspondence of the contact point. The latter congruence relation can be introduced in the finite element formulation referring to a suitable shape functions $\bar{N}^j(x_{ci})$, which is conceived as a row vector of dimension n, with n total number of the bridge's degree of freedom, which holds the shape functions of the j-th bridge finite element in correspondence of the spatial coordinate x_{ci}. Naturally, in the case of the moving quarter-car model the only non-null terms in the aforementioned vector are those related to the vertical displacements of the beam and to the torsional rotation degrees of freedom. This condition is directly derived by the fact that the only excitation terms deriving from the flowing traffic, under the hypothesis of constant velocities are according to the vertical direction and the torsional rotation. Thus, introducing in the formulation the column vector $\bar{d}_b$, of dimension n, in which are stored all the displacements degree of freedom associated with the beam element it is immediate to write

$$\begin{aligned} u_{wi} = \Big\{ 0 \ \ldots \ N_2^{1,i} \ N_2^{2,i} \ \ldots \ -h_i \cdot N_6^{1,i} \ -h_i \cdot N_6^{2,i} \ldots \\ \ldots \ N_2^{3,i} \ N_2^{4,i} \ \ldots \ -h_i \cdot N_6^{3,i} \ -h_i \cdot N_6^{4,i} \ \ldots \ 0 \Big\} \bar{d}_b \end{aligned} \tag{3.4}$$

or shortly

$$u_{wi} = \bar{N}^i \ \bar{d}_b \tag{3.5}$$

by taking advantage of the derivation with respect to time of the mechanical quantity u_{wi} it possible to obtain the associate velocity and accelerations of the i-th wheel on the j-th finite element

$$\begin{aligned} \dot{u}_{wi} &= v_i \cdot \frac{d\bar{N}^i}{dx} \bar{d}_b + \bar{N}^i \dot{\bar{d}}_b \\ \ddot{u}_{wi} &= v_i^2 \cdot \frac{d\bar{N}^{i^2}}{dx^2} \bar{d}_b + 2v_i \cdot \frac{d\bar{N}^i}{dx} \dot{\bar{d}}_b + \bar{N}_i \ddot{\bar{d}}_b \end{aligned} \tag{3.6}$$

substituting eqs. (3.5) and (3.6) in eq. (3.2) the following relation is straightforward

$$\begin{aligned} f_{ci} = m_{wi} \left(v_i^2 \cdot \frac{d\bar{N}^{i^2}}{dx^2} + 2v_i \cdot \frac{d\bar{N}^i}{dx} \dot{\bar{d}}_b + \bar{N}^i \ddot{\bar{d}}_b \right) + c_{vi} \left(v_i \cdot \frac{d\bar{N}^i}{dx} \bar{d}_b + \bar{N}^i \dot{\bar{d}}_b \right) + \\ k_{vi} \bar{N}^i \bar{d}_b - c_{vi} \left(\dot{u}_{vi} - v_i \cdot \frac{dr_i}{dx} \right) - k_{vi} \left(u_{vi} - r_i \right) \end{aligned} \tag{3.7}$$

The mathematical expression for the contact force eq. (3.7), is essential since this is the loophole which allows for the two sub-system to be coupled without any kind of finite element contact formulations. Hence, can be exploited to reduce certainly complex physical phenomenon in a much simpler one, where no additional degrees of freedom need to introduced nor other complex formulation which make the overall procedure non-linear. Moreover, this formulation which follows the theory developed by [31] it seems to be suitable for a further development which can close the gap between two and the three-dimensional behaviour of this mechanical system, without heavily affect the computational effort.

3.2 Coupling of the two sub-systems

Once, that the coupling tool is completely exposed, it is possible to formally state the relations from a principal system standpoint. As a matter of fact, the equations of motion of the associated with to bridge system, which is considered excited by the i-th quarter-car model can be stated in his finite formulation writing

$$\tilde{M}_b\ddot{\bar{d}}_b + \tilde{C}_b\dot{\bar{d}}_b + \tilde{K}_b\bar{d}_b = \left[-f_{ci} + g\left(m_{wi} + m_{vi}\right)\right]\bar{N}^{i^T} \tag{3.8}$$

where g is the acceleration of gravity and $\tilde{M}_b$, $\tilde{C}_b$ and $\tilde{K}_b$ are respectively the bridge mass, damping and stiffness matrix. Those components are determined by the classical approach of finite element method introducing the relations of the previous chapter. Introducing eq. (3.7) in eq. (3.8) the coupled formulation of the bridge is achieved

$$\begin{aligned}\left(\tilde{M}_b + m_{wi}\cdot\bar{N}^i\bar{N}^{i^T}\right)\ddot{\bar{d}}_b + \left(\tilde{C}_b + 2v_i\cdot m_{wi}\frac{d\bar{N}^i}{dx}\bar{N}^{i^T} + c_{vi}\cdot\bar{N}^i\bar{N}^{i^T}\right)\dot{\bar{d}}_b + \\ + \left(\tilde{K}_b + v_i^2\cdot m_{wi}\frac{d^2\bar{N}^i}{dx^2}\bar{N}^{i^T} + v_i\cdot c_{vi}\frac{d\bar{N}^i}{dx}\bar{N}^{i^T} + k_{vi}\cdot\bar{N}^i\bar{N}_i^T\right)\bar{d}_b = \\ = \left[g(m_{wi}+m_{vi}) + c_{vi}\left(\dot{u}_{vi} - v_i\frac{dr_i}{dx}\right) + k_{vi}(u_{vi}-r_i)\right]\bar{N}^{i^T}\end{aligned} \tag{3.9}$$

Furthermore, the mechanical relation associate with the i-th moving vehicle, can be defined in same manner by considering the kinematic relations eqs. (3.5) and (3.6), which can be immediately introduced in the equation of motion of the associated quarter-car model eq. (3.1), hence condensing the degree of freedom associated with respect to the wheel mass m_{wi} the general relations are then re-arranged as function of the upper mass of the quarter-car system and the associated degree of freedom of the bridge on which the quarter-car model relies at the considered instant of time t, as

$$m_{vi}\ddot{u}_{vi} + c_{vi} + \dot{u}_{vi} + k_{vi}u_{vi} = c_{vi}\left(v_i\cdot\frac{d\bar{N}^i}{dx}\bar{d}_b + \bar{N}^i\dot{\bar{d}}_b + v_i\frac{dr_i}{dx}\right) + k_{vi}\left(\bar{N}_i\bar{d}_b + r_i\right) \tag{3.10}$$

Consequently, the latter equations, eq. (3.9) and eq. (3.10), enforce the coupling of the two sub-systems. Those, which are here derived for the simple case of the i-th oscillator which is moving along the bridge, are suitable for the matrix notation, especially in their extend context where in order to simulate the traffic excitation the number of vehicle need to be increased. Indeed, let's assume which the entire system is composed by m moving quarter-car models, thus the aforementioned relations can be arranged

$$\begin{bmatrix}\tilde{M}_{vv} & \tilde{0}\\ \tilde{0} & \tilde{M}_{bb}\end{bmatrix}\begin{Bmatrix}\ddot{\bar{u}}_v\\ \ddot{\bar{d}}_b\end{Bmatrix} + \begin{bmatrix}\tilde{C}_{vv} & \tilde{C}_{vb}\\ \tilde{C}_{bv} & \tilde{C}_{bb}\end{bmatrix}\begin{Bmatrix}\dot{\bar{u}}_v\\ \dot{\bar{d}}_b\end{Bmatrix} + \begin{bmatrix}\tilde{K}_{vv} & \tilde{K}_{vb}\\ \tilde{K}_{bv} & \tilde{K}_{bb}\end{bmatrix}\begin{Bmatrix}\bar{u}_v\\ \bar{d}_b\end{Bmatrix} = \begin{Bmatrix}\bar{f}_v\\ \bar{f}_b\end{Bmatrix} \tag{3.11}$$

where $\tilde{M}_{vv}$, $\tilde{C}_{vv}$ and $\tilde{K}_{vv}$ are respectively the $m\times m$ diagonal matrices associated with the m-th quarter-cars mechanical properties as masses m_{vi}, damping coefficients c_{vi} and stiffness constant k_{vi}

$$\tilde{M}_{vv} = \begin{bmatrix}m_{vi} & \cdots & 0\\ \vdots & \ddots & \vdots\\ 0 & \cdots & m_{vm}\end{bmatrix};\ \tilde{C}_{vv} = \begin{bmatrix}c_{vi} & \cdots & 0\\ \vdots & \ddots & \vdots\\ 0 & \cdots & c_{vm}\end{bmatrix};\ \tilde{K}_{vv} = \begin{bmatrix}k_{vi} & \cdots & 0\\ \vdots & \ddots & \vdots\\ 0 & \cdots & k_{vm}\end{bmatrix} \tag{3.12}$$

the mechanical parameters which are enclosed in the structural matrices associated with respect to the bridge degrees of freedom are time dependent, since the traffic and the quarter-car positions vary with respect to time as function of the associated velocities. Hence, assuming that the bridge can be described by l degrees of freedom it is possible to write the associated matrices as

$$\begin{aligned}
\tilde{M}_{bb} &= \tilde{M}_b + \sum_{i=1}^{m} m_{wi} \cdot \bar{N}_i \bar{N}_i^T \\
\tilde{C}_{bb} &= \tilde{C}_b + \sum_{i=1}^{m} 2v_i \cdot m_{wi} \frac{d\bar{N}_i}{dx} \bar{N}_i^T + c_{vi} \cdot \bar{N}_i \bar{N}_i^T \\
\tilde{K}_{bb} &= \tilde{K}_b + \sum_{i=1}^{m} v_i^2 \cdot m_{wi} \frac{d^2\bar{N}_i}{dx^2} \underline{\mathrm{N}}_i^T + v_i \cdot c_{vi} \frac{d\bar{N}_i}{dx} \bar{N}_i^T + k_{vi} \bar{N}_i \bar{N}_i^T
\end{aligned} \tag{3.13}$$

where the matrices $\tilde{M}_b$, $\tilde{C}_b$ and $\tilde{K}_b$ are derived by the finite element formulation of the principal system. The coupling term which appear in equation (3.11) can be grouped by the support of the column vector $\bar{e}_i$, where all its l rows are nulls except for the ones corresponding to the degree of freedom associated with respect to the j-th element of the beam on which the i-th vehicle is located at the considered time instant t, which are equal to one, therefore

$$\begin{aligned}
\tilde{C}_{vb} &= -\sum_{i=1}^{m} c_{vi} \cdot e_i \bar{N}_i \qquad \tilde{C}_{bv} = -\sum_{i=1}^{m} c_{vi} \cdot \bar{N}_i^T \bar{e}_i^T \\
\tilde{K}_{vb} &= -\sum_{i=1}^{m} \bar{e}_i \left(c_{vi} \cdot v_i \frac{d\bar{N}_i}{dx} + k_{vi} \cdot \bar{N}_i \right) \\
\tilde{K}_{bv} &= -\sum_{i=1}^{m} k_{vi} \cdot \bar{N}_i^T \bar{e}_i^T
\end{aligned} \tag{3.14}$$

Lastly, the two forcing terms f_v and f_b respectively of dimensions equal to m and l, can be formed introducing the column vector $\underline{\mathrm{q}}_i$, of dimension m in which all its components are null except for the one correlated to the i-th vehicles that is set equal to the unity and $\bar{N}_i^T$, hence

$$\begin{aligned}
f_v &= \sum_{i=1}^{m} \bar{q}_i \left(c_{vi} \cdot v_i \frac{dr_i}{dx} + k_{vi} \cdot r_i \right) \\
f_b &= \sum_{i=1}^{m} \left[g(m_{wi} + m_{vi}) - c_{vi} \cdot v_i \frac{dr_i}{dx} - k_{vi} \cdot r_i \right] \bar{N}_i^T
\end{aligned} \tag{3.15}$$

Once, that each component of the eq. (3.11) is defined, the mechanical problem can be easily described for every instant of time. Moreover, the obtained formulation is not dissimilar to the classical formulations which can be drawn for dynamic analysis of beam elements subject to a time varying excitation. Hence, the aforementioned system of equation can be solved at every time increments by some classical familiar numerical solution scheme such as, the Newmark-β method[121], or the previously mentioned (HHT)[110] algorithm.

3.3 Numerical benchmark

In this section numerical benchmark of the proposed finite element framework (*Ghost project*) against the *Abaqus 2023* software is presented. Numerical simulations of the Vehicle-Bridge Interaction can be surely realized by mean of several approaches, ranging from the easiest one, that is the moving force approach, to complex numerical model able to accurately represent both the bridge and the vehicle together with their interaction. Although, this model are essentially based on the sub-system specification, often are translated to numerical representation characterized by a huge amount of active or correlated equations in finite element concept. Moreover, the extensive employment of contact technique in the finite elements code bring furthermore increase in the necessary computational resources. Nevertheless, the deployment of numerical techniques based on the beam finite elements, able to reproduce the overall structural behaviour dynamic and operative conditions, might be a smart remedy especially in the contexts of big data generation. In this regard, the presented numerical analysis are explored to understand, which are the major opportunities and the associated drawbacks of the beam elements modelling. The main focus here, is to show that the adoption of a simple numerical framework, based on the beam approach, is appropriate to obtain significant numerical results if is compared with to a much more complex numerical system, such as the one presented in the previous chapter. Hereafter, the investigated structural element is the same double-tee beam already presented in the previous chapter. Nevertheless, the numerical investigation in this section is performed considering only the *Abaqus 2023*, which is equipped with several contact elements, which allow for these kind of numerical studies. However, many details need to be addressed to bring the finite element software, which is *Abaqus 2023* to convergence. Indeed, the associated mesh of the structural element is refined, including 21004 of S4 linear shell; the increasing amount of finite element is necessary in order to obtain the convergence of the implicit analysis steps with an higher time step Δt. Thus, quarter-car model is modelled by referring to a sprung mass approach, here two reference points are introduced in the three dimensional shell model: the first one aimed to describe the contact point between the two sub-systems and the second host the point mass, which represents the upper mass of the vehicle (fig. 3.2).

Moreover, the two reference points are linked by a connection element, of which stiffness and damping properties are defined. The coupling of the two sub-system is performed by introducing a contact relation, in particular a *friction-less contact*, in the tangential direction and a *hard contact* interaction, in the normal direction, are defined between the master nodes, which are represented by the surface of the interested shells element of the double tee slab, and the slave node, which is represented by the contact reference point. The contact interaction is then enforced by means of the *penalty method*. Despite the well defined framework it is worth noting how some numerical issues can arise due to some boundary condition which need to be addressed. Indeed, the initial positioning of the sprung mass system is critical for the outcome of the analysis. In this context placing the contact node on the edge of the beam would results in convergence issues, this well-known condition can be addressed in different ways. In [122], the authors performed many analysis aimed to the description of the Vehicle-Bridge Interaction problem using several finite elements and condition, in order to simulate different dynamic interaction. They solved the aforementioned issue by considering a slightly modified geometry for the structural element. In particular, they added a little branch to the two beam ends in order to perform the gravity analysis, which is used as starting point for the dynamic analysis. However, the comparison with the theoretical results are not perfectly matching, and this is mainly due to the different geometrical and mechanical characteristic which are enforced between the ideal and the finite model. Moreover, also the gravity condition

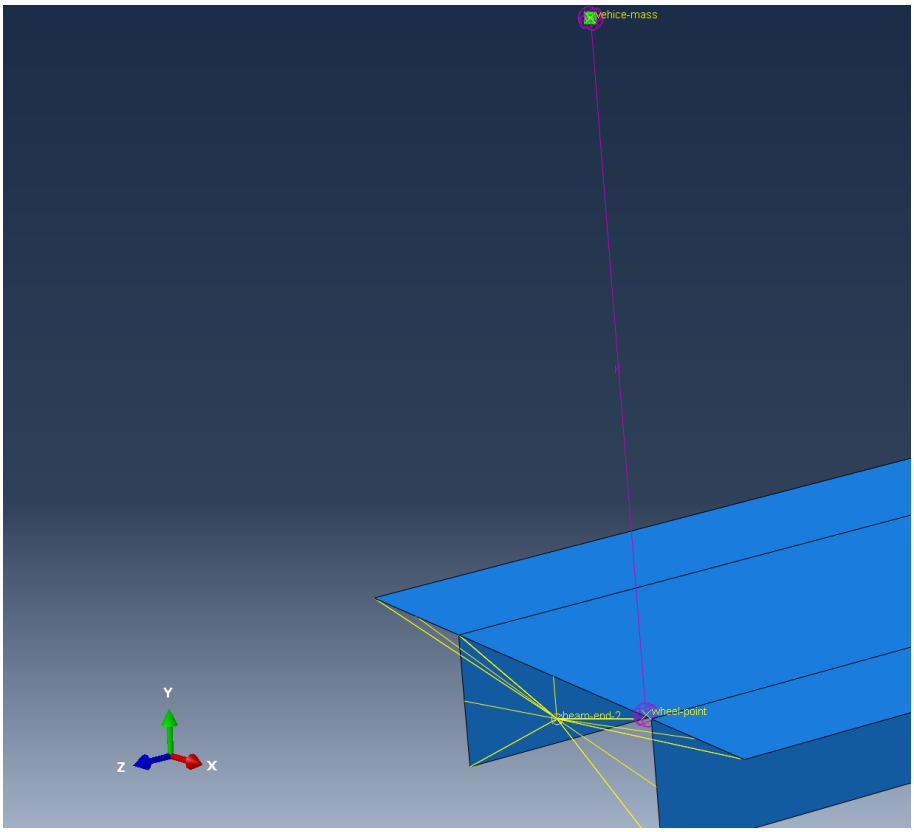

Figure 3.2: *Abaqus 2023* sprung-mass model modelling.

could affect the results because the rest position of the sprung mass could be altered. Thus, in order to overcome this numerical obstacles the actual modelling of the Vehicle-Bridge Interaction system in the *Abaqus 2023* framework is realized by not altering the geometric feature of the double tee beam, but considering the initial position of the sprung at a small distance from the beam edge. In particular, the starting position is moved 1e-5 m from the origin of the coordinate system which coincide with the beam end. This small artifact does not alter in significant manner the analysis nor leads to convergence issues in the afore-mentioned framework. Moreover, the quarter-car model, in the dynamic step doesn't move on the central axes of the beam, but is moved 0.6 m along the z axes. Meanwhile, the dynamic implicit step of the analysis is defined considering a fixed time step with $\Delta t = 0.001s$. In this analysis phase, the boundary condition along the beam axis are suppressed and substituted by an imposed motion in term of velocity v to the two reference nodes, resulting in a total length of 5s of the dynamic analysis. The mechanical parameter associated with to the sprung mass system are briefly reported in table 3.1.

QC Mechanical properties		
m_v	200.00	kg
k_v	7500.00	N/m
c_v	750.00	Ns/m
v	3.00	m/s

Table 3.1: QC mechanical properties numerical benchmark VBI.

The numerical model implemented in the *Abaqus 2023* suite is tested against afore-cited

Ghost project implementation, with the same mesh of the previous chapter. Nevertheless, the time step employed is $\Delta t = 0.01$ with the same vehicle parameters. The higher time step in not restricted by any convergence limitation as for the *Abaqus 2023* case. Indeed, in the commercial software smaller time step is need in order to achieve the convergence. This difference seems to be essentially due to non linearity associated with the contact interaction between the primary and the secondary systems. The time step identification is obviously a critical user choice. Small time steps often are needed especially in strongly non linear problems to achieve the desired accuracy, but at the same time computational effort can be negatively impacted by unnecessary small time-steps. Hence, being able to define a reasoned trade of from this to opposite pole is one of the keys for a good numerical simulation. The quality and the accuracy of the two models could be analysed by considering a different sets of dynamic response of the structure. Two are the adopted approaches in relation to the future use of these numerical simulations. The first recorded quantities are referred to the beam mid-point. This point is introduce in the numerical model employing the same interaction described in the previous chapter and is taken as reference point since coincide with the elastic section of the beam element. The responses obtained in term of vertical displacement, velocities and accelerations together with the ones in terms of torsional rotations, torsional velocities and torsional accelerations are depicted in figs. 3.3 to 3.8.

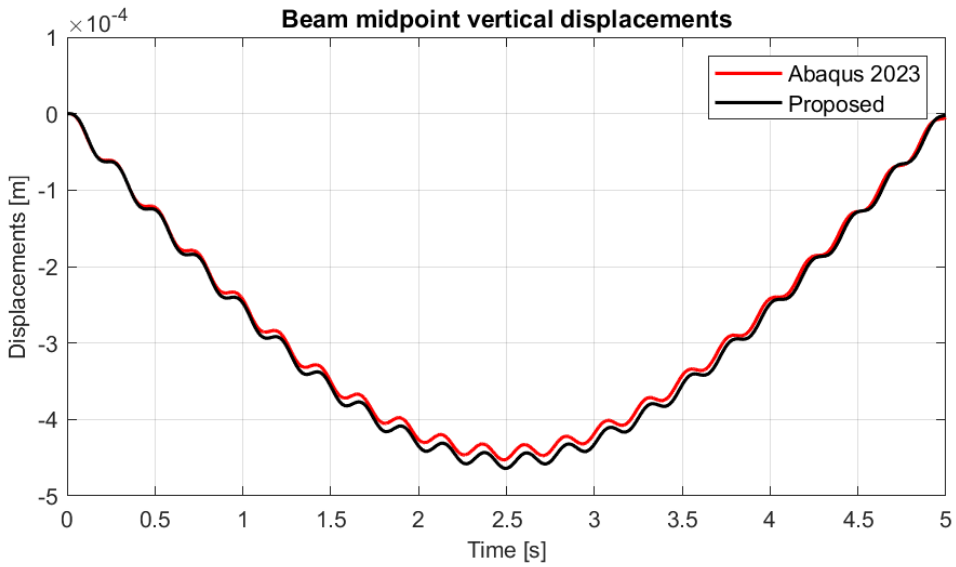

Figure 3.3: Vertical displacement response of the beam midpoint: *Abaqus 2023* Vs. Proposed.

Other interesting mechanical responses which can be analysed in this systems are the reaction forces experienced at the two beam ends. This quantities can be employed to several assessment of the bridge interaction with other structural elements such a the pier or the abutments. The determination of the reaction is performed according to the classical finite element approach. The variation of those values as function of the moving quarter-car in the time domain are depicted in figs. 3.9 and 3.10, from which it is possible to observe the good accuracy of the numerical results.

Moreover, other mechanical responses could be of interest specially in the context it will be used in the further discussions. Indeed, under the assumption of small displacement of the structural artifact, it is possible to re-construct the mechanical behavior in terms

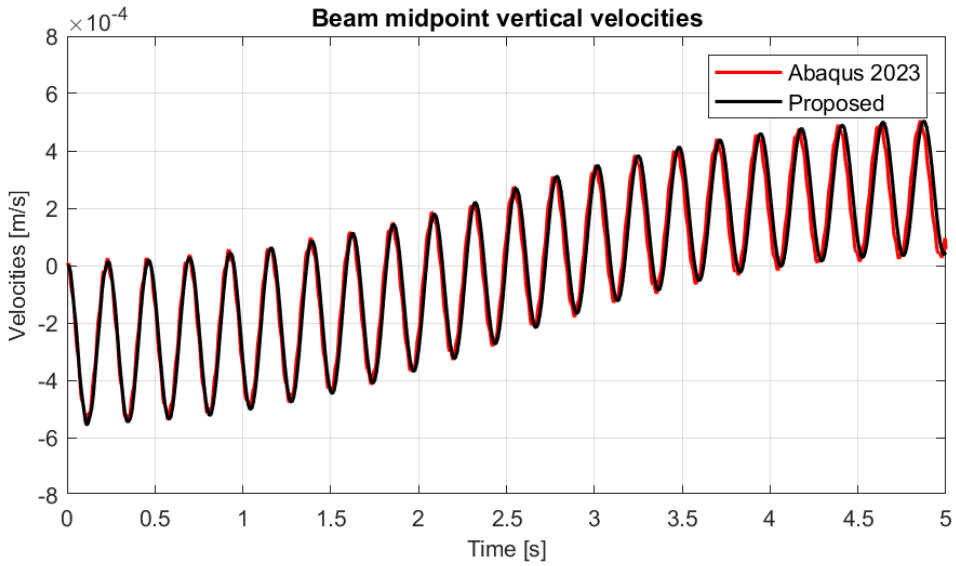

Figure 3.4: Vertical velocity responses of the beam midpoint: *Abaqus 2023* Vs. Proposed.

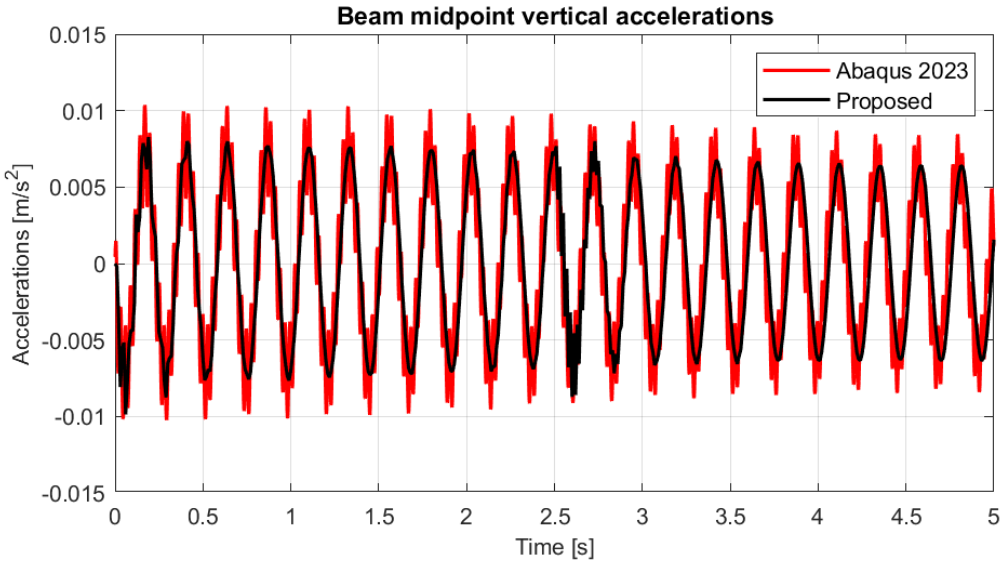

Figure 3.5: Vertical acceleration responses of the beam midpoint: *Abaqus 2023* Vs. Proposed.

of vertical displacements, velocities and accelerations of every node of the cross section by means of eq. (3.3). This premises could be interesting because, in this manner it is possible to simulate the presence of transducers on the beam able to record the desired kinematic component. Hence, additional numerical comparisons can be made taking into account a generic node of the beam cross section in the shell finite element model. The node 9 (see fig. 3.11), is selected. The mechanical responses of node 9 in the two finite element models are illustrated in figs. 3.12 to 3.14.

Furthermore, the secondary system, which is the sprung-mass model, cannot be neglected. As a matter of fact, the accuracy of the response of the vehicle is as critical as the one derived from structure, especially in some experimental context. Being able to obtain

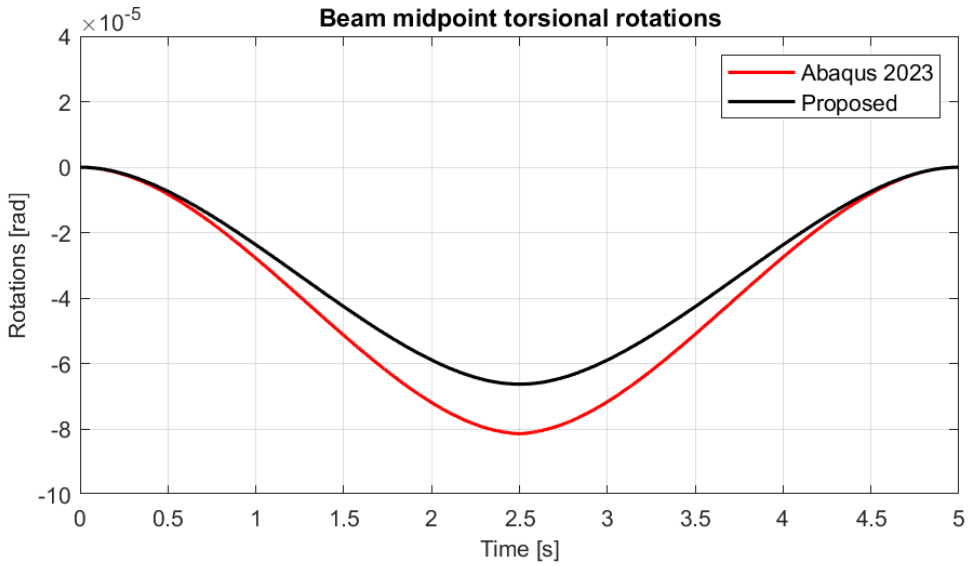

Figure 3.6: Torsional rotation responses of the beam midpoint: *Abaqus 2023* Vs. Proposed.

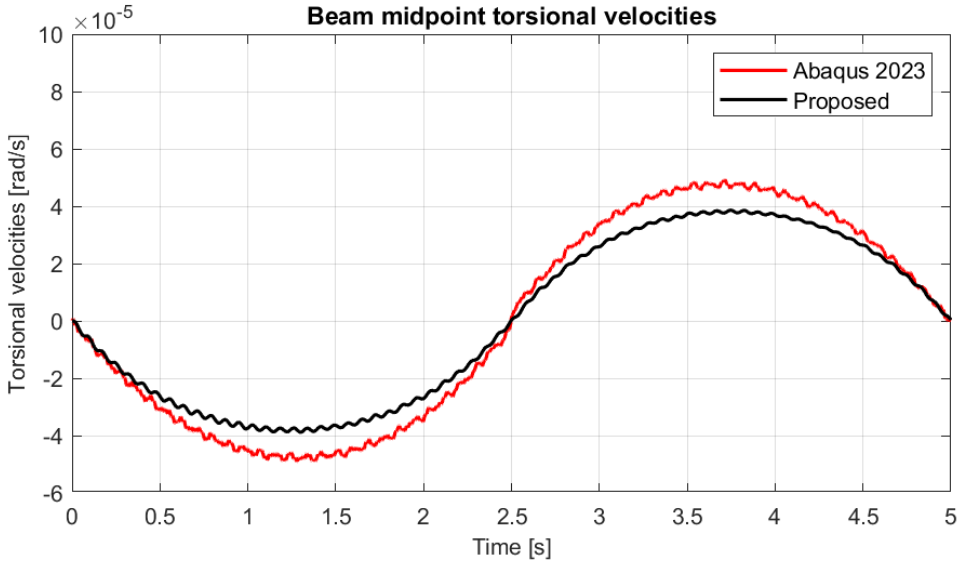

Figure 3.7: Torsional velocity responses of the beam midpoint: *Abaqus 2023* Vs. Proposed.

the vehicles responses opens up to several scenarios, which are essential for the study of the vehicle bridge interaction, such as the indirect methods or the driving frequency impact on bridge, to mention just a few. Thus, the responses recorder in correspondence of the vehicle upper mass derived from the two software are shown is figs. 3.15 to 3.17.

Alongside a qualitative assessment, this section provides a quantitative evaluation of the discrepancies between two distinct simulation software platforms. Here, *Abaqus 2023* serves as the numerical benchmark, while the results from *ghost* are treated as approximations. Similar to the methodology outlined in chapter 2, the quantitative analysis of errors leverages the Mean Absolute Error (MAE, eq. (2.41)), the Root Mean Square Error (RMSE, eq. (2.42)), and the Normalized Root Mean Square Error (NRMSE, eq. (2.43)).

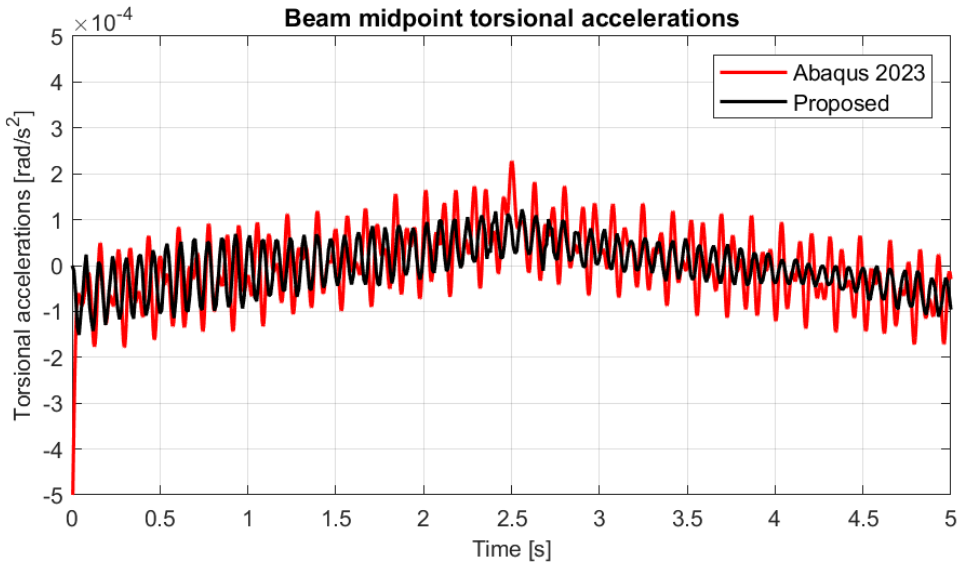

Figure 3.8: Torsional accelerations responses of the beam midpoint: *Abaqus 2023* Vs. Proposed.

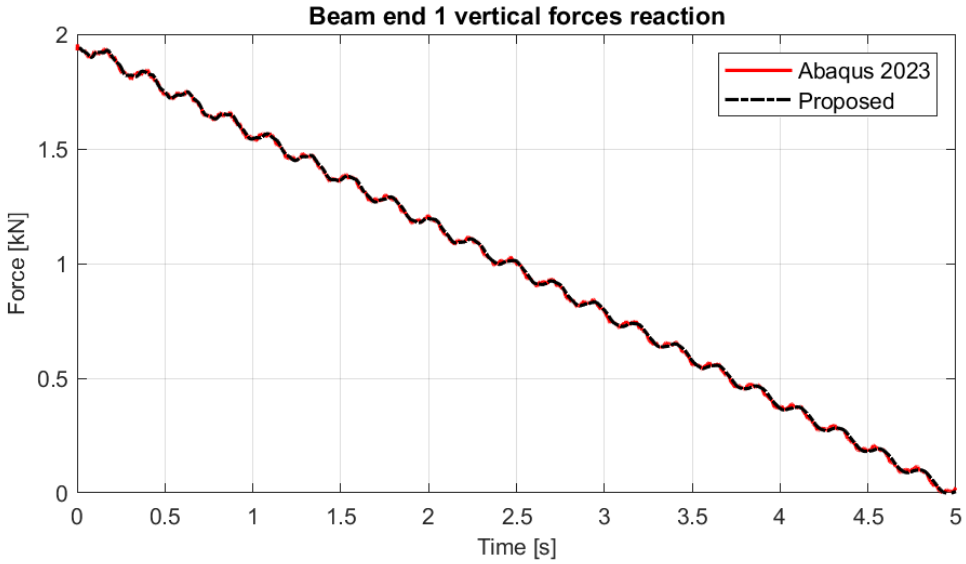

Figure 3.9: Shear vertical reaction measured at the beam end: *Abaqus 2023* Vs. Proposed

In this context, the conventional Mean Relative Error (MRE) is omitted due to its inadequacy in handling values nearing zero. Nonetheless, it's acknowledged that the chosen error metrics, while less susceptible to this issue, are not entirely exempt from it. The quantitative error parameters are detailed in tables 3.2 to 3.4, encompassing all the scenarios under review. Notably, despite the NRMSE metric's superior performance with values close to zero, it can still falter. This is exemplified by the NRMSE in terms of displacement at node 3 (table 3.2) and the corresponding vehicle displacement (table 3.3), which exhibit errors of 50% and 44.36%, respectively. Such levels of error appear significantly unrealistic when considering the quality of the responses, a conclusion supported by figs. 3.3 and 3.15, where the MAE emerges as a more accurate indicator of error. This

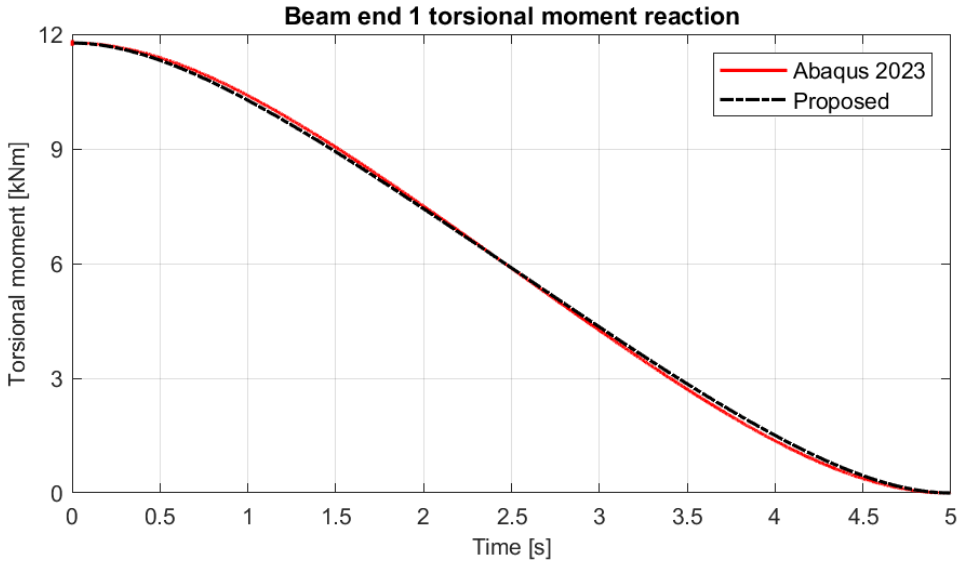

Figure 3.10: Torsional moment reaction measured at the beam end: *Abaqus 2023* Vs. Proposed

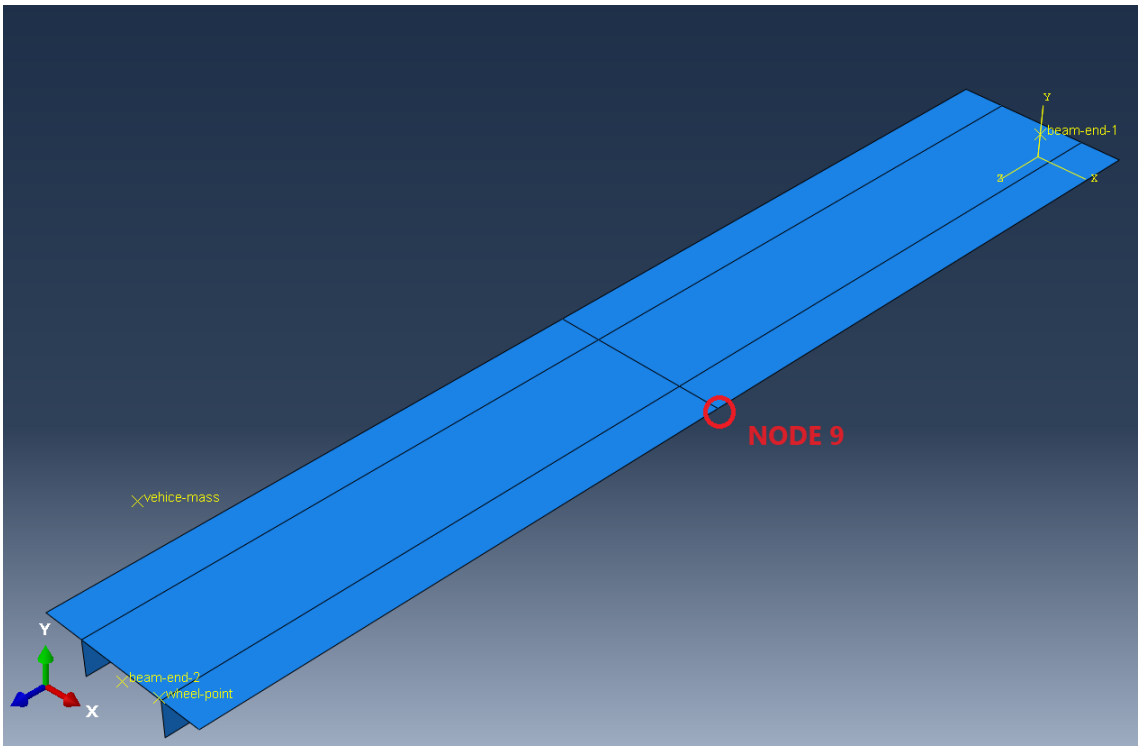

Figure 3.11: Analyzed node from which numerical comparison are performed.

quantitative evaluation underscores the complexity of accurately assessing model performance, particularly when dealing with values that approach zero. Despite the inherent challenges, the analysis highlights the necessity of selecting appropriate error metrics to capture the true quality of the simulation outputs. In this vein, the MAE metric proves to be a reliable measure, offering a more faithful representation of discrepancies between

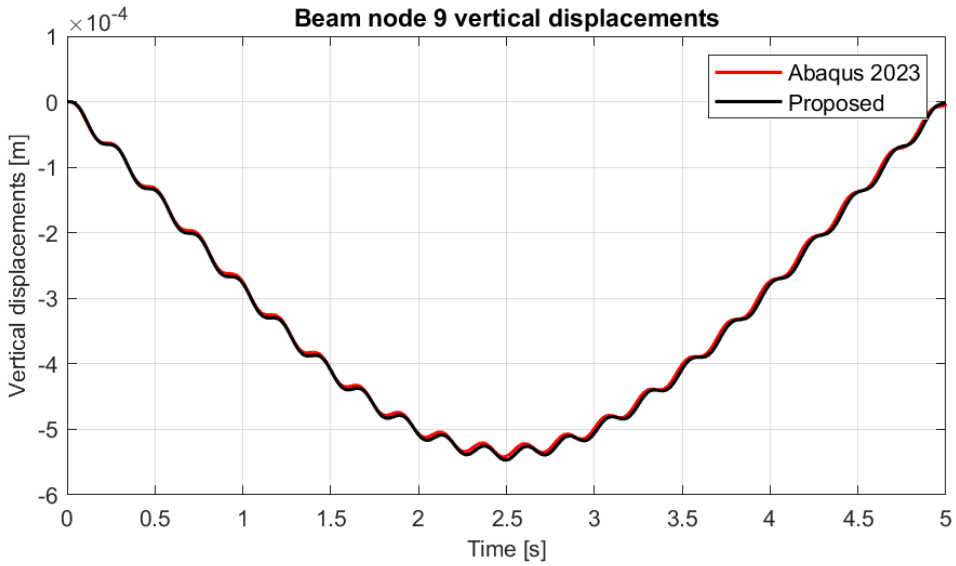

Figure 3.12: Vertical displacements responses of the beam node 9: *Abaqus 2023* Vs. Proposed.

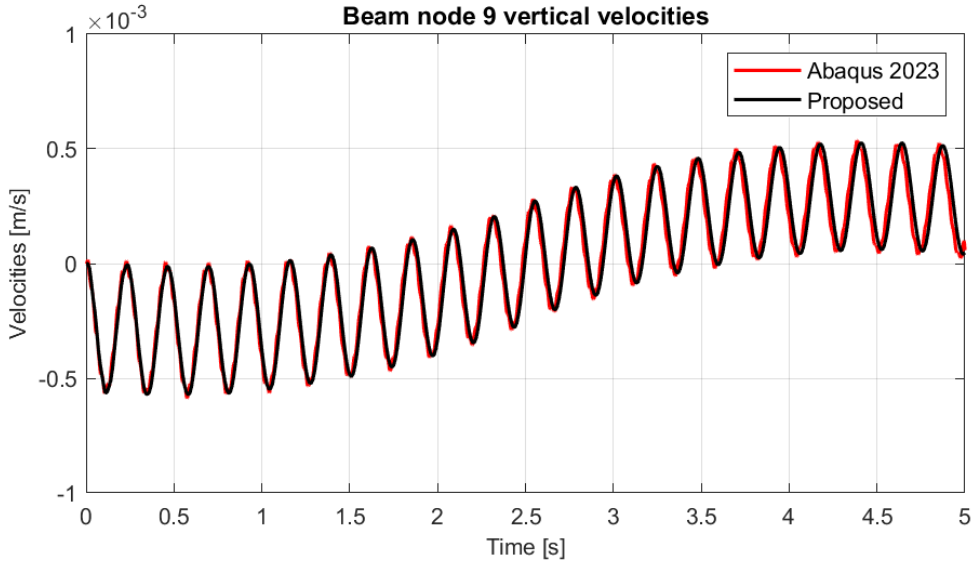

Figure 3.13: Vertical velocities responses of the beam node 9: *Abaqus 2023* Vs. Proposed.

modeled and benchmarked values, thereby reinforcing the importance of critical metric selection in computational modeling studies.

In this section, as in the previous one, our analysis further encompasses the frequency domain outcomes of accelerations linked to nodes 3 and 9, alongside those recorded from the vehicle traversing the beam structure. This juxtaposition importantly highlights the discrepancy in sampling frequencies arising from the numerical simulations conducted with the two distinct software tools. This variation in frequencies is primarily attributed to the model convergence peculiarities within *Abaqus 2023*, which necessitates a time/step that is markedly tenfold smaller than that employed in *Ghost*. As a direct consequence, to align the datasets for a coherent frequency analysis, a downsampling procedure by a factor

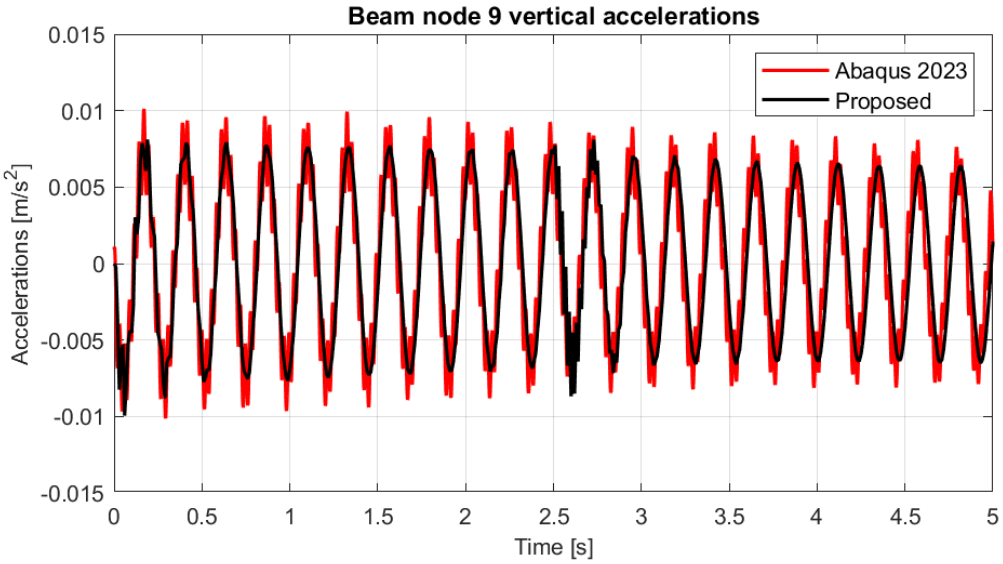

Figure 3.14: Vertical accelerations responses of the beam node 9: *Abaqus 2023* Vs. Proposed.

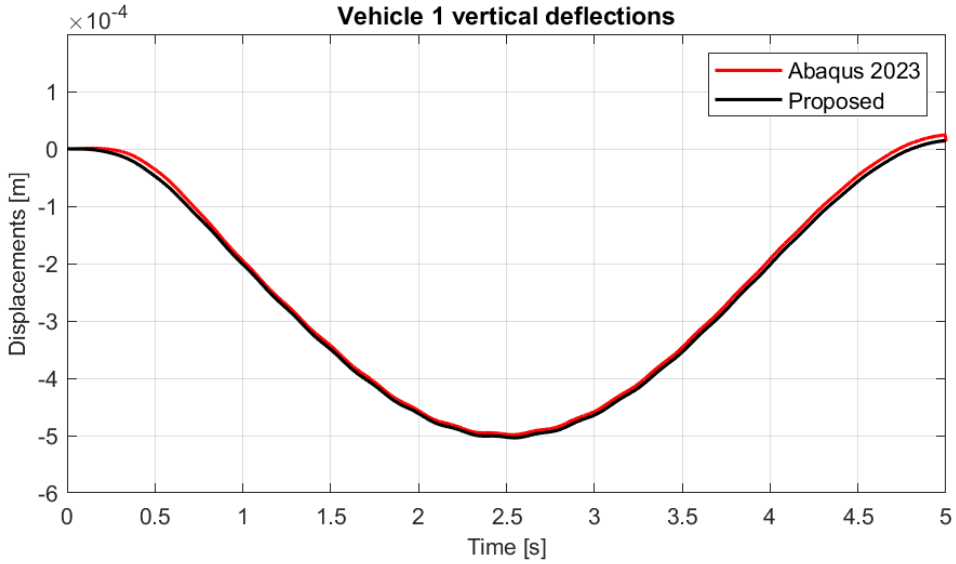

Figure 3.15: Vertical displacement responses of the moving quarter-car model: *Abaqus 2023* Vs. Proposed.

of 10 was imperative before initiating the FFT processes in *matlab*. This step ensures a uniform count of time points across the datasets, facilitating accurate computation of the error metrics such as MAR, MRSE, and NMRSE. The emphasis on acceleration measurements within the models is deliberately chosen, echoing the common practice in dynamic experimental campaigns. These acceleration data are not only frequently utilized but also exhibit minimal influence from the driving frequency effect, an aspect that will be elaborately discussed in chapter 7.

It's noteworthy, as highlighted in the previous section, that the Fourier spectra are presented in decibels to accentuate the differences between the responses. However, the error

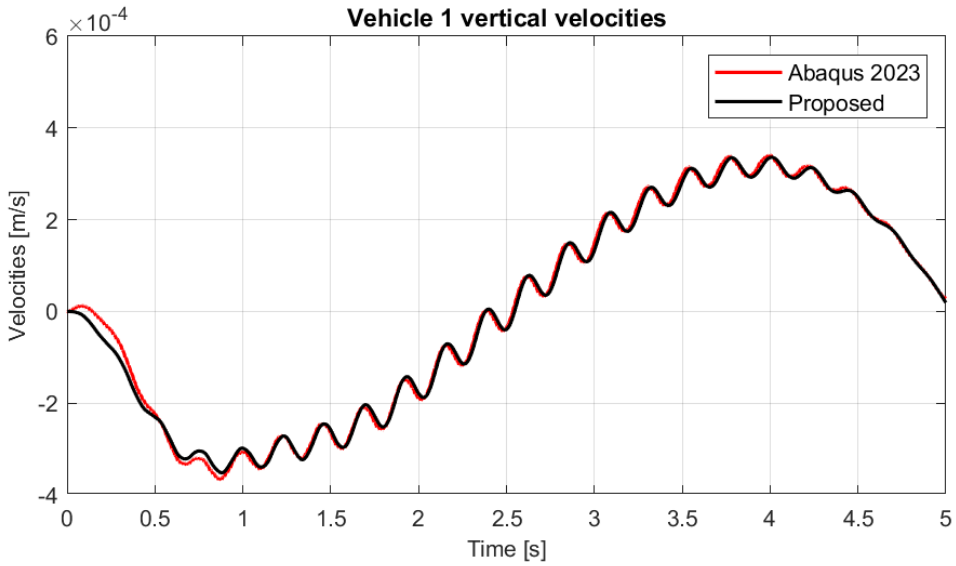

Figure 3.16: Vertical velocity responses of the moving quarter-car model: *Abaqus 2023* Vs. Proposed.

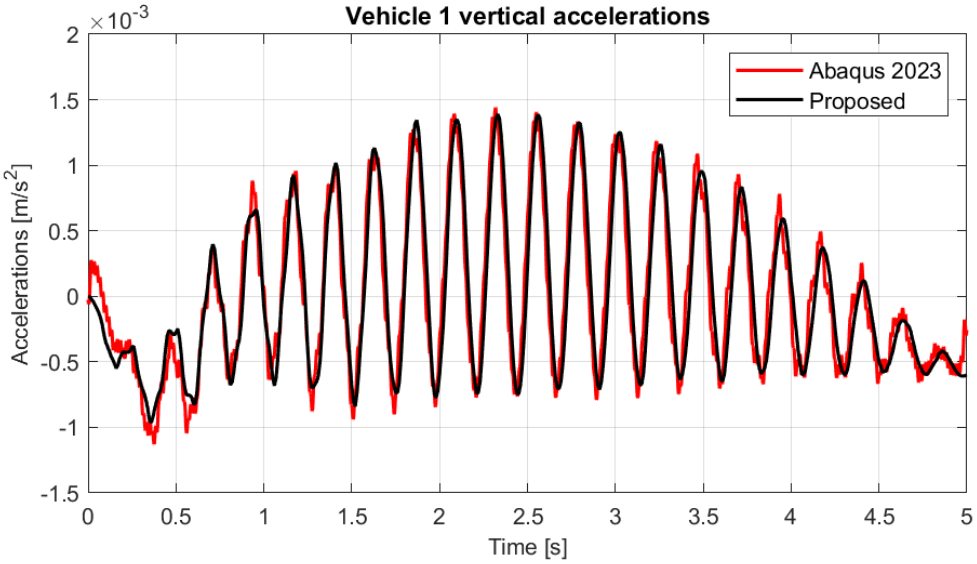

Figure 3.17: Vertical acceleration responses of the moving quarter-car model: *Abaqus 2023* Vs. Proposed.

metrics detailed in table 3.5 rely on the amplitude responses of the spectra to avoid exaggerated NRMSE errors due to the normalization process. As shown in figs. 3.18 and 3.19, which illustrate the spectra for vertical and torsional accelerations at the midpoint control point, there's a commendable match, particularly for vertical accelerations. Nonetheless, in terms of accelerations, significant differences are identified, largely due to the kinematic coupling enforced at the beam's midpoint for the torsional degrees of freedom. This discrepancy is further underscored in table 3.5, where the associated errors are documented. Moreover, it's essential to consider that in testing scenarios focused on the accelerations of the examined structural element, the critical measurements should emanate from the

Node 3 MAE					
Vertical displacement $[m]$	Vertical velocity $[m/s]$	Vertical acceleration $[m/s^2]$	Torsional rotation $[rad]$	Torsional velocity $[rad/s]$	Torsional acceleration $[rad/s^2]$
1.03e-05	5.17e-05	2.10e-03	6.26e-06	5.70e-06	5.78e-05
Node 3 RMSE					
Vertical displacement $[m]$	Vertical velocity $[m/s]$	Vertical acceleration $[m/s^2]$	Torsional rotation $[rad]$	Torsional velocity $[rad/s]$	Torsional acceleration $[rad/s^2]$
2.27E-04	1.31E-05	2.49E-04	1.40E-04	1.31E-05	3.97E-05
Node 3 NRMSE					
Vertical displacement [%]	Vertical velocity [%]	Vertical acceleration [%]	Torsional rotation [%]	Torsional velocity [%]	Torsional acceleration [%]
50.76	1.26	1.22	174.24	0.06	4.81
Node 9 MAE					
Vertical displacement $[m]$	Vertical velocity $[m/s]$	Vertical acceleration $[m/s^2]$			
7.03e-06	5.20e-05	1.90e-03			
Node 9 RMSE					
Vertical displacement $[m]$	Vertical velocity $[m/s]$	Vertical acceleration $[m/s^2]$			
1.55e-04	1.33e-05	2.49e-04			
Node 9 NRMSE					
Vertical displacement [%]	Vertical velocity [%]	Vertical acceleration [%]			
28.86	1.21	1.29			

Table 3.2: MAE, RMSE and NRMSE for the node 3 and 9 reported in numerical benchmarks presented in chapter 3.

behavior of node 9 or nodes situated near the structural element's physical edges. This assertion is confirmed upon reviewing both the graphical representations (fig. 3.20) and the error assessments in table 3.5, demonstrating that the beam element's performance sufficiently mirrors the simulations executed in *Abaqus 2023*, specifically through the incorporation of shell elements. This level of precision and effectiveness is also mirrored in the benchmark analyses conducted on the vertical acceleration responses recorded from

Vehicle MAE		
Vertical displacement $[m]$	Vertical velocity $[m/s]$	Vertical acceleration $[m/s^2]$
1.03e-05	1.16e-05	2.57e-04
Vehicle RMSE		
Vertical displacement $[m]$	Vertical velocity $[m/s]$	Vertical acceleration $[m/s^2]$
2.30e-04	4.49e-05	2.45e-05
Vehicle NRMSE		
Vertical displacement [%]	Vertical velocity [%]	Vertical acceleration [%]
44.36	6.43	1.00

Table 3.3: MAE, RMSE and NRMSE for the idealized vehicle reported in numerical benchmarks presented in chapter 3.

Reaction MAE	
Vertical reaction $[kN]$	Torsional moment $[kNm]$
1.40e-02	7.95e-02
Reaction RMSE	
Vertical reaction $[kN]$	Torsional moment $[kNm]$
2.79e-01	1.69e+00
Reaction NRMSE	
Vertical reaction [%]	Torsional moment [%]
14.53	14.47

Table 3.4: MAE, RMSE and NRMSE for the beam-end reaction reported in numerical benchmarks presented in chapter 3.

the moving vehicle (fig. 3.21 and table 3.5), where the error metrics evaluated in the study are remarkably low. This consistency across various metrics and conditions underscores the robustness and applicability of our computational model in capturing the dynamic behavior of bridges, further validating the use of these specific error indicators in the assessment of numerical simulations.

The preceding numerical analysis furnishes us with insightful conclusions regarding the beam model's fidelity compared to the shell model. Illustrated in the foregoing chapters, the beam model adeptly encapsulates the dynamic behaviors inherent in the three-dimensional model, wherein contact elements delineate the interplay between two distinct subsystems. Observations at the beam's midpoint reveal a quite good alignment of dy-

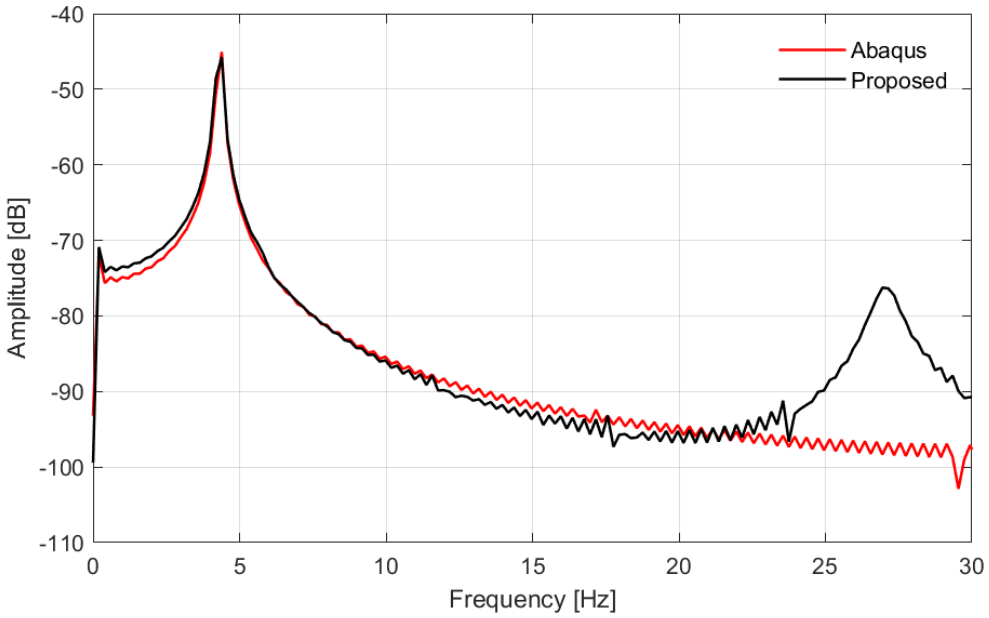

Figure 3.18: FFT of the vertical acceleration for the node 3: *Abaqus 2023* Vs Proposed.

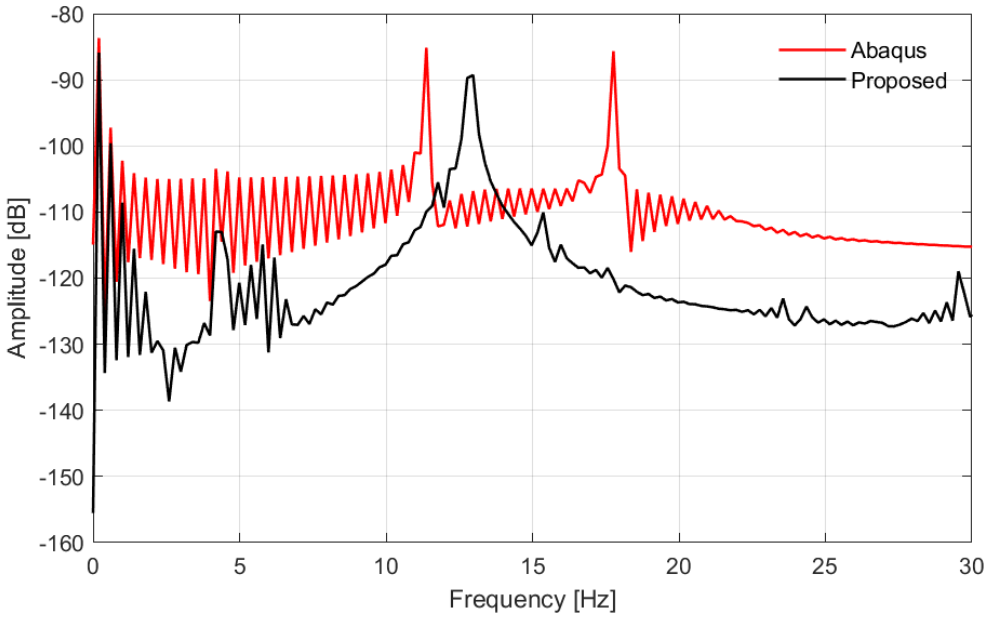

Figure 3.19: FFT of the torsional acceleration for the node 3: *Abaqus 2023* Vs Proposed.

namic responses across these subsystems, even though differences can be noticed especially for the torsional degree of freedom. Much better results are noticeable for the node 9, despite the disparities in finite element counts and the pronounced difference in degrees of freedom, underscoring the beam nodes' displacement, velocity, and acceleration responses as sufficiently precise to mirror the sought quantities. Notwithstanding the contained variations, particularly concerning torsional accelerations as highlighted in fig. 3.6, these

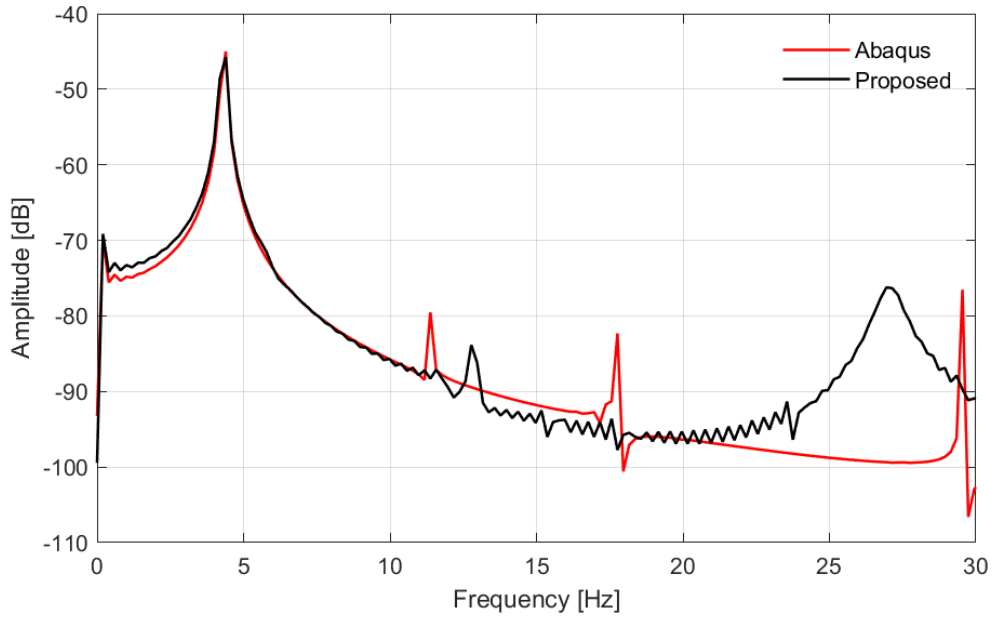

Figure 3.20: FFT of the vertical acceleration for the node 9: *Abaqus 2023* Vs Proposed.

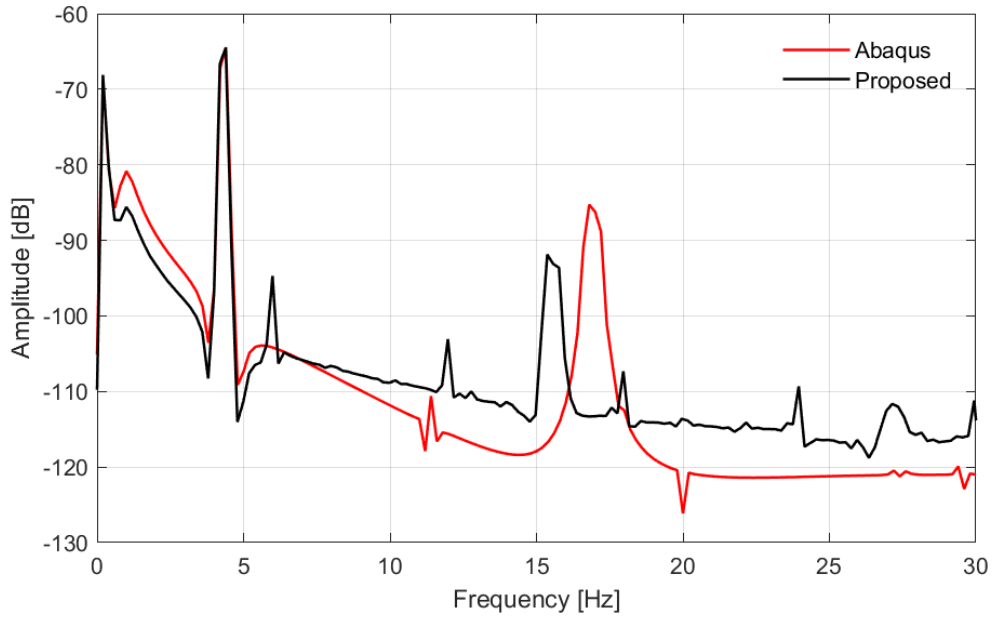

Figure 3.21: FFT of the vertical acceleration for the vehicle: *Abaqus 2023* Vs Proposed.

discrepancies largely stem from the numerical strategies employed in *Abaqus 2023*. Specifically, the impositions at the beam's mid-span exhibit notable peaks coinciding with the vehicle's traversal over that segment. Conversely, the end reactions of the beam provide a response estimate particularly beneficial for fatigue analyses of bridge structures. This aspect becomes paramount when considering numerical simulations aimed towards a big data framework, where achieving a robust model capable of describing a mechanical system

Node 3 vertical accelerations					
MAE	4.06e-05	RMSE	1.52e-04	NRMSE [%]	2.73
Node 3 torsional accelerations					
MAE	2.64e-06	RMSE	2.99e-05	NRMSE [%]	46.12
Node 9 vertical accelerations					
MAE	4.00e-05	RMSE	2.22e-04	NRMSE [%]	3.96
Vehicle vertical accelerations					
MAE	3.04e-06	RMSE	1.03e-05	NRMSE [%]	1.72

Table 3.5: MAE, RMSE and NMRSE for the Fourier spectra in terms of accelerations of the node 3, the node 9 and the vehicle.

with a minimized degree of freedom count stands as a notable advantage for numerical simulation. Moreover, the dynamic responses elicited from the vehicle, particularly through the quarter-car model, align commendably with the proposed framework's simulations in *Abaqus 2023*. While a perfect concordance between the two systems' dynamic responses, given their complexity and spatial resolution differences,remains unattainable, the essence lies in devising a numerical methodology capable of overarching the mechanical behaviors of structural elements. This methodology simplifies and scales different levels without directly incorporating any local effects, which are inherently visible at a microscale. Additionally, the beam model's minor computational demand, coupled with the simplicity of its elements, resonates well with the objectives set forth in this work. Beyond the demonstrated robustness and computational efficiency of the beam model, it's imperative to accentuate the practical ramifications of these insights. The model's ability to authentically represent complex mechanical systems' dynamic behaviors with fewer degrees of freedom presents substantial practical benefits, streamlining computational efforts and enabling broader simulations and analyses within manageable timelines. The congruence between the dynamic responses of the quarter-car model and the *Abaqus 2023* simulations further cements the proposed framework's reliability and applicability. This synergy bolsters confidence in the model's utility for informing real-world considerations pertinent to bridge design, vehicle dynamics, and structural evaluations. Collectively, these insights position the beam model as an invaluable asset in numerical simulation domains for complex mechanical systems, offering a pragmatic solution to reconcile computational efficiency with modeling precision.

Chapter 4

Vehicle-Bridge Interaction and Traffic Related Effects Definition

In the context of bridge-vehicle interaction analysis, despite the large amount of work presented by various scholars over time, it is clear that some points still remain insufficiently explored. Among these areas of uncertainty, the problem of calibrating the mechanical quantities to be associated with dynamic models representing vehicles certainly lies. In this regard, it should be noted that there are numerous models that have been used over time to perform finite simulations of the interaction problem between vehicle and structure. Obviously, it should be highlighted that the choice of one dynamic model over another also derives from the type of analysis to be performed. Indeed, the goal and the phenomenon to be investigated are critical. In this regard, it is straightforward to understand how, for detailed analysis carried out on a single vehicle to understand how the vehicle and the structure behave, it is possible to detail in a meticulous manner different mechanical particulars of the considered vehicle, also exploiting three-dimensional models that have a high computational cost. This choice is partly also due to the fact that such analyses are usually transient analyses which are short in terms of duration and can therefore be resolved, with implicit and explicit algorithms relying on rather small time-steps. Whereas, in the case where the main focus is the study of the interaction of multiple vehicles on a structure or traffic scenarios, or still perform numerical analyses that require prolonged simulations over time, it is not convenient to use complex models, but it would be necessary to have the dynamic model that can return the information of interest with the least number of degrees of freedom so as not to heavily impact the computational cost. Several models have been proposed in the literature to perform such types of analysis in addition to the already mentioned models with concentrated forces and moving masses on the bridge. The first studies in the field presented simple models like the so-called sprung-mass model as in the case of T.Dahlberg et al. [19], who, driven by the development of high-speed trains, performed a parametric study where they exposed all the limits concerning the approach to moving forces and moving masses in favor of a simplified dynamic model like the quarter-car model. They essentially highlighted how as the mass ratio between bridge and structure in favor of vehicles increases, the aforementioned approaches lose accuracy, hence the need to move towards modeling centered on simplified dynamic models. A few years later, P.K. Chatterjee et al [119] proposed a comparative study on three different dynamic models. The first model is a simple quarter-car model characterized by a single vertical degree of freedom, the second model is two-dimensional made up of multi-axial spring and friction devices under each axis of the vehicle, while the third vehicle is the natural extension of the two-dimensional model as it develops in its three-dimensionality incorporating the rotation of the vehicle along its rotational axis together with pitching.

In the same direction subsequently went the studies of Y.B. Yang et al. [36], where the researchers analyzed the differences in dynamic responses due to quarter-car and half-car models and various compositions of these. Although, these studies were aimed and developed for high-speed trains, it will then be the basis for the same research group in the automotive field both for direct and indirect methods. The implementation and the study of new vehicle models aimed at Vehicel-Bridge Interaction is certainly the one from N.Liu et al. [33] who expanded the half-car model where the suspensions are modeled with a double dashpot-spring system to take into account the dissipative effect and stiffness of the tires in such type of simulations. However, it should be noted that the results obtained by adding such devices are very similar to the classic solution of the half-car model. Subsequently, N.Zhang et al [32] described the vehicle-bridge interaction exploiting a particular vehicle model capable of representing the three-dimensional behavior of the system considering a complex model where masses, springs, and dampers are composed to return a complex system characterized by 33 degrees of freedom. The classic quarter-car and half-car models were again taken up and developed further by the work of T. Xiang et al. [123], in these representations the authors interposed an additional mass between the contact element with the road pavement and the upper mass representing the vehicle itself to include the effect of the suspension mass in the analysis. Subsequently, the half-car model was further modified by the study of S.H. Ju et al. [124] who introduced in the analysis the longitudinal contribution due to the speed variations of vehicles, to perform such a study and therefore to take into account the phenomenon, the scholars added a spring-dashpot system in the direction of the longitudinal axis of the vehicle that connects the suspensions to the upper mass of the system. In this way, it is possible to consider in the analysis also the contribution of longitudinal forces due to acceleration and deceleration actions. At the beginning of the new century, along with the idealized dynamic models for the characterization of vehicles, the development of models characterized by three-dimensional elements in finite element software also continued, in this sense it is obvious to cite two works due to Q.Li et al. [42] and J.Oliva et al. [125] who exploited two commercial software to model all the motion acts of the moving vehicle on the beam. In particular, the work of J. Oliva et al. focused more on the introduction and characterization of the dynamic response in the presence of disturbance phenomena such as asphalt roughness. In this work, there are multiple interesting aspects ranging from the multibody modeling of the problem that takes place at this juncture by exploiting the contact between the two subsystems through a technique derived from the use of Lagrange multipliers. Moreover, to achieve their purposes, the scholars developed a new technique aimed at simulating the road profile, to introduce the roughness of the asphalt into the dynamic problem. This method is based on the coherence function, through which it was possible to extract and model two parallel roughness profiles of the asphalt. In this condition, excellent results were obtained both from the point of view of the vehicle-structure interaction model and from the point of view of generating roughness profiles. The development of vehicle-structure interaction models continued, from the mechanical models' perspective, with the work of H. Zhong et al. [126], in which the authors aimed at the interaction between moving vehicles and bridges made of pre-stressed concrete by observing and simulating the interaction with different mechanical vehicle models ranging from the quarter-car model to the half-car model moving on the structure. Moreover, a three-dimensional model of the vehicle was then considered by H.Yu et al. [127], who exploited a combination of two commercial software to perform parametric studies on the effects that the speed of vehicles has on the dynamic response of the bridge using three-dimensional models directly derived from the half-car model, which is characterized by 12 degrees of freedom. More recent activities, concerning dynamic models to be associated with vehicles can finally be found in

the works of Z.Shi et al. [128] and S.S.Eshkevari et al. [129] who developed and analyzed the quarter-car model, particularly in the latter work the authors exploited a new modeling concept by adding an additional degree of freedom to the vehicle at the point of contact with the structure, which becomes the real means through which contact with the structure is established. However, it is precisely in this context of research and development that some points of modeling and in particular the calibration remain rather unclear. Indeed, almost all of the works mentioned above do not pay enough attention to the calibration of the mechanical parameters to be associated with the vehicles. This deficiency turns out to be especially crucial when viewed from the perspective of simulations of actual traffic scenarios on structures. Indeed, under such conditions, it is necessary to take into account the random nature of vehicular traffic, which manifests not only in the quantity of vehicles or their frequency of crossing a structure but also in the diversity of vehicles and therefore their mechanical quantities. In this regard, it is possible to refer to the scientific literature also to analyze how such a phenomenon is normally investigated. There are various models proposed in the literature, which can be used depending on the scale of observation used in this kind of analysis. Specifically, there are models known as microscopic modeling, which corresponds to the modeling of the individual vehicle [130, 131] under the actions of the surrounding vehicles; a statistical framework that consists in the determination of a law of evolution of the phenomenon for the definition of the distribution function on the position and speed of vehicles. Opposite to microscopic modeling, there is macroscopic modeling, a discipline that draws inspiration from fluid dynamics and aims at deriving functional relations for the description of mass densities, linear momentum, and energy. Among the just mentioned frameworks, the one that seems to be most effectively implementable in the context of the numerical simulations presented in this work is certainly the stochastic framework, which allows deriving functions to be associated with vehicles. In this context, it is therefore possible to pursue two approaches: the first purely statistical, of which various applications are known, such as C.C. Minguillon et al. [132] where the authors through a statistical treatment of the variables involved in the phenomenon presented a theoretical model for the development of continuous simulations of traffic flow. Or the works of P.Croce et al. [133] where the authors tried to overcome the problems of local applicability of statistical theories referring to an approach based on the renewal process, which allowed not only to effectively model the traffic phenomenon but also to predict and understand when it is possible to encounter interruptions in the flow of traffic. However, this is not the only approach present in the literature, and among the various, it is certainly worth mentioning the work of R.Mahnke et al. [134] where the authors developed a methodology called probabilistic traffic flow theory based on the stochastic one-step process of growth and shrinkage of a car cluster. A further attempt at estimating traffic parameters was subsequently carried out by L. Cao et al. [135] where the authors developed software based on a Montecarlo algorithm that produced excellent results when compared to real traffic data. Alongside the stochastic methods, it is possible to find another approach that is based on data acquisition from Weigh In Motion platforms capable of providing static distributions of gross weight and velocities of vehicles [136–138]. This technique turns out to be probably the most effective to be implemented in a code provided that traffic data are available. However, even if traffic data are available, this does not guarantee the complete calibration of the mechanical model from which the vehicles are schematized. Indeed, the only mechanical quantities that can be obtained are those just mentioned, and there is no information on the mechanical apparatus of vehicles, such as, for example, suspensions stiffness or damping, and therefore it is impossible to calibrate the mechanical units of which vehicles are composed. Moreover, besides the mechanical characteristics of vehicles, the effects of the interaction between

vehicle and structure, especially in some contexts, cannot disregard the introduction of some disturbance phenomena such as, for example, asphalt roughness, which obviously can be included in the framework referring to different methodologies. In the following treatment, reference will be made to the most used method in the literature, namely the ISO 8606 standard, which allows determining the profile based on some provided parameters, as will be discussed later. But this methodology is indeed not the only one available in the literature. Among the various works available, we can mention, for example, [139] where two different profile generation models are proposed based on two theories, namely, non-homogeneous Laplace process, a hybrid model that combines Gaussian and Laplacian modeling. These profiles are compared with the classic Gaussian methods that represent the most used approach in practice. A technique based always on the Gaussian theory but modified was also introduced by P. Johannesson et al. [140]. The proposed model is locally Gaussian with randomly gamma-distributed variances leading to a generalized Laplace distribution of the road profile. Other methods of generating road profiles can be found in S.Turkay et al. [141] where two different methods are illustrated that have comparable results in terms of effectiveness, one based on measurements in the time domain and on the empirical auto and cross power spectral densities estimated with the Welch method, and the second method is a multi-input/multi-output subspace-based identification algorithm which employs spectral decomposition to derive the spatial domain. In conclusion, traffic simulations need to capture the various facets of the phenomenon. As a matter of fact, traffic is comprised of random events, and this randomness needs to be included in all numerical frameworks developed to deepen the discipline. However, traffic and its related phenomena are not immutable and evolve at the same pace as technological advancements. Indeed, both traffic volumes and traffic loads have increased over the years, and despite the obvious socio-economic benefits, several problems have arisen that need to be addressed. The historical context of traffic evolution, marked by changes in vehicle technology and urban expansion, provides insight into current challenges. As urban centers grow, the environmental impact of traffic becomes a pressing concern, with issues like air and noise pollution and effects on local ecosystems gaining prominence. Advancements in technology and materials have revolutionized bridge design, offering potential solutions to the challenges posed by heavier traffic loads. In this context, the role of policy and urban planning becomes crucial. Effective urban planning can significantly impact traffic flow and the sustainability of infrastructure development, often incorporating initiatives to reduce congestion and promote greener modes of transport. Furthermore, the intersection of big data analytics and artificial intelligence in traffic management opens new avenues for optimizing traffic flow and predicting infrastructural stress points. Smart traffic management systems, which adapt in real-time to changing conditions, are at the forefront of this technological revolution. Case studies from around the world illustrate how these principles have been applied in different contexts, providing practical insights into the challenges and successes of managing traffic and its impact on infrastructure. Looking to the future, challenges such as the integration of autonomous vehicles into existing traffic systems present both opportunities and hurdles. The potential for more resilient and adaptive infrastructure designs is an exciting prospect, but it comes with its own set of complexities. Moreover, the implications of traffic flow and bridge integrity extend beyond mere structural considerations. They play a crucial role in public safety and emergency response. Understanding traffic patterns and bridge behavior under various scenarios is vital for disaster preparedness and effective response strategies. In the following chapter, a new method will be presented to obtain in an automatic and rational manner an estimate of the mechanical parameters to be included in the definition of models for vehicle simulation. This methodology is aimed at reducing the theoretical gap existing in the

definition of the parameters of interest and that often is not treated with the adequate importance in the literature. The main goal, therefore, translates into the definition of a rational procedure to be applied to simulations aimed at representing traffic scenarios. As a matter of fact,this section delves into the development of a robust method to define the mechanical and geometrical vehicle characteristics in a structured manner, exploiting existing databases. We will also explore classical methods to introduce and simulate road profiles for a realistic approximation of road roughness in analyses. These approaches are numerically implemented in *Ghost project* to perform comprehensive numerical analyses aimed at representing Vehicle-Bridge Interaction accurately. By considering these multifaceted aspects, the chapter aim to provide a comprehensive view of the dynamic and complex relationship between traffic, infrastructure, and the environment and their calibration in the numerical framework.

4.1 Quarter-car model: vehicle definition

Quarter-car models are a simplified dynamical system which among many other mechanical models can be implemented to describe the mechanical behaviour of a vehicle axle. They can be also visualized as an oscillator composed of two masses connected by a spring-dashpot system. Obviously, the upper mass represent the vehicle mass, the spring-dashpot system represent the suspension apparatus and the lower mass can be indented as the wheel mass or as a mere connection point with the structural system. Despite its degree of freedom is the vertical one, which activate the vertical response forces of the system and its motion takes place along the beam axes, in the investigated case, at constant velocity. Moreover, a single vehicle is usually composed by two or more axles which maintain the same reciprocal distance along the ride. Hence, a vehicle can be intended as a succession of a series of quarter-car moving at the same velocity characterized by a null relative displacement along the beam axes, as show in fig. 4.1.

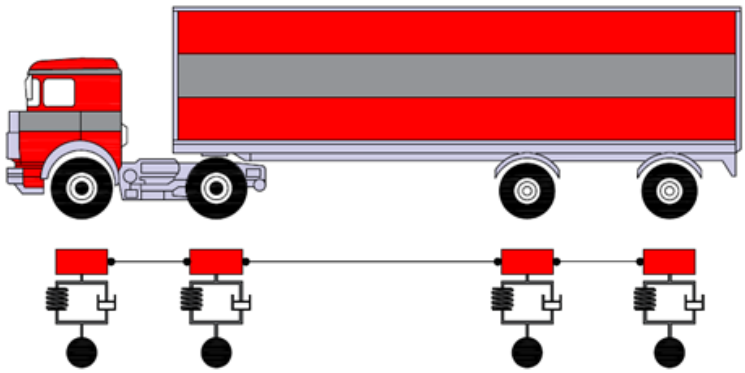

Figure 4.1: Vehicle idealization as a succession of quarter-car models.

In such a condition, it is necessary to obtain the values of each mechanical values associated to each employed quarter-car. Moreover, apart from the mechanical characteristics of the axles is crucial to retrieved both the velocity to be associated with a single vehicle and the mutual distance between two consecutive vehicles. Hence, being able to obtain in a smart and appropriate manner all the cited quantities is the minimal requirement to depict a good picture of the traffic phenomenon to be introduced in the numerical simulations. Unfortunately, is not an easy ride to obtain all the desired quantities to introduce

in the vehicle description. Although, some mechanical aspects, such as the gross mass of a truck, are easily to understand, others such as the velocity or the mutual distances can be deduced from some legal limits, meanwhile other mechanical quantities are almost impossible to be a-priori known. For instance, the stiffness parameters of the suspension apparatus often are not an immediate available data as well as the damping constants. However, is not all unknown. Indeed, it possible to exploit the existence of the so-called Weigh In Motion database, some of which are available. Weigh In Motion systems have emerged as a transformative technology in the realm of transportation engineering, revolutionizing the way to monitor and manage the dynamic characteristics of moving vehicles. At the core of these systems lies a sophisticated integration of advanced sensor technologies and intricate data processing methodologies, collectively contributing to a more efficient and intelligent approach to traffic management. The fundamental principle of Weigh In Motion systems revolves around the concept of non-intrusive measurement. Advanced sensors, including load cells and piezoelectric sensors, are strategically embedded in the road surface. These sensors detect and measure the forces exerted by vehicles as they pass over, providing real-time data without necessitating any interruption to the flow of traffic. This non-disruptive nature is a key advantage, as it allows for the seamless integration of Weigh In Motion systems into existing road infrastructure. One of the primary objectives of Weigh In Motion systems is the accurate measurement of key parameters associated with moving vehicles. Vehicle weight, axle load, axle spacing, and speed are among the critical metrics captured by these systems. The accuracy of these measurements is paramount, as they form the basis for a multitude of applications, ranging from ensuring compliance with weight regulations to informing infrastructure design and maintenance decisions. The technology employed in Weigh In Motion systems extends beyond the physical sensors to the intricate realm of data processing and analysis. Collected data from the sensors is transmitted to a central control unit, where it undergoes a series of complex algorithms and computations. This processing stage is crucial in transforming raw data into actionable insights. The result is a comprehensive understanding of traffic patterns, weight distributions, and the overall utilization of road infrastructure. This wealth of information proves invaluable in making informed decisions that enhance the efficiency and safety of transportation networks. Weigh In Motion systems are not a one-size-fits-all solution; they come in various typologies, each designed to cater to specific scenarios and requirements. In-road sensor systems, for instance, involve the integration of sensors directly into the road surface, providing continuous and uninterrupted monitoring. Portable Weigh In Motion systems, on the other hand, offer a level of versatility that allows for temporary deployment, making them ideal for research studies, special monitoring projects, or temporary weight enforcement zones. High-speed and low-speed Weigh In Motion systems address the diverse speed limits encountered on different types of roadways. High-speed systems are optimized for highways and expressways, where vehicles travel at elevated speeds. In contrast, low-speed systems are tailored for urban environments or areas with lower speed limits, ensuring accurate measurements even in slower traffic conditions. The significance of Weigh In Motion systems extends beyond immediate applications, contributing to broader objectives within the transportation landscape. By eliminating the need for vehicles to stop at traditional weigh stations, Weigh In Motion systems enhance traffic flow and reduce congestion. This not only improves the overall efficiency of transportation logistics but also minimizes fuel consumption and decreases wear and tear on road infrastructure. They represent a paradigm shift in transportation engineering, blending technological innovation with practical applications. With their non-intrusive approach, diverse typologies, and intricate data processing capabilities, Weigh In Motion systems stand as a cornerstone in the pursuit of safer, more efficient, and sus-

tainable transportation networks. The ongoing evolution of this technology holds promise for further advancements, shaping the future of how we monitor and manage the dynamic aspects of vehicular traffic on our roadways. By exploiting this robust framework is than possible to tune a numerical procedure to obtain the interested parameters from this data. However, the definition of some characteristics, such as the the stiffness coefficients and the damping parameters to be mapped to the dynamical vehicle models cannot be retrieved easily, but other technique need to be involved. Nevertheless, it is still possible to exploit the data deriving from this equipment to developed the desired algorithm. They global aim to is define a procedure to retrieved all the required mechanical parameters from the available data. Usually, the Weigh In Motion database available are able to describe by a statistical means the typology, the number of axles and their reciprocal distance and the associated velocity of a truck. Unfortunately, often car vehicle are not included in the data because their weight can be not sufficient to trigger the sensors or are intentionally discarded. However, it is possible to develop the procedure for the truck and then expand that to vehicles.

Pseudo-code of the developed algorithm aimed to quarter-car calibration can be found in fig. 4.2. Once, that the probability distribution of the masses associated with each axle of the quarter-car are known, the selected value of mass m_{vi} can be introduced in a simple computation to obtain the associated stiffness value. As a matter of fact, the suspension system are calibrated and designed in order to ensure an adequate comfort to vehicle passengers, that allows the definition of a frequency range which can be represented as [142]

$$f_{min} = 0.5\ Hz \qquad f_{max} = 1.5Hz \tag{4.1}$$

this frequency range is able to return an upper and a lower limit, to be associated with the stiffness k_{vi} of quarter-car once the mass value is known, indeed by mean of a simple relation

$$\begin{aligned} k_{vi,min} &= m_{vi} \cdot (2\pi f_{min})^2 \\ k_{vi,max} &= m_{vi} \cdot (2\pi f_{max})^2 \end{aligned} \tag{4.2}$$

the value to be associated with the stiffness of the i-th quarter-car model, can be extrapolated by mean of a uniform $\mathcal{U}_{[k_{vi,min},\, k_{vi,max}]}$ distribution where the lower and the upper bound are respectively $k_{vi,min}$ and $k_{vi,max}$. The remaining parameter to be addressed from a quarter-car perspective is the damping coefficient which is related to the dashpot of the suspension system, that is c_{vi}. This can be found by means of relation [143]

$$c_{vi} = \beta_i \cdot c_{i,cr} = 2 \cdot \beta \cdot m_{vi} \cdot \omega_i \tag{4.3}$$

where thee quantity $c_{i,cr}$ refers to the critical damping, which is function of the i-th vehicle mass m_{vi} and the undamped circular natural frequency of the quarter-car model ω_i. Moreover, the β parameter is a constant, which can varies from a restricted interval, featured with a lower bound of 0.2 and an upper bound of 0.6. Thus, it can be also be obtained assuming and uniform distribution $\mathcal{U}_{[0.2,\, 0.6]}$. In order to complete the calibration of the heavy vehicles, is necessary to consider the velocity v_i and a mutual distance between two consecutive vehicles. Those, if available, can be retrieved directly from the considered WIM database, or can be stated by assuming some hypothesis which are based on the road traffic regulations. As mentioned before, this procedure is directly derived from some

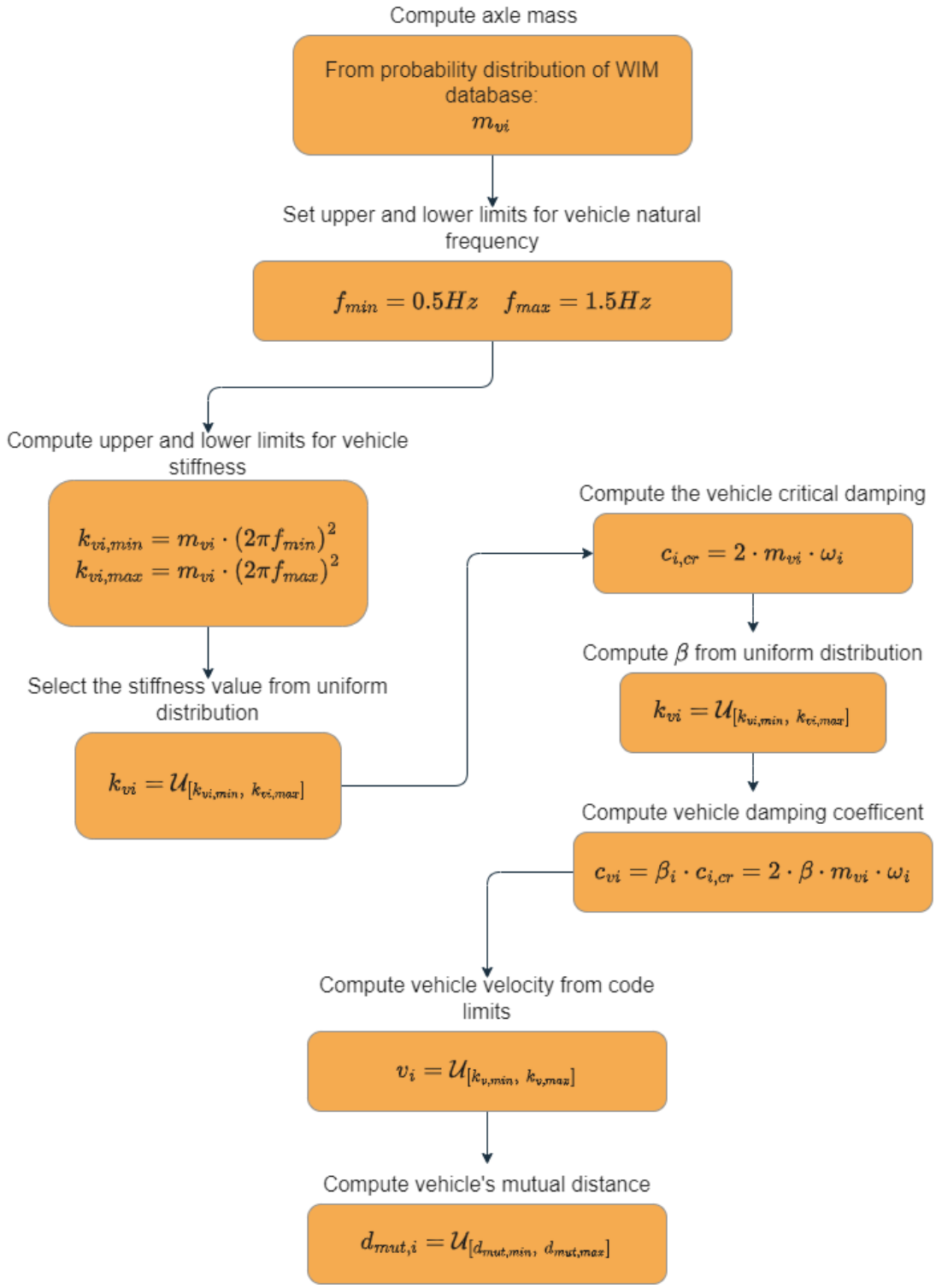

Figure 4.2: Pseudo code vehicle calibration from WIM database.

WIM data where often only truck are measured. Nevertheless, the mass $m_v i$ and the single wheel distance of a standard car could be retrieved, directly from the data make available from the car industries. They unlike the great diversity of the heavy vehicle categories, usually are characterized by a minor variations.

4.2 Road roughness definition

Among all traffic related phenomena, surely the road roughness is something which cannot be neglected. Numerical and experimental studies carried out in the past years have highlighted how severe levels of this quantity can negatively impact the whole numerical analysis or the experimental campaign especially for the case of indirect methods approaches. The road roughness is introduced in the analysis by determining the road profile in stochastic manner. However, to accomplish this objective it is possible to rely on a well known method based on the standard ISO 8608 [144–146]. The latter, classifies the road profiles in eight different categories ranging from A to H as function of the severity of the associated road profile. Herein, class A represents a good road profile, while H indicates the worst conditions. However, it is worth to noticing how for advanced and modern infrastructure the profile can be easily restricted to the C or D class. Indeed, often perform numerical simulation or trying to include profile with a grade H severity seems to be inappropriate for the heavy excitation which is derived. The generation of the numerical road profile is based on the prescribed values of the Power Spectral Density (PSD) (m^3/rad) $\psi_d(n)$ whose value for each angular spatial frequency per meter n (rad/m)might be find as

$$\psi_d(n) = \psi_d(n_0) \cdot \left(\frac{n}{n_0}\right)^{-w} \tag{4.4}$$

here, the profile is treated as a Gaussian random function, which can be fully described by its PSD. In the further analysis, in according to the standard ISO-8608 a constant waviness w equal to 2 is considered. The spatial frequency n is equal to

$$n = \frac{2\pi}{L} \tag{4.5}$$

where L is the wavelength. The prescribed values associated with n_0 and $\psi(n_0)$ are listed in the standard ISO 8608. The value of the constant w in eq. (4.4), which is introduced to describe the wavelength distribution in a certain range spatial frequency bands. The amplitude of the desired road profile for every spatial coordinate x of the investigated beam can be easily be generated by means of

$$r(x) = \sum_{i=1}^{N} R_i \cdot cos(n_i x + \phi_i) \tag{4.6}$$

where the amplitude R_i can be derived from

$$R_i = \sqrt{2 \cdot \psi_d(n) \cdot \Delta n} \tag{4.7}$$

here Δn is the sampling interval of the spatial frequency. Meanwhile, the terms in the cosine argument in eq. (4.6) are respectively the i-th spatial frequency n_i and a random phase angle ϕ_i. Known all the aforementioned quantities it is trivial to generate road profile for the desired road classes. An example of this numerical road generation is reported in fig. 4.3, where three different road profiles are reported, respectively belonging to class A, class B and class C.

Hereby, (fig. 4.3), for the class A and B the geometric mean values for the unevenness index $\psi_d(n_0)$ is selected, meanwhile the upper limit for the last case, that is the class C road

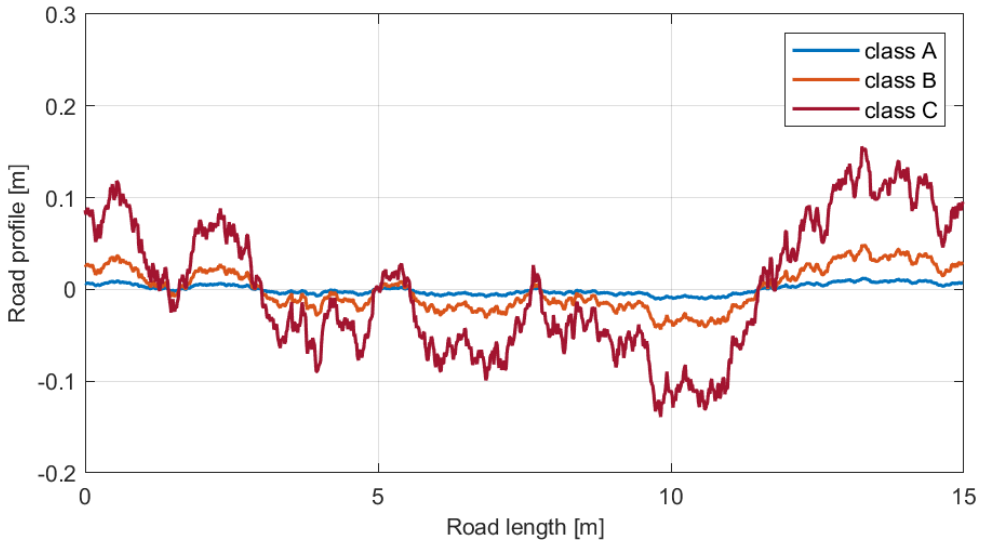

Figure 4.3: Road roughness profile example.

profile is taken into consideration. The road profile generation, is not a secondary aspect in the numerical simulations. As a matter of fact, the sampling interval is a critical aspect since an adequate number of points along the beam need to issued. A coarse spatial subdivision has a very small impact into the numerical time involved in the analysis, especially because the closest point to a moving quarter-car model is identified with some kind of search algorithm. However, if this interval is to coarse it might happen that among two subsequent analysis steps the vehicle could lies on the same point of the profile, leading to a non physical representation of the phenomenon. Obviously, this situation can be avoid calibrating the spatial interval in relation of two analysis parameters, that are the velocity the minimum velocity associated to a vehicle class and the analysis time step involved into the simulation. Hence, the number of spatial coordinate of the beam can be tuned ensuring that at minimum velocity the slowest vehicle doesn't lies on the same profile coordinate for the imposed analysis time step. Moreover, also the profile class choice can influence the dynamical analysis especially if the obtained responses need to be processed with algorithms for other purposes. Indeed, having worst, characterized by higher heights elevations of the road profile increase the excitation level and this might imply unrealistic responses. Moreover, since that this formulation can be seen as the realization of a Gaussian stochastic process, the levels of noise introduced in the analysis, by assuming a defined road profile, can introduce a disturbance in the dynamical output and be impactfull especially in the context of frequency analysis, which are one the most employed methodology for the OMA algorithm.

Chapter 5

Environmental Effects Definition

Bridges and infrastructure, in general, are inherently subject to excitation by various environmental phenomena, such as wind, thermal variations, and other effects that often cannot be neglected. Among all the environmental excitations typically present under operational bridge conditions, this chapter focuses on developing a new user-friendly technique that is easy to implement for incorporating environmental noise into the analysis, as well as the implications of temperature changes that these structures may encounter. It is essential to consider the unique environmental conditions of each location, as these effects are strongly dependent on the local site where the structures are situated. Therefore, a site-specific analysis, which takes into account local geography, climate, and ecosystem, is crucial. The potential integration of advanced sensor technologies and real-time monitoring systems could enhance our understanding and response to these environmental conditions. The use of historical environmental data and predictive modeling plays a significant role in anticipating the long-term effects of environmental factors on infrastructure. A multidisciplinary approach that combines civil engineering with climatology, material science, and data science is advocated to create a more holistic method of structural analysis. This methodologies would obviously influence regulatory standards and building codes, leading to safer and more reliable infrastructure. Public safety implications are paramount, and the importance of sharing these findings with a broader audience, including engineers, policymakers, and the public, is emphasized to foster a culture of informed decision-making. Global case studies where environmental factors have played a critical role in the integrity and performance of bridges are also referenced, underscoring the universal relevance of this research. The main objective of the following chapter is to develop a robust method capable of efficiently reproducing the environmental effects on structures while considering a minimal impact on computational effort and time. Two main aspects are investigated herein. The first is the introduction of environmental noise into the vibration analysis through a calibrated set of equivalent generalized forces, and the second aspect concerns the dynamic effects that a change in temperature can have from a structural perspective. All these environmental agents, together with the calibration discussed in the previous chapter, will later be integrated to carry out numerical simulations aimed at framing various test layouts under different levels of excitation.

5.1 Environmental noise definition

Environmental excitation is often overlooked in numerical simulations, and this can have significant consequences, especially in the context of structures like bridges. In traditional analyses, the focus might be primarily on static or dynamic loads generated by daily use or exceptional events. However, environmental factors such as wind, traffic vibrations,

and even seismic effects are critical to fully understand real-world structural behavior. Integrating environmental excitation into numerical simulations allows for a more accurate assessment of structural performance. For example, considering traffic vibrations enables predicting how the bridge will respond to the passage of vehicles of different sizes and weights. Similarly, incorporating the effects of wind allows evaluating the dynamic response of the structure at different wind speeds and directions. This more holistic approach not only improves the precision of simulations but is also crucial for ensuring the long-term safety and durability of infrastructure. In fact, ignoring environmental excitation could lead to designs that do not account for critical factors, jeopardizing structural stability over time. Moreover, incorporating environmental excitation into numerical simulations not only refines the accuracy of structural assessments, but also extends its application to include the simulation of acquisition systems like operational modal analysis. This broader approach allows for a more comprehensive understanding of how structures respond to real-world conditions and how measurement systems can capture and interpret these responses. It's a step towards creating simulations that mirror the complexity and nuances of actual environmental influences on structures. In numerical simulations, the environmental noise effects can be introduced and modelled in several manners, in fact this environmental excitation is numerically measured and recorded by taking into account its effects in terms of velocity or accelerations. Both of these quantities can be easily introduced in the model as a single point constraints on each beam node. Hence, in accordance with this methodology some sort of boundary condition need to be enforced in the numerical model. Usually, finite element software have several ways to handle single and multi-point constraints, such as the transformation method, the penalty method or the Lagrange multipliers. All the aforementioned, constraint methods exhibit both merits and drawbacks. For instance, the transformation method is a condensation techniques, which involve some matrix manipulation in order to eliminate some degrees of freedom or make them depends from another, which is probably the easiest way to operate, but not always the convenient one. The penalty method doesn't alter in any way the number of active equation in the mechanical problem, but add some penalty factor in correspondence of the degree of freedom of the restrained degrees of freedom. This convenient approach if not employed judiciously can lead to numerical issues due to ill-conditioning of matrices. On the hand hand, the Lagrange multipliers method has the major drawback which is essentially related to the increase in equations in the model as the number of constraints grows. Hence, in the following discussion a force based environmental noise technique is introduced. Here, the environmental noise is introduced in the analysis considering a set of equivalent forces, which needs to be adequately calibrated in order to describe the phenomenon. This approach is numerically beneficial if is compared to the aforementioned ones, indeed does not introduce any additional equation to the analysis, unlike the Lagrange multiplier, nor potentially determine some ill-condition of the matrix or introduce some condensation or elimination in the finite element model. On the other hand, the calibration of both the spatial and temporal description of the loads which need to be applied to the structural element nodes needs to be addressed. With respect to this matter, the ample literature developed in the field of OMA can be exploit. Indeed, the OMA techniques, unlike the EMA counterpart, are essentially based on some assumption, which are made on the environmental noise acting on structures. The fundamental OMA assumption about the analysed system are the linearity, the stationarity and the observability. In this context the environmental noise, under operative condition of a structural artifact, is assumed to be a broadband excitation, which ensure a sufficient excitation of all the modes in the investigated spectrum. Thus, the excitation can be referred the a Gaussian distribution $\mathcal{N}_{[0,1]}$, with zero mean and unitary standard deviation. Moreover, the

levels of environmental noise are often measured by referring to the Root Mean Squared of the acceleration on the structure, which allows to set some ranges to discriminate the so-called *weak ambiental excitation* to the *strong ambiental excitation*. However, this are not well posed or fixed limits because are strongly dependent from the studied structure and the surrounding environment. Common limits for the aforementioned interval are typically 10^{-5} g to 10^{-3} g for weak excitation and over 10^{-3} g for strong environmental excitation [147]. Based on this assumptions, the nodal forces can be calibrated by means of parametric analysis, deriving the force vector as

$$\bar{f}_{ii} = \mathcal{N}_{[0,1]} \cdot \varepsilon \tag{5.1}$$

the force vector $\bar{f}_{ii}$ is characterized by a random function, described by a Guassian distribution, and its amplitudes are determined by ε parameter which is made parametrically change for all the desired values. Thereafter, the components of $\bar{f}_{ii}$ are substituted to the interested degree of freedom ii, such as the vertical, horizontal or torsional one. In this regard, an example of this approach is reported below, where the double-tee beam element is excited with with a set of stochastic forces along the vertical and the horizontal degrees of freedom. The resulting time histories of accelerations for the node place every quarter of the beam length along vertical direction are depicted in fig. 5.1. The duration of the entire analysis is taken equal to 250 s, which respect the minimum registration for modal analysis purposes, typically taken as thousand times the fundamental period of the structure.

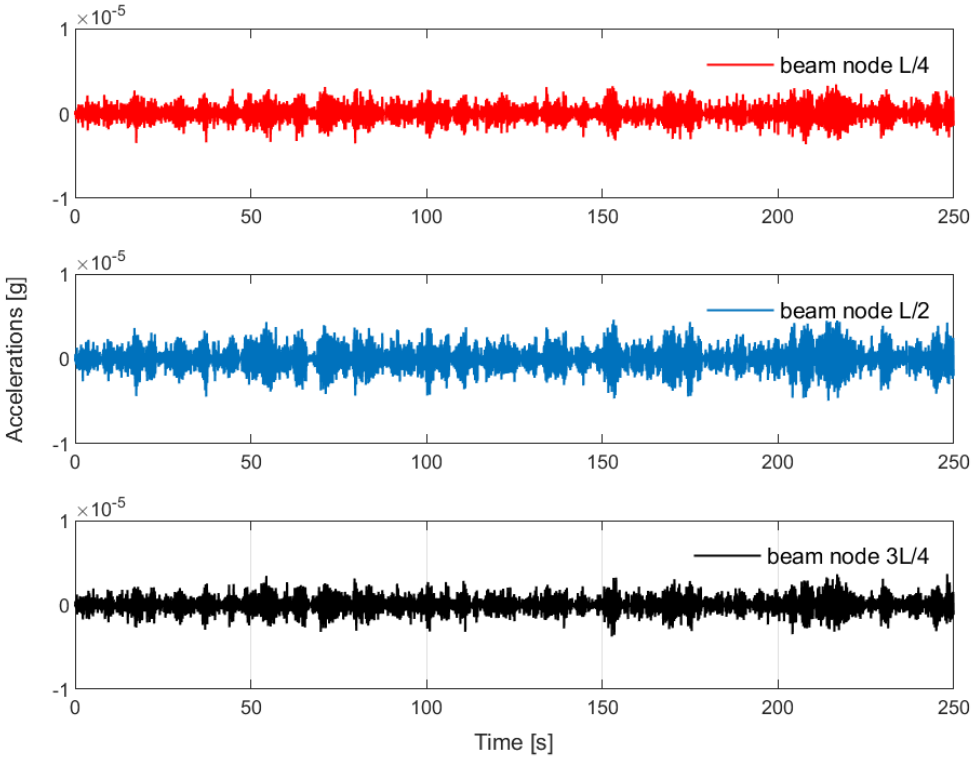

Figure 5.1: Acceleration responses of nodes located at L/4, L/2 and 3L/4, for a value of $\varepsilon = 0.01$.

The values of the RMS of the accelerations responses for the three nodes are illustrated in fig. 5.2, where is possible to notice, that despite the different location of the virtual transducers, the values assumed by the different values of RMS is of the same order. Those transient analysis take the ε and make it range from the following interval (0.01, 0.10, 1.00, 2.50, 5.00, 50.00, 100.00, 500.00, 1000.00, 1500.00 2000.00). In fig. 5.1 are reported the responses in terms of accelerations of the three virtual transducers for a value of ε equal to 0.01.

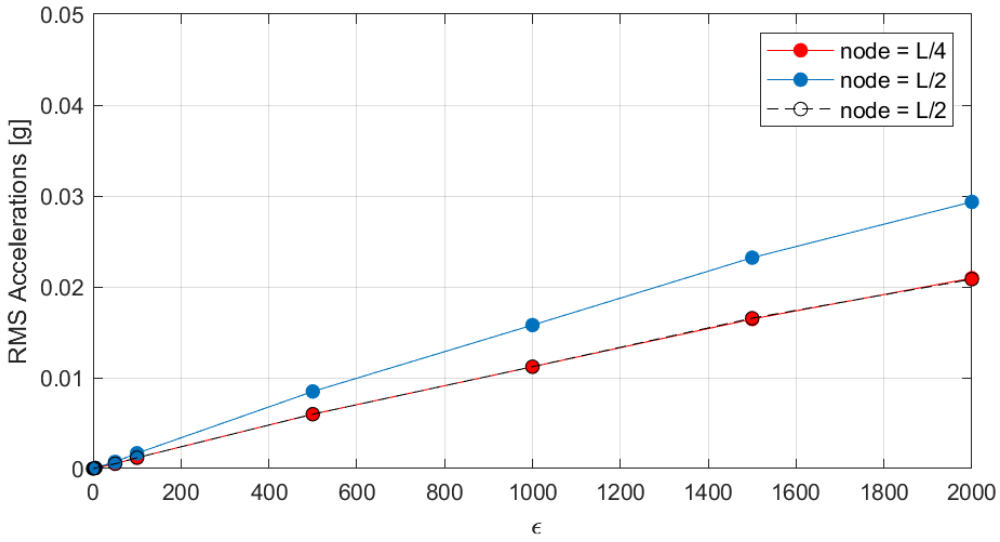

Figure 5.2: RMS of accelerations responses of node located at L/4, L/2 and 3L/4, along the vertical degree of freedom, for several values of ε.

The trends shown in fig. 5.2, allows to draw some interesting observation about the phenomenon, in particular since that only operational condition are involved in the numerical simulation, the obtained evolution of the RMS over the ε parameter is almost linear for the investigate excoriation levels. Moreover, the close response of the three nodes in the analysis enables to consider as a reference measurements the midpoint node, which obviously exhibit the worst effects in terms of accelerations committing a minor oversight. Furthermore, in the optic of an OMA test the highlighted nodes are likely to be chosen as a layout for transducers. The same numerical artifact can be applied to the horizontal degree of freedom of the double-tee beam element, in order to compare the different dynamical responses in term of RMS of accelerations between the two kinematic components (see fig. 5.3).

Here, in fig. 5.3 the dynamic picture already drawn from previous chapters is framed. Indeed, the sectional shapes with respect to the elastic center exhibit an higher stiffness along the horizontal axes if is compared with the vertical one. Hence, for the same value of ε it is possible the observe an lower response in term of RMS of the accelerations. Moreover, the trends of the RMS values is close to a linear behaviour. So in this condition the number of parametric analysis need to calibrate the equivalent forces can be drastically reduced by considering a simple linear regression, computing the angular coefficient of the curves. As a matter of fact, those curves both pass through the origin of the reference system, due to the null excitation for $\varepsilon = 0$.

Thus, the real behaviour of the curves can be approximated by a simple line, whose

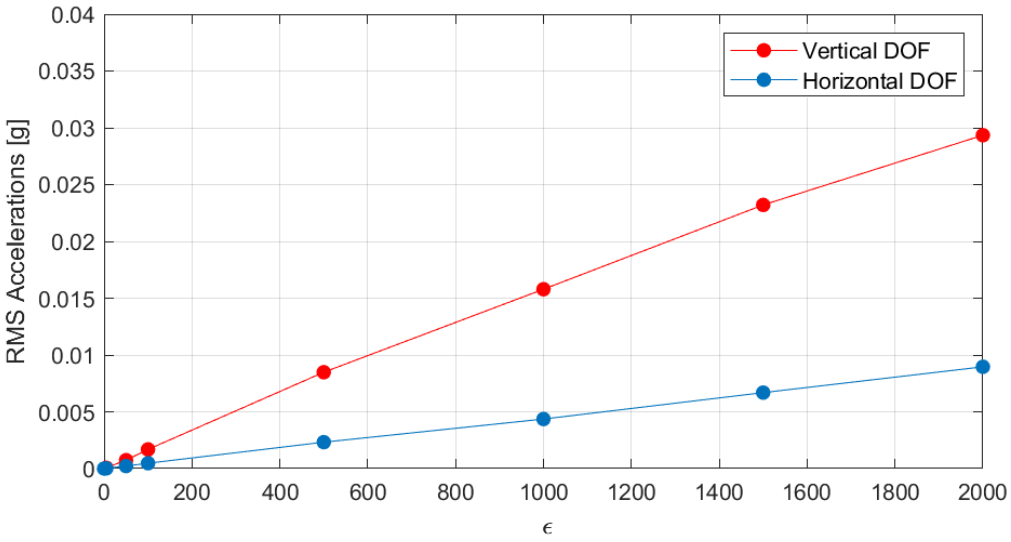

Figure 5.3: RMS of accelerations vertical Vs. horizontal responses of the double-tee beam.

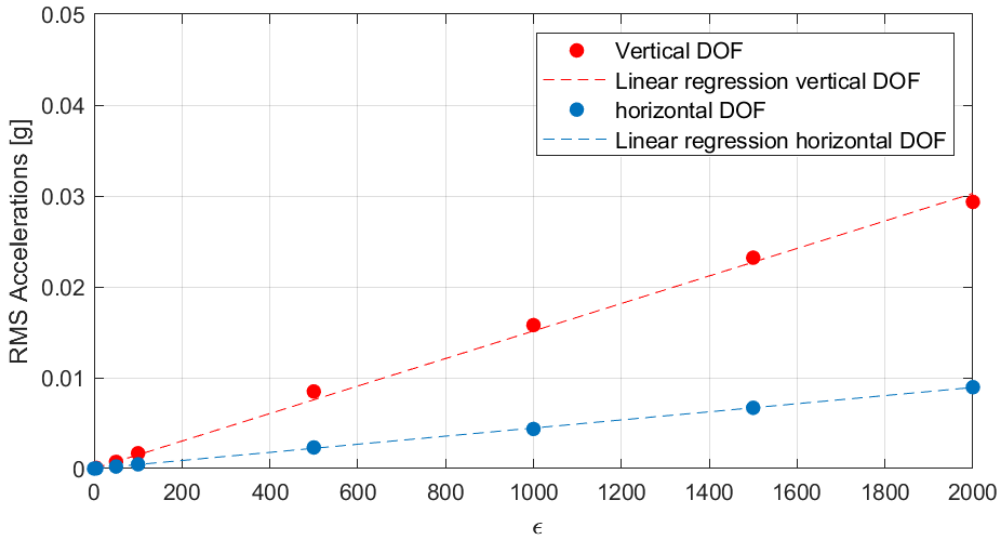

Figure 5.4: Comparison between the RMS point compute and linear regression.

mathematical relation is

$$y = \beta_1 \cdot x \tag{5.2}$$

where the coefficient β_1, is the slope or the so-called regression coefficient. In the current case and in all the future examples, this coefficient is computed by a *Matlab R2023b* [148] script. For the investigated case the values associated with the two curves are respectively $\beta_1 = 1.51e{-}05$ for the vertical degree of freedom and $\beta_1 = 4.46e{-}06$ for the horizontal one. The Comparison between the punctual realization of the RMS in term of accelerations and the linear regressions are reported in fig. 5.4. Where the quality of the aforementioned function is immediate to show. Moreover, the development of this calibration technique

allows to easily identify the value to be associated with the ε parameter to obtain the desired levels of environmental noise in the numerical analysis. What it is worth to mention is that the noise calibration aimed to reproduce the environmental effects is strictly related to the time step employed in the numerical simulations. This condition is the obvious consequence of the dynamic analysis framework since that considering a reduced time step causes an increasing in the level of RMS in term of accelerations due to the greater excitation applied to the structure in the same time interval for the same equivalent set of forces. Hence, in the calibration phase it is crucial to perform the aforementioned parametric analysis considering the same time step employed in the further numerical simulations.

5.2 Environmental temperature modeling and introduction into the numerical model

Bridges, as vital components of our infrastructure, are subjected to a myriad of environmental factors that can significantly influence their structural behavior. Among these factors, temperature variation emerges as a dynamic force that can have profound effects on the natural frequencies of bridges. Understanding the intricate relationship between temperature and structural dynamics is paramount for ensuring the resilience and safety of these critical structures. The impact of temperature on bridges is inherent in the fundamental behavior of structural materials. As temperatures fluctuate, materials expand or contract in response to thermal expansion coefficients. This thermal movement introduces deformations and stresses into the bridge elements, affecting the overall structural response. The interplay between these temperature-induced deformations and the natural frequencies of the bridge creates a complex dynamic scenario. Temperature-induced deformations generate dynamic effects that manifest in the natural frequencies of the bridge. The dynamic response is particularly pronounced in slender and flexible structures, where even subtle temperature changes can lead to significant alterations in vibrational characteristics. Understanding these variations is crucial for predicting potential resonances and ensuring that the bridge remains within safe operational limits. To comprehend the intricate relationship between temperature and natural frequencies, sophisticated measurement and monitoring techniques become indispensable. Modal analysis, for instance, allows engineers to identify the natural frequencies of a bridge under various temperature conditions. Advanced sensor systems placed strategically on the bridge enable real-time monitoring, providing valuable data on dynamic responses to temperature variations. Hence, introducing also the temperature influence on the bridges structures, is a main aspect especially to simulate experimental campaign in order to collect numerical data on the investigated structure. As mentioned before, temperature variation impact on material performance and mechanical characteristics. This aspect can be incorporate in the numerical analysis, where the material feature are obviously needed for the structural definition. In the scientific literature several scholars over the years have dedicated their effort in the study on how material in general reaction to the thermal variations [149–151], in our case scenario the majority of the numerical simulation are carried out considering concrete structures. in this regard, many works populate the academic shelves, regarding the mechanical behaviour of such material to several temperature ranges. From very low temperature [152–154] to very high temperature [150, 155, 156]. In the pertinent case study, the variation law of the Young modulus of the concrete, employed to include the effect of this parameter on the structural behaviour is [157]

$$E_{28}(T) = E_{28}(20^\circ) - 0.10627(T - 20^\circ) \tag{5.3}$$

where E_{28} is the Young modulus in GPa after 28 days of aging and T is the temperature. This mathematical relation (eq. (5.3)), is more than general and easily implementable in a specific code. Its temperature range is from $-20°$ to $50°$, which is more than acceptable for ordinary structure. As example, already presented double-tee beam element is here analysed, which is characterized by a Young modulus equal to 35 GPa, at ambient temperature here considered at $20°$, and the associated modes of vibration are reported in table 2.2. Those data are then reprocessed considering the influence of the temperature on the mechanical properties of the system. The Young modulus evolution over the temperature in accordance with eq. (5.3) is depicted in fig. 5.5

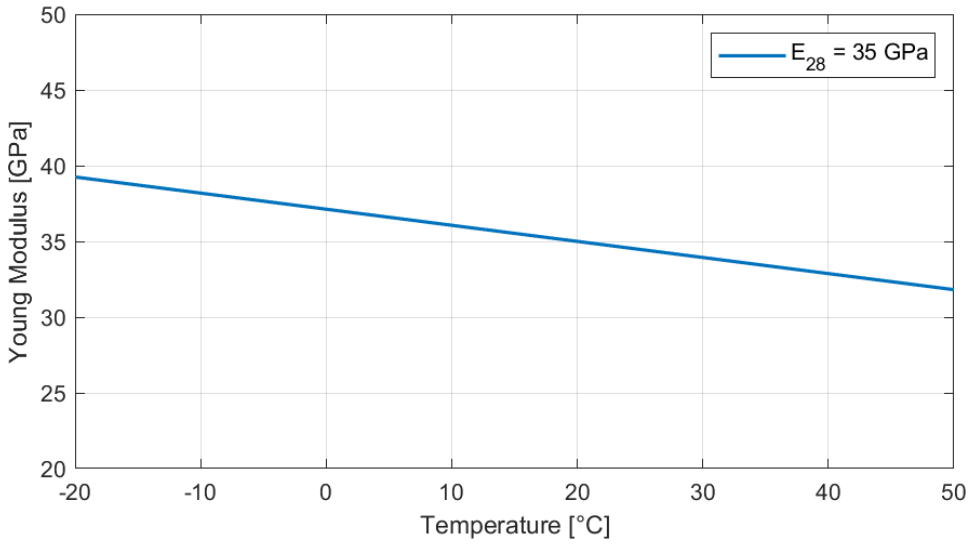

Figure 5.5: The evolution of Young modulus with the temperature.

On the other hand the effect on the modal properties of the double-tee beam due to the variation of the elastic modulus which impact directly on the beam stiffness are illustrated in fig. 5.6. Where it is easy to observe how the temperature variations act on the modal characteristics of the investigated structural elements. Indeed, for low temperature an increase in the elastic modulus is observed, meanwhile at higher temperatures a relaxation of this mechanical property is observed. This phenomenon is reflected directly on the natural frequencies of the structures, which are interest by a shift, whose severity strongly depend on the mode. In fact, from the trend showed in fig. 5.6 is immediate to understand how the higher modes are essentially the ones more sensible to this phenomenon in accordance with the literature. Moreover, the first mode, which here is uncoupled and associated with the vertical deflection of the beam, is almost graphically represented by a straight line on the plot showing a small frequency shift from 4.53 Hz to 4.14 Hz, which is a minimum amount, especially if compared with the respect the fifth mode which has shift of 2.57 Hz, changing from 29.45 Hz to 26.88 Hz.

Nevertheless, this illustrate how performing experimental tests on structure, such as bridges which are perpetually subject to environmental phenomena could potentially be misleading especially when the same test is performed with a complete different environmental boundary conditions, which corrupt the modal and hence the dynamical behavior of the investigated structure.

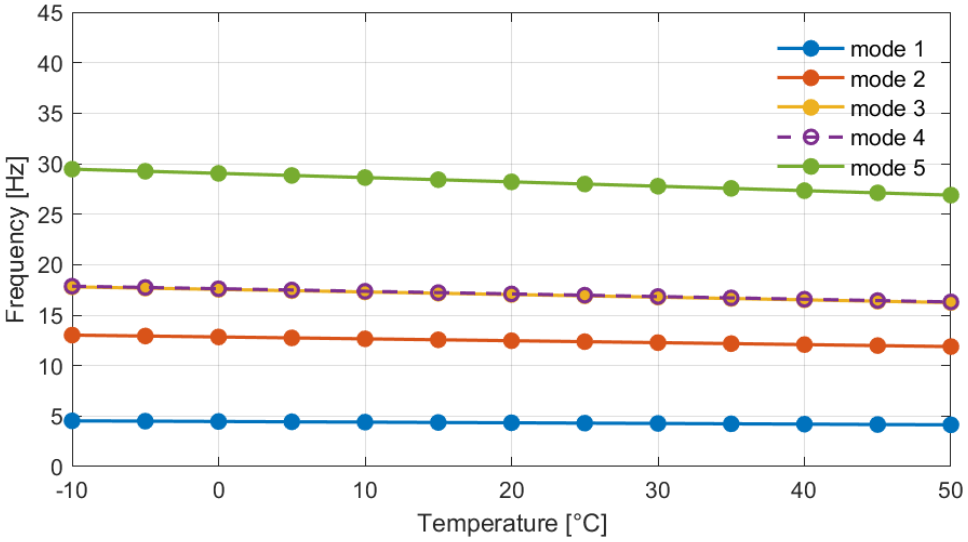

Figure 5.6: The evolution of modes of vibration of the double-tee beam with the temperature.

Chapter 6

"Ghost Project" a Numerical Framework for Vehicle Bridge Interaction simulations

The *Ghost Project* is a general-purpose finite element software designed for linear analysis. It is conceived to implement Vehicle-Bridge Interaction through the integration of beams and idealized mechanical models that describe vehicle dynamic behavior, such as the quarter-car model. The extension of this software to handle non-linear problems is planned as a future development within the presented framework. Currently, several finite element software packages are available for a wide range of applications, including structural engineering, geotechnical engineering, and aerospace engineering, to name a few. However, when it comes to describing and analyzing specific or niche problems, it is not always possible to rely on existing software. In such cases, it becomes necessary to develop a tailored framework capable of addressing the desired problems. Nevertheless, many moving loads problems can also be modeled using various techniques, involving mechanical systems that may be more or less detailed. Indeed, the issue of moving loads has garnered significant interest, particularly with the development of high-speed trains and in general bridge design. Several techniques and models have been developed in this area. While simple dynamic problems focused on the moving force approach are easily implementable and found in many existing software packages, more complex dynamic systems, such as the quarter-car model moving along a bridge, are not always straightforward to implement. This is especially true in software that are already structured or originally designed to address other mechanical problems. Furthermore, it is evident that complex models capable of describing dynamic systems, such as high-speed trains or trucks, can be addressed through the implementation of 3D modeling. This approach involves employing complex meshes and, more often than not, managing contact relationships between different subsystems. Although, this seems like a good approach, it is clear that as the number of vehicles increases, the simulations require significant computational effort. Hence, it is more convenient to rely on simpler mechanical models, which can provide accurate responses while saving on computational costs. In this context, beam models capable of describing the interaction between the primary system and the vehicle can be outstanding. Various beam elements and types of vehicles, ranging from a simple quarter-car model to more complex mechanical systems that also consider the pitching and rolling of a vehicle, can obviously be implemented. This approach results in significant gains in terms of computational cost and time efficiency in simulations. And it is within this complex numerical context that the *Ghost Project* is situated. Its primary aim is to develop a new finite element code capable not only of performing Vehicle Bridge Interaction simulations, complete

with all the classical elements necessary for analysis, but also of conducting both static and dynamic analyses of beam structures. In the present chapter the afore-mentioned software is presented and all its features are depicted. Naturally, for the sake of conciseness and since this is not a software documentation, the software insight is aimed at highlighting in a general manner its potentialities while also providing a comprehensive description of all its functionalities.

6.1 General introduction

The *Ghost Project* is entirely coded in C++ [158, 159], extensively utilizing the object-oriented paradigm due to its numerous key advantages, such as *encapsulation*, *inheritance*, and *polymorphism*, among others. Encapsulation binds together data and the functions that manipulate this data, protecting both from outside interference and misuse. *Inheritance* is a vital feature that allows the creation of a new class derived from an existing one, leading to a hierarchical structure in the code. *Polymorphism* enables methods to perform different actions based on the object they act upon, even with the same name. This feature enhances code flexibility and allows for a unified interface for various data types. All these features contribute to excellent code modularity; indeed, classes and objects can be treated as self-contained units, simplifying code maintenance. Many existing software programs are based on these premises, with one of the best examples being *OpenSees* [160]. *OpenSees*, short for "Open System for Earthquake Engineering Simulation," is a software framework developed primarily for simulating the seismic response of structural and geotechnical systems. It is an open-source, object-oriented application designed to support complex, multi-domain, nonlinear dynamic analysis. *OpenSees* is widely used in the engineering community for research and educational purposes, offering a versatile platform for developing custom models and algorithms in earthquake engineering and beyond. Its flexibility and extensive library of material models, elements, and algorithms make it a valuable tool for in-depth seismic analysis and understanding structural behavior under earthquakes. In the current case, C++ is employed together with the *Eigen* library [161]. *Eigen* is an open-source C++ template library renowned for its high-performance matrix and linear algebra operations, widely used in scientific computing. It is characterized by ease of use and efficiency. *Eigen* provides a comprehensive set of tools for matrix manipulations, solving linear equations, and performing sophisticated operations like eigenvalue decomposition and singular value decomposition. Its versatility and compatibility with various types of matrices and algebraic operations make it popular among developers and researchers in fields such as robotics, physics, and computer graphics. Additionally, *Eigen*'s syntax is intuitive and integrates seamlessly with standard C++ code, enhancing its appeal for complex mathematical computations. Moreover, it offers specialized data structures for sparse matrices, optimizing memory usage and computational efficiency in cases where matrices have a large number of zero elements. It supports operations like sparse-dense matrix multiplication, solving sparse linear systems, and sparse matrix decompositions (e.g., Cholesky, LU). Furthermore, *Eigen* uses efficient storage schemes like Compressed Sparse Column (CSC) or Compressed Sparse Row (CSR) to store sparse matrices. In the following sections, a general description of the code is provided, along with a discussion of the main classes and methods. The code is organized as follows: two primary classes are pivotal. The **Domain** class, where all objects concerning the model — such as mesh, constraints, and traffic patterns — are stored, and the **Analysis** class, where the equations of motion for dynamic cases or equilibrium equations for static cases are solved. Subsequently, the structure of the code is reviewed. A brief description of the class relationship is depicted in fig. 6.1 according to Rumbaugh notation [162]. A concise

and accurate description of this notation and its relationships can be found in [107] and is reported in the following. The aforementioned notation, often associated with the Object Modeling Technique (OMT), is a methodology for object-oriented analysis and design. It is based on key features such as the **object model**, which is the core of the notation, and includes the **dynamic** and **functional model**, among others. Classes are depicted as rectangles divided into three parts, in their complete form, where the top part contains the class name, the middle part lists the attributes, and the bottom part includes operations or methods. Moreover, Rumbaugh notation defines several types of relationships between classes:

- **Association**: depicted as a solid line between classes, indicates that objects of one class are connected to object of another.
- **Aggregation**: a special form of association representing a *whole-part* relationship. Illustrated with an empty diamond at the aggregate (whole) end of the line.
- **Composition**: another form of aggregation but more tightly coupled. Shown with a filled diamond to indicate that the part cannot exist independently of the whole.
- **Inheritance**: Shown with a line ending in a triangle. The triangle points to the general class, while the other end of the line connects to the specialized class.

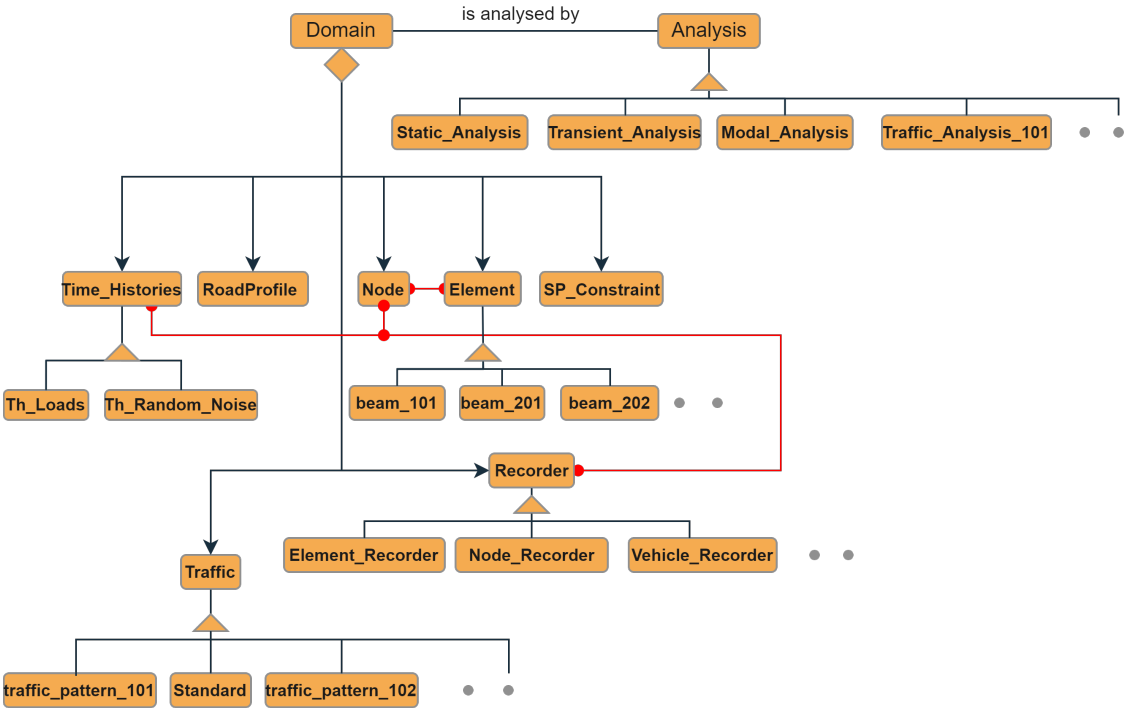

Figure 6.1: *Ghost project* class diagrams.

6.2 Domain Class

The domain class is the main class of the code where all the information about the model are stored. The class definition is depicted in listing 6.1 .In particular, the main methods populating the **Domain** class primarily focus on adding specific objects to the class. This

is where all the pointers to the classes, which are indispensable for defining the numerical model, are aggregated. All pointers are then organized and listed in a collection, composed of *unordered maps*. The *unordered map* is a powerful and efficient container for managing key-value pairs with fast access times, making it suitable for application where rapid lookup, insertions, and deletions are necessary and where the order of the elements is not a concerns. Underneath, it uses a hash table for storage. This means it applies a hash function to the keys to determine where the values will be stored in the container. The average time complexity for searching, inserting, and deleting elements is $O(1)$, assuming a good hash function. Unlike *std::map*, the *unordered map* does not store elements in any ordered sequence. The order of elements is unpredictable and based on the internal hash function. Furthermore, alongside the aforementioned functions and key-values containers some basic member are stored in the zero initialized. In particular, the vector responses, which are uploaded each analysis step are stored. Vectors associated with the road profiles coordinates and values are initialized. Furthermore, some internal members are zero initialized and are updated during the geometric model constructions, such as the dofs number, the number of vehicles and the number of single points constrained defined. Moreover, this section defines all the **Add**— functions, which are designed to check if an object with the same tag already exists in the corresponding unordered map; if not, they store the pointer to the considered object. Every object in the code is mandatorily associated with a reference tag, whether it is a node, an element, or even the **Domain** itself.

```
    class Domain
{
public:
    Domain(int domain_tag);
    ~Domain();


    //Add Domain Methods
    void AddNode(Node* node);
    void AddElement(Element* element);
    void AddSP_Constraint(SP_Constraint* constr);
    void AddNode_Load(int node, int dofs, double load);
    void AddTH_Load(TH_Load* thLoad);
    void AddTrafficPattern(Traffic* theTraffic);
    void AddNode_Recorder(Node_Recorder* node_rec);
    void AddElement_Recorder(Element_Recorder* ele_rec);
    void AddModal_Recorder(Modal_Recorder* modal_rec);
    void AddVehicle_Recorder(Vehicle_Recorder* veh_rec);
    void setDampingCoefficients(const double& a1, const double& a2);

    // Free the Heap
    void ClearAll();

    //Define Class Members
    std::unordered_map<int, Node*> Node_Pointer_List;
    std::unordered_map<int, Element*> Element_Pointer_List;
    std::unordered_map<int, SP_Constraint*> SP_Constraint_Pointer_List;
    std::unordered_map<int, Node_Recorder*> Node_Recorder_List;
    std::unordered_map<int, Element_Recorder*> Element_Recorder_List;
    std::unordered_map<int, Modal_Recorder*> Modal_Recorder_List;
    std::unordered_map<int, TH_Load*> TH_Load_Pointer_List;
    std::unordered_map<int, Traffic*> Traffic_Pattern_Pointer_List;
    std::unordered_map<int, Vehicle_Recorder*> Vehicle_Recorder_Pointer_List;

    //Define the Responses from the Analysis
    VectorXd disp;
```

```
    VectorXd vel;
    VectorXd acc;
    VectorXd force;

    //RoadProfile
    VectorXd roadCoordinates;
    VectorXd roadProfile;
    VectorXd Droadprofile;

    //Vector of Elements of which the Road is commposed of
    std::vector <int> eleRoad;
    double Road1 = 0;
    double Road2 = 0;

    //Model members
    int nVehicles = 0;
    int nFixedVehicles = 0;
    int ndofs = 0;
    int nele = 0;
    int nSP = 0;

    //Domain Tag
    int TAG;
private:

};
```

Listing 6.1: Domain class declaration.

6.2.1 Node and constraint classes

Node and **constraint** classes are two of the classes which are defined once that a domain is declared. The **Node** class is crucial in order to create the model geometry. Being in 2 dimensional coordinate system the **class**, whose class definition is reported in listing 6.2, is defined by only the coordinates X and Y.

```
class Node
{
public:
        Node(int node_tag, double x_coordinate, double y_coordinate);
        ~Node();

        //Define Class Methods
        int getTag();

        //Define Class Members
        int TAG;
        double X, Y;

        //ID Associated with respect to the dof
        std::vector <int> dofs_idx;

        //Constrained == 0 -- Unconstrained == 1
        std::vector <int> dofs_act;

        //Vector of Nodal Loads
        std::vector <double> node_load;
        std::vector <double> node_load_th;

};
```

Listing 6.2: Node class declaration.

Each node, like many other objects in the following sections, is uniquely identified by means of a tag. A **getTag** method can return the integer associated with the node's tag. Furthermore, the element class maintains a standard vector where unique tags of degrees of freedom are stored. Consequently, another vector of the same dimension is composed and initialized with unit values. This vector indicates which degrees of freedom are restrained and is manipulated by the constraint handler. In this analysis, only single-point constraints are considered. Single-point constraints are managed by the *SP Constrain* class (see listing 6.3). This class iterates over the node list in the domain and sets the restrained degrees of freedom to 0 in the *unordered map* of the nodes in the domain.In particular, in the *Ghost Project* code, constraints are enforced using the so-called penalty methods, a widely recognized approach in the field of computational mechanics. The penalty method is a technique used for enforcing constraints in the solution of Partial Differential Equations (PDEs) and in finite element analysis. This method involves adding a penalty term to the system's governing equations, which imposes a high cost for violating the constraints. In the context of finite element analysis, the penalty method is often applied to manage boundary conditions and internal constraints of a model. It works by introducing stiff springs or forces at the points of constraint violation, effectively penalizing any deviation from the prescribed conditions. The magnitude of the penalty parameter is crucial; it must be large enough to enforce the constraint effectively, yet not so large as to cause numerical instability or ill-conditioning in the system matrix. This method offers a straightforward way to implement constraints, particularly useful in complex simulations where traditional methods might be challenging to apply.

```
class SP_Constraint
{
public:
        SP_Constraint(int constraint_tag,int node_tag, int node_dofs);
        ~SP_Constraint();

        //Method to look for restrained dofs in the domain
        void SP_Constraint_Node(std::unordered_map<int,Node*> dofs_list);
        int getTag();

        //Define Members
        int CON_TAG, NODE_TAG, DOFS;

};
```

Listing 6.3: SP Constraint class declaration.

As for the **Node** class scenario also in the **SP Constraint** class each constrained is uniquely identified by a tag. In Finite Element Method (FEM) simulations, the use of tags as unique identifiers for entities like nodes, elements, materials, and boundary conditions is crucial for efficient and accurate analysis. Tags facilitate easy identification and tracking of each entity, essential in models with numerous components. They enhance data organization and management, allowing for streamlined storage and retrieval of entity-specific information. Furthermore, tags are instrumental in error checking and model validation. They ensure the uniqueness of each entity, preventing errors from duplicate entries, and help verify the correct establishment of connections and relationships within the model. Efficiency in computational processes is another key advantage. Tags enable quick indexing and access to entity properties, a critical factor in the performance of large-scale simulations. They also simplify model modifications and extensions, making it easier to update the model without disrupting its structure. Not to mention, that tags play a vital role in interoperability and data exchange between different FEM software, maintaining entity consistency and integrity across platforms. Additionally, they are ben-

eficial in scripting and automation, providing a clear and consistent reference point for specific entities, which is crucial for advanced FEM analysis.

6.2.2 Element class

The **Element** class is an interface class which act as a base for other specific class able to fully describe the desired beam finite element. It is an abstract class, which is a class that cannot be instantiated on its own and is designed to serve as a base class for other classes. The key characteristic of a pure virtual class is that it contains at least one pure virtual function. This classes act as a foundation for other classes. They define a set of functionalities that derived classes must implement, ensuring a consistent interface. They are primarily used to achieve *polymorphism* in C++. Derived classes that inherit from a pure virtual class must implement all its pure virtual functions, thereby providing their own behavior. The specific class definition is reported in listing 6.4.

```
class Element
{
public:
        Element(int ele_tag);
        Element();
        ~Element();

        //Define methods
        int getTag() { return TAG; };
        //Method to set the number of DOFS to interested node
        virtual void setNodeDofs
            (int &idx, std::unordered_map<int,Node*> Node_List_Ptr) = 0;
        //Compute the element length
        double getLength(Node* ptr1, Node* ptr2);
        //Get local matrices
        virtual void getLocalStiffness() = 0;
        virtual void getLocalMass() = 0;
        virtual void getLocalDamping() = 0;
        //Compute the element reaction to the two ends
        virtual VectorXd computeReaction(const VectorXd& disp) = 0;
        virtual VectorXd computeReaction(const VectorXd& disp,
                const VectorXd vel, const VectorXd& acc,
                const VectorXd& force) = 0;
        //Get the shape functions -> traffic analysis no Torsion
        virtual VectorXd getN(double zita);
        virtual VectorXd getdN(double zita);
        virtual VectorXd getddN(double zita);
        //Get the shape functions -> traffic analysis Torsion
        virtual VectorXd getN(double zita, double d);
        virtual VectorXd getdN(double zita, double d);
        virtual VectorXd getddN(double zita, double d);
        //Initialize local matrices and vectors
        std::vector <int> node_vector;
        MatrixXd Local_Stiffness;
        MatrixXd Local_Mass;
        MatrixXd Local_Damping;
        //Element length
        double ele_length;
        //Element TAG
        int TAG;
        //Damping parameters
        double a1, a2;
```

```
};
```

Listing 6.4: Abstract element class declaration.

In the **Element** interface class, some basic quantities are necessary for computation, such as local matrices and the element length. The element tag can also be retrieved using the **getTag** method. Furthermore, a series of methods are defined as either *virtual* or *pure virtual*. Among the pure virtual methods, it's important to mention **setNodeDofs**. This method is responsible for setting the number of degrees of freedom (DOFs) and their tags in the domain. Different elements have varying numbers of DOFs, and this method determines the appropriate number for the selected element. Additionally, functions that compute and return essential matrices of the problem are declared. For instance, **getLocalStiffness** returns the local stiffness matrix of the element, and **getLocalMass** typically returns the local mass matrix in dynamic analysis. Meanwhile, the damping matrix is retrieved by **getLocalDamping**, which utilizes the proportional damping formulation; hence, a prior modal analysis is essential for its effectiveness. Moreover, the virtual functions **getN**, **getdN** and **getddN** are able to return the local shape functions and their derivatives in traffic analysis conditions. Currently, the finite beam elements available in *Ghost* are ten, of which five support the Euler-Bernoulli formulations and five the Timoshenko formulations. Those element are resumed in the following list for the sake of clarity

- **Beam 101**: Euler-Bernoulli formulation with 2 DOFs per node, only vertical deflection;
- **Beam 102**: Euler-Bernoulli formulation with 4 DOFs per node, uncoupled flexural behavior along the two cross-sectional axis;
- **Beam 112**: Euler-Bernoulli formulation with 5 DOFs per node, uncoupled flexural behaviour along the two cross-section axis, uniform torsion;
- **Beam 201**: Timoshenko formulation with 2 DOFs per node, only vertical deflection;
- **Beam 202**: Timoshenko formulation with 4 DOFs per node, uncoupled flexural behavior along the two cross-sectional axis;
- **Beam 212**: Timoshenko formulation with 5 DOFs per node, uncoupled flexural behaviour along the two cross-section axis, uniform torsion;
- **Beam 232**: Timoshenko formulation with 7 DOFs per node, axial displacement, flexural-torsional coupling, non-uniform torsion;

All the finite beam element inserted in the **Element** class are formulated exploiting the iso-parametric formulation and gauss quadrature. An example of child element class, is reported below where the class **beam232** declaration is resumed.

```
class beam232 :public Element {
public:
    //Class constructor
    beam232(int ele_tag, int Node_1, int Node_2, double den,
    double Young, double Shear_Mod, double Area,
    double Inertia_z, double Inertia_y,
    double Shear_cor_fact_y, double Shear_cor_fact_z,
    double Polar_Inertia, double Torsional_Constant,
    double Warping_Constant, double Static_zs,
    double Static_ys, double Inertia_wz,
```

```
    double Inertia_wy, double Inerzia_yz);
    //Class destructor
    ~beam232();
    //Define virtual methods
    void setNodeDofs(int& idx,
        std::unordered_map<int, Node*> Node_List_Ptr);
    void getLocalStiffness();
    void getLocalMass();
    void getLocalDamping();
    VectorXd computeReaction(const VectorXd& disp);
    VectorXd computeReaction(const VectorXd& disp,
    const VectorXd vel, const VectorXd& acc);
    VectorXd computeReaction(const VectorXd& disp,
    const VectorXd vel, const VectorXd& acc, const VectorXd& force);
    //Define Class Memebers
    double A, Iz, Iy, Ky, Kz, IP, Jt, Iomega;
    double Szs, Sys, Iwz, Iwy, Izy;
    double rho, E, G;
    int N1, N2;
    int DOF = 6, NODES = 2;
    double ele_length;
    VectorXd getN(double zita, double d);
    VectorXd getdN(double zita, double d);
    VectorXd getddN(double zita, double d);

private:
        //Shape function vertical dof
        VectorXd NN2(double csi);
        VectorXd NN2x(double csi);
        VectorXd NN4(double csi);
        VectorXd NN4x(double csi);
        //Shape function horizzontal dof
        VectorXd NN3(double csi);
        VectorXd NN3x(double csi);
        VectorXd NN5(double csi);
        VectorXd NN5x(double csi);
        //Shape function torsional dof
        VectorXd NN6(double csi);
        VectorXd NN6x(double csi);
        VectorXd NN6xx(double csi);
        //Gauss quadrature methods
        MatrixXd gaussQuadrature(int n,
        VectorXd(beam232::*N1)(double),
        VectorXd(beam232::*N2)(double));

        MatrixXd gaussQuadrature2(int n,
        VectorXd(beam232::* N1)(double),
        VectorXd(beam232::* N2)(double));

        MatrixXd gaussQuadrature3(int n,
        VectorXd(beam232::* N1)(double),
        VectorXd(beam232::* N2)(double));

};
```

Listing 6.5: beam232 class declaration.

6.2.3 Time histories class

The **Time_Histories** (see listing 6.6) class is responsible to the definition of the several load cases, which are implemented in the *Ghost project*. Although, the name it is able the

handle both the nodal loads which are statically applied, or the dynamical time histories which can be stored in an external *.txt* or *.csv* file. It is the abstract class in term of load defining.

```
class Time_Histories {
public:
        Time_Histories(int loadTag);
        ~Time_Histories();
        // Get tag method
        int getTag() { return TAG; }
        // Main members
        int TAG;
        std::string PATH;
        int DOFS;
        std::vector<int> NODE;
        std::vector<double> thData;
        double DURATION, DT, EPSILON;

};
```

Listing 6.6: Abstract TimeHistories class declaration.

This class has only one method in its base configuration which is able to return the tag of a defined load case. Is populated with two different classes which are been defined for the numerical simulation in this case. The first is called **TH_Loads**, where it is possible to assign a static or dynamic load to a specified node and a specified degree of freedom associated with the node. If the load is static no external reference is needed to describe the evolution of the load over the time domain. On the other hand in case of dynamic analysis the also the path the associated file is mandatory to perform the desired analysis. Here, the **readData** method (see listing 6.7 owns all the needed tools the open read and store the data deriving from an external file and is based on the c++ library **fstream**.

```
class TH_Load : public Time_Histories
{
public:
        TH_Load(int loadTag, std::string path_file,
            std::vector <int> node, int dofs, double dt, double duration);
        ~TH_Load();
        //Read data from a file .csv or .txt
        void readData();
};
```

Listing 6.7: TH_Loads class declaration.

Obviously, also the analysis time step of for the specified case need to be acknowledge by the constructed object. Together, with the classical nodal loads, which can be handled by the previous class another class is defined in the framework and it is aimed to the simulations where the environmental noise or a Gaussian noise need to be added to the analysis. It is called **TH_Random_Noise** and just as the previous class the main focus of this is to construct an object which is stored through a pointer in the appropriate domain container, or unordered map. The constructor is similar to the previous one, but no path to file is allowed and is mandatory pass the ε parameter, which is able to define the noise amplitude, as already pointed out in the previous chapters for the environmental noise calibration.

6.2.4 Road profile and traffic pattern classes

The traffic description is a crucial component of all simulations presented in the *Ghost Project*. Although the project is capable of performing simple generic static or dynamic

analyses, it is primarily designed to replicate and conduct analyses aimed at Vehicle-Bridge Interaction (VBI). Therefore, two main concepts must be introduced into the aforementioned framework: the generation of road profiles, which describe road roughness and are a significant component in certain simulations of the interaction between the two subsystems, and the generation of traffic patterns. Both are described in the current section. Starting with road profiles, they can be generated according to several standards. The ISO 8608 standard has been previously cited, but it is not the only one available in the scientific literature. It is worth mentioning that, although it may be the most widespread, other definitions for road profiles, such as the BSI proposal [163], are also possible. However, in this context, only the well-established ISO standard is employed. This decision allows the author to avoid defining an abstract class specifically for road roughness profile generation. The **RoadProfile** class constructor is capable of generating a discretized spatial domain with a prescribed total number of samples. In addition to a unique tag and the pointer to the domain, two other mandatory parameters need to be addressed: the k parameter, as already described in the previous section, and the desired number of samples. What it is worth to mention is that only one road profile can be added to the **Domain** without encountering an error.

```
class RoadProfile
{
public:
        RoadProfile(int roadProfileTag, Domain* domain_ptr,
            double kIso, int nSample);
        ~RoadProfile();
        // Get tag method
        int getTag() {return TAG;}
        // Compute the road profile
        void computeRoadProfile();
        int TAG, sample;
        double K;
        Domain* ptrDomain;
        double totalLength;


};
```

Listing 6.8: RoadProfile class declaration.

From this class three different vectors are then composed in the **Domain** class, from the **computeRoadProfile** method. Those vectors are respectively, **roadCoordinates**, **roadProfile** and **DroadProfile**, where are stored the road coordinates as function of the desired number of samples, the road profile and the associated derived with respect to the spatial coordinate. Subsequently, the **Traffic** class is the abstract class responsible to defined the desired traffic pattern. The interface declaration is illustrated in listing 6.9. Several traffic patterns can be defined by the users. the focus is to compose the so-called **TrafficReferenceMatrix**, which is the matrix able to define the starting and the ending instant for each vehicle moving along the beam finite elements. Moreover, the last column is representative of the traffic direction, more specifically unitary value in the last column equal to vehicle moving along the positive x coordinate and a zero value in negative sense.

```
class Traffic
{
public:
        // Class constructor
        Traffic(int trafficTag, Domain* domain_ptr);
        Traffic();
        ~Traffic();
        // getTag methods definition
```

```
        int getTag() { return TAG; }
        //Define Virtual Methods
        virtual void getMatrices() = 0;
        //Define Member
        std::vector<double> Mass, Damp, Stiffness, Wheel, Vel, inter, d;
        std::string Ways;
        double beam_length;
        int TAG, nVehicle;
        MatrixXd Vehicle_Mass;
        MatrixXd Vehicle_Damp;
        MatrixXd Vehicle_Stiffness;
        MatrixXd TrafficReferenceMatrix;

        Domain* ptrDomain;


};
```

Listing 6.9: Traffic abstract class declaration.

Furthermore, the object-oriented framework and some of its unique features are fully exploited here. Indeed, several traffic patterns can be implemented. All derived classes are required to provide certain features mandatorily. These features include the mass, damping, and stiffness matrices, referred to as **Vehicle_Mass**, **Vehicle_Damp**, and **Vehicle_Stiffness**, the total number of vehicles, and, notably, the **TrafficReferenceMatrix**. The pure virtual method **getMatrices** is responsible for returning and computing the matrices associated with the mass, damping, and stiffness, and it needs to be defined in every derived class. In this context, two different situations can arise. In the first scenario, the user wishes to specify mechanical quantities associated with the traffic scenario for each vehicle individually. This requirement can be met by the derived class named **Standard**. As demonstrated in the class constructor, shown in listing 6.10, the user can provide all the desired quantities using *std::vectors*. Some default quantities are set, such as the **massWheel** vector, which is not always indispensable, the direction of the traffic flow, and the presence of the **d** vector. The components of the **d** vector represent the distances relative to the x-axis of the beam, and thus, this vector is necessary only in cases where torsional behavior is under investigation.

```
class Standard: public Traffic
{
public:
        Standard(int trafficTag, Domain* domain_ptr, int vehicleNumber,
            std::vector <double> mass, std::vector <double> damping,
            std::vector <double> stiffness, std::vector<double> velocity,
            std::vector<double> interAxle,
            std::vector <double> massWheel = {},
            std::string ways = "One",
            std::vector<double> dist_centre = {});

        ~Standard();

        //Define Methods
        void getMatrices();
        void ReferenceMatrix();

};
```

Listing 6.10: Standard traffic class declaration.

On the other hand, there may be situations where the user wants to provide a class in which all the mechanical quantities of interest are automatically computed by referencing

a Weigh-In-Motion (WIM) database. In such cases, the classes to be added are fully customizable, with the only limitation being the requirement to implement the pure virtual methods. These methods are essential to ensure both the compilation and the functionality of the overall software. To achieve this, a different approach needs to be selected. In this context, the class **traffic_pattern102** is introduced (see listing 6.12). This class is designed to retrieve traffic data based on the WIM database from [164]. The implementation allows for an automated computation of mechanical quantities, leveraging the detailed data available from WIM sources. This class will be extensively employed in the numerical simulations presented in the next chapter.

```
class traffic_pattern_102 : public Traffic
{
public:
        //Define the class constructor
        traffic_pattern_102(int trafficTag, Domain* domain_ptr,
            double duration, std::string ways);

        ~traffic_pattern_102();
        //Class methods
        void getMatrices();
        void twoWaytraffic();
        void oneWaytraffic();
        double computeTime(double velocityVehicle, double interAxles);

private:
        //Define class private members
        int ndofs;
        double dmin, dmax;
        std::vector<int> flag_vector;
        double max_duration;
};
```

Listing 6.11: Traffic pattern 102 class declaration.

Indeed, this class is capable of defining an entire **TrafficReferenceMatrix** based on the desired analysis duration. In this class, besides the mandatory pure virtual method **getMatrices**, other methods are defined to compose the traffic reference matrix for a specified duration in seconds. Depending on the selected number of traffic directions, the class constructor can invoke methods like **twoWayTraffic** or **oneWayTraffic**. Following the method outlined in the chapter on vehicle calibration, it can compose the reference matrix using known values derived from the WIM database. Furthermore, all necessary matrices and vectors are then assigned to the corresponding quantities in the domain through its pointers. This includes the total number of vehicles along with the associated number of degrees of freedom, which are crucial not only for defining the analysis but also from an output perspective. The pseudo-code for the traffic pattern **traffic_pattern102** is illustrated in fig. 6.2. This is where the calibration method described in fig. 4.2 is called to calibrate the various vehicle categories derived from the aforementioned database. It should be emphasized that this is one of the cases, along with the one already presented for the elements, where it is possible to intelligently exploit object-oriented programming. In fact, it would be straightforward to insert data and methods for vehicle calibration derived from other databases, knowing the conditions dictated by the code, and in particular the members and functional elements that are necessary to construct both the domain class and the class related to numerical analyses.

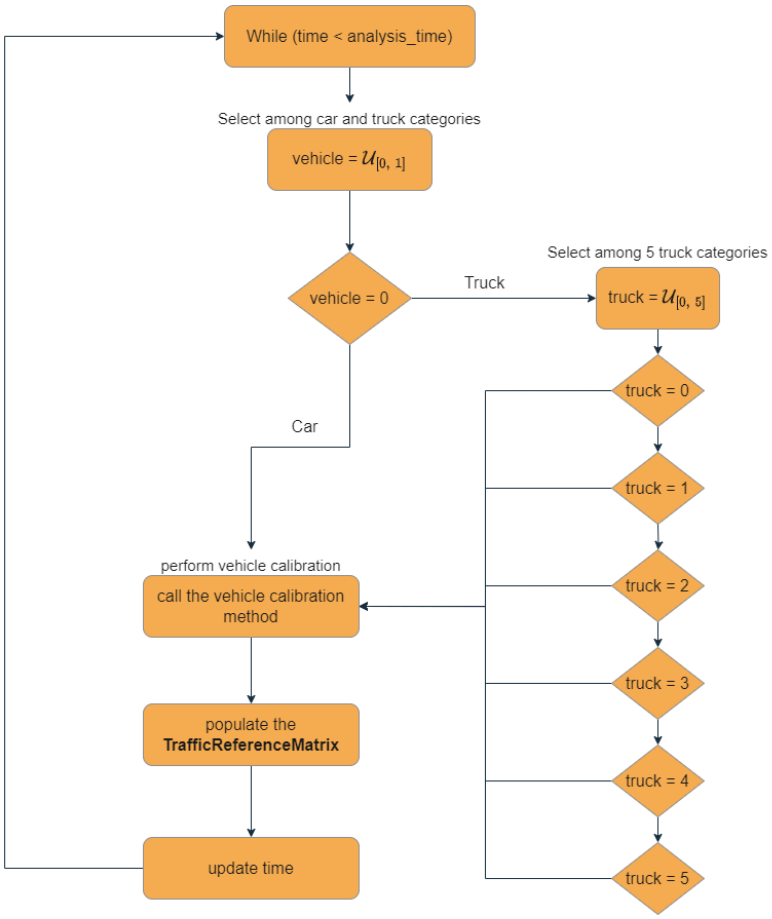

Figure 6.2: **traffic_pattern102** flow chart.

6.2.5 The recorder class

In a finite element software the outputs are as much important as the numerical simulations because the hold the data, which can be exchanged, modified or passe to other algorithms. In *Ghost* a single class is responsible for handle and print the recorder in the desired file format. This abstract class is called **Recorder**, just like the *OpenSees* framework, and as usual acts like interface for the other recorder class defined. Several recorder are present in ghost each one able to absolve a specific task.

```
class Recorder
{
public:
        // Class constructor
        Recorder(int recorderTag, std::string filePath);
        Recorder();
        //Class destrcutor
        ~Recorder();
        //Get TAG method
        int getTag();
        //Define class memebers
        int TAG;
        std::string PATH;

};
```

Listing 6.12: Traffic pattern 102 class declaration.

The interface is very user-friendly and offers extensive customization possibilities. The key elements that play a significant role in the framework include the associated **Tag**, which allows storage in the domain, and the mandatory **PATH** string. This string identifies the folder where the recorder needs to be stored, and it is saved considering its tag number. Several recorders are defined based on the desired response types. In particular, the **Node_Recorder**, if defined and stored in the domain, can provide output concerning the displacements, velocities, and accelerations of the selected node. Conversely, the reactions from elements are retrieved using the **Element_Recorder**. It should be noted that the responses available from an element recorder depend heavily on the elements and their degrees of freedom. Moreover, the **Modal_Recorder** is available for use; the user can specify the number of desired modes, and all data concerning natural periods, natural frequencies, and mode shapes are stored in a **.txt** or *.csv* file. Lastly, a specific recorder for VBI analysis focuses on the vehicle responses. The **Vehicle_Recorder** derived class allows the user to easily select data such as displacements, velocities, and accelerations associated with the upper mass of the quarter-car model.

6.3 The analysis class

Beside the **Domain** class, the **Analysis** class is another crucial aspect of the code, it is an interface class, where each of the derived classes allow to the user to implement the desired analysis typology suitable for the investigated mechanical problem. In listing 6.13 the definition of the header file associated with the abstract **Analysis** class is provided.

```
class Analysis
{
public:
        //Define class constructor
        Analysis(int analysisTag, Domain* domain_Ptr);
        Analysis();
        ~Analysis();
        //Define pure virtual methods
        //Methods to compute matrices of structural elements
        virtual MatrixXd getK() = 0;
        virtual MatrixXd getM();
        virtual MatrixXd getD();
        //Compose the force vector
        virtual VectorXd getF() = 0;
        //Method to perform the analysis
        virtual void Analyse() = 0;
        //Class memebers
        Domain* ptrDomain;
        int TAG;
private:
        //Define integration methods
        void Newmark_Beta();
        void HHT-alpha();
};
```

Listing 6.13: Analysis class declaration.

As for the other investigated object in the framework every analysis object in order to be correctly defined needs two main ingredients which are the classic tag associated with the analysis and the pointer to the analyzed domain. Several, virtual methods are defined, such as the *getter*, which compute and define the mass, damping and stiffness local matrices and build up the global counterparts, together with the **getF** method able to define the force vector for every instant of time. The main actor in the method named **Analyse**, is responsible to compute the results for every instant of time, in transient analysis or

to perform the eigen-decomposition associated with the modal analysis of the structure. Two algorithm for the transient analysis are actually implemented in the framework, one is the so called $Newmark - \beta$ method [121] and the second is the HHT method [110]. The first it is a widely used numerical algorithm for solving differential equations in structural dynamics and earthquake engineering. The method approximates the integrals in the equations of motion using a linear combination of the accelerations, velocities, and displacements at different time steps. It involves two parameters, usually denoted as γ and β. These parameters control the numerical stability and accuracy of the method. If $\gamma = 0.5$ and $\beta = 0.25$ the method is unconditionally stable but only conditionally accurate. Increasing the value of β it is possible to improves accuracy but can affect the numerical damping properties. On the other hand, the HHT algorithm can be seen as a natural extension of $Newmark - \beta$. It introduces an additional parameter α to the Newmark method, which is introduced to modify the method's response to high-frequency components of the motion. In fact, α controls the amount of numerical damping and a negative value of α increases damping, which can be beneficial for reducing the effects of spurious high frequencies. The analysis class diagram is shown in fig. 6.3, where all the

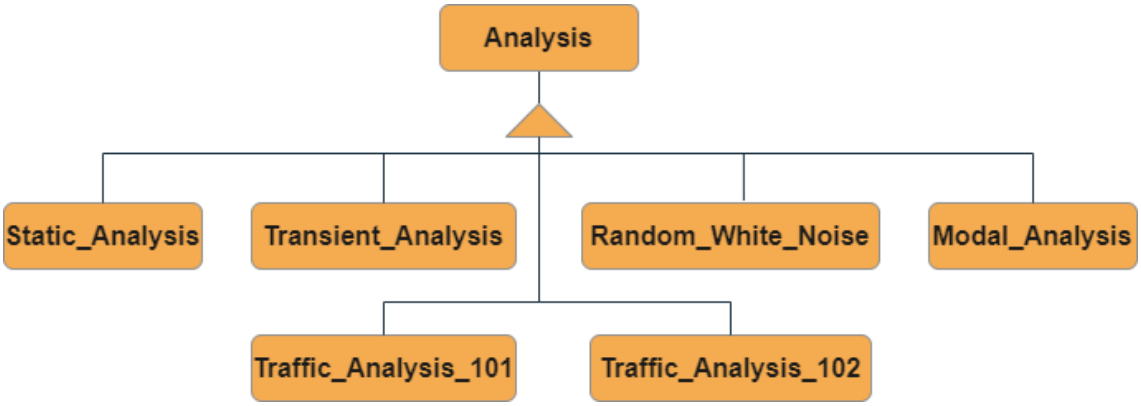

Figure 6.3: Analysis class diagrams.

available options are reported. Ranging from classical analysis, such as the static, modal and transient analysis to more specific ones. Among them **Random_Noise_Analysis** is implemented in order to construct the parametric analysis for the environmental noise calibration and **Traffic_analysis_101** and **Traffic_Analysis_102**, which are both able to take into account for the traffic analysis and the only difference lies in the fact that the latter has the possibilities to take into account thermal variation and the environmental noise in the same analysis. The **Static_Analysis** class exploit the *Eigen* algorithm *LDLT* or *LDLT Cholesky Decomposition*, which is a numerical technique used for efficiently solving systems of linear equations, particularly suited for symmetric, positive-definite matrices. This method decomposes a matrix into a product of three matrices: L (a lower triangular matrix), D (a diagonal matrix), and LT (the transpose of L). This specialized decomposition is highly efficient for computational purposes, especially when handling large matrices. *LDLT* is particularly tailored for symmetric, positive-definite matrices, which are common in various scientific and engineering fields, such as optimization and numerical solutions of differential equations. One of its key advantages is its computational efficiency, which simplifies solving linear equations by breaking down a complex matrix into simpler components. Moreover, it offers better numerical stability compared to other methods, making it more accurate for ill-conditioned matrices. On the other hands for the *Modal_Analysis* class the eigen-value problem is solved by means of the *GeneralizedSelfAdjoint* algorithm.

This is a specialized tool for solving eigenvalue problems, particularly tailored for pairs of self-adjoint (Hermitian) matrices. It efficiently addresses generalized eigenvalue problems formulated as $Ax = \lambda Bx$, where A and B are self-adjoint matrices, λ represents the eigenvalues, and x is the eigenvectors. This functionality is crucial in many fields, including structural and vibration analysis, as well as in the solution of differential equations in physics and engineering. One of the key strengths of this solver is its numerical efficiency and stability, making it well-suited for large-scale and high-performance computing applications. The solver is part of the Eigen library, renowned for its user-friendly design and seamless integration with other library components, enhancing its appeal among developers and researchers for complex numerical simulations.

6.4 Ghost application on numerical benchmark

In this section a brief example of a simple analysis performed by *Ghost* on an existent example is reported. This moving sprung-mass problem can be found in [31] and is here briefly explored for the sake of clearness. A 25-meter span simple beam experiences a moving sprung mass. Key parameters include: Young's modulus E at $2.87\,GPa$, moment of inertia I at $2.90\,m^4$, mass per unit length m at $2303\,kg/m$, and a vehicle mass M_v of $5750\,kg$. Additional specifics are a suspension stiffness k_v of $1595\,kN/m$, velocity v at $100\,km/h$, and a mass ratio (vehicle to bridge) M_v/mL of 0.1. The bridge's vibration frequency is ω_1 at $30.02\,rad/s$, and for the sprung mass, it's ω_v at $16.66\,rad/s$. The results of this simple case is compared against the analytical displacement response of the beam midpoint. The close form solution for this cases, focused on the response of an Euler-Bernoulli beam is reported in [18]. This is a typical example for Vehicle-Bridge Interaction where the scholar tested the accuracy of the finite element formulation against the close form solution. Here, no dashpot is considered and vehicle move on an Euler-Bernoulli beam with no road roughness is introduced on the analysis in order to eliminate all uncertainty arising from the stochastic phenomenon. All the necessary passages from the *Ghost* perspective, to model and analyze the mechanical problem are reported in listing 6.14. This is an explanatory example of a *main* file which need to be provided in order to perform numerical simulations, with the aforementioned framework. The main function, which need to be provided in the ghost framework *Ghost* is illustrated and fully commented in listing 6.14. According to [18] the displacement responses of the midpoint of the investigated beam on which a sprung-mass system is moving at constant velocity can be compute as

$$u(x,t) = \sum_{i=1}^{n} \frac{\Delta_{stn}}{1 - S_n^2} \left\{ sin\left(\frac{n\pi x}{L}\right) \left[sin\left(\frac{n\pi vt}{L}\right) - S_n sin\left(\omega_{bn} t\right) \right] \right\} \tag{6.1}$$

where Δ_{stn} is static deflection caused by the sprung-mass system with respect to the n-th mode, which can be computed as

$$\Delta_{stn} = -\frac{2m_v g L^3}{n^4 \pi^4 EI} \tag{6.2}$$

and S_n is the speed parameter for the n-th mode, that is

$$S_n = \frac{n\pi v}{L\omega_{bn}} \tag{6.3}$$

In eqs. (6.1) and (6.3) the quantity ω_{bn} is the n-th natural circular frequency of the beam.

```
//BenchMark Yang for the QC moving on the Euler Bernoulli Beam
//Create Domain
Domain* Dominio = new Domain();
//Define Nodes
Node* Nodo_1 = new Node(1, 0,00 0.00);
Node* Nodo_2 = new Node(2, 1.25, 0.00);
Node* Nodo_3 = new Node(3, 2.50, 0.00);
Node* Nodo_4 = new Node(4, 3.75, 0.00);
Node* Nodo_5 = new Node(5, 5,00, 0.00);
Node* Nodo_6 = new Node(6, 6.25, 0.00);
Node* Nodo_7 = new Node(7, 7.50, 0.00);
Node* Nodo_8 = new Node(8, 8.75, 0.00);
Node* Nodo_9 = new Node(9, 10.00, 0.00);
Node* Nodo_10 = new Node(10, 11.25, 0.00);
Node* Nodo_11 = new Node(11, 12.50, 0.00);
Node* Nodo_12 = new Node(12, 13.75, 0.00);
Node* Nodo_13 = new Node(13, 15.00, 0.00);
Node* Nodo_14 = new Node(14, 16.25, 0.00);
Node* Nodo_15 = new Node(15, 17.50, 0.00);
Node* Nodo_16 = new Node(16, 18.75, 0.00);
Node* Nodo_17 = new Node(17, 20.00, 0.00);
Node* Nodo_18 = new Node(18, 21.25, 0.00);
Node* Nodo_19 = new Node(19, 22.50, 0.00);
Node* Nodo_20 = new Node(20, 23.75, 0.00);
Node* Nodo_21 = new Node(21, 25.00, 0.00);
//Add nodes to Domain
Dominio->AddNode(Nodo_1);
Dominio->AddNode(Nodo_2);
Dominio->AddNode(Nodo_3);
Dominio->AddNode(Nodo_4);
Dominio->AddNode(Nodo_5);
Dominio->AddNode(Nodo_6);
Dominio->AddNode(Nodo_7);
Dominio->AddNode(Nodo_8);
Dominio->AddNode(Nodo_9);
Dominio->AddNode(Nodo_10);
Dominio->AddNode(Nodo_11);
Dominio->AddNode(Nodo_12);
Dominio->AddNode(Nodo_13);
Dominio->AddNode(Nodo_14);
Dominio->AddNode(Nodo_15);
Dominio->AddNode(Nodo_16);
Dominio->AddNode(Nodo_17);
Dominio->AddNode(Nodo_18);
Dominio->AddNode(Nodo_19);
Dominio->AddNode(Nodo_20);
Dominio->AddNode(Nodo_21);
//Define Mechanical Properties
double E = 2.87e9;
double I = 2.90;
double rho = 2500.;
double A = 0.9212;
//Define Euler-Bernoulli beam elements
beam101* Element_1 = new beam101(1, 1, 2, A, I, E, rho);
beam101* Element_2 = new beam101(2, 2, 3, A, I, E, rho);
beam101* Element_3 = new beam101(3, 3, 4, A, I, E, rho);
beam101* Element_4 = new beam101(4, 4, 5, A, I, E, rho);
beam101* Element_5 = new beam101(5, 5, 6, A, I, E, rho);
beam101* Element_6 = new beam101(6, 6, 7, A, I, E, rho);
beam101* Element_7 = new beam101(7, 7, 8, A, I, E, rho);
beam101* Element_8 = new beam101(8, 8, 9, A, I, E, rho);
```

```
beam101* Element_9 = new beam101(9, 9, 10, A, I, E, rho);
beam101* Element_10 = new beam101(10, 10, 11, A, I, E, rho);
beam101* Element_11 = new beam101(11, 11, 12, A, I, E, rho);
beam101* Element_12 = new beam101(12, 12, 13, A, I, E, rho);
beam101* Element_13 = new beam101(13, 13, 14, A, I, E, rho);
beam101* Element_14 = new beam101(14, 14, 15, A, I, E, rho);
beam101* Element_15 = new beam101(15, 15, 16, A, I, E, rho);
beam101* Element_16 = new beam101(16, 16, 17, A, I, E, rho);
beam101* Element_17 = new beam101(17, 17, 18, A, I, E, rho);
beam101* Element_18 = new beam101(18, 18, 19, A, I, E, rho);
beam101* Element_19 = new beam101(19, 19, 20, A, I, E, rho);
beam101* Element_20 = new beam101(20, 20, 21, A, I, E, rho);
//Add Elements to Domain
Dominio->AddElement(Element_1);
Dominio->AddElement(Element_2);
Dominio->AddElement(Element_3);
Dominio->AddElement(Element_4);
Dominio->AddElement(Element_5);
Dominio->AddElement(Element_6);
Dominio->AddElement(Element_7);
Dominio->AddElement(Element_8);
Dominio->AddElement(Element_9);
Dominio->AddElement(Element_10);
Dominio->AddElement(Element_11);
Dominio->AddElement(Element_12);
Dominio->AddElement(Element_13);
Dominio->AddElement(Element_14);
Dominio->AddElement(Element_15);
Dominio->AddElement(Element_16);
Dominio->AddElement(Element_17);
Dominio->AddElement(Element_18);
Dominio->AddElement(Element_19);
Dominio->AddElement(Element_20);
//Impose BC
SP_Constraint* Const1 = new SP_Constraint(1, 1, 0);
SP_Constraint* Const2 = new SP_Constraint(2, 21, 0);
//Add Constraint to the Domain
Dominio->AddSP_Constraint(Const1);
Dominio->AddSP_Constraint(Const2);
//Set the Recorder
std::string path = "D:\\steve-rodger\\matlab-yang-analytical";
std::vector<int> node_rec = { 11 };
std::vector<int> dofs_rec = { 0 };
//Node Recorder
//Displacement recorder
Node_Recorder* Rec_1 = new Node_Recorder(1, path, node_rec, dofs_rec, "disp");
//Add Recorders to Domain
Dominio->AddNode_Recorder(Rec_1);
//Set the element of which the Road is composed of
std::vector <int> roadEle = { 1,2,3,4,5,6,7,8,9,
    10,11,12,13,14,15,16,17,18,19,20 };
//Add them to Domain
Dominio->eleRoad = roadEle;
//Select vehicle properties
int nVehicles = 1;
std::vector <double> Mass = { 5750. };
std::vector <double> Damp = { 0. };
std::vector <double> Stif = { 1595.e3 };
std::vector <double> vel = { 27.7778 };
std::vector <double> interAxles = { };
//Define a Standard traffic Pattern
Standard* Traffic_1 = new Standard(1, Dominio, nVehicles,
```

```
    Mass, Damp, Stif, vel, interAxles);
//Add traffic pattern to Domain
Dominio->AddTrafficPattern(Traffic_1);
//Create a traffic analysis object
Traffic_Analysis* Analisi = new Traffic_Analysis(1,
    Dominio, 0.001, 25./ 27.7778);
//Add analysis to Domain
Analisi->Analyse();
//Clear the memory
Dominio->ClearAll();
```

Listing 6.14: *Ghost* main c++ file for the Yang example.

Here the structure is discretized taking advantage of 20 **beam101** elements, each of the 21 nodes is equally spaced for a distance of 1.25 m. Once that nodes are defined the are added to the **Domain** object by the method **AddNode**, which is able to store the object address in the unordered_map of which the Domain is composed of. Same procedure can be followed for the elements. Once that, the spatial domain is created the boundary condition can added to the **Domain** through the function **AddSP_Constraint** method. The node **Recorder**s are defined to return the displacements of the node 11, which is the beam midpoint. Hence, the element on which the vehicle moves on are specified in the vector **roadEle**, which is added to the **Domain** as well. Furthermore, the vehicle parameters need to be set, for this simple case the traffic patter creted and added to the **Domain** is the **Standard**, where apart from the tag the vehicle mechanical characteristics need to specified as a double vectors. Hence, it is possible to create the **Traffic_Analysis** object, which once populated by all the required parameters is analyzed by the **Analyse** method. Lastly the dynamic memory which is allocated during all the entire process is deleted calling a **Domain** method named **ClearAll**. The results in terms of midpoint beam displacements over the time are depicted in fig. 6.4. Where it is possible to observe the accuracy between to the original formulation developed and reported in [31].

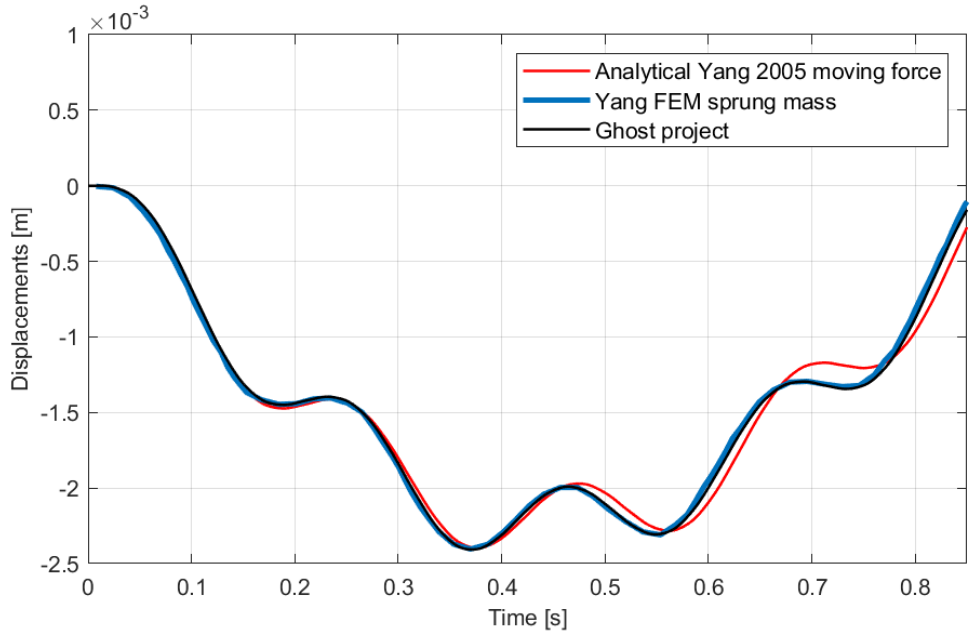

Figure 6.4: Comparison between the analytical and finite elements formulation of the Yang example.

In the analytical solution results, the first five modes of the associated Euler-Bernoulli beam are used to compute the displacement response through eq. (6.1). Notably, the results obtained from the *Ghost Project* align with the finite element formulation presented in [31] for the same mechanical problem.

Chapter 7

Numerical Simulation of Vehicle-Bridge Interaction

In the constantly evolving field of engineering, numerical simulations have emerged as indispensable tools, revolutionizing the understanding and analysis of complex systems. A particularly intriguing and vital area of study is the interaction between vehicles and bridges. As infrastructure expands and transportation systems become more sophisticated, the need for a comprehensive understanding of vehicle-bridge dynamics is more critical than ever. This interaction is a multifaceted phenomenon, influenced by factors such as vehicle dynamics, road conditions, environmental effects, and the structural characteristics of bridges themselves. Numerical simulations offer a platform for modeling these intricate interactions, enabling engineers to gain insights into the dynamic forces at play. With the role of numerical simulations becoming increasingly significant in the realm of infrastructure, they prove essential for modeling the dynamics of vehicle-bridge interactions. These simulations are crucial for understanding the various factors involved, including vehicle dynamics, road conditions, environmental influences, and the bridges' structural features. This comprehensive approach is key for optimizing bridge design and maintenance strategies, ensuring safety and long-term cost-effectiveness. Engineers use these simulations to explore different designs and materials, aiming to enhance the resilience and efficiency of bridges. Numerical simulations are invaluable for predicting the long-term performance of bridges. They allow engineers to proactively address potential issues by considering factors such as material degradation and changing traffic patterns, thereby extending the lifespan of bridges. The innovative application of simulations leads to groundbreaking solutions in bridge design and construction, incorporating advanced materials and technologies. Various simulations are presented, focusing on traffic scenarios and experimental investigations on bridges. The forthcoming chapter delves into diverse simulation methodologies, building upon the numerical tools discussed previously. The objective is to establish a robust and precise framework that emulates real-world bridge monitoring systems. This involves systematic calibration of parameters, including environmental and other factors, using methodologies outlined in previous chapters. The potential applications of these simulations are vast, ranging from comprehensive continuous monitoring systems to specific investigative campaigns. By integrating parameters like temperature trends, traffic variations, and the bridges' geometric and mechanical properties, a detailed numerical representation of these systems is achieved. The insights from these simulations are applicable to a wide range of objectives. In today's era of big data, algorithms and hardware capable of handling large datasets make these simulations even more valuable. They can be tailored for monitoring and analyzing damage to structures under traffic loads and more, utilizing artificial intelligence techniques. This opens new

possibilities for the maintenance and safety of infrastructure. In the subsequent sections, numerical simulations performed with the *Ghost project* are presented. These simulations serve a dual purpose: they showcase the software's potentialities and highlight key considerations about Vehicle-Bridge Interaction, which emerge as natural consequences of studying this specific interaction phenomenon. The simulations are meticulously designed to demonstrate not only the capabilities of the software but also to shed light on the complexities and nuances of Vehicle-Bridge Interaction. By delving into this particular interaction, the simulations reveal critical insights that are essential for understanding and improving the interaction between vehicles and bridges. Through these simulations, various aspects of Vehicle-Bridge Interaction are explored. The findings not only reinforce existing knowledge but also unveil new perspectives and understandings of the interaction. This contributes to the ongoing development of more sophisticated and resilient infrastructure. The 'ghost project' thus stands as a pivotal tool in advancing the field, offering both a practical application in the form of software and a theoretical expansion in the understanding of vehicle-bridge dynamics. In the following several numerical simulations are presented aimed to the representations of real scenarios. Both *direct* and *indirect methods* are investigated, with some emphasis on the effects of the so-called *driving frequency*, which can be impctfull on modal estimations.

7.1 Bridge description and external factors calibration

In the pursuit of a comprehensive understanding of the intricate dynamics inherent in vehicle-bridge interaction, the following numerical simulations have been meticulously conducted on an existing bridge structure (see fig. 7.2). Building upon the foundation laid in the preceding chapter, where various simulation types and their significance were delineated, these simulations delve into the realms of real-world application. Focused on the nuanced interplay between vehicles and a singular-span bridge composed of three precast reinforced concrete beams with an extended transverse deck, the simulations aim to elucidate the diverse scenarios and potential outcomes within the purview of this complex phenomenon.

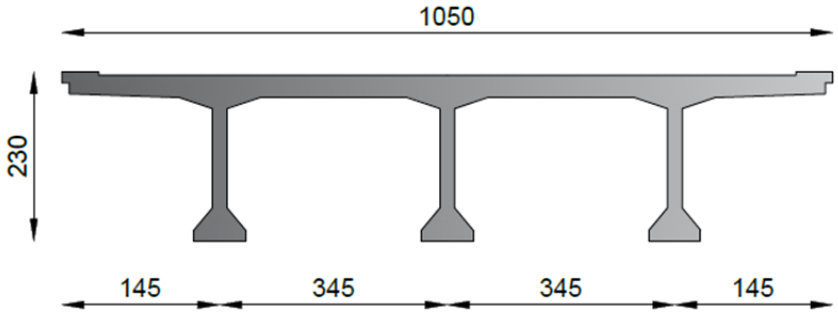

Figure 7.1: Exemplification of the beam cross-section.

A single-span simply supported bridge comprises three precast reinforced concrete beams and a transversely extended deck with a length of 10.50 meters. The three beams have a height of 1.95 meters, while the thickness of the concrete deck is 30 cm. The three beams beneath the deck are evenly spaced at 345 cm, with the central beam positioned at the symmetry axis of the section. The applied boundary conditions are the same of the double-tee beam case in the previous chapters, which are here modelled restraining the vertical and the horizontal degrees of freedom together with the degrees of freedom associate with the uniform and the non-uniform torsion. The mechanical and geometrical

feature of the above mentioned cross-section are collected in table 7.1

Section properties			
Area	A	4.93E+00	m^2
Shear Factor y-y	χ_y	5.12E-01	m^2
Shear Factor z-z	χ_z	2.56E-01	m^2
Second moment of area y-y	I_y	4.23E+01	m^4
Second moment of area z-z	I_z	2.59E+00	m^4
Torsional constant	J	1.63E-01	m^4
Second moment of warping	I_ω	2.15E+01	m^6
Mixed moment ω-y	$I_{\omega y}$	3.50E+01	m^5
Material properties			
Density	ρ	2.50e+03	kg/m^3
Young modulus	E	4.00e+10	N/m^2
Poisson's coefficient	ν	3.00e-01	–

Table 7.1: Section and material properties of the beam cross-section.

Also in this case, as in the previous numerical benchmarks, the geometric characteristics of the section were computed using the *Sectionproperties* python library. In particular, this software exploit a triangular mesh for the desired section and in the current case the choose dimension is equal to 0.05 m. The mesh dimension is calibrated by a sensitivity analysis in term of computed cross-sectional characteristics.

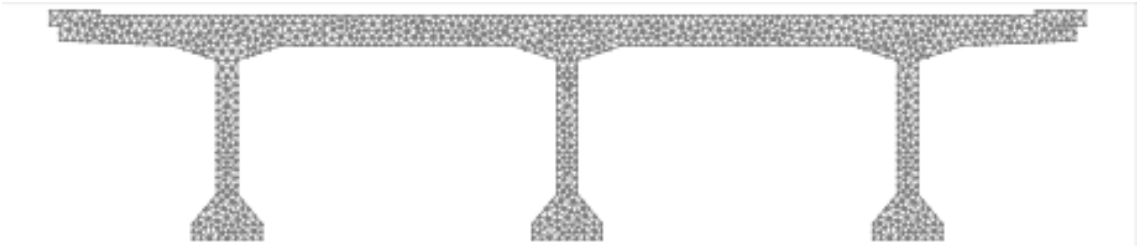

Figure 7.2: Meshed cross section: *Sectionproperties* python library.

Moreover, Young modulus variation due to temperature changing is as well shown in fig. 7.3.

The overall length of the bridge structure between the two supported end is equal to 30 m. The bridge is characterized by one carriageway and two lane one for each direction. This observation is somewhat important because allows to consider an adequate deviation of the two traffic direction with respect to the central axes of the beam. Due to the following numerical configurations of the beam problem, in this section some of the basic properties of the bridge are investigated. In particular, a modal analysis with a standard Young modulus of 40 GPa is carried out in order to asses what are the modes of vibration of the bridge, which are taken as a reference values at temperature equal to $20°C$. Natural frequencies and the associated modes of vibration of the analysed structure are summarized in table 7.2. Additionally, in the upcoming numerical simulations, all previously mentioned disturbance phenomena will be introduced. Therefore, concerning thermal variations, it is pertinent to analyze the modal frequency behavior of the structure with respect to ambient temperature fluctuations. Here, it is assumable that the beam is fabricated utilizing reinforced concrete, hence eq. (5.3) can be employed. The same

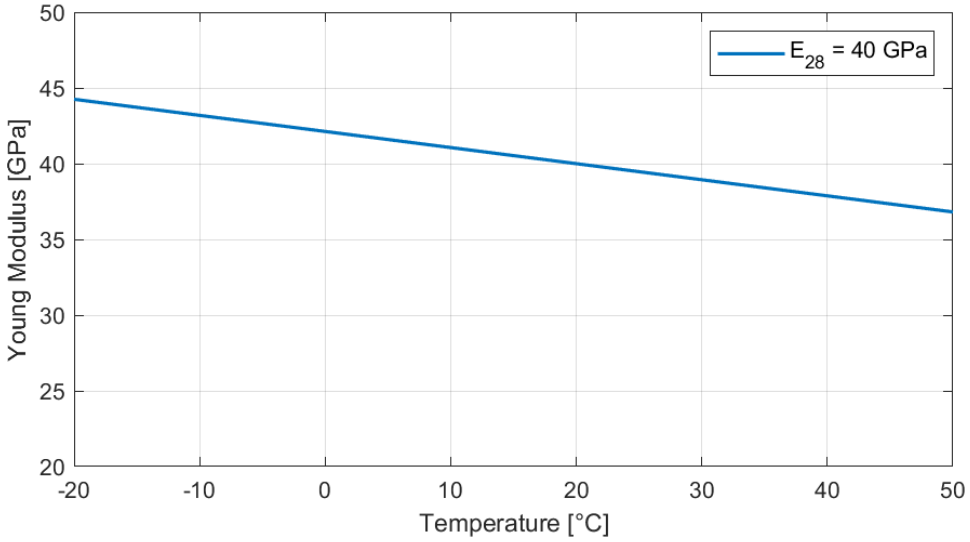

Figure 7.3: Young modulus variation with temperature.

temperature range, from $-20°C$ to $50°C$, is investigated and the natural frequency shifts are illustrated in fig. 7.4.

Bridge Modal Properties		
	Frequency [Hz]	Mode
1	4.97	Vert
2	10.52	Tors - Hor
3	15.50	Hor - Tors
4	18.98	Vert
5	28.27	Tors - Hor

Table 7.2: Bridge modal analysis, $T = 20°$.

Furthermore, the environmental excitation needs to be addressed. Performing parametric analysis make the ε parameter varying from 10 to 100000, multiplying by a factor ten for each simulation, over the vertical and the horizontal degrees of freedom. The value of the RMS in terms of the accelerations retrieved at the beam mid-point, are the treated by implementing the same procedure, mediated through a linear regression already showed in the previous chapters. Hence, the resulting punctual results, derived from the parametric analysis, together with the linear regression line, obtained by computing the slope coefficients β_1 and β_2, respectively for the vertical and the horizontal degree of freedom, can be plotted (see fig. 7.5).

Where the slope coefficients are equal respectively to $\beta_1 = 3.46e-08$ and $\beta_2 = 1.09e-08$. Hence, known all the desired values it easy to exploit the plot reported in fig. 7.5 the selected the desired values of ε selecting the target RMS in terms of accelerations. Once that, the environmental factors are calibrated, the traffic related phenomena need to be addressed. Several tests can be conducted numerically using the developed tool. Examples include the classical dynamic tests such as Experimental Modal Analysis (EMA), Operational Modal Analysis (OMA) in the presence of ambient excitation alone, and with active traffic-induced excitation. Various monitoring systems, ranging from sea-

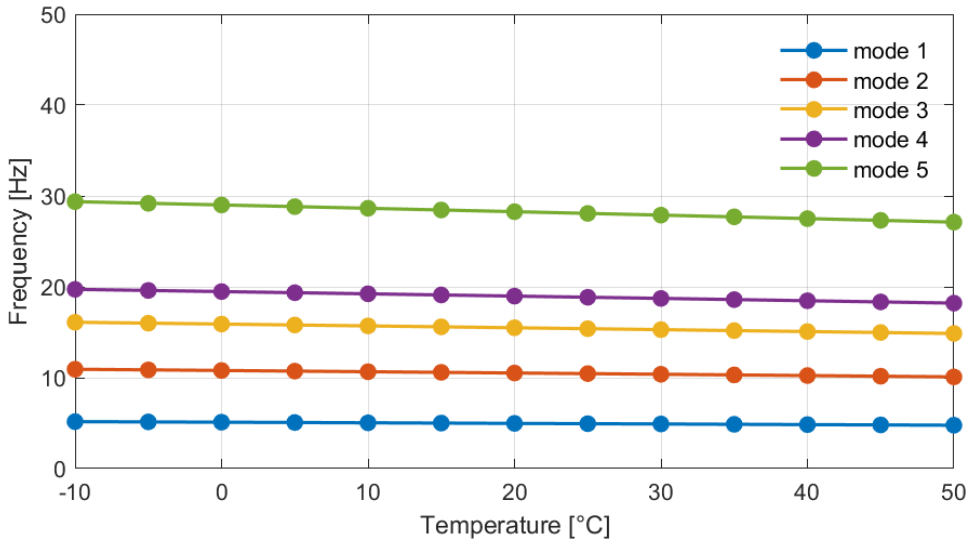

Figure 7.4: Natural frequency shifts due to temperature variation.

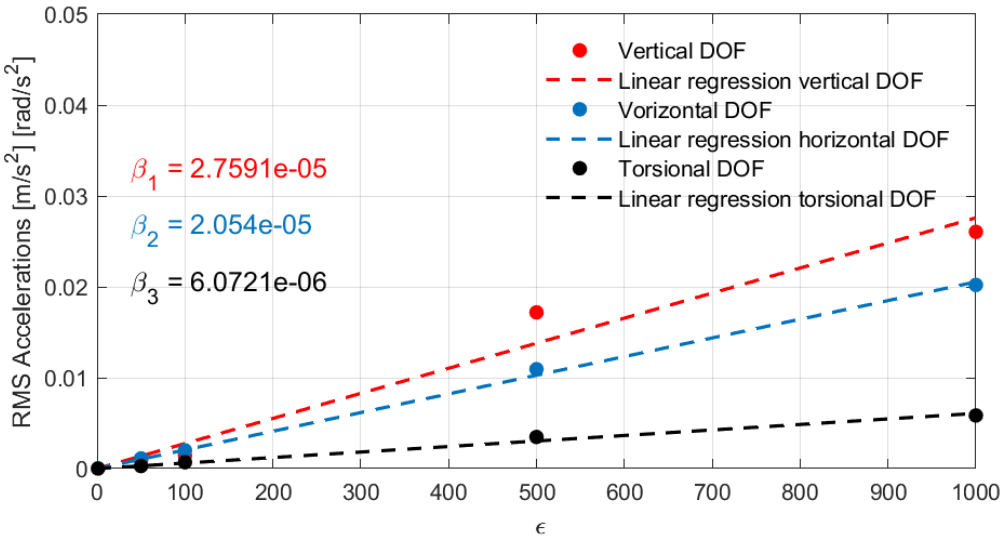

Figure 7.5: Environmental excitation calibration ε Vs RMS of accelerations.

sonal assessments to continuous monitoring, can be evaluated. Additionally, the tool enables the examination of the structural elements' responses to external loads. Of particular interest is the analysis of phenomena induced by *driving frequencies* on monitoring systems, especially in the context of autonomous vehicles moving at constant speeds. The versatility of these numerical tests facilitates a comprehensive exploration of the bridge's behavior under diverse conditions, contributing to a nuanced understanding of its dynamic response to varying dynamic situations.

7.2 Simulation of periodic tests

Simulation of a seasonal experimental campaign involves emulating the dynamic responses of the bridge structure under the influence of changing environmental conditions throughout the year. This comprehensive numerical test aims to capture the variations in temperature, traffic patterns, and other seasonal factors that can impact the structural behavior. By incorporating these dynamic elements into the simulation, it provides insights into how the bridge responds to the dynamic interplay of environmental and traffic-related influences across different seasons. The sensors placements is fully described in fig. 7.6. It consists in a total number of 9 acceleration transducers, of which 6 are dedicated to the vertical degree of freedom and 3 to the horizontal one. Each sensor station is evenly spaced for a length equal to a quarter of the entire beam. The numerical simulations carried out are of two different categories aimed at the simulations of two experimental scenarios. The first typology concerns the test performed on the bridge structures periodically in order to investigate the dynamics of the manufacts with active traffic flow, in order to retrieve the modal information of the bridge under operative conditions. The second scenario, represents the experimental campaign, where the bridge is closed to traffic to exploit the environmental excitation. The hypothesized tests are designed to be performed four times per year, where for each day of field test three different tests are simulated, two where the bridge is open to traffic, and one test where only the environmental vibrations are exploited, considering the bridge closed to traffic. As a matter of fact, environmental OMA tests tend to be performed during the night hours, especially in very busy roads to minimize the effects of the traffic interruptions. The table 7.3 reports the nomenclature associated with every single tests together with the temporal information related to the test execution. The temperature variations along the days are retrieved by real registrations deriving from a measurement station, named *AL007* placed in Rome, whose spatial coordinates in terms of latitude and longitude are respectively 41.909317° and 12.496543°. The sampling frequency of the temperature is equal to 30 minutes. Since the 60 minutes duration of each test two environmental temperature are experienced, which however don't show strong variations during the simulated process as shown in table 7.3.

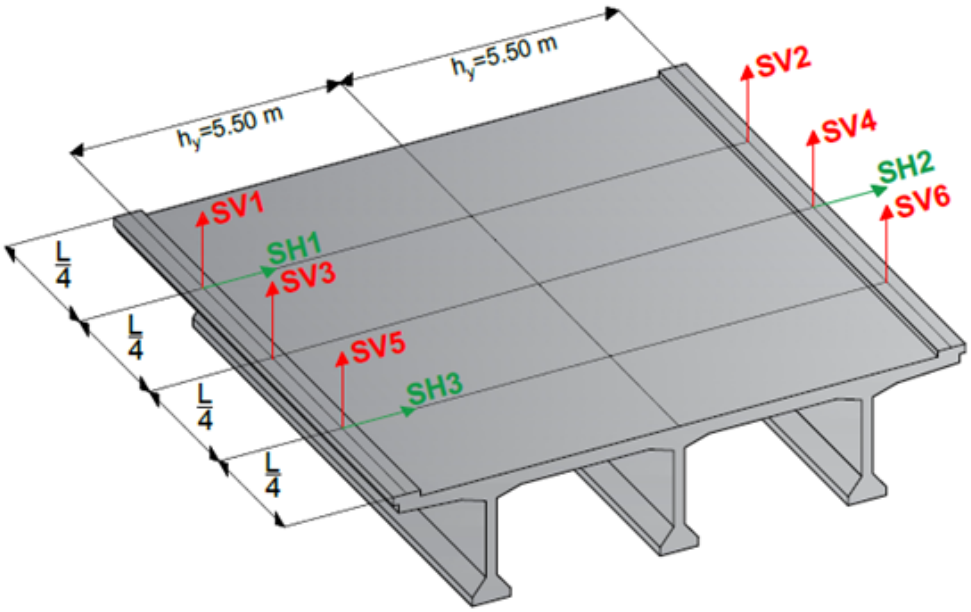

Figure 7.6: Sensor placement investigated beam.

Tag	Date	Start time	End time	T_1[°C]	T_2[°C]	Excitation
A1	15/01/2018	08:30	09.30	6.04	6.76	Traffic
A2	15/01/2018	16:00	17:00	12.32	12.51	Traffic
A3	15/01/2018	22:30	23:30	7.84	8.14	Environmental
B1	15/04/2018	08:30	09:30	12.13	13.23	Traffic
B2	15/04/2018	16:00	17:00	19.22	19.43	Traffic
B3	15/04/2018	22:30	23:30	8.21	8.55	Environmental
C1	15/07/2018	08.30	09:30	23.07	23.57	Traffic
C2	15/07/2018	16:00	17:00	26.49	26.45	Traffic
C3	15/07/2018	22:30	23:30	23.23	22.94	Environmental
D1	15/10/2018	08.30	09:30	20.66	22.23	Traffic
D2	15/10/2018	16:00	17:00	19.22	19.77	Traffic
D3	15/10/2018	22:30	23:30	16.46	15.93	Environmental

Table 7.3: Periodic test description.

Furthermore, instrumental or electric noise can also be introduced in the analysis selecting a desired level of SNR, once the the RMS in term of acceleration of the signal is computed. The instrumental noise is then modelled as a Gaussian process as well for the desired level of SNR. As a matter of fact, this disturbance phenomena is manly due to the experimental equipment and can both be reduced or a-priori known.
Each test is conducted over a duration of one hour, adhering to a well-established Operational Modal Analysis (OMA) technique. It is recommended that the test duration be at least a thousand times the fundamental period of the structure to ensure robust results. Some results in terms of accelerations for the sensors named SV3 and SH2 are reported respectively in figs. 7.7 and 7.8, where it is possible to observe both the different responses in terms of vertical and horizontal components, as well as for the two different tests carried out with the beam open and closed to traffic, where only ambient noise is present

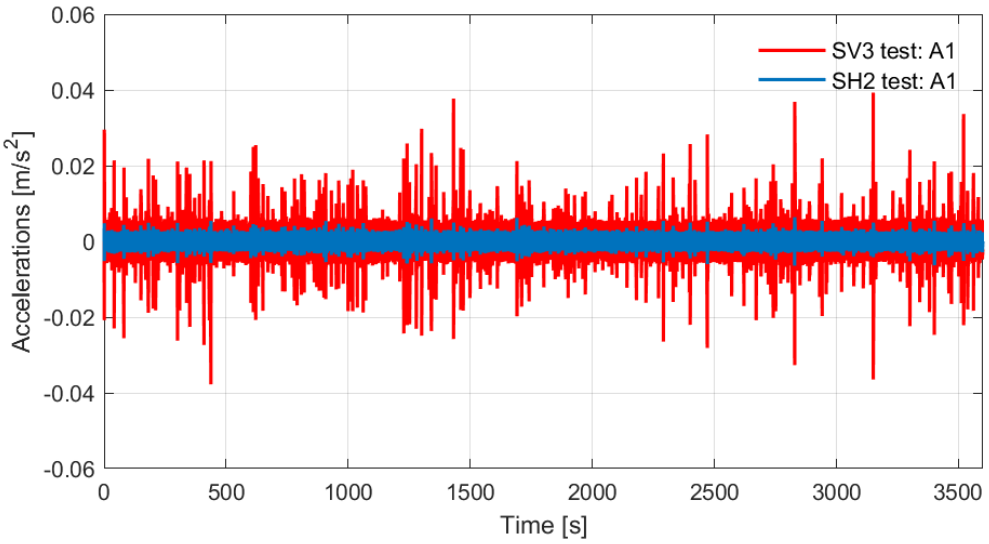

Figure 7.7: Accelerations response of sensors SV3 ad SH2 for test A1.

Environmental excitation is incorporated into the analysis by considering a set of

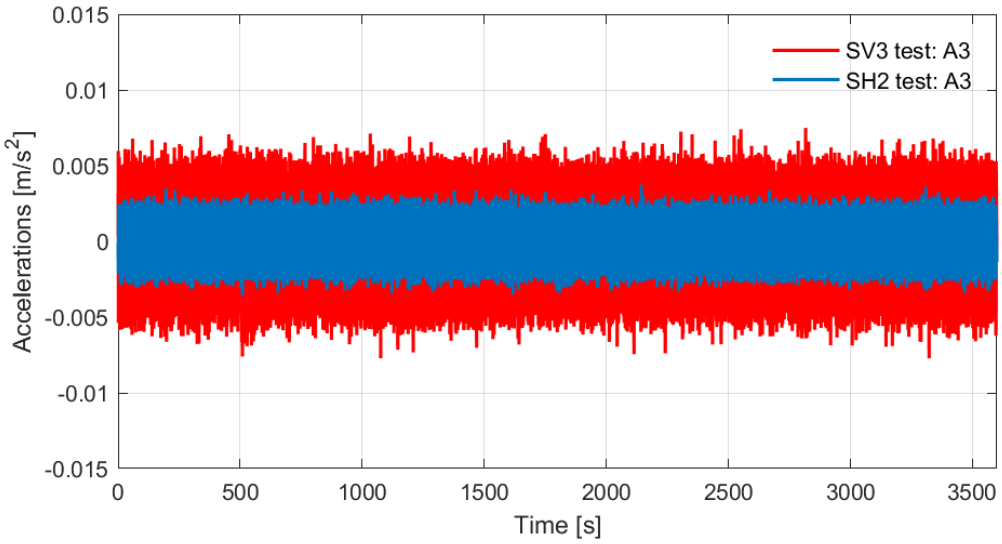

Figure 7.8: Accelerations response of sensors SV3 ad SH2 for test A3.

equivalent forces. These forces are stochastically generated using the technique previously described, with predefined values of ε set at 4, 5 and 50 for the vertical, the horizontal and the torsional degrees of freedom, respectively. These values are chosen to accurately replicate an environmental noise level, whose order in term of RMS of accelerations is about 10^{-4} g for the selected degrees of freedom. Furthermore, the road profile used in this analysis falls under Category A of the ISO 8608 standard, and it is characterized by a beam extension with 1000 discrete points. Vehicle calibration is performed using Weigh-in-Motion (WIM) data obtained from [164]. The study defines six distinct truck categories, specifying the probability distribution of inter-axle distances and axle forces for each category. To account for passenger cars, relevant data regarding mass limits and inter-axle distances are collected from various car manufacturers, and a uniform distribution is assigned to these quantities. The mechanical properties of the spring-dashpot devices are determined using the algorithm detailed in the previous chapter. Vehicle velocities are selected based on a uniform distribution, while adhering to Italian highway speed limits corresponding to each vehicle category. Moreover, the mutual distances between consecutive vehicles within each lane are calculated using traffic regulations from the same traffic code. To simulate realistic mechanical conditions and excitations, the traffic flow is organized into different lanes, with two directions of travel. Finally, the numerical model is discretized using 20 Timoshenko finite elements, which can adequately account for non-uniform torsion introduced in earlier chapters. Structural damping is incorporated using the widely accepted *proportional damping*, also known as 'Rayleigh damping.' This damping is calibrated based on the first and the fifth natural frequencies, achieving a damping ratio of 0.02, a value compatible with the operational conditions of typical bridge structures. Numerical simulations, employ a time step of $\Delta t = 0.0025$ s to advance the simulation. Such small time step is necessary to obtain accurate modal estimation on the structure, indeed acting with a larger time steps would certainly affect in positive manner the computational times associated with the analysis, but on the other hand a slightly decreasing in the accuracy of the signals is experienced. However, it is essential to note that in practical situations, expert technicians typically use specific instrumentation with defined sampling frequencies for conducting these types of analyses on real structures. To

align the numerical results with this real-world scenario, down-sampling on the generated data is performed. This down-sampling allows to achieve a sampling frequency that is consistent with the instrumentation typically employed by expert technicians in these kinds of structural analyses. The down-sampled is performed by a factor of 4 reaching a sampling frequency of 100 Hz. The responses in term of accelerations are processed by two well-known algorithms in the field of OMA, such as the Frequency Domain Decomposition (FDD) and the Covariance Driven Stochastic Sub-Space Identification (Cov-SSI). Hence, the channels are subject to a windowing technique with Hanning windows with 66% of overlapping resulting in a frequency resolution of 0.02 Hz. On the other hand, the Cov-SSi analysis is tuned by a sensitivity analysis able to give back the most suitable model order and time shifts for the analysed test. Here, the scatter limits for the stability of the identified poles are respectively, 1%, 2% and 5%, for frequency, Modal-Assurance-Criterion (MAC) and damping. The estimated natural frequencies from both the FDD and the Cov-SSI are reported for each test in tables 7.4 to 7.7 together with the resulting damping ratio retrieved from the Cov-SSI. The accelerations data were processed to a software named *S2-OMA*. This software allows to performed some basic procedure consdering some of the most employed algorithm for the modal estimation in the OMA context, such as the FDD, the Cov-SSI or the Second Order Blind Identification (SOBI).

Tag	**Mode**	**Natural Freq. FDD [Hz]**	**Natural Freq. Cov-SSi [Hz]**	**Damping** [%]
A1	1	5.06	5.06	5.28
A1	2	10.74	10.68	2.10
A1	3	15.76	15.69	1.72
A1	4	19.14	19.20	1.63
A1	5	28.26	28.25	1.77
A2	1	5.04	5.00	4.70
A2	2	10.62	10.59	2.14
A2	3	15.58	15.57	1.79
A2	4	19.08	19.04	1.74
A2	5	27.96	28.02	1.77
A3	1	5.08	5.05	3.92
A3	2	10.72	10.65	2.20
A3	3	15.68	15.65	1.74
A3	4	19.10	19.12	1.74
A3	5	28.20	28.18	1.75

Table 7.4: Natural frequencies estimation for test A.

In fig. 7.9 are reported the first singular values plot for the test with tag A, here are represented the three simulated experimental tests, where it is possible to notice how in the third test, the one where only environmental excitation is present, the peaks associated with the vertical modes resulting attenuate. This is manly due to the different levels of excitation along the vertical degrees of freedom between the two conditions, since that the quarter-car model excited mostly the beam along its vertical. Moreover, a graphical report about the result of the mode estimation is reported in fig. 7.10, where the previous fig. 7.4 is populated with the estimated natural frequencies as function of the temperature. Naturally, since the hour duration of the simulated test and the two associated temperature values, a single point in term of x coordinate is defined by the average between the two test temperatures.

Tag	Mode	Natural Freq. FDD [Hz]	Natural Freq. Cov-SSi [Hz]	Damping [%]
B1	1	5.04	4.99	5.02
B1	2	10.64	10.60	2.18
B1	3	15.62	15.57	1.80
B1	4	18.98	19.00	1.74
B1	5	27.96	28.04	1.73
B2	1	4.98	5.00	5.38
B2	2	10.52	10.51	2.18
B2	3	15.42	15.42	1.77
B2	4	18.86	18.85	1.71
B2	5	27.78	27.78	1.76
B3	1	5.04	5.05	4.28
B3	2	10.62	10.65	2.18
B3	3	15.66	15.63	1.77
B3	4	19.12	19.11	1.67
B3	5	28.18	28.19	1.80

Table 7.5: Natural frequencies estimation for test B.

Tag	Mode	Natural Freq. FDD [Hz]	Natural Freq. Cov-SSi [Hz]	Damping [%]
C1	1	4.94	4.88	4.47
C1	2	10.40	10.45	2.13
C1	3	15.36	15.35	1.79
C1	4	18.76	18.72	1.94
C1	5	27.56	27.63	1.77
C2	1	4.90	4.95	5.69
C2	2	10.44	10.39	2.20
C2	3	15.30	15.27	1.88
C2	4	18.74	18.67	1.76
C2	5	27.60	27.53	1.67
C3	1	4.92	4.95	3.96
C3	2	10.38	10.45	2.14
C3	3	15.36	15.35	1.76
C3	4	18.78	18.75	1.67
C3	5	27.78	27.65	1.70

Table 7.6: Natural frequencies estimation for test C.

The results in term of estimated frequencies and damping ratio deriving from the data treatment testimony the feasibility and reliability of the developed numerical framework. Here, all the main components which be found in a real situation are integrated ranging from the road roughness, the temperature variations or the effect of traffic on the investigated beam. Moreover, some of the employed data are easily accessible from the users, such as the temperature variations or the traffic data deriving from WIM procedures. Furthermore, analysing the obtained results in term of modal estimation is easy to observe or reliable is the modal estimation even though active traffic is acting on the bridge. This

Tag	Mode	Natural Freq. FDD [Hz]	Natural Freq. Cov-SSi [Hz]	Damping [%]
D1	1	4.94	4.93	5.27
D1	2	10.44	10.47	2.17
D1	3	15.46	15.39	1.84
D1	4	18.82	18.82	1.74
D1	5	27.72	27.69	1.74
D2	1	4.98	4.93	5.25
D2	2	10.46	10.50	2.09
D2	3	15.44	15.43	1.76
D2	4	18.88	18.84	1.71
D2	5	27.84	27.78	1.80
D3	1	5.00	4.99	3.82
D3	2	10.52	10.55	2.14
D3	3	15.60	15.49	1.77
D3	4	18.90	18.92	1.70
D3	5	27.92	27.89	1.77

Table 7.7: Natural frequencies estimation for test D.

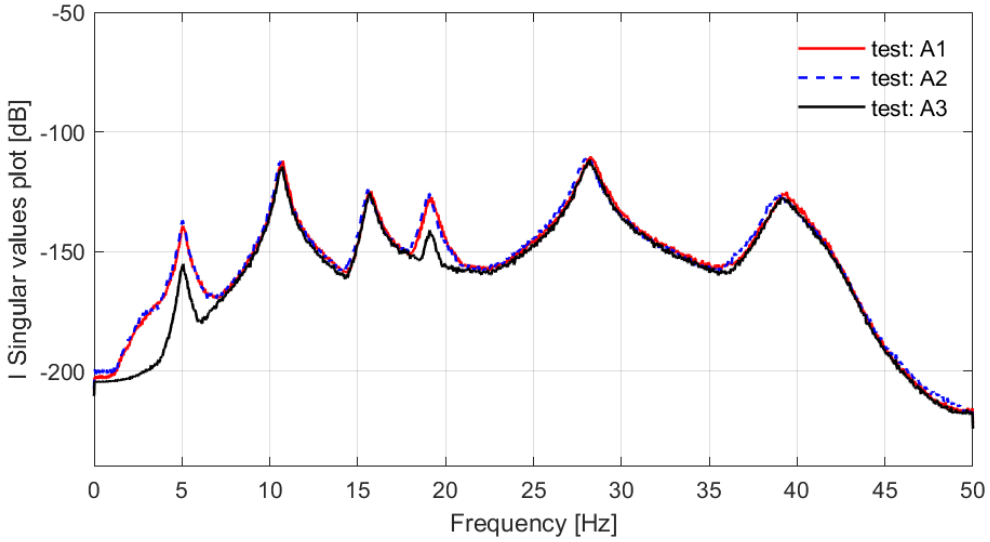

Figure 7.9: FDD, first singular values plot of tests: A1, A2 and A3.

point is crucial, indeed in some codes, such as the italian guidelines form bridges [60, 165], OMA tests with active traffic is allowable only with the presence of a WIM system. Although, this seems a pretty generic advise from the code, it is possible to demonstrate, that despite the excitation of the traffic a modal estimation, able to calibrate the numerical model for further numerical analysis does not necessary need a integrated WIM system. Surely, the levels of noise and excitation, whit respect to the classical OMA test can be altered by the traffic presence but at the same time the natural frequencies seem to be detectable. Those statements become even more clear observing the plot where the singular values of the FDD are depicted where it is possible to notice how for this level of

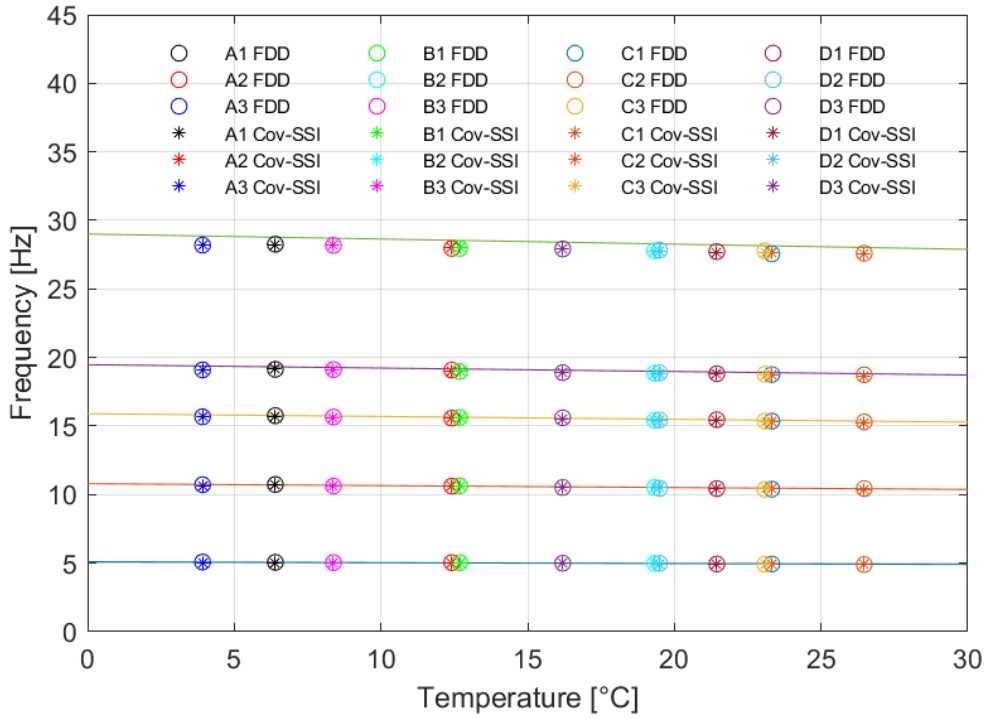

Figure 7.10: Results comparison: estimated natural frequencies Vs. modal shift due to temperature variation.

noise, the natural frequencies of the bridge are surely identifiable. Indeed, from fig. 7.9 is straightforward to notice how the two simulated tests where the also the traffic excite the structure are overlapping themselves, meanwhile the third test, that is a classical OMA test where only the environmental excitation is presented a downshift in for the vertical frequencies is observed. This situation seems to be quite normal since the quarter-car models own only a vertical degree of freedom which amplify the vertical dynamical effects on the bridge and the horizontal and the torsional peaks remain basically the same on the plot. In conclusion, it is possible to state that the experimental campaign should work also for the bridge open traffic. Hence, the modal estimation can happen without any traffic restriction and without interfere with the operative conditions of bridges.

7.3 Constant velocity simulation: the impact of the driving frequency on dynamic identification

Numerical simulations aimed to VBI can be used and implemented to verify and test several scenarios. Real traffic simulations are obliviously an immediate subject, but at the same time this kind of simulations can be implemented also study several effects, which traffic can imposed to real bridge structures. In particular in this section a particular scenarios and its related issued is analysed, where all the vehicle move along the bridge with the same velocity. Even though, this situation can seems, at least at first impact, far from reality, in the last few years the development of the autonomous vehicles reached high levels of reliability and it is not difficult to imagine that over the next ten years this framework can be fully implemented in the every day life. This traffic scenario could

amplify some mechanical phenomena, which can impact on the bridges structure. As a matter of fact, the of dynamic component, such as the so called *driving frequency* is not unknown and is well described in the scientific literature. This frequency component could certainly impact over the bridge modal estimation. *Driving frequency* in the investigated structural scheme, where a simply supported beam with a torsional restrain is considered, is function of both the bridge geometry and the vehicle speed, indeed can be estimated as

$$\omega_d = \frac{\pi \cdot v}{L} \tag{7.1}$$

Where v represents the vehicle velocity and L denotes the beam length. The following paragraph examines the impact and presence of this frequency component. It aims to understand how it detrimentally affects modal estimation and explores how this issue can be partially or fully addressed from a dynamical perspective. In the subsequent simulations, the same bridge structure with identical boundary conditions is considered. Environmental temperature is kept constant and equal to $20°C$, in order to exclude thermal phenomena from the current investigation. Traffic is generated considering both directions of flow, using the same WIM database [164]. However, cars and similar vehicles are excluded. The mutual distance between consecutive vehicles on the bridge is randomly determined based on a uniform distribution, with lower and upper limits set at 30 m and 40 m, respectively. This configuration represents a relatively busy road in terms of traffic, necessary for adequate excitation by vehicles passing over the bridge. Analyses are conducted both with and without environmental excitation to investigate the impact of this random component on the traffic scenario. The road roughness profile used is identical to that in previous simulations, incorporating a class A profile according to ISO standards. The beam length is consistently maintained at 30 meters. Meanwhile, vehicle velocities are parametrically investigated, ranging from 5 m/s to 30 m/s, in increments of 5 m/s. Each generated time history has a duration of 1500 seconds, which exceeds a thousand times the fundamental period of the structure, adhering to OMA specifications. The sensor layout hypothesized for the experimental campaign is the same as in the previous example. The responses of the vertical sensors are reconstructed by considering both the vertical responses of the beam and its torsional behavior. The same distance from the beam axis is maintained for the placement of the transducers, which is 5.5 m. A sample recorded responses for the vertical transducers SV1, SV3 and SV5 is shown in fig. 7.11 and **??**.

In the following section, the impact that the *driving frequency* has on such signals will be highlighted. This analysis will focus on understanding how the driving frequency, a crucial component in signal processing, influences the characteristics and behavior of the signals under study. This examination is essential for comprehending the dynamics of these signals and for optimizing their analysis and application in various contexts. . In this regard, the Power Spectral Density (PSD) can be employed as indicator. Indeed, the PSD is defined as the Fourier Transform of the auto-correlation function of a signal if the signal is continuous, or the Discrete Fourier Transform (DFT) if the signal is discrete. This transformation allows us to analyze how much power exists at different frequencies within the signal. The primary purpose of the PSD is to identify the dominant frequencies in a signal. It helps in understanding the frequency composition of the signal and in identifying any periodic components. This allows for the comparison of the power contributions of different frequency components. In this case the PSDs are computed by *Matlab R23*. Also in these cases the signals are down-sampled for a decimation factor equal to 4 and they are pre-processed by a 100 Hanning window functions. As a matter of facts, in signals application window functions are often applied to the signal before computing the PSD.

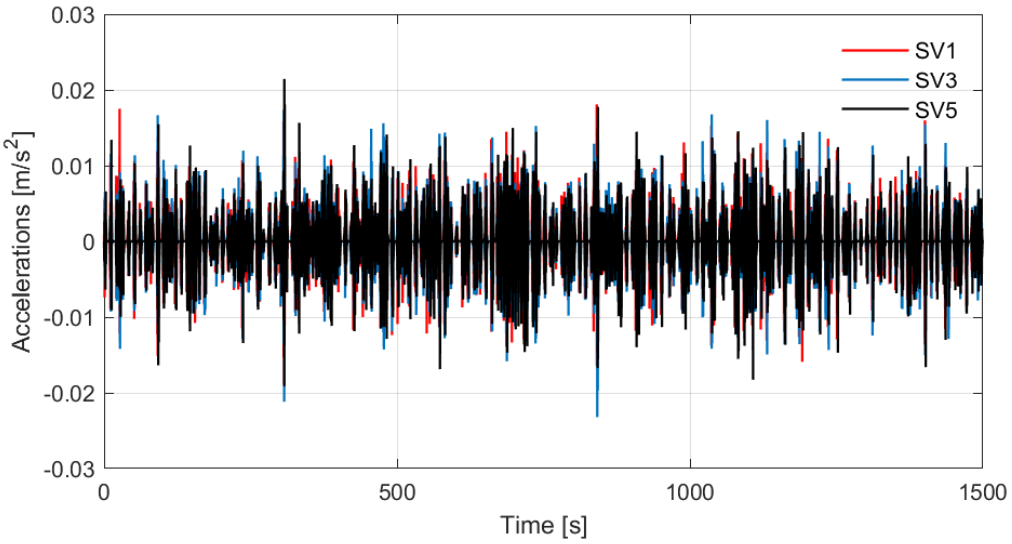

Figure 7.11: Acceleration responses measured for the transducers SV1, SV3 and SV5: environmental excitation not applied.

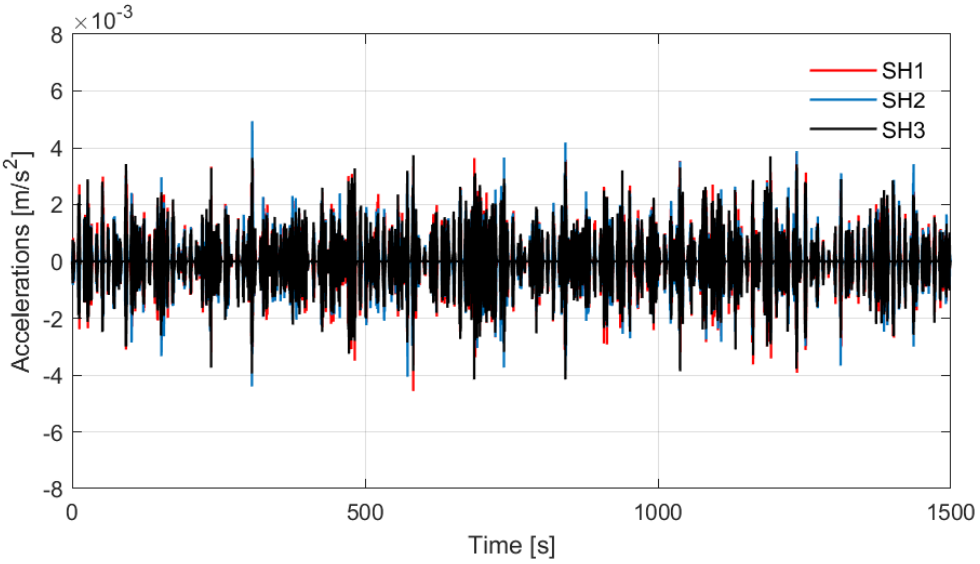

Figure 7.12: Acceleration responses measured for the transducers SH1, SH2 and SH3: environmental excitation not applied.

This is to mitigate the effects of discontinuities at the boundaries of the sampled signal, a phenomenon known as spectral leakage. In the following the PSD of the displacements, velocities and accelerations of the transducers named SV3 are presented for the different levels of vehicles speeds (see figs. 7.13 to 7.15).

Upon examination of the Power Spectral Density (PSD) plots, it is manifest that the influence of the *driving frequency* varies across different kinematic components. Particularly noteworthy is the impact on displacements, as illustrated in fig. 7.13, where the driving frequency components conspicuously emerge as predominant elements within the spectral distribution. Furthermore, a discernible shift in the peaks corresponding to the *driving*

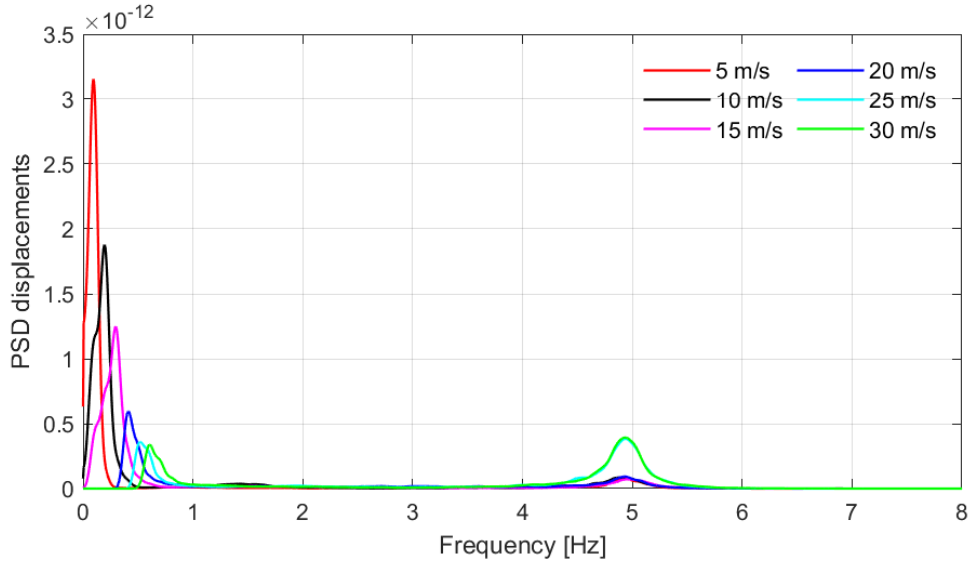

Figure 7.13: Displacements PSD of transducer SV3 in absence of environmental excitation.

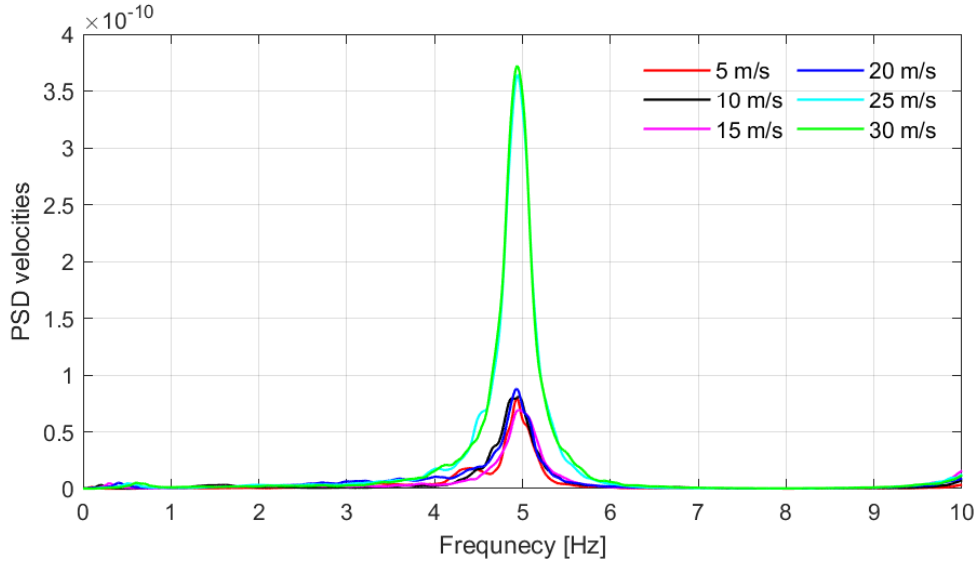

Figure 7.14: Velocities PSD of transducer SV3 in absence of environmental excitation.

frequencies is observed in relation to the increment in constant vehicle velocities. This phenomenon is a logical consequence, stemming from the intrinsic velocity-dependence of the physical process under consideration, given the constancy of the beam length. Conversely, the impact of the driving frequency on both velocity and acceleration is minimal. Within the velocity spectral analysis, the peaks attributable to the *driving frequency* are scarcely perceptible, and in the acceleration spectrum, they are virtually absent. This delineation elucidates a definitive scenario, from which pertinent conclusions can be drawn. Specifically, in the context of OMA estimations under the prevailing traffic conditions, a predilection for employing transducers calibrated for measuring acceleration or velocity is advisable, as opposed to those configured to monitor temporal displacement. The previous analysis are considered without the environmental effects. However, this excitation is

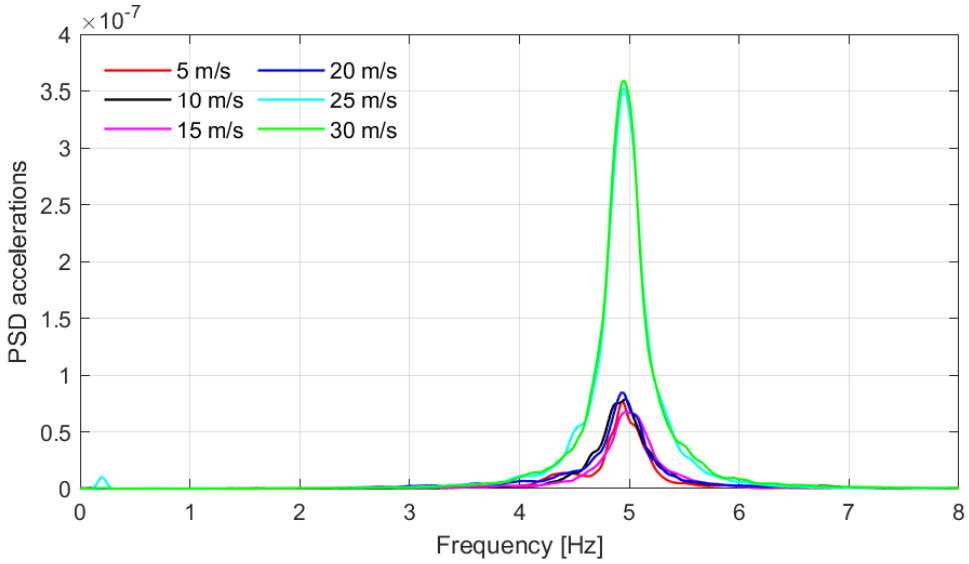

Figure 7.15: Accelerations PSD of transducer SV3 in absence of environmental excitation.

something that every structure experience for several levels. In the following the impact of the *driving frequency* are also investigated in presence of environmental excitation. The considered levels of environmental excitation are the same of the previous chapter that is a resulting RMS in term of accelerations of magnitude $10^{-4}g$. The focus, here is to investigate if the presence of this stochastic excitation can somewhat influence the *driving frequency* impact on the analysis estimation. In the following, only three values of velocity are considered, that are 10 m/s, 15 m/s and 25 m/s. The useful tool is once again the comparison in term PSD of the investigated kinematic components. Hereafter, the PSD of the accelerations is neglected because is trivial understand that the impact of the *driving frequency* on this mechanical quantity is negligible.

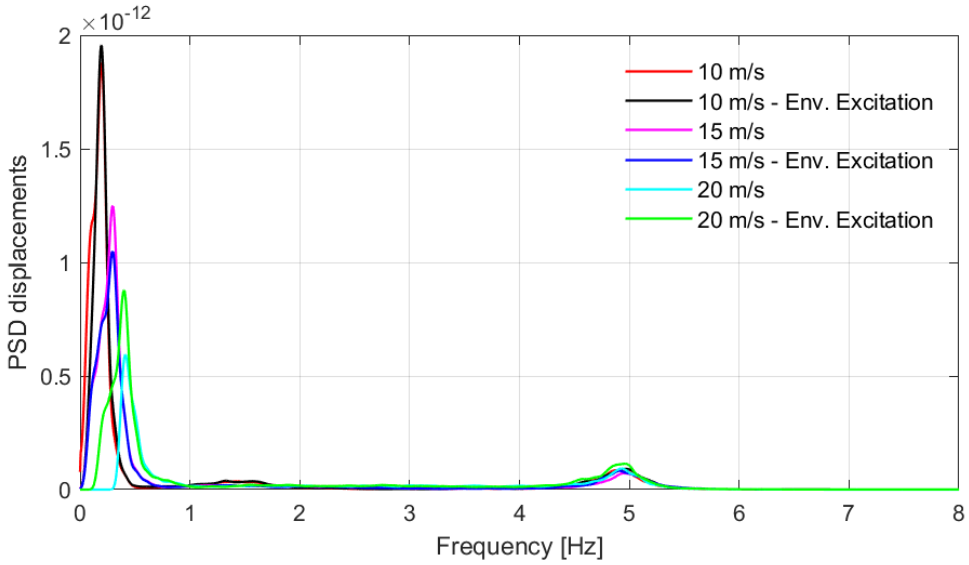

Figure 7.16: Displacements PSD of transducer SV3 comparison between presence or absence of environmental excitation.

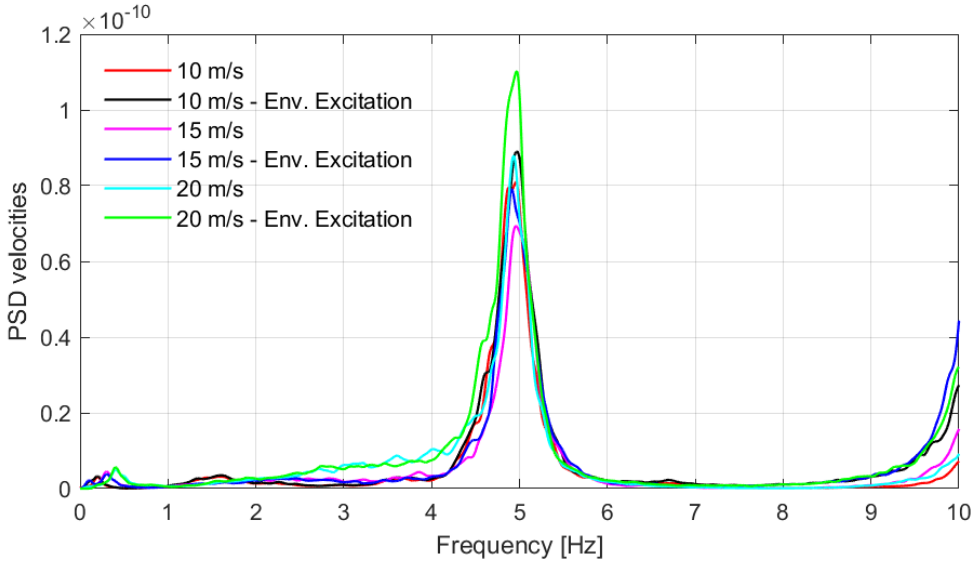

Figure 7.17: Velocity PSD of transducer SV3 comparison between presence or absence of environmental excitation.

Moreover, the impact of this frequency can also be investigated by inspecting the associated stabilization diagram deriving from a CoV-SSI application. In the fig. 7.18 is illustrated the comparison in term of stable poles of the stabilization diagram between the same numerical test, that is conducted with the vehicular traffic with constant speed equal to 25 m/s. Here, the stabilization plot holds all the kinematic components involved in the analysis. This visual approach is suitable for an immediate comparison of the impact of the *driving frequencies* for the diverse components. Indeed, is immediate to observe all the stables poles of all the three components aliened along the natural frequencies of the bridge, for the investigated temperature. Furthermore, only the stable poles which are associated with the displacements components show a concentration and an alignment around 0.4 Hz, which is the *driving frequency* owned by a vehicle which moves at 25 m/s over a bridge whose characteristic length is equal to 30 m. The same behavior is also evidenced by figs. 7.19 and 7.20, where the same procedure are taken into account for several levels of constant velocities ranging from 15 m/s to 25 m/s. Where it becomes even more evident how the unwanted frequency component is present, and thus causes a disturbance in identification only when measurements in terms of displacements are used.

Therefore, this observation is crucial for the existence and use of such methodologies. Indeed, from the previous chapter, it can be stated that experimental campaigns in the presence of traffic are not only possible, from the perspective of dynamic identification, but at the same time the presence of traffic excitation can even amplify frequency components, making their identification easier. Moreover, the negative effect that is substantially determined by the presence of the driving frequency can be greatly limited or mitigated by adopting an adequate acquisition chain that should essentially consist of speed transducers, or even better, acceleration transducers. Indeed, in the case where traffic develops in such a way that vehicles must maintain a constant speed, the use of displacement measurements could be hindered by the presence of this frequency component. It is also true that if the speed of the vehicles and the bridge's associated geometries are known, this frequency could be trivially filtered out by using signals that are not characterized by this negative element for dynamic identification.

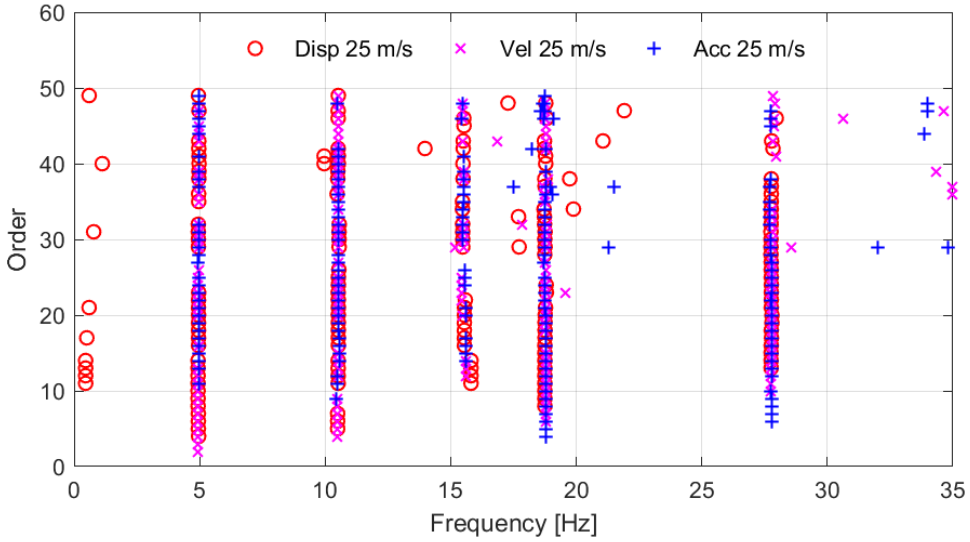

Figure 7.18: Stabilization diagram: comparison between displacements, velocities and accelerations. Traffic constant velocity equal to 25 m/s

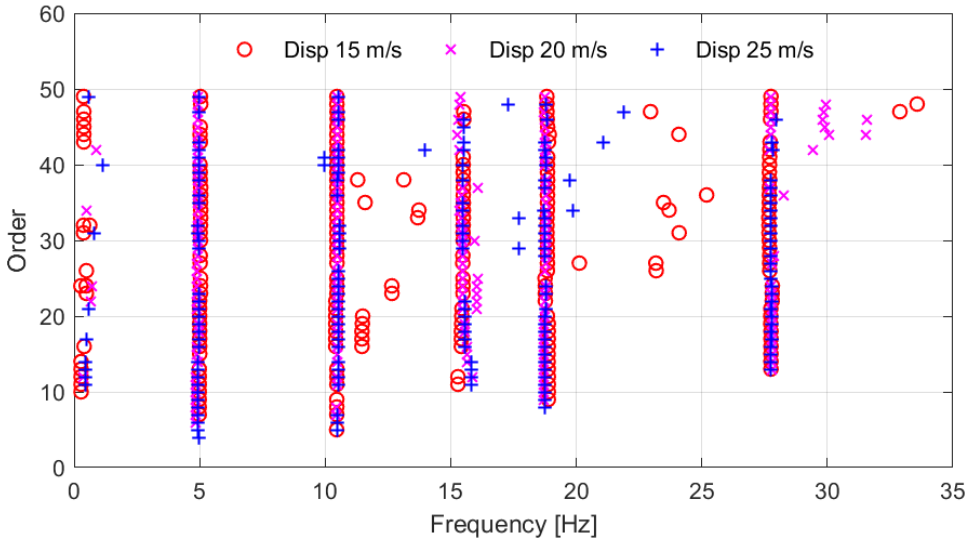

Figure 7.19: Stabilization diagram: displacements, constant vehicle velocities, 15 m/s, 20 m/s and 25 m/s.

7.4 Indirect method simulations

In this section, we explore the potential of the ghost project in numerical simulations, with a particular emphasis on the so-called indirect methods. The direct methods in vibration analysis, such as Experimental Modal Analysis (EMA) and Operational Modal Analysis (OMA), are classical methodologies aimed at estimating or obtaining the mechanical or dynamical properties of bridges from their responses, where these responses are directly acquired from the infrastructure. The first type, Experimental Modal Analysis (EMA), is a traditional approach where an external force is applied to the structure, and the resulting

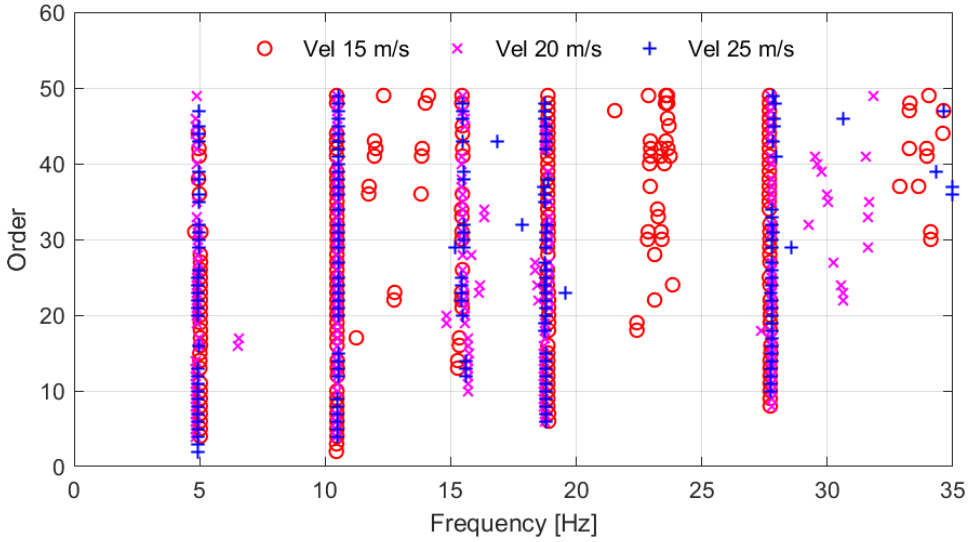

Figure 7.20: Stabilization diagram: velocities, constant vehicle velocities, 15 m/s, 20 m/s and 25 m/s.

vibrations are measured. EMA allows for precise control and understanding of the input forces, which leads to an accurate determination of the structure's modal parameters, such as natural frequencies, damping ratios, and mode shapes. This method is particularly useful for understanding how a structure behaves under known conditions, making it ideal for testing and validating theoretical models. However, it can be intrusive and expensive, requiring specialized equipment and often necessitating operational interruptions during testing. On the other hand, Operational Modal Analysis (OMA) represents a more modern approach, where the focus is on analyzing vibrations during the normal operation of the structure, without applying any artificial force. This method utilizes ambient vibrations caused by natural forces like wind, traffic, or other operational activities. The main advantage of OMA is its non-intrusive nature, allowing for continuous monitoring without disrupting the structure's function. Additionally, OMA is more practical and cost-effective, especially for large structures like bridges. However, the lack of control over input forces means that the results from OMA can sometimes be less precise than those obtained from EMA. Over the past 40 years, OMA has grown significantly as a field, offering a valuable alternative to EMA. It allows engineers to infer the modal properties of a structure by recording responses with appropriate sensors and making informed assumptions about the input forces. This approach provides several advantages over EMA, including easier installation, a more flexible layout, and reduced economic effort, making it an increasingly popular choice in the field of structural health monitoring. Despite the relatively minor impact of Operational Modal Methods compared to Experimental Modal Analysis, they still require some operational interaction with the infrastructure, such as sensor placement. There are times when responses due to environmental excitation are needed, and this necessitates closing the roads to traffic. It is in this context that the so-called *indirect methods* have emerged. In these methods, the modal characteristics of the bridges are not directly retrieved by transducers placed on the structures. Instead, the analyzed responses are derived from another mechanical system that has some relationship with the primary system, namely the bridge. In this perspective, vehicles are suitable for this purpose, as they have a contact relationship with the bridges when moving on them. Several studies

in recent years have focused on this constantly growing field. These studies often utilize a moving instrumented vehicle or some sort of truck-trailer system as moving transducers on bridges. Despite the appeal of these methodologies, many drawbacks have limited their implementation in a robust framework. Perhaps the most impactful aspect is the very poor frequency resolution achieved in these situations. Indeed, a moving instrumented vehicle traveling along a bridge does not provide recordings that are long enough for effective signal treatment. Additionally, the presence of the *driving frequency* and contamination from external factors, such as road roughness, also negatively impact the modal estimation of the bridges. Furthermore, these methods are often only capable of identifying and estimating a limited number of modal frequencies of the bridges. However, the limitations highlighted in this framework can be mitigated by a simple consideration of vehicle velocity. In fact, issues such as poor frequency resolution and the impact of road roughness can be diminished by using an instrumented vehicle that remains stationary at a precise spot on the beam, functioning as a real transducer. Indeed, reducing the vehicle's velocity to zero has a dual beneficial effect: firstly, it eliminates the influence of the driving frequency on the analyzed spectrum. Consequently, the vehicle is not affected by the road profile, allowing for longer recordings. In the following paragraph, numerical simulations for the *indirect method* framework are conducted. The primary objective is to investigate the feasibility of using stationary instrumented vehicles on bridge structures as transducers, and to assess the impact of various disturbing phenomena on the modal estimation. The bridge structure under consideration is the same beam discussed in previous chapters, with its section depicted in fig. 7.2. Thermal effects are neglected here, and the bridge, along with the Young's modulus, is assumed to be at a stable temperature of $20°C$. Three instrumented vehicles, each modeled as a single oscillator, are placed at three specific locations on the beam. These positions correspond essentially to the locations of the transducers named SV1, SV4, and SV5, as shown in fig. 7.6. The associated distance from the first beam end are respectively, 7.5m ,15m and 22.5m. In this condition only one vehicle axle is considered instrumented. Each vehicle is characterized by identical mechanical parameters, which are detailed in table 7.8.

Instrumeted vehicles properties		
Mass	500.00	kg
Stiffness coef.	19739.21	N/m
Damping coef.	3141.59	Ns/m

Table 7.8: Instrumented vehicles properties.

On the other hand, the principal system, namely he bridge, is considered to have two lanes accommodating one direction of traffic flow. The traffic is calibrated based on the same database [164] as used in the previous chapter, with cars being excluded from the probability selection. Indeed, the most impactful dynamic effects on bridge structures are attributed to trucks transiting on the investigated beam. The total duration of the recordings and simulations is set to 1500 seconds. However, an important consideration in these simulations is the introduction of fixed vehicles on the beam. Introducing these physical systems in the numerical simulations is akin to applying an impulse to the bridge, which needs to stabilize. The duration of this load assessment depends on several parameters, particularly the bridge damping. In this case, the same bridge damping as in the previous simulations is implemented, which is based on *proportional damping* calibrated on the first five modal frequencies of the unloaded system for a damping ratio of 0.02. Consequently, the numerical simulations are divided into two distinct phases. In the first phase, the

instrumented vehicles are introduced on the beam. Once the acceleration stabilizes to zero, traffic is then introduced into the model. The first phase is calibrated referring to (figs. 7.21 and 7.22) the bridge response and instrumented vehicles responses. It is possible to observe in figs. 7.21 and 7.22 how after 7.5s both the system reach a stationary conditions.

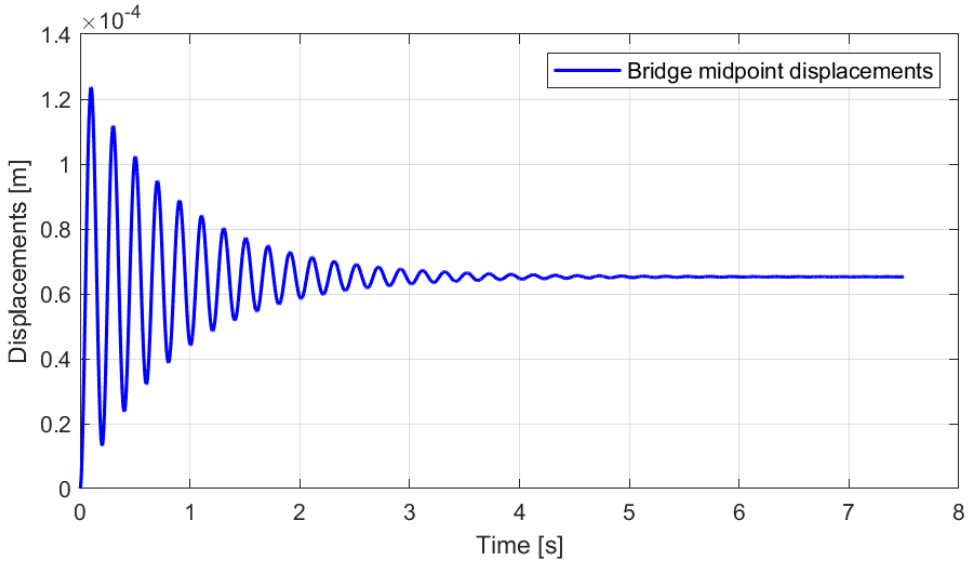

Figure 7.21: Bridge midpoint displacements due to the three instrumented vehicles.

Hence, each analysis is characterized by an initial 7.5-second period during which only the instrumented vehicles are on the bridges. Subsequently, a 1500-second traffic phase is simulated. The current simulations are carried out considering a time step of $\Delta t = 0.001s$, resulting in a sampling frequency of 1000 Hz. Prior to the application of the Frequency Domain Decomposition and Covariance-driven Stochastic Subspace Identification to the acceleration responses, a pre-processing step is required. Specifically, a down-sampling of the recordings is performed using a decimation factor of 10. Additionally, windowing is conducted by introducing 30 Hamming windows with 66% overlap, resulting in a frequency resolution of approximately 0.01 Hz. In this discussion, two main aspects are analyzed: the impact of road profile and environmental excitation on the numerical simulations of *indirect methods*. For the first aspect, three different road roughness conditions are tested: the first condition is a smooth road without any roughness; the second and third conditions correspond to a class A and a class B profile, respectively, as illustrated in fig. 4.3, using the same parameters employed to achieve the aforementioned conditions.

In scenarios involving a moving instrumented vehicle, road roughness introduces notable constraints, particularly in extreme conditions. For dynamic identification, a significant road profile acts as a disruptive element for the instrumented vehicle, potentially masking the bridge's intrinsic frequencies and adversely influencing modal analysis. In contrast, when the instrumented vehicles are stationary, the effect is diametrically opposite. The roughness of the road leads to better excitation of the primary system, an effect readily apparent in the accelerations recorded by the vehicle. As a result, vehicular motion induces stronger structural stimulation compared to what is observed under perfectly smooth conditions. This effect is clearly demonstrated in fig. 7.23, where the initial singular values obtained from the Frequency Domain Decomposition are shown. These graphs display significant variations in excitation levels relative to different road

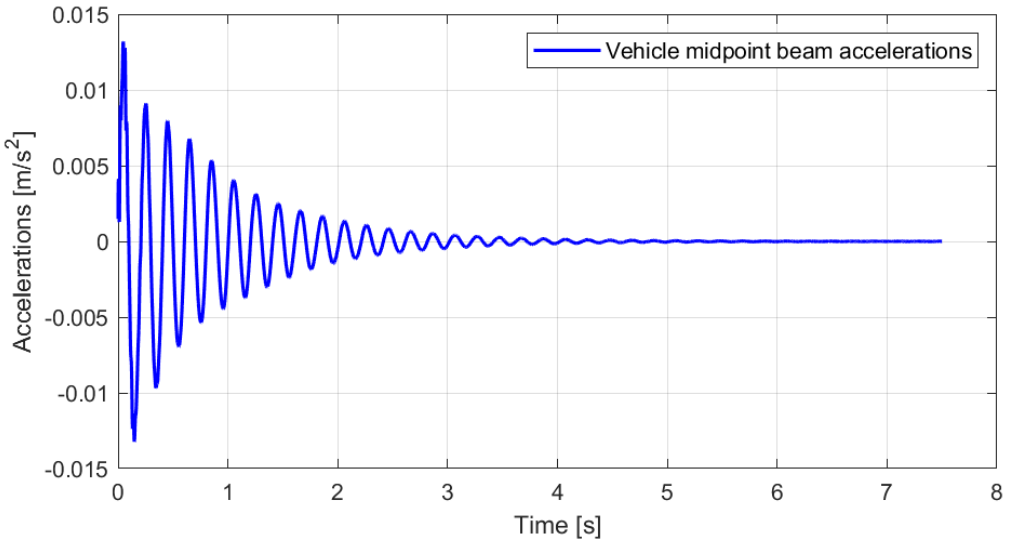

Figure 7.22: Instrumented vehicle, placed at beam midpoint, acceleration stabilization.

roughness profiles.

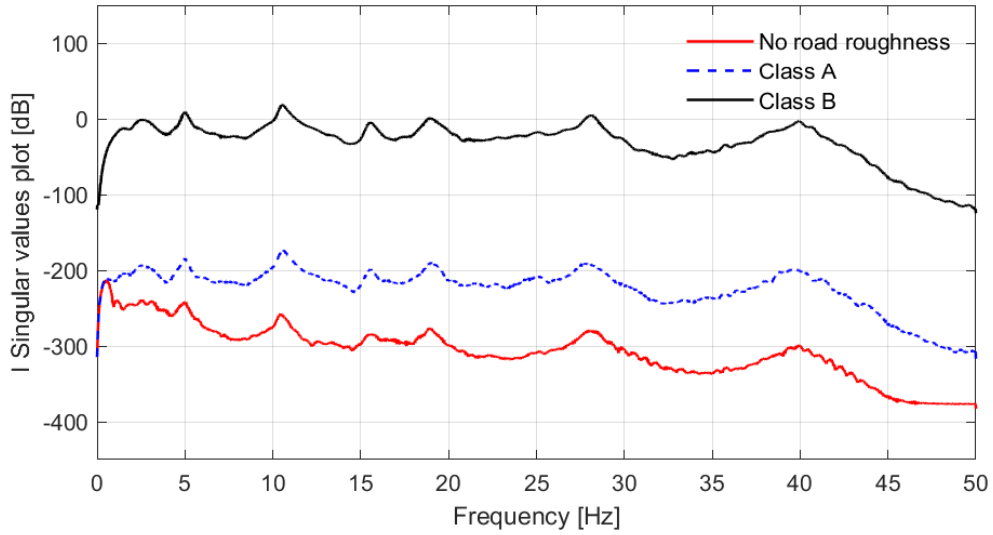

Figure 7.23: First singular value plots for different levels of road roughness.

It becomes evident that the class B road profile significantly increases signal energy in identical traffic simulations. This phenomenon is a natural consequence of the dynamic problem investigated. Indeed, road surface irregularities contribute to elevated contact force levels, as oscillators are driven not only by bridge deflections but also by an additional component from the road profile. Consequently, this reveals an advantage of using a stationary, instrumented vehicle system for *indirect* measurements. Further analysis of figs. 7.23 and 7.24 shows that as road quality diminishes, the frequency response attributable to the instrumented vehicle becomes more pronounced. The mechanical characteristics of stationary vehicles yield a natural frequency around 1Hz. This is clearly

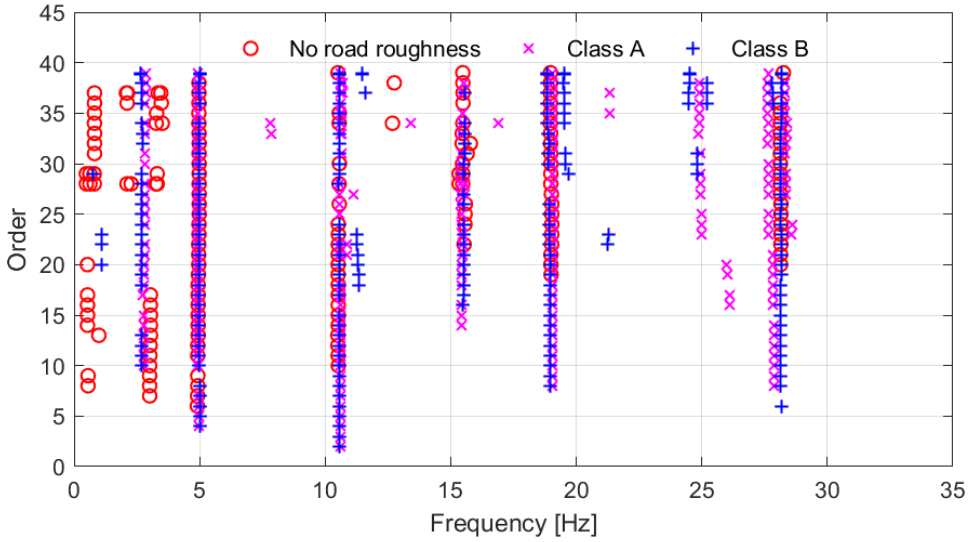

Figure 7.24: Stabilization diagram for different levels of road roughness.

marked by a peaks in fig. 7.23 and by stable poles in the same frequency range in fig. 7.24. Additionally, these graphs reveal how vehicular traffic manifests as peaks or stable poles at frequencies near 2.5Hz. However, these modes are readily identifiable and can be disregarded due to their associated damping levels, which exceed 15%. Moreover, these adverse effects can be further mitigated or eliminated through signal filtering, particularly if basic information about the bridge's modal parameters is available, ensuring that the natural frequencies of the bridge remain unaffected.

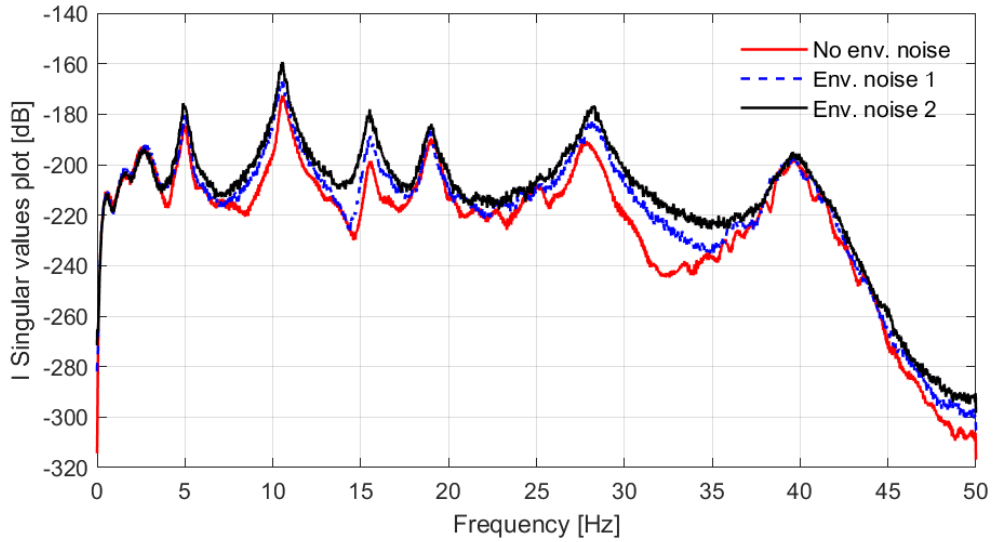

Figure 7.25: First singular value plots for different levels of environmental excitation.

Environmental excitation represents another crucial external factor in *indirect method* analyses within the numerical framework, especially regarding its impact on modal estimation. To explore this, three distinct simulations are conducted, each adopting a class

A road profile but varying in levels of environmental excitation. The first simulation excludes environmental noise, serving as a baseline for comparison. Conversely, the second and third simulations introduce environmental factors, calibrated to produce equivalent forces with an Root Mean Square (RMS) of acceleration values of $10^{-4}g$ and $10^{-3}g$, respectively. These are denoted in the figures as Env. noise 1 and Env. noise 2.

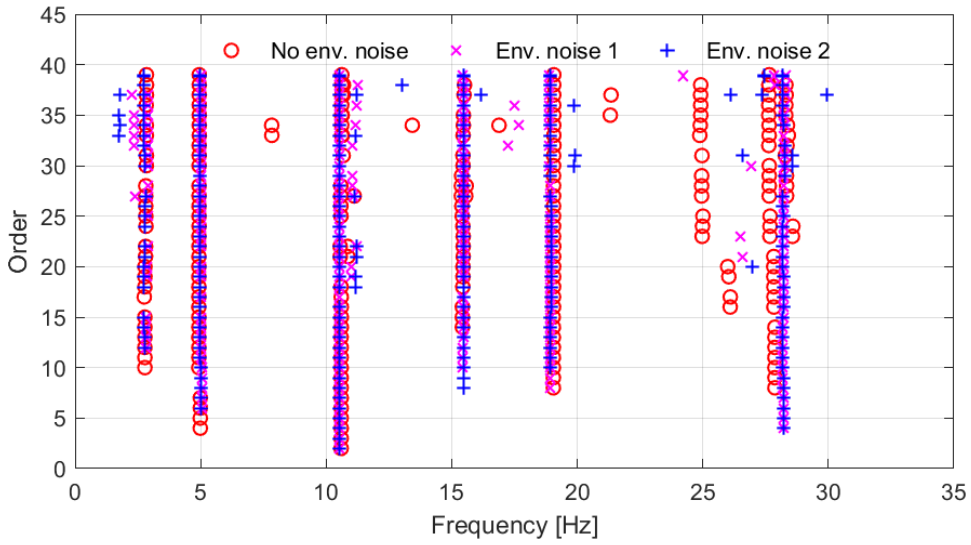

Figure 7.26: Stabilization diagram for different levels of environmental excitation.

Under these specific conditions, the impact of environmental excitation on the results of numerical simulations is clearly distinct. It is apparent that different levels of excitation yield varied responses in modal estimation, yet these variations are subtler compared to those observed in scenarios involving road roughness. In particular, fig. 7.23 shows only minor discrepancies among the three scenarios, a stark contrast to the significant variations noted in the road roughness case. Despite perceptible differences in excitation levels, the pronounced increase seen in the first singular values plot with road roughness is not replicated in fig. 7.23. Thus, concluding that the impact of the road roughness over the environmental excitation is a main aspect to take into account is trivial. Furthermore the presented data leads to some general considerations about the *indirect methods*. Indeed, employing stationary vehicles in *indirect methods* is not only viable but also significantly mitigates many drawbacks noted in literature regarding the use of moving instrumented vehicles. Key limitations, such as the disturbance effects of vehicle velocity and road roughness on modal estimation, are effectively addressed. Additionally, the influence of environmental excitation on simulation results is minimal compared to when this factor is absent. This point is crucial considering the often complex calibration of environmental excitation, influenced by various ambient phenomena. Moreover, the estimation of natural frequencies, as reported in table 7.9 and table 7.10, appears quite accurate when compared to the theoretical frequencies outlined in table 7.2. From these findings, two key insights emerge. First, from a numerical perspective, incorporating road roughness and defining a road profile in the analysis is pivotal, having the potential to significantly alter data interpretation. Second, utilizing stationary instrumented vehicles enables a more robust and precise analytical framework compared to moving vehicle conditions. This finding is intriguing as it paves the way for developing a new, flexible investigation methodology. Such a method would minimally disrupt bridge operations while leveraging established

techniques from classical Operational Modal Analysis. Therefore, this innovative investigative approach is particularly appealing due to its flexibility, cost-effectiveness, and the ability to conduct multiple investigative campaigns with various test layouts without impeding traffic flow on the bridge. However, it is crucial for operators to understand and identify the primary modal characteristics of the instrumented vehicle. While this requirement may initially seem like a complex hurdle, it can be effectively overcome by characterizing the vehicle through dynamic testing in the given scenario.

Tag	**Mode**	**Natural Freq. FDD [Hz]**	**Natural Freq. Cov-SSi [Hz]**	**Damping** [%]
No road rough.	1	4.94	4.96	4.17
No road rough.	2	10.41	10.52	2.19
No road rough.	3	15.66	15.48	1.78
No road rough.	4	18.90	18.99	1.88
No road rough.	5	27.98	28.14	1.68
Class A	1	4.98	4.94	3.43
Class A	2	10.53	10.61	1.96
Class A	3	15.6	15.44	1.30
Class A	4	19.01	19.06	1.62
Class A	5	27.76	27.85	1.46
Class B	1	4.98	4.98	3.64
Class B	2	10.52	10.57	2.18
Class B	3	15.52	15.52	1.27
Class B	4	18.90	18.92	1.79
Class B	5	28.17	28.15	1.24

Table 7.9: Natural frequencies estimation for test different values of road roughness.

Tag	**Mode**	**Natural Freq. FDD [Hz]**	**Natural Freq. Cov-SSi [Hz]**	**Damping** [%]
No env. noise	1	4.98	4.94	3.43
No env. noise	2	10.53	10.61	1.96
No env. noise	3	15.60	15.44	1.30
No env. noise	4	19.01	19.06	1.62
No env. noise	5	27.76	27.85	1.46
Env. noise 1	1	5.04	5.00	3.10
Env. noise 1	2	10.52	10.51	2.15
Env. noise 1	3	15.59	15.46	1.74
Env. noise 1	4	18.86	18.91	1.29
Env. noise 1	5	28.14	28.23	2.06
Env. noise 2	1	4.90	4.97	3.61
Env. noise 2	2	10.55	10.53	1.89
Env. noise 2	3	15.52	15.48	1.69
Env. noise 2	4	19.02	18.94	1.54
Env. noise 2	5	28.27	28.21	1.68

Table 7.10: Natural frequencies estimation for test different values of environmental excitation.

Chapter 8

Conclusions and future developments

This work presents a numerical analysis of the Vehicle-Bridge Interaction phenomenon, delving into several key aspects. The primary focus is on implementing a finite element formulation of this dynamic problem, progressing from one-dimensional problem—which only accounts for deflection and utilizes a sprung-mass system on a more elaborate framework that explores the three-dimensional nature of the beam problem. The formulation of the simple beam element is enhanced by incorporating shear deformation and torsional behavior. Notably, the torsion is extended beyond uniform cases to include an additional degree of freedom for non-uniform torsion, effectively coupling the Timoshenko and Vlasov theories. The Chapter 2 details the system's fundamental equations of motion, founded on the stationarity of the Hamilton's functional. The problem's strong form is transformed into a weak formulation, and the Finite Element Method, using the Galerkin approach, is applied to solve the system of coupled Partial Differential Equations (PDEs). This method, part of the broader weighted residual approach, is chosen for its consistency and stability. It guarantees the capture of the exact PDE solution if it exists within the approximation space. The method's efficacy in handling complex geometries and its excellent convergence properties, particularly with suitable finite elements, make it ideal for bridge simulations. The Finite Element formulation's accuracy is validated against dynamic solutions obtained from commercial software like *Abaqus 2023* and *OpenSees*, where the same mechanical problems is modelled using shell elements. The achieved accuracy, coupled with reduced computational efforts, underscores this approach's potential. However, this is not the endpoint but rather a strong foundation for developing the Vehicle-Bridge Interaction framework. In fact, Chapter 3 introduces a coupling formulation between the primary system (the bridge) and the secondary system (the vehicle), represented as a basic dynamic system capturing the vehicle's general dynamic response. This coupling is based on the assumption of perfect contact, utilizing contact forces conceptually defined as the reciprocal forces exchanged at the contact points. This elegant Finite Element formulation describes the interaction between bridges and traffic effectively. Additionally, employing realistic dynamic models over simpler approaches, like moving forces or masses, is crucial in Vehicle-Bridge Interaction analysis. Introducing vehicles that simulate not only inertial effects on the bridge but also continuous force exchange during motion is indispensable, especially in applications like the *indirect methods*. Here, the bridge's response, mediated through another system like a vehicle, could be altered by the vehicle's suspension system, making physical representation in numerical simulations vital. In this context, numerical benchmarks are conducted and presented to the reader, comparing the formulated model with *Abaqus 2023* software. The inherent challenges of multidimensional model-

ing are addressed and detailed. This includes solutions to various problems that users may encounter, primarily those associated with non-linearities resulting from the use of contact elements. Furthermore, the system's responses are comprehensively compared. The bridge's behavior, in terms of displacements, velocity, accelerations, and reactions, is thoroughly analyzed, demonstrating the model's high accuracy. Good agreement in terms of results is also achieved with respect to the outcomes derived from the moving vehicle along the bridge. Furthermore, in the sections mentioned above, different error estimation metrics such as MAR, RMSE, and NRMSE have been introduced and compared to analyze which error parameter yields consistent results in terms of simulating both the responses of structures and their interaction with vehicles. Indeed, the issues associated with processes exhibiting mean values close to zero are well known, leading to the potential failure of traditional error estimates like the MRE. Specifically, it becomes clear that even NRMSE, despite being much more robust in terms of error estimation in this context, still falls prey to the same issues in some of the presented cases. Therefore, utilizing metrics such as MAR or RMSE emerges as the most reasoned way to analyze the deviations between two signals.

Once the numerical aspects, including the accuracy and performance of the developed formulation, are validated, the focus shifts to another critical aspect of Vehicle-Bridge Interaction simulations: traffic or vehicle calibration. There is a noticeable gap in the literature between finite element framework implementation and vehicle calibration for these analyses. In the context of simulations aimed at representing traffic, which realistically involves a large number of vehicles over an observation period, a robust calibration algorithm is essential. Available resources, such as the Weigh In Motion database, offer valuable data, are able to provide probability distributions for mechanical characteristics like gross weight or inter-axle distance. These data are utilized in chapter 4 to establish a calibration procedure. This procedure incorporates three main components: the Weigh In Motion database, considerations made on vehicle suspensions aimed to the passenger comfort, and regional code limitations. This approach demonstrates significant potential in accurately describing traffic, particularly in the context of automatic vehicle generation. Moreover, it is well-suited for numerical implementation in Finite Element suites. These phenomena, including the well-known challenge of incorporating road roughness in numerical simulations for Vehicle-Bridge Interaction, are addressed. Despite being a complex disturbance effect, road roughness has been extensively studied, and various formulations have been developed, as presented in chapter 4. Among these, the standard ISO 8608 is chosen as the reference point due to its proven effectiveness and robust performance, as evidenced in scientific literature over the years. As a matter of fact, this standard is able to reproduce the randomness of several road profile proving a minimal set of input parameters.

Traffic-related phenomena are not the only challenges faced by bridges. These structures are also constantly exposed to various environmental effects that significantly impact their integrity and lifespan. Factors like temperature fluctuations, wind, rain, and humidity lead to material degradation, corrosion, and structural fatigue. Seasonal changes induce thermal expansion and contraction in bridge materials, causing stress and potential damage. Extreme weather events, such as floods and hurricanes, pose additional risks, testing the resilience of these structures. Therefore, designing bridges for durability and adaptability is crucial, using materials and engineering solutions resilient to these diverse conditions. Regular maintenance and monitoring are essential for their safety and functionality, protecting this critical part of our transportation infrastructure against nature's forces. However, it's not feasible to include every aspect in numerical simulations. Chapter 5 focuses on two main effects: daily thermal variations and environmental excitation,

pertinent in Operational Modal Analysis. Thermal effects are simulated by altering the Young's modulus value for concrete based on an empirical relationship. Environmental excitation, on the other hand, is numerically introduced as equivalent forces or moments, a more straightforward approach than single or multi-point constraints. This methodology involves parametric analyses to determine the appropriate level of environmental excitation for each degree of freedom, using linear regression between analyzed points. Thus, an ε parameter is introduced, representing the amplitude of a Gaussian distribution, as a set of equivalent generalized forces to achieve the desired excitation level.

Chapter 6 details the finite element software developed by the author, known as the *Ghost project*. This general-purpose software, written entirely in C++ and utilizing the *Eigen* library, is designed for Vehicle-Bridge interaction simulations. It leverages the object-oriented features of the programming language. The chapter introduces several classes to the reader and provides a basic explanation of the main features. All numerical simulations in this work use the *Ghost project*. The software can define various finite elements, based on both Euler-Bernoulli and Timoshenko formulations, using a basic mesh defined by nodes in a 2D coordinate system. It allows for the easy definition of different traffic patterns by specifying mandatory parameters. Additionally, road roughness and environmental excitation can be incorporated into the analysis. The software supports static, modal, and transient linear analyses, as well as traffic analysis. While this chapter outlines the general structure and key dependencies of the software, it is not a comprehensive documentation, hence only the principal features are described.

Finally, Chapter 7 presents a collection of numerical simulations exploring various traffic scenarios, methodologies, and analyses within the realm of Vehicle-Bridge Interaction finite element formulation. This section covers diverse topics. It features a detailed examination of a real bridge section under multiple traffic analyses, primarily focusing on a feasibility study and accuracy assessment of the entire developed framework. This includes a discussion on the advantages and limitations of both *direct* and *indirect methods* in Vehicle-Bridge Interaction simulations. Classical traffic analyses are conducted under various environmental conditions to mimic regular tests performed on such structures. These are then compared in terms of responses and excitations to the classical Operational Modal Analysis framework, where only environmental excitation impacts the bridge. Specific traffic scenarios, especially those related to the influence of the *driving frequency* on the structure, are also scrutinized. The effects of this phenomenon are analyzed and compared with different measurable responses of the vehicles, including displacements, velocities, and accelerations. Additionally, strategies to mitigate or simplify the impact of the *driving frequency* on modal estimation are discussed. The chapter also delves into *indirect methods*, examining the use of stationary instrumented vehicles on the bridge as transducers. The potential and practical insights of this methodology are elucidated through the data presented.

In conclusion, it can be stated that Vehicle-Bridge Interaction numerical simulations can be effectively conducted using simpler principal systems from a finite element discretization perspective, coupled with streamlined mechanical systems to represent vehicles. The primary benefits of this approach are computational, as significant results are attainable with basic beam models. Additionally, these simulations can be robustly structured to incorporate various external factors often present in real structures but commonly overlooked in numerical models. Both *direct* and *indirect methods* have demonstrated adequate performance across all analyzed contexts, allowing for the identification of main effects caused by various external factors. The use of beam models, as opposed to more complex three-dimensional objects, notably enhances computational efficiency. Looking forward, the development of this work will follow two main directions: numerical and ex-

perimental. Numerically, the *Ghost project* will be expanded to include different vehicle models, like the half-car model, and other traffic patterns to simulate diverse traffic conditions. Non-linearities, both material and geometrical, will be integrated into the software, which is also planned to be released as an open-source resource. Experimentally, specific tests will be conducted on real vehicles and structures with multiple objectives. These range from verifying the quality of data obtained from Operational Modal Analysis tests in open traffic conditions to assessing the effects of the *driving frequency*. Additionally, vehicles will be studied to gather information on instrumented vehicles, which will then be used in real-world applications of the *indirect methods* on an actual bridge.

Moreover, it's important to mention how the work presented here is not seen as a conclusion, but rather as a starting point, albeit a well-advanced one, for the creation of a comprehensive framework. This framework is aimed not only at simulating the traffic phenomenon on real bridges with a detailed treatment of disturbance phenomena but also at calibrating numerical models. Indeed, it represents a crucial step towards the development of a reasoned model for the creation of a broad-spectrum technique aimed at producing large quantities of data. These data can be seamlessly integrated into paradigms dictated by artificial intelligence, and its natural progression undoubtedly leads to the development of surrogate models. Surrogate models in structural engineering are simplified representations or approximations of complex structural systems, used to predict the system's behavior under various conditions without the need for detailed and computationally expensive simulations. These models act as stand-ins for the actual physical models, offering a balance between accuracy and computational efficiency. They are particularly valuable in optimization, sensitivity analysis, and uncertainty quantification tasks where numerous evaluations of the model are required. To achieve this goal, the next step will naturally involve planning and conducting experimental campaigns on both vehicles and bridges. This phase is crucial for defining the models in the first place and for obtaining feedback regarding the developed methodology.

Appendix A

Shape functions Timoshenko Flexural-Torsional Finite Element

In this section are reported the shape functions which are employed in order to obtain the finite element formulation for the developed beam element. Those are referred to the isoparametric formulation of the problem, which is more suitable for the Gauss quadrature method in order to achieve the definition of the associate matrices and vectors. Here, the parameter ξ is the adimensioanl coordinate of the beam, referred to a coordinate system which has its origin in the beam midpoint, and the integration boundaries are respectively -1 and 1, which in the natural coordinate system are the two beam ends. Each degree of freedom is characterized by different shape functions, due to different number of act of motion at the extreme nodes.
The axial degrees of freedom is treated in the classical fashion by providing a linear polynomial, which in the natural coordinates, can bewhich are the two component of the row vector $\bar{N}_1(x)$ can be expressed as

$$N_1^1 = \frac{1}{2} \cdot (1 - \xi) \qquad N_1^2 = \frac{1}{2} \cdot (1 + \xi) \tag{A.1}$$

and the corresponding the derivatives with respect to x of the previous functions are

$$N_{1,x}^1 = -\frac{\xi}{L} \qquad N_{1,x}^2 = \frac{\xi}{L} \tag{A.2}$$

Furthermore, the shape functions associated with respect to the vertical deflection w_y in the Timoshenko hypothesis can be written as follow

$$\begin{aligned}
N_2^1 &= \frac{1}{2} - \frac{3(L^2 + 8\Lambda_y)}{4(L^2 + 12\Lambda_y)}\xi + \frac{L^2}{4(L^2 + 12\Lambda_y)}\xi^3 \\
N_2^2 &= \frac{L}{8} - \frac{L^3}{8(L^2 + 12\Lambda_y)}\xi - \frac{L}{8}\xi^2 + \frac{L^3}{8(L^2 + 12\Lambda_y)} \\
N_2^3 &= \frac{1}{2} + \frac{3(L^2 + 8\Lambda_y)}{4(L^2 + 12\Lambda_y)}\xi - \frac{L^2}{4(L^2 + 12\Lambda_y)}\xi^3 \\
N_2^4 &= -\frac{L}{8} - \frac{L^3}{8(L^2 + 12\Lambda_y)}\xi + \frac{L}{8}\xi^2 + \frac{L^3}{8(L^2 + 12\Lambda_y)}\xi^3
\end{aligned} \tag{A.3}$$

where the parameter Λ_y is the parameter

$$\Lambda_y = \frac{EI_z}{GA_y} \tag{A.4}$$

by deriving with respect to the x coordinate and multiplying by the inverse of the Jacobian

$$\begin{aligned}
N^1_{2,x} &= -\frac{3(L^2+8\Lambda_y)}{2L(L^2+12\Lambda_y)} + \frac{3L^2}{2L(L^2+12\Lambda_y)}\xi^2 \\
N^2_{2,x} &= \frac{L^2}{4(L^2+12\Lambda_y)} + \frac{\xi}{2} - \frac{3L^2}{4(L^2+12\Lambda_y)}\xi^2 \\
N^3_{2,x} &= \frac{3(L^2+8\Lambda_y)}{2L(L^2+12\Lambda_y)} - \frac{3L}{2(L^2+12\Lambda_y)}\xi^2 \\
N^4_{2,x} &= \frac{L^2}{4(L^2+12\Lambda_y)} - \frac{\xi}{2} - \frac{3L^2}{4(L^2+12\Lambda_y)}\xi^2
\end{aligned} \tag{A.5}$$

meanwhile the shape function for the associate rotational degree of freedom θ_z can be stated as

$$\begin{aligned}
N^1_3 &= -\frac{3(L^2+8\Lambda_y)}{2L(L^2+12\Lambda_y)} + \left(\frac{6\xi^2}{L} + \frac{48\Lambda_y}{L^3}\right)\left(\frac{L^2}{4(L^2+12\Lambda_y)}\right) \\
N^2_3 &= -\frac{L^2}{4(2+12\Lambda_y)} - \frac{\xi}{2L} + \left(\frac{6\xi^2}{L} + \frac{48\Lambda_y}{L^3}\right)\left(\frac{L^3}{8(L^2+12\Lambda_y)}\right) \\
N^3_3 &= \frac{3(L^2+8\Lambda_y)}{2(L^2+12\Lambda_y)} - \left(\frac{6\xi^2}{L} + \frac{48\Lambda_y}{L^3}\right)\left(\frac{L^2}{4(L^2+12\Lambda_y)}\right) \\
N^4_3 &= -\frac{L^2}{4(L^2+12\Lambda_y)} + \frac{\xi}{2L} + \left(\frac{6\xi^2}{L} + \frac{48\Lambda_y}{L^3}\right)\left(\frac{L^3}{8(L^2+12\Lambda_y)}\right)
\end{aligned} \tag{A.6}$$

and its derivatives with respect to their derivatives with respect to the x coordinates

$$\begin{aligned}
N^1_{3,x} &= \frac{6\xi}{L^2+12\Lambda_y} \\
N^2_{3,x} &= -\frac{1}{L^2} + \frac{3L}{L^2+12\Lambda_y}\xi \\
N^3_{3,x} &= -\frac{6\xi}{L^2+12\Lambda_y} \\
N^4_{3,x} &= \frac{1}{L^2} + \frac{3L}{L^2+12\Lambda_y}\xi
\end{aligned} \tag{A.7}$$

by performing the same operations on the other coupled degrees of freedom, that are w_z and θ_y the shape functions can be computed by the following relations

$$\begin{aligned}
N_4^1 &= \frac{1}{2} - \frac{3(L^2+8\Lambda_z)}{4(L^2+12\Lambda_z)}\xi + \frac{L^2}{4(L^2+12\Lambda_z)}\xi^3 \\
N_4^2 &= -\frac{L}{8} + \frac{L^3}{8(L^2+12\Lambda_z)}\xi + \frac{L}{8}\xi^2 - \frac{L^3}{8(L^2+12\Lambda_z)} \\
N_4^3 &= \frac{1}{2} + \frac{3(L^2+8\Lambda_z)}{4(L^2+12\Lambda_z)}\xi - \frac{L^2}{4(L^2+12\Lambda_z)}\xi^3 \\
N_4^4 &= \frac{L}{8} + \frac{L^3}{8(L^2+12\Lambda_z)}\xi - \frac{L}{8}\xi^2 - \frac{L^3}{8(L^2+12\Lambda_z)}\xi^3
\end{aligned} \tag{A.8}$$

$$\begin{aligned}
N_{4,x}^1 &= -\frac{3(L^2+8\Lambda_z)}{2L(L^2+12\Lambda_z)} + \frac{3L^2}{2L(L^2+12\Lambda_z)}\xi^2 \\
N_{4,x}^2 &= \frac{L^2}{4(L^2+12\Lambda_z)} + \frac{\xi}{2} - \frac{3L^2}{4(L^2+12\Lambda_z)}\xi^2 \\
N_{4x}^3 &= \frac{3(L^2+8\Lambda_z)}{2L(L^2+12\Lambda_z)} - \frac{3L}{2(L^2+12\Lambda_z)}\xi^2 \\
N_{4,x}^4 &= \frac{L^2}{4(L^2+12\Lambda_z)} - \frac{\xi}{2} - \frac{3L^2}{4(L^2+12\Lambda_z)}\xi^2
\end{aligned} \tag{A.9}$$

$$\begin{aligned}
N_5^1 &= \frac{3(L^2+8\Lambda_z)}{2L(L^2+12\Lambda_z)} - \left(\frac{6\xi^2}{L} + \frac{48\Lambda_z}{L^3}\right)\left(\frac{L^2}{4(L^2+12\Lambda_z)}\right) \\
N_5^2 &= -\frac{L^2}{4(2+12\Lambda_z)} - \frac{\xi}{2L} + \left(\frac{6\xi^2}{L} + \frac{48\Lambda_z}{L^3}\right)\left(\frac{L^3}{8(L^2+12\Lambda_z)}\right) \\
N_5^3 &= -\frac{3(L^2+8\Lambda_z)}{2(L^2+12\Lambda)} + \left(\frac{6\xi^2}{L} + \frac{48\Lambda_z}{L^3}\right)\left(\frac{L^2}{4(L^2+12\Lambda_z)}\right) \\
N_5^4 &= -\frac{L^2}{4(L^2+12\Lambda_z)} + \frac{\xi}{2L} + \left(\frac{6\xi^2}{L} + \frac{48\Lambda_z}{L^3}\right)\left(\frac{L^3}{8(L^2+12\Lambda_z)}\right)
\end{aligned} \tag{A.10}$$

$$\begin{aligned}
N_{5,x}^1 &= -\frac{6\xi}{L^2+12\Lambda_z} \\
N_{5,x}^2 &= -\frac{1}{L^2} + \frac{3L}{L^2+12\Lambda_z}\xi \\
N_{5,x}^3 &= \frac{6\xi}{L^2+12\Lambda_z} \\
N_{5,x}^4 &= \frac{1}{L^2} + \frac{3L}{L^2+12\Lambda_z}\xi
\end{aligned} \tag{A.11}$$

with the position of

$$\Lambda_z = \frac{EI_y}{GA_z} \tag{A.12}$$

On the other hand, the shape functions associated with the torsional degrees of freedom are retrieved by a classical third order Hermite polynomial in their adimensional formulation, which by considering the inverse of the Jacobian for the change of the coordinate systems are

$$\begin{aligned} N_6 &= \frac{1}{2} - \frac{3}{4}\xi + \frac{1}{4}\xi^3 \\ N_6 &= \frac{L}{(8}\left(1 - \xi - \xi^2 + \xi^3\right) \\ N_6 &= \frac{1}{2} + \frac{3}{4}\xi - \frac{1}{4}\xi^3 \\ N_6 &= \frac{L}{8}\left(-1 - \xi + \xi^2 + \xi^3\right) \end{aligned} \tag{A.13}$$

$$\begin{aligned} N^1_{6,x} &= -\frac{3}{2L}\left(1 - \xi^2\right) \\ N^2_{6,x} &= \frac{1}{4}\left(-1 - 2\xi + 3\xi^2\right) \\ N^3_{6,x} &= \frac{3}{2L}\left(1 - \xi^2\right) \\ N^4_{6,x} &= \frac{1}{4}\left(-1 + 2\xi + 3\xi^2\right) \end{aligned} \tag{A.14}$$

$$\begin{aligned} N^1_{6,xx} &= \frac{6\xi}{L^2} \\ N^2_{6,xx} &= \frac{1}{L}\left(1 - 3\xi\right) \\ N^3_{6,xx} &= -\frac{6\xi}{L^2} \\ N^4_{6,xx} &= \frac{1}{L}\left(1 + 3\xi\right) \end{aligned} \tag{A.15}$$

All the aforementioned shape functions are then implemented in combination with the classical Gauss quadrature rule in order to obtain the matricial and vectorial quantities suitable for the finite element formulation.

Bibliography

[1] ZhiWu Zhou, Julián Alcalá, and Víctor Yepes. "Environmental, economic and social impact assessment: Study of bridges in China's five major economic regions". In: *International journal of environmental research and public health* 18.1 (2021), p. 122.

[2] Tae Hyoung Kim and Sung Ho Tae. "Proposal of environmental impact assessment method for concrete in South Korea: An application in LCA (life cycle assessment)". In: *International journal of environmental research and public health* 13.11 (2016), p. 1074.

[3] Ya Hong Dong and S Thomas Ng. "A social life cycle assessment model for building construction in Hong Kong". In: *The international journal of life cycle assessment* 20 (2015), pp. 1166–1180.

[4] Xiaoling Zhang. *Toward a regenerative sustainability paradigm for the built environment: from vision to reality*. 2014.

[5] Luís AC Neves, Dan M Frangopol, and Aruz Petcherdchoo. "Probabilistic lifetime-oriented multiobjective optimization of bridge maintenance: Combination of maintenance types". In: *Journal of Structural Engineering* 132.11 (2006), pp. 1821–1834.

[6] Sherif Yehia, Osama Abudayyeh, Imran Fazal, and Dennis Randolph. "A decision support system for concrete bridge deck maintenance". In: *Advances in Engineering Software* 39.3 (2008), pp. 202–210.

[7] Ayaho Miyamoto, Kei Kawamura, and Hideaki Nakamura. "Bridge management system and maintenance optimization for existing bridges". In: *Computer-Aided Civil and Infrastructure Engineering* 15.1 (2000), pp. 45–55.

[8] Danhui Dan and Houjin Li. "Monitoring, intelligent perception, and early warning of vortex-induced vibration of suspension bridge". In: *Structural Control and Health Monitoring* 29.5 (2022), e2928.

[9] Guang-Ming Wu, Ting-Hua Yi, Dong-Hui Yang, Hong-Nan Li, and Hua Liu. "Early warning method for bearing displacement of long-span bridges using a proposed time-varying temperature–displacement model". In: *Journal of Bridge Engineering* 26.9 (2021), p. 04021068.

[10] Hai-Bin Huang, Ting-Hua Yi, Hong-Nan Li, and Hua Liu. "Sparse Bayesian identification of temperature-displacement model for performance assessment and early warning of bridge bearings". In: *Journal of Structural Engineering* 148.6 (2022), p. 04022052.

[11] Xuzhao Lu, Chul-Woo Kim, and Kai-Chun Chang. "Finite element analysis framework for dynamic vehicle-bridge interaction system based on ABAQUS". In: *International Journal of Structural Stability and Dynamics* 20.03 (2020), p. 2050034.

[12] Qing Xie, Wanshui Han, and Yangguang Yuan. "Refined Vehicle-Bridge Interaction Analysis Using Incompatible Solid Finite Element for Evaluating Stresses and Impact Factors". In: *Advances in Civil Engineering* 2020 (2020), pp. 1–15.

[13] Leslaw Kwasniewski, Hongyi Li, Jerry Wekezer, and Jerzy Malachowski. "Finite element analysis of vehicle–bridge interaction". In: *Finite Elements in Analysis and Design* 42.11 (2006), pp. 950–959.

[14] Ladislav Fryba. *Vibration of solids and structures under moving loads*. Thomas Telford, 1999.

[15] Pawet Śniady. "Vibration of a beam due to a random stream of moving forces with random velocity". In: *Journal of Sound and Vibration* 97.1 (1984), pp. 23–33.

[16] George Michaltsos, Dimitrios Sophianopoulos, and Antonios N Kounadis. "The effect of a moving mass and other parameters on the dynamic response of a simply supported beam". In: *Journal of sound and Vibration* 191.3 (1996), pp. 357–362.

[17] Masami Ichikawa, Yoshio Miyakawa, and Akira Matsuda. "Vibration analysis of the continuous beam subjected to a moving mass". In: *Journal of Sound and Vibration* 230.3 (2000), pp. 493–506.

[18] YB Yang and Chi Way Lin. "Vehicle–bridge interaction dynamics and potential applications". In: *Journal of sound and vibration* 284.1-2 (2005), pp. 205–226.

[19] Tore Dahlberg. "Vehicle-bridge interaction". In: *Vehicle System Dynamics* 13.4 (1984), pp. 187–206.

[20] XQ Zhu and Siu-Seong Law. "Recent developments in inverse problems of vehicle–bridge interaction dynamics". In: *Journal of Civil Structural Health Monitoring* 6 (2016), pp. 107–128.

[21] XQ Zhu and Siu-Seong Law. "Moving forces identification on a multi-span continuous bridge". In: *Journal of sound and vibration* 228.2 (1999), pp. 377–396.

[22] Radosław Iwankiewicz and Paweł Śniady. "Vibration of a beam under a random stream of moving forces". In: *Journal of Structural Mechanics* 12.1 (1984), pp. 13–26.

[23] Ladislav Fryba. "Non-stationary response of a beam to a moving random force". In: *Journal of Sound and Vibration* 46.3 (1976), pp. 323–338.

[24] Arturo O Cifuentes. "Dynamic response of a beam excited by a moving mass". In: *Finite Elements in Analysis and Design* 5.3 (1989), pp. 237–246.

[25] John E Akin and Massood Mofid. "Numerical solution for response of beams with moving mass". In: *Journal of Structural Engineering* 115.1 (1989), pp. 120–131.

[26] Heow Pueh Lee. "Dynamic response of a beam with a moving mass". In: (1996).

[27] Mehdi Dehestani, Massod Mofid, and Abolhassan H Vafai. "Investigation of critical influential speed for moving mass problems on beams". In: *Applied mathematical modelling* 33.10 (2009), pp. 3885–3895.

[28] Neda Mostafa, Dario Di Maio, Richard Loendersloot, and Tiedo Tinga. "The influence of vehicle dynamics on the time-dependent resonances of a bridge". In: *Advances in Bridge Engineering* 4.1 (2023), p. 22.

[29] Charikleia D Stoura and Elias G Dimitrakopoulos. “Additional damping effect on bridges because of vehicle-bridge interaction”. In: *Journal of Sound and Vibration* 476 (2020), p. 115294.

[30] Y Zhan and Francis TK Au. “Bridge surface roughness identification based on vehicle–bridge interaction”. In: *International Journal of Structural Stability and Dynamics* 19.07 (2019), p. 1950069.

[31] Yeong-Bin Yang, JD Yau, Zhongda Yao, and YS Wu. *Vehicle-bridge interaction dynamics: with applications to high-speed railways*. World Scientific, 2004.

[32] Nan Zhang, He Xia, and Weiwei Guo. “Vehicle–bridge interaction analysis under high-speed trains”. In: *Journal of Sound and Vibration* 309.3-5 (2008), pp. 407–425.

[33] Nengguang Liu, Wei Gao, Chongmin Song, Nong Zhang, and Yong-Lin Pi. “Interval dynamic response analysis of vehicle-bridge interaction system with uncertainty”. In: *Journal of Sound and Vibration* 332.13 (2013), pp. 3218–3231.

[34] Yeong-Bin Yang and Jong-Dar Yau. “Vehicle-bridge interaction element for dynamic analysis”. In: *Journal of Structural Engineering* 123.11 (1997), pp. 1512–1518.

[35] YB Yang, MC Cheng, and KC Chang. “Frequency variation in vehicle–bridge interaction systems”. In: *International Journal of Structural Stability and Dynamics* 13.02 (2013), p. 1350019.

[36] Yeong-Bin Yang and Bing-Houng Lin. “Vehicle-bridge interaction analysis by dynamic condensation method”. In: *Journal of Structural Engineering* 121.11 (1995), pp. 1636–1643.

[37] Patrick J McGetrick, Arturo Gonzlez, and Eugene J OBrien. “Theoretical investigation of the use of a moving vehicle to identify bridge dynamic parameters”. In: *Insight-Non-Destructive Testing and Condition Monitoring* 51.8 (2009), pp. 433–438.

[38] Eugene J O’Brien and Jennifer Keenahan. “Using Instrumented Quarter-Cars for’Drive By’Bridge Inspection”. In: *The 2013 International Association for Bridge and Structural Engineering Conference (IABSE 2013), Rotterdam, The Netherlands, 6-8 May 2013*. IABSE. 2013.

[39] Daniel Cantero and Arturo González. “Location and evaluation of maximum dynamic effects on a simply supported beam due to a quarter-car model”. In: *Bridge and Infrastructure Research In Ireland (BRI 2008), Galway, Ireland, December, 2008*. 2008.

[40] Ebrahim Esmailzadeh and Nader Jalili. “Vehicle–passenger–structure interaction of uniform bridges traversed by moving vehicles”. In: *Journal of Sound and Vibration* 260.4 (2003), pp. 611–635.

[41] Judy P Yang and Jyu-Yi Sun. “Pitching effect of a three-mass vehicle model for analyzing vehicle-bridge interaction”. In: *Engineering Structures* 224 (2020), p. 111248.

[42] Qiang Li, You-Lin Xu, DJ Wu, and ZW2759244 Chen. “Computer-aided nonlinear vehicle-bridge interaction analysis”. In: *Journal of Vibration and Control* 16.12 (2010), pp. 1791–1816.

[43] Arturo González, Eugene J OBrien, and PJ McGetrick. “Identification of damping in a bridge using a moving instrumented vehicle”. In: *Journal of Sound and Vibration* 331.18 (2012), pp. 4115–4131.

[44] Charikleia D Stoura and Elias G Dimitrakopoulos. “A Modified Bridge System method to characterize and decouple vehicle–bridge interaction”. In: *Acta Mechanica* 231 (2020), pp. 3825–3845.

[45] Qing Zeng, Charikleia D Stoura, and Elias G Dimitrakopoulos. “A localized lagrange multipliers approach for the problem of vehicle-bridge-interaction”. In: *Engineering Structures* 168 (2018), pp. 82–92.

[46] Qiling Zou, Lu Deng, Tieding Guo, and Xinfeng Yin. “Comparative study of different numerical models for vehicle–bridge interaction analysis”. In: *International Journal of Structural Stability and Dynamics* 16.09 (2016), p. 1550057.

[47] Brian J Schwarz and Mark H Richardson. “Experimental modal analysis”. In: *CSI Reliability week* 35.1 (1999), pp. 1–12.

[48] Peter Avitabile. “Experimental modal analysis”. In: *Sound and vibration* 35.1 (2001), pp. 20–31.

[49] Randall J Allemang. “Experimental modal analysis”. In: (1983).

[50] Carlo Rainieri and Giovanni Fabbrocino. “Operational modal analysis of civil engineering structures”. In: *Springer, New York* 142 (2014), p. 143.

[51] Filipe Magalhães and Álvaro Cunha. “Explaining operational modal analysis with data from an arch bridge”. In: *Mechanical systems and signal processing* 25.5 (2011), pp. 1431–1450.

[52] Matthew J Whelan, Michael V Gangone, Kerop D Janoyan, and Ratneshwar Jha. “Real-time wireless vibration monitoring for operational modal analysis of an integral abutment highway bridge”. In: *Engineering Structures* 31.10 (2009), pp. 2224–2235.

[53] Jiawang Zhan, Junjie You, Xuan Kong, and Nan Zhang. “An indirect bridge frequency identification method using dynamic responses of high-speed railway vehicles”. In: *Engineering Structures* 243 (2021), p. 112694.

[54] Xudong Jian, Ye Xia, and Limin Sun. “An indirect method for bridge mode shapes identification based on wavelet analysis”. In: *Structural Control and Health Monitoring* 27.12 (2020), e2630.

[55] Sean P Brady, Eugene J O’Brien, and Aleš Žnidarič. “Effect of vehicle velocity on the dynamic amplification of a vehicle crossing a simply supported bridge”. In: *Journal of Bridge Engineering* 11.2 (2006), pp. 241–249.

[56] Chengjun Tan, Ahmed Elhattab, and Nasim Uddin. ““Drive-by”bridge frequency-based monitoring utilizing wavelet transform”. In: *Journal of Civil Structural Health Monitoring* 7 (2017), pp. 615–625.

[57] Yong Lu, Lei Mao, and Peter Woodward. “Frequency characteristics of railway bridge response to moving trains with consideration of train mass”. In: *Engineering Structures* 42 (2012), pp. 9–22.

[58] Stefano Ercolessi, Giovanni Fabbrocino, and Carlo Rainieri. “Indirect measurements of bridge vibrations as an experimental tool supporting periodic inspections”. In: *Infrastructures* 6.3 (2021), p. 39.

[59] Stefano Ercolessi, Giovanni Fabbrocino, Danilo Gargaro, and Carlo Rainieri. “Theoretical and Experimental Assessment of Indirect Dynamic Measurements for Periodic Inspections of Road Bridges”. In: *Proceedings of the 1st Conference of the European Association on Quality Control of Bridges and Structures: EUROSTRUCT 2021 1*. Springer. 2022, pp. 1064–1072.

[60] Italian Ministry of infrastructure and transportation. “Linee Guida per la classificazione e gestione del rischio, la valutazione della sicurezza ed il monitoraggio dei ponti esistenti”. In: *D.M. 204-01/07/2022* (2022).

[61] Ge-Wei Chen, Piotr Omenzetter, and Sherif Beskhyroun. “Operational modal analysis of an eleven-span concrete bridge subjected to weak ambient excitations”. In: *Engineering Structures* 151 (2017), pp. 839–860.

[62] Zhenpeng Wang, Minshui Huang, and Jianfeng Gu. “Temperature effects on vibration-based damage detection of a reinforced concrete slab”. In: *Applied Sciences* 10.8 (2020), p. 2869.

[63] Harsh Nandan and Mahendra P Singh. “Effects of thermal environment on structural frequencies: Part I–A simulation study”. In: *Engineering Structures* 81 (2014), pp. 480–490.

[64] EJ Cross, KY Koo, JMW Brownjohn, and K Worden. “Long-term monitoring and data analysis of the Tamar Bridge”. In: *Mechanical Systems and Signal Processing* 35.1-2 (2013), pp. 16–34.

[65] Carlo Rainieri, Filipe Magalhaes, Danilo Gargaro, Giovanni Fabbrocino, and Alvaro Cunha. “Predicting the variability of natural frequencies and its causes by Second-Order Blind Identification”. In: *Structural Health Monitoring* 18.2 (2019), pp. 486–507.

[66] Stephan P Timoshenko. “X. On the transverse vibrations of bars of uniform cross-section”. In: *The London, Edinburgh, and Dublin Philosophical Magazine and Journal of Science* 43.253 (1922), pp. 125–131.

[67] Vasili Zakharovich Vlasov. “Thin-walled elastic beams”. In: *PST Catalogue* 428 (1959).

[68] MM Black and HM Semple. “Torsion-bending analysis of continuous thin-walled beams”. In: *International Journal of Mechanical Sciences* 11.10 (1969), pp. 791–810.

[69] MM Black. “The unstable behaviour of thin-walled unsymmetrical section beams subjected to combined bending and torsion”. In: *Journal of Strain Analysis* 1.1 (1965), pp. 50–56.

[70] RED Bishop, SM Cannon, and S Miao. “On coupled bending and torsional vibration of uniform beams”. In: *Journal of sound and vibration* 131.3 (1989), pp. 457–464.

[71] Richard Evelyn Donohue Bishop, William Geraint Price, and Zhang Xi Cheng. “On the structural dynamics of a Vlasov beam”. In: *Proceedings of the Royal Society of London. A. Mathematical and Physical Sciences* 388.1794 (1983), pp. 49–73.

[72] PO Friberg. “Coupled vibrations of beams—an exact dynamic element stiffness matrix”. In: *International Journal for numerical methods in engineering* 19.4 (1983), pp. 479–493.

[73] PO795740 Friberg. “Beam element matrices derived from Vlasov’s theory of open thin-walled elastic beams”. In: *International Journal for Numerical Methods in Engineering* 21.7 (1985), pp. 1205–1228.

[74] Eduardo N Dvorkin, Diego Celentano, Alberto Cuitino, and Gustavo Gioia. “A Vlasov beam element”. In: *Computers & structures* 33.1 (1989), pp. 187–196.

[75] AS Gendy, AF Saleeb, and TYP Chang. “Generalized thin-walled beam models for flexural-torsional analysis”. In: *Computers & structures* 42.4 (1992), pp. 531–550.

[76] S Mohammad Hashemi and Marc J Richard. “Free vibrational analysis of axially loaded bending-torsion coupled beams: a dynamic finite element”. In: *Computers & Structures* 77.6 (2000), pp. 711–724.

[77] A Arpaci and E Bozdag. “On free vibration analysis of thin-walled beams with nonsymmetrical open cross-sections”. In: *Computers & structures* 80.7-8 (2002), pp. 691–695.

[78] A Arpaci, SE Bozdag, and E Sunbuloglu. “Triply coupled vibrations of thin-walled open cross-section beams including rotary inertia effects”. In: *Journal of Sound and Vibration* 260.5 (2003), pp. 889–900.

[79] Li Jun, Shen Rongying, Hua Hongxing, and Jin Xianding. “Coupled bending and torsional vibration of axially loaded Bernoulli–Euler beams including warping effects”. In: *Applied Acoustics* 65.2 (2004), pp. 153–170.

[80] Li Jun, Li Wanyou, Shen Rongying, and Hua Hongxing. “Coupled bending and torsional vibration of nonsymmetrical axially loaded thin-walled Bernoulli–Euler beams”. In: *Mechanics Research Communications* 31.6 (2004), pp. 697–711.

[81] JR Banerjee and H Su. “Free transverse and lateral vibration of beams with torsional coupling”. In: *Journal of Aerospace Engineering* 19.1 (2006), pp. 13–20.

[82] YL Kuo, WL Cleghorn, and K Behdinan. “Stress-based finite element method for Euler-Bernoulli beams”. In: *Transactions of the Canadian Society for Mechanical Engineering* 30.1 (2006), pp. 1–6.

[83] Diego Lisi. “A beam finite element model including warping. Application to the dynamic and static analysis of bridge decks”. In: (2011).

[84] João Serra, Ricardo Vieira, and Francisco Virtuoso. “DYNAMIC ANALYSIS OF BRIDGE GIRDERS UNDER MOVING LOADS CONSIDERING WARPING AND MASS EFFECTS: NUMERICAL AND ANALYTICAL BEAM MODELS”. In: (2017).

[85] Gregory J Hancock, Kim JR Rasmussen, et al. “Formulation and Implementation of General Thin-Walled Open-Section Beam-Column Elements in Opensees (No. R961)”. In: (2016).

[86] TM Wang and TA Kinsman. “Vibrations of frame structures according to the Timoshenko theory”. In: *Journal of Sound and Vibration* 14.2 (1971), pp. 215–227.

[87] R Davis, RD Henshell, and GB Warburton. “A Timoshenko beam element”. In: *Journal of Sound and Vibration* 22.4 (1972), pp. 475–487.

[88] RED Bishop and WG Price. “Coupled bending and twisting of a Timoshenko beam”. In: *Journal of Sound and Vibration* 50.4 (1977), pp. 469–477.

[89] Geir A Gunnlaugsson and P Terndrup Pedersen. “A finite element formulation for beams with thin walled cross-sections”. In: *Computers & Structures* 15.6 (1982), pp. 691–699.

[90] A Tessler and SB Dong. “On a hierarchy of conforming Timoshenko beam elements”. In: *Computers & structures* 14.3-4 (1981), pp. 335–344.

[91] JR Banerjee. “Coupled bending–torsional dynamic stiffness matrix for beam elements”. In: *International journal for numerical methods in engineering* 28.6 (1989), pp. 1283–1298.

[92] JR Banerjee and FW Williams. “Coupled bending-torsional dynamic stiffness matrix for Timoshenko beam elements”. In: *Computers & Structures* 42.3 (1992), pp. 301–310.

[93] JR Banerjee, S Guo, and WP Howson. “Exact dynamic stiffness matrix of a bending-torsion coupled beam including warping”. In: *Computers & structures* 59.4 (1996), pp. 613–621.

[94] Ricardo Daniel Ambrosini, Jorge Daniel Riera, and Rodolfo Francisco Danesi. “Dynamic analysis of thin-walled and variable open section beams with shear flexibility”. In: *International Journal for Numerical Methods in Engineering* 38.17 (1995), pp. 2867–2885.

[95] Ricardo Daniel Ambrosini, Jorge Daniel Riera, and Rodolfo Francisco Danesi. “A modified Vlasov theory for dynamic analysis of thin-walled and variable open section beams”. In: *Engineering Structures* 22.8 (2000), pp. 890–900.

[96] AN Bercin and M Tanaka. “Coupled flexural–torsional vibrations of Timoshenko beams”. In: *Journal of sound and vibration* 207.1 (1997), pp. 47–59.

[97] Sung Y Back and Kenneth M Will. “A shear–flexible element with warping for thin-walled open beams”. In: *International Journal for Numerical Methods in Engineering* 43.7 (1998), pp. 1173–1191.

[98] JR Hutchinson. “Shear coefficients for Timoshenko beam theory”. In: *J. Appl. Mech.* 68.1 (2001), pp. 87–92.

[99] JN1709059 Reddy. “On the dynamic behaviour of the Timoshenko beam finite elements”. In: *Sadhana* 24 (1999), pp. 175–198.

[100] EJ Sapountzakis and JA Dourakopoulos. “Shear deformation effect in flexural–torsional vibrations of beams by BEM”. In: *Acta mechanica* 203.3-4 (2009), pp. 197–221.

[101] M.H. Kahrobaiyan, M. Asghari, and M.T. Ahmadian. “A Timoshenko beam element based on the modified couple stress theory”. In: *International Journal of Mechanical Sciences* 79 (2014), pp. 75–83. ISSN: 0020-7403. DOI: https://doi.org/10.1016/j.ijmecsci.2013.11.014. URL: https://www.sciencedirect.com/science/article/pii/S0020740313003160.

[102] R Van Leeuwen. “Cross-Section Analysis in Python”. In: (2017).

[103] LE Elsgolts. “Differential equations and variational calculus”. In: *Moscu: MIR* (1969).

[104] Walter Rudin. “Functional analysis, mcgrawhill”. In: *Inc, New York* 45.46 (1991), p. 4.

[105] Haim Brezis and Haim Brézis. *Functional analysis, Sobolev spaces and partial differential equations*. Vol. 2. 3. Springer, 2011.

[106] Michael Smith. *ABAQUS/Standard User's Manual, Version 6.9*. English. United States: Dassault Systèmes Simulia Corp, 2009.

[107] Francis Thomas McKenna. *Object-oriented finite element programming: frameworks for analysis, algorithms and parallel computing*. University of California, Berkeley, 1997.

[108] M Petracca, F Candeloro, and G Camata. "STKO user manual". In: *ASDEA Software Technology: Pescara, Italy* 551 (2017).

[109] Eduardo N Dvorkin and Klaus-Jürgen Bathe. "A continuum mechanics based four-node shell element for general non-linear analysis". In: *Engineering computations* 1.1 (1984), pp. 77–88.

[110] Hans M Hilber, Thomas JR Hughes, and Robert L Taylor. "Improved numerical dissipation for time integration algorithms in structural dynamics". In: *Earthquake Engineering & Structural Dynamics* 5.3 (1977), pp. 283–292.

[111] Timothy O Hodson. "Root mean square error (RMSE) or mean absolute error (MAE): When to use them or not". In: *Geoscientific Model Development Discussions* 2022 (2022), pp. 1–10.

[112] Dulakshi Santhusitha Kumari Karunasingha. "Root mean square error or mean absolute error? Use their ratio as well". In: *Information Sciences* 585 (2022), pp. 609–629.

[113] Weijie Wang and Yanmin Lu. "Analysis of the mean absolute error (MAE) and the root mean square error (RMSE) in assessing rounding model". In: *IOP conference series: materials science and engineering*. Vol. 324. IOP Publishing. 2018, p. 012049.

[114] Davide Chicco, Matthijs J Warrens, and Giuseppe Jurman. "The coefficient of determination R-squared is more informative than SMAPE, MAE, MAPE, MSE and RMSE in regression analysis evaluation". In: *Peerj computer science* 7 (2021), e623.

[115] Sir George Gabriel Stokes. *Discussion of a differential equation relating to the breaking of railway bridges*. Printed at the Pitt Press by John W. Parker, 1849.

[116] Great Britain. Commissioners appointed to inquire into the application of iron to railway structures. *Report of the Commissioners Appointed to Inquire Into the Application of Iron to Railway Structures...* Vol. 1. William Clowes and sons, 1849.

[117] SP Timoshenko. "CV. On the forced vibrations of bridges". In: *The London, Edinburgh, and Dublin Philosophical Magazine and Journal of Science* 43.257 (1922), pp. 1018–1019.

[118] Arnold N Lowan. "LIV. On transverse oscillations of beams under the action of moving variable loads". In: *The London, Edinburgh, and Dublin Philosophical Magazine and Journal of Science* 19.127 (1935), pp. 708–715.

[119] PK Chatterjee, TK Datta, and CS Surana. "Vibration of suspension bridges under vehicular movement". In: *Journal of Structural Engineering* 120.3 (1994), pp. 681–703.

[120] Yufeng Dong, Wenyang Zhang, Anoosh Shamsabadi, Li Shi, and Ertugrul Taciroglu. "A Vehicle–Bridge Interaction Element: Implementation in ABAQUS and Verification". In: *Applied Sciences* 13.15 (2023), p. 8812.

[121] Nathan M Newmark. "A method of computation for structural dynamics". In: *Journal of the engineering mechanics division* 85.3 (1959), pp. 67–94.

[122] Xuzhao Lu, Chul-Woo Kim, and Kai-Chun Chang. "Finite element analysis framework for dynamic vehicle-bridge interaction system based on ABAQUS". In: *International Journal of Structural Stability and Dynamics* 20.03 (2020), p. 2050034.

[123] Tianyu Xiang, Renda Zhao, and Tengfei Xu. “Reliability evaluation of vehicle–bridge dynamic interaction”. In: *Journal of Structural Engineering* 133.8 (2007), pp. 1092–1099.

[124] Shen-Haw Ju and Hung-Ta Lin. “A finite element model of vehicle–bridge interaction considering braking and acceleration”. In: *Journal of sound and vibration* 303.1-2 (2007), pp. 46–57.

[125] Javier Oliva, José M Goicolea, Pablo Antolín, and Miguel Á Astiz. “Relevance of a complete road surface description in vehicle–bridge interaction dynamics”. In: *Engineering structures* 56 (2013), pp. 466–476.

[126] Hai Zhong, Mijia Yang, and Zhili Jerry Gao. “Dynamic responses of prestressed bridge and vehicle through bridge–vehicle interaction analysis”. In: *Engineering Structures* 87 (2015), pp. 116–125.

[127] Helu Yu, Bin Wang, Yongle Li, Yankun Zhang, and Wei Zhang. “Road vehicle-bridge interaction considering varied vehicle speed based on convenient combination of Simulink and ANSYS”. In: *Shock and Vibration* 2018 (2018).

[128] Zhenhua Shi and Nasim Uddin. “Theoretical vehicle bridge interaction model for bridges with non-simply supported boundary conditions”. In: *Engineering Structures* 232 (2021), p. 111839.

[129] Soheil Sadeghi Eshkevari, Thomas J Matarazzo, and Shamim N Pakzad. “Simplified vehicle–bridge interaction for medium to long-span bridges subject to random traffic load”. In: *Journal of Civil Structural Health Monitoring* 10 (2020), pp. 693–707.

[130] Nicola Bellomo, Marcello Delitala, and V Coscia. “On the mathematical theory of vehicular traffic flow I: Fluid dynamic and kinetic modelling”. In: *Mathematical Models and Methods in Applied Sciences* 12.12 (2002), pp. 1801–1843.

[131] Colin C Caprani, Eugene J OBrien, and Alessandro Lipari. “Long-span bridge traffic loading based on multi-lane traffic micro-simulation”. In: *Engineering Structures* 115 (2016), pp. 207–219.

[132] Cesar Crespo-Minguillon and Juan R Casas. “A comprehensive traffic load model for bridge safety checking”. In: *Structural safety* 19.4 (1997), pp. 339–359.

[133] Pietro Croce and Walter Salvatore. “Stochastic model for multilane traffic effects on bridges”. In: *Journal of Bridge Engineering* 6.2 (2001), pp. 136–143.

[134] Reinhard Mahnke, Jevgenijs Kaupužs, and I Lubashevsky. “Probabilistic description of traffic flow”. In: *Physics Reports* 408.1-2 (2005), pp. 1–130.

[135] Li Cao and Limin Sun. “Research on Random Flow Simulation Model of Bridges”. In: *2018 International Conference on Computer Science, Electronics and Communication Engineering (CSECE 2018)*. Atlantis Press. 2018, pp. 295–297.

[136] Bernard Jacob. “Assessment of the accuracy and classification of weigh-in-motion systems Part 1: Statistical background”. In: *International Journal of Heavy Vehicle Systems* 7.2-3 (2000), pp. 136–152.

[137] Bernard Jacob, Eugene J O’Brien, and William Newton. “Assessment of the accuracy and classification of weigh-in-motion systems. Part 2: European specification”. In: *International Journal of Heavy Vehicle Systems* 7.2-3 (2000), pp. 153–168.

[138] Muhammad Munum Masud and Syed W Haider. "Effect of static weight errors on Weigh-in-Motion (WIM) system accuracy". In: *Measurement* 206 (2023), p. 112301.

[139] Klas Bogsjö, Krzysztof Podgórski, and Igor Rychlik. "Models for road surface roughness". In: *Vehicle System Dynamics* 50.5 (2012), pp. 725–747.

[140] Par Johannesson, Krzysztof Podgórski, and Igor Rychlik. "Modelling roughness of road profiles on parallel tracks using roughness indicators". In: *International journal of vehicle design* 70.2 (2016), pp. 183–210.

[141] Semiha Türkay and Hüseyin Akçay. "Road roughness modelling by using spectral factorization methods". In: *2016 16th International Conference on Control, Automation and Systems (ICCAS)*. IEEE. 2016, pp. 51–56.

[142] Venu Muluka. "Optimal suspension damping and axle vibration absorber for reduction of dynamic tire loads". PhD thesis. Concordia University, 1998.

[143] Z Lozia and P Zdanowicz. "Optimization of damping in the passive automotive suspension system with using two quarter-car models". In: *IOP Conference Series: Materials Science and Engineering*. Vol. 148. 1. IOP Publishing. 2016, p. 012014.

[144] Peter Múčka. "Simulated road profiles according to ISO 8608 in vibration analysis". In: *Journal of Testing and Evaluation* 46.1 (2017), pp. 405–418.

[145] Kong Yat Sheng, Shahrum Abdullah, Sallehuddin Mohamed Haris, Mohd Zaidi Omar, and Dieter Schramm. "Generation of artificial road profile for automobile spring durability analysis". In: *Jurnal Kejuruteraan* 30.2 (2018), pp. 123–128.

[146] Prashant R Pawar, Arun Tom Mathew, and MR Saraf. "IRI (International Roughness Index): an indicator of vehicle response". In: *Materials Today: Proceedings* 5.5 (2018), pp. 11738–11750.

[147] Carlo Rainieri, Matilde A Notarangelo, and Giovanni Fabbrocino. "Experiences of dynamic identification and monitoring of bridges in serviceability conditions and after hazardous events". In: *Infrastructures* 5.10 (2020), p. 86.

[148] The MathWorks Inc. *MATLAB version: 9.13.0 (R2022b)*. Natick, Massachusetts, United States, 2022. URL: https://www.mathworks.com.

[149] Dan J Naus and HL Graves III. "A review of the effects of elevated temperature on concrete materials and structures". In: *International Conference on Nuclear Engineering*. Vol. 42428. 2006, pp. 615–624.

[150] Long T Phan and Nicholas J Carino. "Code provisions for high strength concrete strength-temperature relationship at elevated temperatures". In: *Materials and Structures* 36 (2003), pp. 91–98.

[151] Melvin S Abrams. "Compressive strength of concrete at temperatures to 1600F". In: *Special Publication* 25 (1971), pp. 33–58.

[152] GC Lee, TS Shih, and Kuei-Chung Chang. "Mechanical properties of concrete at low temperature". In: *Journal of cold regions engineering* 2.1 (1988), pp. 13–24.

[153] Y Yuan and ZL Wan. "Prediction of cracking within early-age concrete due to thermal, drying and creep behavior". In: *Cement and concrete research* 32.7 (2002), pp. 1053–1059.

[154] Charles J Korhonen. "Off-the-shelf antifreeze admixtures". In: (2002).

[155] J Randall Lawson, Long Thanh Phan, and Frank Davis. *Mechanical properties of high performance concrete after exposure to elevated temperatures*. US Department of Commerce, Technology Administration, National Institute of ..., 2000.

[156] Jaesung Lee, Yunping Xi, and Kaspar Willam. "Properties of concrete after high-temperature heating and cooling". In: *ACI Materials Journal* 105.4 (2008), p. 334.

[157] Samir N Shoukry, Gergis W William, Brian Downie, and Mourad Y Riad. "Effect of moisture and temperature on the mechanical properties of concrete". In: *Construction and Building Materials* 25.2 (2011), pp. 688–696.

[158] Bjarne Stroustrup. *The C++ Programming Language Fourth Edition*. 2013.

[159] Bjarne Stroustrup. "An overview of C++". In: *Proceedings of the 1986 SIGPLAN workshop on Object-oriented programming*. 1986, pp. 7–18.

[160] Frank McKenna. "OpenSees: a framework for earthquake engineering simulation". In: *Computing in Science & Engineering* 13.4 (2011), pp. 58–66.

[161] Gaël Guennebaud, Benoît Jacob, et al. *Eigen v3*. http://eigen.tuxfamily.org. 2010.

[162] James Rumbaugh, Michael Blaha, William Premerlani, Frederick Eddy, William E. Lorensen, et al. *Object-oriented modeling and design*. Vol. 199. 1. Prentice-hall Englewood Cliffs, NJ, 1991.

[163] BSI MEE. "158/3/1, Proposals for Generalised Road Inputs to Vehicles". In: *British Standard Institution (BSI), London, BSI* 72 (1972), p. 34562.

[164] Tong Guo, Dan M Frangopol, and Yuwen Chen. "Fatigue reliability assessment of steel bridge details integrating weigh-in-motion data and probabilistic finite element analysis". In: *Computers & Structures* 112 (2012), pp. 245–257.

[165] Matthew J Fox, Marco Furinghetti, and Alberto Pavese. "Application of the new Italian assessment guidelines to a 1960s prestressed concrete road bridge". In: *Structural Concrete* 24.1 (2023), pp. 583–598.